

*Adaptations of Prevotella bryantii B₁₄ to Short-Chain
Fatty Acids and Monensin Exposure*

**Dissertation for Obtaining the Doctoral Degree of Natural Sciences
(Dr. rer. nat.)**

**Faculty of Natural Sciences
University of Hohenheim**

Institute of Animal Sciences & Institute of Biology

Submitted by
Andrej Trautmann

Born in Moscow, Russia

2022

Dean: Prof. Dr. Uwe Beifuss

1st reviewer: Prof. Dr. Jana Seifert

2nd reviewer: Prof. Dr. Julia Fritz-Steuber

Submitted on: 25.Nov.2022

Oral examination on: 17.Mar.2023

This work was accepted by the Faculty of Natural Sciences at the University of Hohenheim on 25.Nov.2022 as “Dissertation for Obtaining the Doctoral Degree of Natural Sciences”. The subject was defended via an oral examination on the 17.Mar.2023.

Thesis abstract

The rumen microbiome constitutes a complex ecosystem including a vast diversity of organisms that produce and consume short-chain fatty acids (SCFAs). It is of great interest to analyze these activities as they are of benefit for both, the microbiome and the host. This dissertation aims to display the proteome and metabolome of the predominant ruminal representative *Prevotella bryantii* B₁₄ in presence of various SCFA and under exposure of the antibiotic monensin in pure and mixed culture (*in vitro*). Due to the strong contributing abundance of Prevotellaceae in the rumen microbiome, the representative *P. bryantii* B₁₄ (DSM 11371) was chosen to investigate biochemical factors for the success of withstanding monensin and the impact of SCFA on their growth. The current work is composed of two effective publications [1, 2] which are inserted in chapter 2 and 3 as well as a submitted manuscript in chapter 4. The formatting was aligned to the dissertation.

The first publication (Chapter 2), studying the supplementation of various SCFAs, showed SCFAs as growth promoting but not essential for *P. bryantii* B₁₄. Pure cultures of *P. bryantii* B₁₄ were grown in Hungate tubes under anaerobic conditions. Gas chromatography time of flight mass spectrometry (GC-ToF MS) was used to quantify long-chain fatty acid (LCFA) profiles of *P. bryantii* B₁₄. Proteins of *P. bryantii* B₁₄ were identified and quantified by using a mass spectrometry-based, label-free approach. Different growth behavior was observed depending on the supplemented SCFA. An implementation of SCFAs on LCFAs and the composition on membrane proteins became evident. Supplementing *P. bryantii* B₁₄ with branched-chain fatty acids (BCFAs), in particular isovaleric acid, showed an increase of the 3-IPM pathway, which is part of the branched-chain amino acid (BCAA) metabolism. Findings point out that the structure similarity of isovaleric acid and valine is most likely enhancing the conversion of BCFA into BCAA. The required set of enzymes of the BCAA metabolism supported this perspective.

The ionophore monensin has antibiotic properties which are used in cattle fattening but also for treating ketosis and acidosis in ruminants. In the second publication (Chapter 3), *P. bryantii* B₁₄ was exposed to different concentrations of monensin (0, 10, 20 and 50 μ M) and to different exposure times (9, 24, 48 and 72 h) with and without monensin. Growth behavior, glucose and intracellular sodium concentration were determined. Proteins were analyzed by label-free quantification method using the same method as in chapter 2. Fluorescence microscopy was used to observe extracellular polysaccharides (EPS) of *P. bryantii* B₁₄. A

progressing monensin exposure triggered disconnection between *P. bryantii* B₁₄ cells to the sacrificial EPS layer by increasing its number and amount of carbohydrate active enzymes (CAZymes). Simultaneously, an increase of extracellular glucose was monitored. Reduction of intracellular sodium was likely to be performed by increasing the abundance of ion-transporters and an increased activity of Na⁺-translocating NADH:quinone oxidoreductase under monensin supplementation.

The role of monensin supplemented *Prevotella* in a mixed culture of the rumen microbiome was described in the last manuscript (Chapter 4). Extracted rumen fluid from cows was incubated anaerobically by using the rumen simulation technique (Rusitec). Proteomics of the solid phase was applied by using a similar approach as in chapter 2 and 3. Metabolomics of the liquid phase from the Rusitec content was performed by using ¹H-nuclear magnetic resonance (NMR) spectroscopy. Further parameters such as pH, gas and methane production were monitored over time. The experiment was constituted out of three phases starting with an adaptation phase of 7 days. A subsequent treatment phase followed, where monensin was supplemented via the daily introduced total mixed ration (TMR) for further 7 days. The elution phase was the final phase when monensin supplementation was stopped and monitoring was continued for further 3 days. Metabolomics and proteomics showed that members of the genus *Prevotella* remained most abundant under monensin supplementation. Furthermore, shifting the ruminal metabolism to an increased production of propionate by shifting the metabolism of *Prevotella* sp. to an enhanced succinate production.

The current work shows the impact of SCFAs on various metabolic functions of *P. bryantii* B₁₄. Diverse defence mechanisms of *Prevotella* sp., in particular *P. bryantii* B₁₄, were shown to avoid the antibiotic effects of monensin.

Thesis Zusammenfassung

Das Pansenmikrobiom ist ein komplexes Ökosystem mit einer großen Vielfalt an Organismen, die kurzkettige Fettsäuren (SCFAs) produzieren und verbrauchen. Es ist von großem Interesse, diese Aktivitäten zu analysieren, da sie sowohl für das Mikrobiom als auch für den Wirt von Nutzen sind. Ziel dieser Arbeit ist es, das Proteom und Metabolom des vorherrschenden Pansenvertreterers *Prevotella bryantii* B₁₄ in Gegenwart verschiedener SCFA und unter Einwirkung des Antibiotikums Monensin in Rein- und Mischkultur (*in vitro*) darzustellen. Aufgrund der großen Anzahl von Prevotellaceae im Pansenmikrobiom wurde der Vertreter *P. bryantii* B₁₄ (DSM 11371) ausgewählt, um die biochemischen Faktoren für die erfolgreiche Resistenz gegenüber Monensin und die Auswirkungen von kurzkettigen Fettsäuren auf ihr Wachstum zu untersuchen. Die aktuelle Arbeit besteht aus zwei Publikationen [1, 2], die in Kapitel 2 und 3 eingefügt sind, sowie einem eingereichten Manuskript in Kapitel 4. Die Formatierung der Publikationen und des Manuskriptes wurde an die Dissertation angepasst.

Die erste Veröffentlichung (Kapitel 2) befasste sich mit der Supplementierung verschiedener SCFAs und zeigt, dass SCFAs wachstumsfördernd, aber nicht essentiell für *P. bryantii* B₁₄ sind. Reinkulturen von *P. bryantii* B₁₄ sind in Hungate-Röhrchen unter anaeroben Bedingungen durchgeführt worden. Gaschromatographie-Flugzeit-Massenspektrometrie (GC-ToF MS) wurde zur Quantifizierung der langkettigen Fettsäuren (LCFA) von *P. bryantii* B₁₄ verwendet. Die nicht-markierte und nicht-angereicherte Proteine von *P. bryantii* B₁₄ wurden mit Hilfe von Massenspektrometrie identifiziert und quantifiziert. Es wurde ein unterschiedliches Wachstumsverhalten in Abhängigkeit von der zugeführten SCFA beobachtet. Eine Auswirkung der strukturellen Eigenschaften der SCFAs hat sich auf die LCFAs und ebenso auf die Anwesenheit verschiedener Membranproteine bemerkbar gemacht. Die Supplementierung von *P. bryantii* B₁₄ mit verzweigt-kettigen Fettsäuren (BCFAs), insbesondere Isovaleriansäure, hat einen Anstieg des Stoffwechsels von 3-Isopropylmalat (IPM) gezeigt, welcher Teil des Stoffwechsels von verzweigt-kettigen Aminosäuren (BCAAs) ist. Die Ergebnisse deuten darauf hin, dass die Strukturähnlichkeit von Isovaleriansäure und Valin höchstwahrscheinlich die Umwandlung von BCFA in BCAA begünstigt. Der relative Anstieg der erforderlichen Enzyme BCAA-Stoffwechsel unterstützen diese Sichtweise.

Das Ionophor Monensin hat antibiotische Eigenschaften, welche in der Rindermast, aber auch zur Behandlung von Ketose und Azidose bei Wiederkäuern eingesetzt wird. Die

zweiten Veröffentlichung (Kapitel 3) zeigte den Einfluss verschiedenen Konzentrationen von Monensin (0, 10, 20 und 50 μM) und verschiedenen Expositionszeiten (9, 24, 48 und 72 h) mit und ohne Monensin auf *P. bryantii* B₁₄. Das Wachstumsverhalten, extrazelluläre Glukose- und intrazelluläre Natriumkonzentration wurde unter den beschriebenen Bedingungen ermittelt. Das Proteom von *P. bryantii* B₁₄ wurde mittels markierungsfreier Quantifizierung nach der gleichen Methode wie in Kapitel 2 analysiert. Fluoreszenzmikroskopie wurde zur Untersuchung der extrazellulären Polysaccharide (EPS) von *P. bryantii* B₁₄ eingesetzt. Mit fortschreitender Monensin-Exposition hat sich gezeigt, dass *P. bryantii* B₁₄ die Verbindung zur äußeren EPS abbaute, indem es die Anzahl und Menge der kohlenhydrataktiven Enzyme (CAZyme) erhöhte. Der Anstieg an extrazellulärer Glukose bestätigte die Vermutung, dass die „Opferschicht“ abgebaut wurde. Die beobachtete Reduktion des intrazellulären Natriums ist wahrscheinlich mit der Zunahme der Menge an Ionentransportern verbunden. Weiterhin wurde eine erhöhte Aktivität der Na⁺-transferrierenden NADH:Quinon-Oxidoreduktase (NQR) unter Monensin-Supplementierung dokumentiert.

Die Rolle von mit Monensin supplementierten *Prevotella* in einer Mischkultur des Pansenmikrobioms ist im letzten Manuskript beschrieben worden (Kapitel 4). Pansensaft ist mit Hilfe der Pansensimulationstechnik (Rumen simulation technique = Rusitec) anaerob inkubiert worden. Das Proteom der festen Phase ist mit einem ähnlichen Ansatz wie in Kapitel 2 und 3 durchgeführt worden. Das Metabolom der flüssigen Phase aus dem Rusitec ist anhand der ¹H-Kernresonanz (Nuclear magnetic resonance = NMR) spektroskopie ermittelt worden. Weitere Parameter wie pH-Wert, Gas- und Methanproduktion wurden im Zeitverlauf überwacht. Das Experiment bestand aus drei Phasen, beginnend mit einer Anpassungsphase von 7 Tagen. Es folgte eine Behandlungsphase, in der Monensin über das tägliche verabreichen der totalen Mischration (TMR) für weitere 7 Tage durchgeführt wurde. Die Elutionsphase war die letzte Phase, in der die Monensinzugabe eingestellt und die Überwachung für weitere 3 Tage fortgesetzt wurde. Metabolomics und Proteomics haben gezeigt, dass Mitglieder der Gattung *Prevotella* unter Monensinzugabe am häufigsten vorkommen. Außerdem verlagerte sich der Pansenstoffwechsel auf eine erhöhte Propionatproduktion. Der Stoffwechsel von *Prevotella* sp. wurde auf eine erhöhte Succinatproduktion umgestellt.

Die vorliegende Arbeit zeigt die Auswirkungen von SCFAs auf verschiedene Stoffwechselfunktionen von *P. bryantii* B₁₄. Es wurde gezeigt, dass verschiedene

Abwehrmechanismen von *Prevotella* sp. und insbesondere von *P. bryantii* B₁₄ die anti-biotische Wirkung von Monensin verhindern.

Table of contents

Thesis abstract.....	III
Thesis Zusammenfassung	V
Table of contents.....	VIII
List of abbreviations	XIV
1. Introduction & motivation	1
1.1 Rumen and microbiome.....	1
1.2 <i>Prevotella bryantii</i> B ₁₄	2
1.2.1 Essential requirements of <i>Prevotella</i> species	3
1.2.2 Carbon sources & metabolism.....	4
1.2.3 Short-chain fatty acids (SCFA) & metabolism	5
1.2.4 Vitamins & supplements.....	6
1.3 Monensin in nutrition	7
1.3.1 Mode of action of monensin.....	8
1.3.2 Monensin impact on rumen microbiome, function and metabolites	9
1.3.3 Monensin resistance of <i>Prevotella</i> species.....	9
1.4 Methodologies	10
1.4.1 Cultivation technologies	10
1.4.2 Proteomics	12
1.4.3 Metabolite Analysis.....	12
1.5 Motivation, hypothesis & objectives	13
2. Short-chain fatty acids modulate metabolic pathways and membrane lipids in <i>Prevotella bryantii</i> B₁₄.....	15
2.1 Abstract	15
2.2 Introduction	16

Table of contents

2.3	Material & methods.....	17
2.3.1	Cultivation in medium M2-A for proteome analysis	17
2.3.2	Cultivation for long-chain fatty acid determination	18
2.3.3	Glucose based medium M2-B.....	18
2.3.4	Short-chain fatty acid determination	18
2.3.5	Long-chain fatty acid determination	19
2.3.6	Protein extraction	20
2.3.7	In gel protein digestion	20
2.3.8	LC-ESI-MS/MS	21
2.3.9	Data analysis for proteomics	21
2.4	Results.....	23
2.4.1	Cultivation of <i>P. bryantii</i> B ₁₄ Using Single SCFAs.....	23
2.4.2	Proteome inventory of <i>P. bryantii</i> B ₁₄	25
2.4.3	Effect of SCFA exposure on LCFA in membranes from <i>P. bryantii</i>	29
2.4.4	Effect of carbon source on growth of <i>P. bryantii</i>	30
2.5	Discussion.....	32
2.5.1	SCFAs replace rumen fluid for cultivation of <i>P. bryantii</i> B ₁₄	32
2.5.2	SCFA Influence the Abundance of Iron Transport Proteins.....	32
2.5.3	SCFAs incorporated into long-chain fatty acids of lipid membranes	34
2.5.4	Isovaleric acid enhance branched-chain amino acid synthesis.....	34
2.5.5	Conclusions	35
2.6	Miscellaneous information of publication.....	36
2.6.1	Funding.....	36
2.6.2	Acknowledgments.....	36
2.6.3	Conflicts of interest.....	36
2.7	Supplementary tables	37

Table of contents

2.8	Supplementary figures	44
3.	Na⁺-coupled respiration and reshaping of extracellular polysaccharide layer counteract monensin-induced cation permeability in <i>Prevotella bryantii</i> B₁₄	57
3.1	Abstract	57
3.2	Introduction	58
3.3	Results	59
3.3.1	Inhibition of <i>Prevotella bryantii</i> B ₁₄ growth by increasing monensin concentrations	59
3.3.2	Growth adaptations towards monensin over time	61
3.3.3	Dose-dependent modulation of the proteome of <i>Prevotella bryantii</i> B ₁₄ by monensin	62
3.3.4	Protein modification in monensin cultures over time	65
3.3.5	Altered EPS structure in monensin cultivations	67
3.4	Discussion	68
3.4.1	Degrassive dose-response to monensin	68
3.4.2	Cation permeability affects proteome and metabolism	68
3.4.3	Monensin triggers extracellular polysaccharide degradation by <i>P. bryantii</i> with a concomitant release of glucose	69
3.5	Conclusions	71
3.6	Materials and methods	72
3.6.1	Cultivation	72
3.6.2	Growth in presence of monensin	72
3.6.3	Determination of intracellular sodium content	72
3.6.4	Determination of D-glucose and glucose-6-phosphate in cell cultures	73
3.6.5	Membrane isolation and enzyme kinetics	74
3.6.6	Fluorescence microscopy	74

Table of contents

3.6.7	Proteome analysis preparation.....	75
3.6.8	Tandem mass spectrometry	75
3.6.9	Proteome analysis.....	76
3.6.10	Statistical analysis	76
3.7	Miscellaneous information of publication.....	78
3.7.1	Data availability statement	78
3.7.2	Acknowledgement	78
3.7.3	Competing interest	78
3.8	Supplementary tables	78
3.9	Supplementary figures.....	90
4.	A shift towards succinate-producing <i>Prevotella</i> in the ruminal microbiome challenged with monensin	94
4.1	Abstract.....	94
4.2	Introduction	94
4.3	Material and methods	96
4.3.1	Diet and treatment preparation	96
4.3.2	Inoculation and Rusitec design	96
4.3.3	Parameter measurement and sampling	97
4.3.4	Experimental setup	99
4.3.5	Gas slope calculations.....	99
4.3.6	Monensin quantification via LC-MS.....	99
4.3.7	Quantification of [NH ₃ + NH ₄ ⁺].....	99
4.3.8	Metabolome analysis by ¹ H-NMR spectroscopy.....	100
4.3.9	Protein extraction and purification.....	100
4.3.10	Tandem mass spectrometry	101
4.3.11	Metaproteomic data analysis	101

Table of contents

4.3.12	Data analysis	102
4.4	Results	102
4.4.1	Gas and methane emission.....	102
4.4.2	Fermentation and metabolites	102
4.4.3	Monensin in reactor effluent.....	106
4.4.4	Metaproteome is altered by monensin exposure	106
4.4.5	<i>Prevotella</i> species are less affected by monensin	108
4.4.6	Functional metaproteome influenced by monensin	109
4.4.7	Monensin leads to reduced fiber digesting and assimilating capabilities of the microbiome.....	111
4.5	Discussion.....	113
4.5.1	Proteolytic activities influenced by monensin.....	113
4.5.2	Reduced fibre degradation in the presence of monensin	113
4.5.3	Monensin affects fermentation activities.....	114
4.5.4	Accumulation and elution of monensin.....	116
4.6	Miscellaneous information of manuscript.....	117
4.6.1	Associated Data.....	117
4.6.1	Acknowledgments.....	117
4.7	Supplementary tables	118
4.8	Supplementary figures	120
5.	Requirements of semi-defined media for <i>Prevotella bryantii</i> B₁₄.....	126
5.1	Gas phase requirements	126
5.2	Optimal Starting pH	127
5.3	Dispensable supplements	127
6.	Discussion	129
6.1	Major findings	129

Table of contents

6.2	Versatile functions of SCFA in <i>Prevotella bryantii</i> B ₁₄	130
6.2.1	SCFA a non-essential growth promotor.....	130
6.2.2	Influence of SCFA on LCFA and membrane proteins.....	130
6.2.3	Iron uptake via SCFAs.....	131
6.2.4	Production and deconstruction of BCAAs and BCFAs.....	132
6.3	Reactions & countermeasures of <i>P. bryantii</i> towards monensin	133
6.3.1	Increased Na ⁺ -translocating proteins, NQR and QFR promote succinate formation	134
6.3.2	Prevent monensin binding.....	134
6.3.3	Increased transcription & translation.....	135
6.3.4	Outer membrane proteins as biomarkers	136
6.3.5	Key role of <i>Prevotella</i> under monensin exposure	137
6.4	Reclassification of <i>P. bryantii</i> to <i>Segatella bryantii</i>	139
7.	Outlook.....	140
8.	Literature References	143
9.	Author contributions	162
9.1	First publication in chapter 2	162
9.2	Second publication in chapter 3	162
9.3	Third publication/manusript in chapter 4.....	163
	Curriculum Vitae (CV).....	XVIII
	Publications.....	XIX
	Acknowledgements	XX
	Eidesstattliche Versicherung	XXII

List of abbreviations

%	Percentage
°C	Degree Celsius
x g	Times the gravitational force equivalent
μL	Microliter
μm	Micrometer
μM	Micromolar
¹ H	Hydrogen isotope with an electron and proton
² H	Hydrogen isotope with an electron, proton and neutron
2MB	Treatment with 2-methyl butyric acid
3-IPM	3-Isopropylmalate
ABC-transporter	ATP-binding cassette transporters
Acet	Treatment with acetic acid
Acetyl-CoA	Ethyl bound Co enzyme A
AIB	Anti-isobutyrate factor
ANOSIM	Analysis of similarities
ATP	Adenosine triphosphate
Av.	Average
BCFA	Branched-chain fatty acid
But	Treatment with butyric acid
CAZyme	Carbohydrate-active enzyme
CCCP	Carbonylcyanid-m-chlorophenylhydrazon
CE	Carbohydrate esterase
CH ₃	Methyl group
COOH	Carboxyl group
CON	Condition referred as control without monensin
COG	Clusters of orthologous groups
d	Day(s)
D ₂ O	Deuterium, has the ² H isotope
Da	Dalton
DNA	Desoxyribonuclease

List of abbreviations

e.g.	Example given
ESI	Electron spray ionization
EPS	Extracellular polysaccharides
Fe ^{2+/3+}	Iron ion with two or three positive charges
FeS	Iron-sulfur complex
FDR	False discovery rate
g	Gram
GC-MS	Gas chromatography coupled to mass spectrometry
GH	Glycoside hydrolase
GIT	Gastrointestinal tract
h	Hour(s)
H ⁺	Hydrogen ion / proton
H ₂	Molecular Hydrogen
H ₂ O	Water
iBut	Treatment with iso-butyric acid
IC	Ion Chromatography
iVal	Treatment with iso-valeric acid
HPLC	High performance liquid chromatography
HSP	Heat shock protein
K ⁺	Potassium ion
KEGG	Kyoto encyclopedia of genes and genomes
KO	KEGG orthology
L	Liter
LC	Liquid chromatography
LCFA	Long-chain fatty acid
LC-MS/MS	LC coupled tandem mass spectrometry
LD ₅₀	Lethal doses at which 50% of test animals die
LFQ	Label-free quantification
Log ₂	Logarithm with basis of 2
Log ₁₀	Logarithm with basis of 10
LPS	Lipopolysaccharides

List of abbreviations

LSD	Least significant difference
M	Molar
mA	Milli-ampere
<i>mcrA</i>	Methyl-coenzyme-M-reductase
mg	Milli-gram
min	Minute(s)
mL	Milli-liter
mM	Milli-molar
MON	Condition with monensin supplementation
mV	Milli-volt
Na ⁺	Sodium Ion
NADH	Nicotinamide adenine dinucleotide
nL/min	Nano-liter per minute
NMR	Nuclear magnetic resonance
No.	Number
∅	Average
OD ₆₀₀	Optical density at $\lambda = 600$ nm
<i>p</i>	Probability
PABA	<i>p</i> -Aminobenzoic acid
PBS	Phosphate buffered saline
PCO	Principal component
PCoA	Principal component analysis
PCR	Polymerase chain reaction
pH	Potential of hydrogen ($-\log_{10}[\text{H}^+]$)
PMSF	Phenylmethylsulfonyl fluoride
PPIX	Protoporphyrin IX
ppm	Parts per million
Prop	Treatment with propionic acid
QFR	Quinol:fumarate reductase
qPCR	Quantitative PCR
R ²	Coefficient of determination, squared Pearson correlation

List of abbreviations

Rusitec	Rumen simulation technique
SCFA	Short-chain fatty acid
SCFA-Mix	A mixture of the SCFAs: acetic, propionic, butyric, iso-butyric, iso- valeric, valeric and 2-methyl butyric acid
SD	Standard deviation
SDS-PAGE	Sodium dodecyl sulfate polyacrylamide gel electrophoresis
SIMPER	Similarity percentage
sp.	Species
TCA	Trichloro-acetic acid
TMR	Total mixed ration consisting of grinded: 20% soy meal, 20% corn grains, 20% grass silage and 40% corn silage
TopN	Number of tandem mass-spectra fragments
Trypticase	Trypsin digested casein (milk protein)
TSP	Trimethyl-silyl-propanoic acid
UDP	Uridin-diphosphat (nucleotide)
VFA	Volatile fatty acid (synonym for SCFA)

1. Introduction & motivation

1.1 Rumen and microbiome

Ruminants on their own are incapable of digesting plant fiber [3]. The required enzymes for digesting plant fiber in animals derive from microorganisms. The microorganisms enable them to access nutrients which they could not get on their own [3]. This evolutionary shaped symbiosis formed the forestomach system which created the suborder of ruminants. The forestomach system consists of the segments: esophagus, rumen, reticulum, omasum and abomasum. The digestive system of ruminants allows to ruminate (to chew the cud and shred it) and digest plant fiber by microorganisms in an extremely efficient way, as compared to most of the non-ruminant animals. The rumen is the largest digestive segment in adult cattle [3] and provides a suitable location for anaerobic microbial growth and feedstuff digestion. Microbes benefit from the stable environment while ruminants gain a majority of their energy supply from fermentation products out of the rumen [3]. This fermentation products, to which short-chain fatty acids (SCFAs) contribute proportionally the most [3], are provided due to the broad spectrum of enzymes of microorganisms[3]. The rumen microbiome is composed by a large number of bacteria, archaea and fungi. The most abundant found bacterial phyla based on 16S rRNA sequencing are: *Proteobacteria*, *Bacteroidetes*, *Firmicutes* *Spirochaetes*, *Verrucomicrobia*, *Actinobacteria* and other in the rumen microbial community [4-6]. Most present phyla based on 16S rRNA sequencing from archaea are *Euryarchaeota*, *Crenarchaeota*, and *Thaumarchaeota* [7]. Predominant eukaryotic phyla based on 16S rRNA sequencing are *Ciliophora*, *Chytridiomycota*, *Amoebozoa*, *Metamonada* and *Rhodophyta* [6].

The family Prevotellaceae contributes with a major part to the large phylum *Bacteroidetes*. Sequencing and metaproteomic analyses revealed that Prevotellaceae was one of the quantitatively most contributing family of the rumen microbiome [8, 9]. The genus *Prevotella* originally derived from *Bacteroides* and is named “after the French microbiologist A. R. Prévot, a pioneer in anaerobic microbiology” [10]

1.2 *Prevotella bryantii* B₁₄

The Prevotellaceae include multiple species such as *Prevotella copri*, *Prevotella multisaccharivorax*, *Prevotella brevis*, *Prevotella albensis*, *Prevotella ruminicola* and *Prevotella bryantii*. Latter two are characteristic representatives of ruminal *Prevotella* species due to their ability to degrade hemicellulose and pectin via their broad spectra of carbohydrate active enzymes (CAZymes) [11]. It is assumed that the high genetic diversity of CAZymes within the genus *Prevotella* allows an efficient adaptation to changing environments such as the change of feed [11, 12]. Besides the hemi-cellulolytic and cellulolytic activity [13] the strain *P. bryantii* B₁₄ is known to have a strong proteolytic activity with a preference to grow fast on casein as a N-source [14].

The first appearance of *Prevotella bryantii* B₁₄ was documented by Bryant, M., *et al.* [15], who isolated and classified the strain as *Bacteroides ruminicola* ssp. *brevis* strain B₁₄. The strain number four originated from eight strains of the group B₁ (B₁18, B₁19, B₁25, B₁28, B₁38, B₁4, B₁45, B₁49) that have been isolated “from a Holstein cow fed alfalfa hay” [15]. *B. ruminicola* B₁₄ cells were coccoid to oval shaped cells with an approximate length of 4 μm and had a width in a range between 0.7 to 0.8 μm [15]. One of the observed unique feature of *B. ruminicola* B₁₄ was its vast carbohydrate degrading capabilities and its lacking ability in fermenting gum arabic [15]. Later analysis depicted *B. ruminicola* B₁₄ as a very distinct strain that shares only very little DNA similarity with the other relatives [16]. With the study of Avguštin, G., *et al.* [17], *Prevotella bryantii* B₁₄ was reclassified and named after its discoverer M. P. Bryant. The phylogenetic tree from Purushe, J., *et al.* [11] illustrated species similarity on basis of 16S rRNA gene analysis (Figure 1).

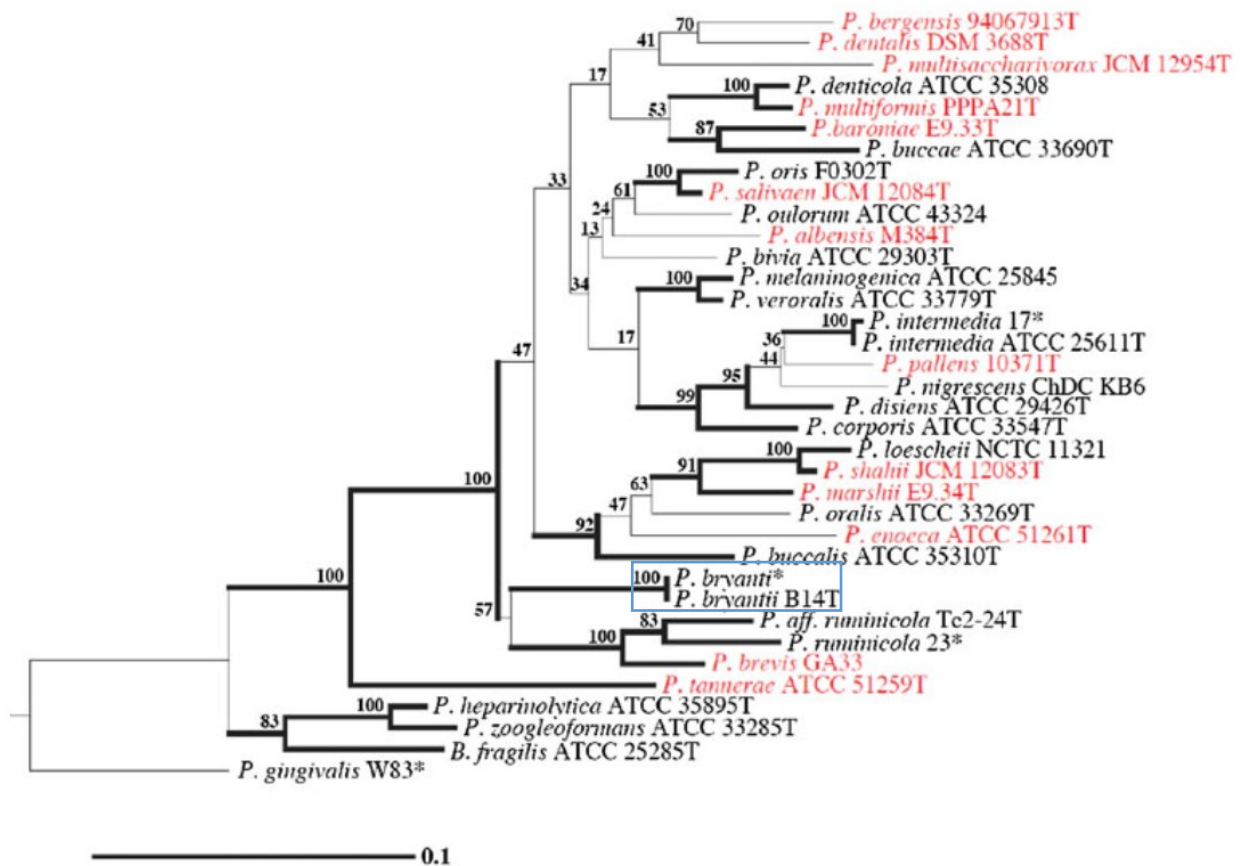


Figure 1: Phylogenetic tree based on the 16S rRNA gene sequences calculated by Purushe et al. (2010), which “infer the maximum-likelihood branch length values for the tree. Increased line thickness infers strength of bootstrap value while the numbers along the branches denote percent occurrence of nodes among 100 bootstrap replicates”. The blue box indicates phylogenetic location and its proximity to its neighbors.

The related species *P. bivia*, *P. denticola* and *P. intermedia* are less rumen-associated and known to cause inflammatory diseases such as vaginosis or periodontitis [18-20]. *P. bryantii* also shares virulence factors such as hemolysin from pathogenic *Prevotella* species that remain as an evolutionary residue [21]. Many virulence factors of *P. bryantii* are also familiar to *Porphyromonas gingivalis*, which growth is also depending on short-chain fatty acid (SCFA) and hemin [22]. As mentioned, *Prevotella* species are well-known for their proteolytic activity especially for their dipeptidyl aminopeptidase [23]. The so far best growth promoting nitrogen source is the milk protein casein [14].

1.2.1 Essential requirements of *Prevotella* species

The requirements of each organism develop throughout the evolution and can be observed by the point of view of Darwin’s theory of evolution “survival of the fittest” [24]. The ruminant as a host provides a stable environment for *P. bryantii* B₁₄ resulting in stable anoxic condition, pH, temperature (39°C), agitation and feed supply. The first listed factor includes

the contribution of carbon dioxide (CO₂), which is found in the liquid phase as bicarbonate (HCO₃⁻) and becomes introduced into the metabolism via the pyruvate pathway [25]. The optimal pH for *P. bryantii* B₁₄ was so far not determined but is assumed to be similar to the optimal conditions for ruminal fermentation in the pH range from 5.8 to 6.8 [26]. The identification of required organic factors was challenging and that is how also the first complex media was used. The creation of the optimal growth media for *P. bryantii* began with the isolation the microorganism, which was known before the work of Avguštin, G., *et al.* [12] as *Prevotella ruminicola* subsp. *brevis*. By that time, *P. ruminicola* was isolated from rumen of cattle by intubation and isolated by serial dilution [15]. At the beginning, utilized media contained rumen fluid as a growth enhancer [27]. Around the 1960s it was clear that SCFAs appeared to be a main factor for growth of numerous rumen microorganisms, which was deeper investigated in chapter 2. By release of the study from Caldwell, D., *et al.* [28] a recommendation for growth media of anaerobic rumen microorganisms was set and the Medium 2 (M2) was created. This media omitted rumen fluid and replaced with a mixture of SCFAs, yeast extract, hemin and trypsin digested casein (trypticase). A later study showed that the enzymatic hydrolysate of the milk protein casein was able to compensate the absence of SCFAs as a growth factor [15]. Whereas an acid hydrolysis of casein was unable to substitute the SCFA mixture. Pittman, K. and Bryant, M. [29] suspected certain peptides of casein to be responsible for growth promotion without SCFAs.

1.2.2 Carbon sources & metabolism

The nutritional basis of the ruminants is a heterogeneous mixture of forage and grains which can be found in a total mixed ration (TMR) [3, 30], which is consequently also the feed for *P. bryantii*. One main characteristic of *P. bryantii* is its capability of digesting multiple plant based polysaccharides [11], such as hemicellulose and cellobiose [31], of which latter was used for its isolation on selective media [15]. Additionally, *P. ruminicola* and *P. bryantii* are known to have a large set of carbohydrate active enzymes (CAZymes) to digest the introduced carbohydrates, originating from plant fiber [11].

In case of glucose excess, UDP-glucose is formed and used as a building block for glycogen synthase [31, 32]. The two described main catabolic pathways for glucose are acetate formation via glycolysis and pyruvate metabolism and the succinate production via the glycolysis and the Krebs-Cycle [33], which are described in Figure 2.

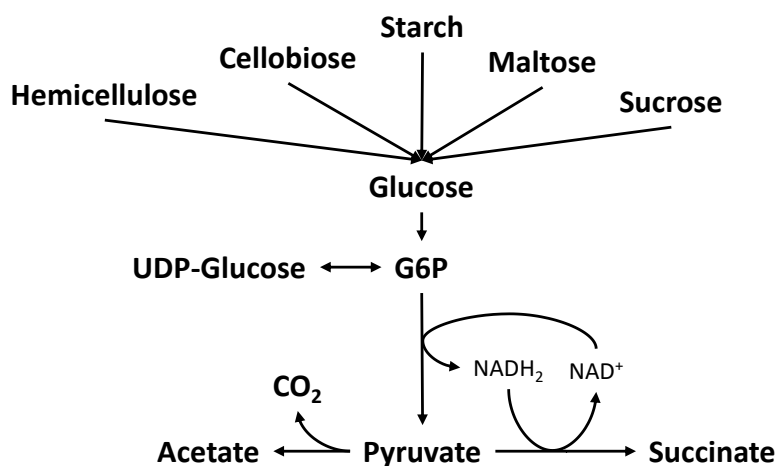


Figure 2: Carbon flow from substrates to fermentation products in *Prevotella bryantii* B₁₄. G6P: Glucose-6-phosphate; UDP: Uridin-diphosphate.

1.2.3 Short-chain fatty acids (SCFA) & metabolism

Short-chain fatty acids (SCFAs) – also known as volatile fatty acids (VFAs) – have due to their volatile property a remarkably intense smell, which can be found as a product in the digestive process of animals and especially ruminants [34]. Those fermentation products are used by the host as the major energy source [35]. The acids consist of a short alkyl chain of maximal five carbon atoms including a terminal carboxyl group. The alkyl chains can appear in linear or branched forms. Branched-chain fatty acids (BCFAs) can only occur in carboxylic acids of four or more carbon atoms. Most of the SCFAs are produced by microbial fermentation of plant fiber [34]. The well-known and most abundant SCFAs are acetic, propionic and butyric acid, which are linear-chain fatty acids. Less familiar and abundant are BCFAs, such as isobutyric, isovaleric and 2-methyl butyric acid (Figure 3A), which can be found after ruminal protein degradation [36]. Those BCFAs can be divided into iso- or anteiso-branched types. Examples for the iso-branched fatty acid are isobutyric and isovaleric acid, which hold a methylation at the pre-last carbon atom. 2-Methyl-butrate is an anteiso BCFA, which hold a methylation at the last but two linear carbon chain (see below: Figure 3B). Isovaleric and 2-methyl butyric acid are, due to their similar structure to valine, leucine and iso-leucine, suspected to be bioactive compounds [37]. Isovaleric acid showed also a dosage depending inhibition of ruminal protein degradation *in vivo* [38] and certain *Ruminococcus* strains required those for growth promotion [39].

A lack of research was found about the reasons for SCFA requirements in some rumen bacteria. It was shown that species like *Fusobacterium prausnitzii*, *Ruminococcus albus* and *Porphyromonas gingivalis* require SCFAs for their growth [39-41], but no biochemical explanation is given so far. Studies assume the implementation of SCFAs into the lipid metabolism to form long-chain fatty acids (LCAFs) [42]. However, their necessity from a biochemical perspective is not explained so far. A possible impact of the LCFA may be to effect the membrane property with respect to the fluidity or integration of crucial membrane proteins [43-45]. Furthermore, in multiple studies the role of SCFAs as a chelating agent was proposed, which also allow the transport of ions through membranes [46-49].

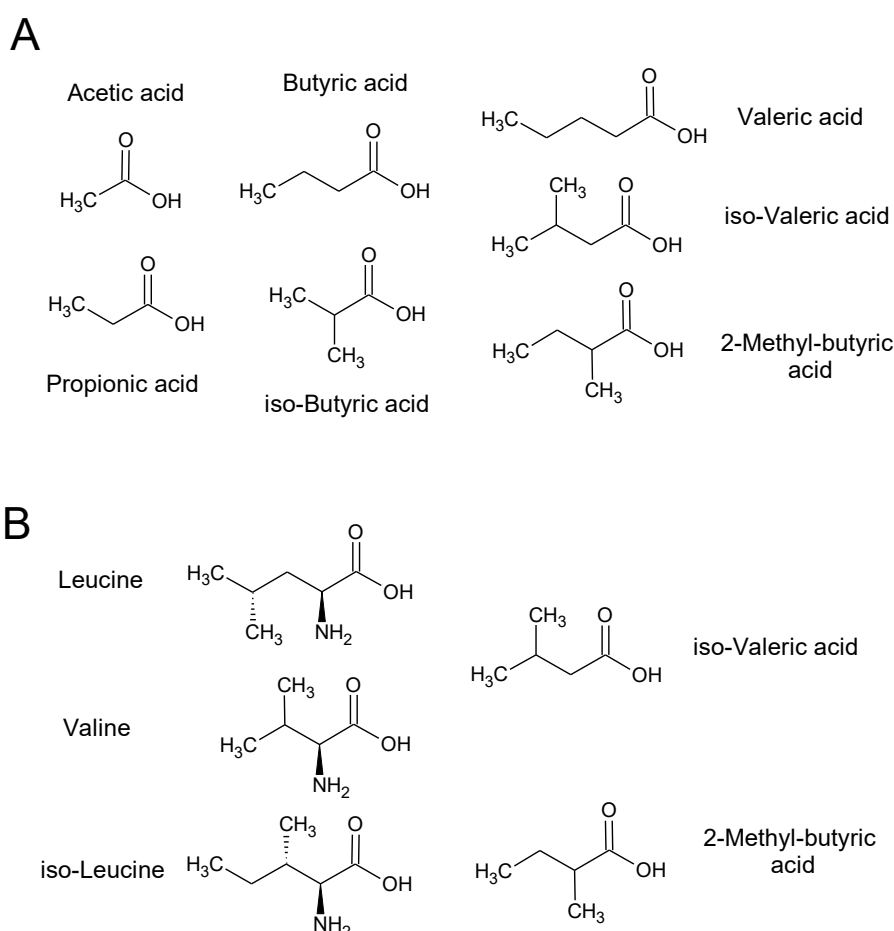


Figure 3: Chemical structure of short-chain fatty acids (SCFA) and branched-chain amino acids. **A:** Illustration of investigated studies from chapter 2 SCFAs. **B:** Structural lineup of branched-amino acids and branched-chain fatty acids.

1.2.4 Vitamins & supplements

Aside from the mineral, carbon and nitrogen sources, vitamins appear to be essential for ruminal microbes grown under *in vitro* conditions. Various vitamins such as *p*-aminobenzoic acid (PABA), menadion (Vitamin K₃), biotin (Vitamin B₇) and cyanocobalamin

(Vitamin B₁₂) emerged to be important for cellolytic bacteria [50-52]. PABA is known as a growth promotor for many bacterial species as an intermediate for folic acid synthesis [53]. Vitamin K₃ is found to be associated with anaerobic respiration [54]. Vitamin B₇ acts as a prosthetic group for enzymatic reactions especially for carboxylases in fixating carbon dioxide [55]. Vitamin B₁₂ is with its porphyrin ring structure an important co-factor for methylmalonyl mutase in the propionate synthesis of *Prevotella* [51].

Another porphyrin ring structure with a Fe^{2+/3+} as a central ion, is hemin. It was found to be a growth promoting supplement for *Prevotella* sp. [52]. Hemin seemed to originate from the host in form of decomposed blood plasma proteins [56] and appeared to be up taken by the outer membrane proteins of *Prevotella* [22, 57]. Studies proposed the usage of hemin in form of an anti-oxidative coating for anaerobes [58, 59]. However, hemin was not required for the growth of *Prevotella bryantii* B₁₄ [16].

1.3 Monensin in nutrition

The discovery of antibiotic growth promotor in life stock farming enforced the search for new compounds and led to the group of ionophores [60]. This group included compounds such as monensin, nigericin, carbonylcyanid-m-chlorophenylhydrazon (CCCP), tetranosin and others [61]. Ionophores are known to transport ions through a lipid bilayer, by binding ions and pass them through membranes. Thereby the ion gradient of bacterial cells can get disrupted, which resolves in a disorder of the mineral and pH homeostasis with a consecutive malfunctioning of cellular metabolism [61-63]. The overuse of antibiotic growth promotors in animal nutrition provided the formation of antibiotic resistances and cross-resistances [64] and led to a restricted regulation for veterinary purposes in many countries [65-67]. Since 2006, monensin became prohibited as an antibiotic growth promotor in the European Union but since 2020 monensin supplementation in broiler feed was reintroduced legally [68]. Other nations such as the United States still use monensin as an antibiotic growth promotor in life stock farming, but its use over the last four years decreased [69]. A subtle antibiotic treatment also occurs via consumption of foods originated from a drug contaminated environment [70-73]. For example, monensin traces (0.022-0.068 ppm) were found in the liver of ruminants when fed contained 10 ppm monensin per feed wet mass [74]. A study of Todd, G., *et al.* [75] showed the oral LD₅₀ of monensin for diverse animals such as: horses, with about 2-3 mg/kg body weight [76], sheep with about 11 mg/kg body weight, or cattle with 26 mg/kg body

weight. In humans monensin is known to inhibit the recycling of low density lipoprotein (LDL) receptors *in vivo* [77], as well as on cell superficial sugars of macrophages and lysosomes [78], which are a major part of the innate immune system. Those findings indicate subtle effects of monensin on human health by consuming animal products raised with antibiotic growth promoters [63].

1.3.1 Mode of action of monensin

Monensin, known as pharmaceuticals Kexxtone or Rumensin[®], was originally used as a coccidiostat in poultry farming and is the most commonly used ionophore in ruminant nutrition nowadays [79]. The first appearance of monensin and its derivatives was described in *Streptomyces cinnamonensis*, which produced this crown ether compound on basis of butyrate and isobutyrate [80, 81]. Monensin is applied orally in form of a bolus where it affects the sodium- (Na^+), potassium- (K^+) and proton gradient (H^+) of microorganisms [61], by integrating into membranes via its lipophilic property [82]. The affected mineral and proton homeostasis of ruminal microbes lead to a diminished acetate and methane production, while propionate production was increased as seen in Figure 4 from Wischer, G. [83]. Inhibition of the H^+ -dependent adenosine tri-phosphate (ATP) production in monensin treated *Streptococcus bovis* seem also to contribute to the metabolic shift [84, 85].

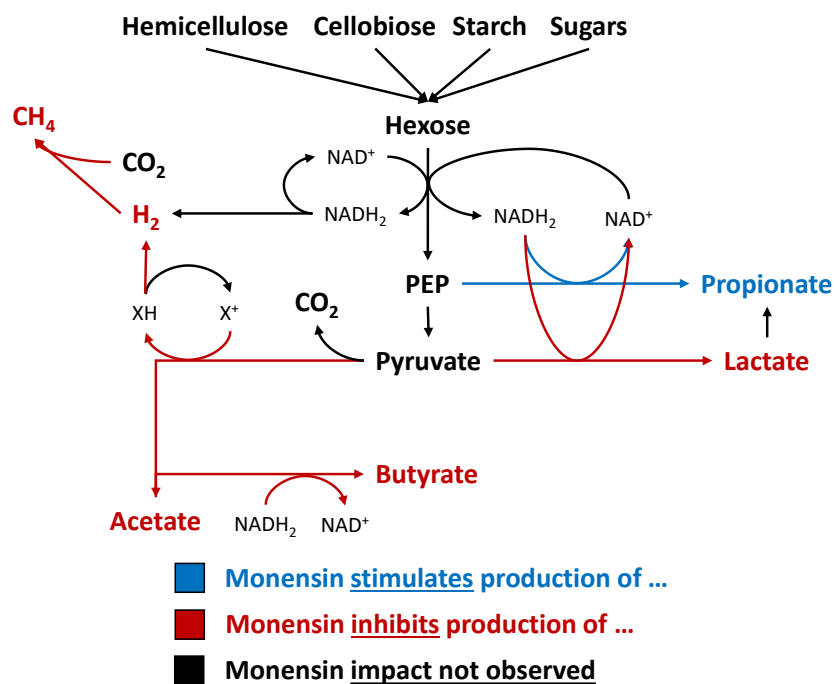


Figure 4: Monensin effects ruminal microbiome metabolism. Figure is based on Wischer et al. (2012) and is modified by indicating not only affected metabolites but also the connected pathways. Modifications are assigned to following references: Hemicellulose - Purushe et al. (2010); Lactate - Dennis et al. (1981); Butyrate - Perry et al. (1976).

1.3.2 Monensin impact on rumen microbiome, function and metabolites

An inhibiting effect of monensin was shown mainly on Gram-positive microbes, while Gram-negative appeared to have an advantage due to their outer membrane [85]. However, certain Gram-positive species with low G+C content in their DNA appeared to resist monensin too [86]. Same withstanding effects were seen for hydrogen producing protozoa [87], which are living in symbiosis with methane producing archaea. *P. bryantii* B₁₄ remained unchanged towards monensin under *in vivo* conditions in mixed cultures, while species such as *P. ruminicola* or *P. brevis* took advantage of antibiotic effect and showed higher proportional contribution [88].

In vitro and *in vivo* studies with monensin exposure described an increase of propionate and succinate in the culture supernatant and a reduced formation of methane [89, 90]. This elevated propionate concentration led to an increased hepatic gluconeogenesis, which supports the process of cattle fattening. Ruminal fiber degradation [91, 92] as well proteolytic activity [90, 93] were found to be reduced under monensin supplementation.

1.3.3 Monensin resistance of *Prevotella* species

Prevotella bryantii B₁₄ proved to be one of the most resistant *Prevotella* strains withstanding concentrations up to 20 μM *in vitro*, while most species were able to grow up to 1 μM or less [82]. Experiments from Callaway, T.R. and Russell, J.B. [82] showed an adaptive effect of *Prevotella* sp. to sub-lethal concentrations of monensin. In a former study, Callaway, T.R. and Russell, J.B. [85] also concluded a change of outer membrane composition by observing a lack of agglutination for monensin exposed cells. Some of those outer membrane proteins were expected to be porins [94]. Callaway, T.R. and Russell, J.B. [85] indicated that ATP is not necessarily needed to regenerate the proton gradient due to the cytochrome linked quinol:fumarate reductase (QFR). Another defense mechanism of *P. bryantii* B₁₄ appears to be reduced monensin binding, shown by studies with radiolabeled monensin [95]. Those findings point out multiple factors that make *Prevotella* species, especially *P. bryantii* B₁₄, an outstanding monensin resistant organism.

1.4 Methodologies

1.4.1 Cultivation technologies

In order to cultivate anaerobic microorganisms, such as *P. bryantii*, a cultivation flask known as Hungate tube was used. The Hungate tube is a 16 x 125 mm thick and long glass tube with a plastic screw cap and a septum in-between the cap and glass. The tube was named after the microbial ecologist Robert Hungate, who was a pioneer in the field of rumen ecology [96]. The gas tight screw cap with the septum allows to hold anaerobic microbes with a gas such as carbon dioxide (CO₂). The first media for isolating rumen microorganisms contained rumen, which resulted in a complex medium. In order to elucidate the growth promoting substances of the rumen fluid, several defined media were used. The current most recommendable media composition for growing *P. bryantii* appeared to be a semi-defined media with components such as: a mineral solution, SCFAs, lactate, carbohydrates (glucose, maltose and cellobiose), peptone (trypsin digested casein), yeast extract and a mixture of vitamins [97]. For the purpose and the requirements of those ingredients see chapter 1.2. Investigating the interactions of *P. bryantii* with other members of the rumen microbiome a different cultivation technique was required. Therefore fresh rumen fluid is was used for this cultivation approach, which is called, the Rumen Simulation Technique. The Rusitec is an *in vitro* technique to study digestive processes in the rumen without a direct effect on the animal [98]. It is mainly used for *in vitro* test of feed compounds or supplements such as for monensin [93]. The used Rusitec is a continuous culture bioreactor equipped with constant heating,

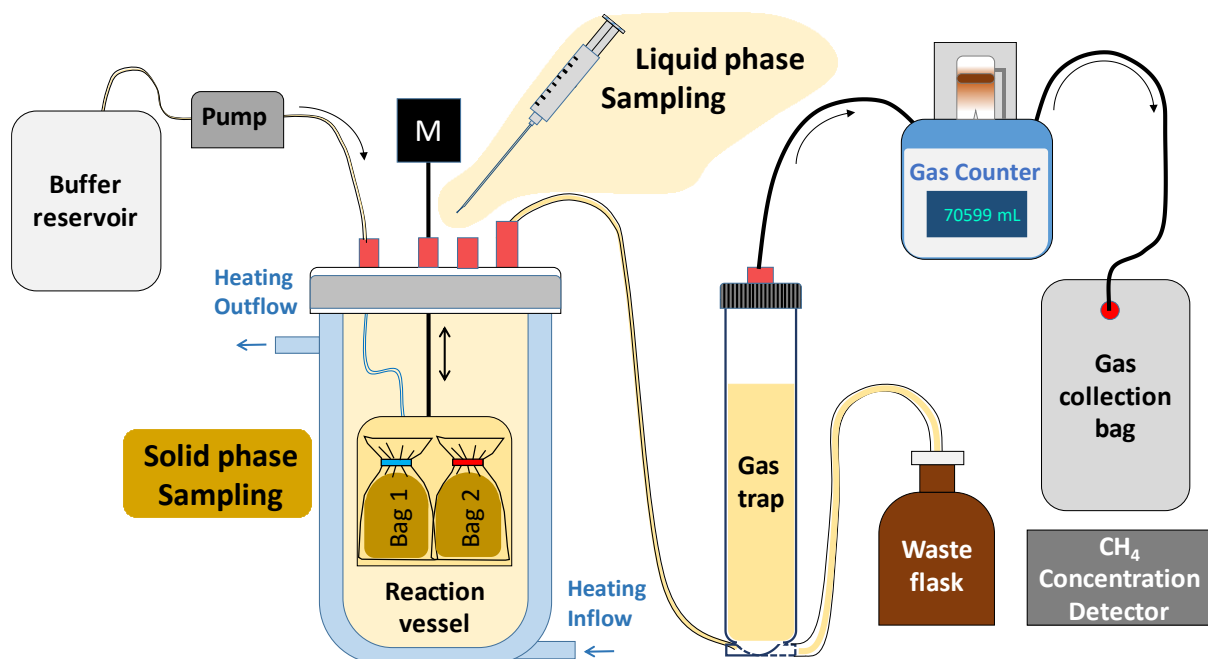


Figure 5: Schematic design of Rumen Simulation Technique (Rusitec)

agitation and an online measurement for gas production (see below Figure 5). The Rusitec provides features regarding abiotic factors, such as anaerobic- and temperature-control as well as agitation and pH adjustment. Host secreted compounds as bicarbonate and further inorganic salts are simulated by introducing buffer continuously via a peristaltic pump from a reservoir. The reaction vessel content is mixed by an up- and downward agitated cage. The cage serves as a reservoir for nylon bags filled with plant-based animal feed material called total mixed ration (TMR). The excess of liquid and produced gas is eluded into the gas trap for separation of both phases. The measured gas is collected in gas-proof bags for later determination of methane concentration. The liquid phase departs from the gas trap into a waste flask. The Rusitec provides standardized conditions with an online measurement for gas and an easy access for sampling the liquid phase via a screwcap-opening through the lid of the reactor.

Metabolism is usually viewed how organic substrates are converted via intermediate-form by an enzyme with corresponding co-factors into organic products [99]. Metabolomics is an approach to describe chemical processes by investigating metabolites – mainly smaller molecules – that appear as substrates, intermediate forms and products [100]. A complementary method is called proteomics, which is primarily defined as the “protein complement expressed by a genome”, which allows to investigate the whole spectrum of proteins within a cell [101]. A vast majority of proteins act as enzymes, which can be monitored using functional proteomics. Metabolomics together with proteomics allow to understand the flow of metabolites by considering respective tools (enzymes) to form them. The benefit of all omics tools (gene-, transcript-, prote- and metabolomics) is the wide spectrum for identifying and quantifying the respective group of chemicals. However, the limitations are that all those tools show only a state of a certain moment under a certain condition. This disadvantage can be compensated by monitoring time points in a sequential manner and applying different conditions with different states. This allows to monitor the flow of metabolites, which is known as metabolism. A further benefit of proteomics compared to genomics and transcriptomics is the ability to detect the products of active genes in their final processed form after translation and transcription. Despite detecting the finalized products of active genes, the functionality of the products, for example enzymatic activity, needs to be

monitored by additional tests. Proteomics and metabolomics are still the closest approach to describe the flow of metabolism and represent the current state of art.

1.4.2 Proteomics

The proteomics in a non-targeted from pure cell cultures usually undergo a cell rupture with a subsequent protein extraction and protein digestion into peptides. Obtained peptides were purified and analyzed by label-free (proteins and consequently the peptides were not marked) tandem-mass spectrometry (MS/MS). The analysis usually began with a separation of peptides by liquid chromatography (LC). The LC is usually performed by a reversed phase column, which allows to separate the peptides by their hydrophobicity [102]. By this separation, peptides are allowed to be fragmented in the mass spectrometer in various combinations, so that the amino acid sequence of each peptide can be reconstructed [102]. The MS/MS means, that peptides are fragmented and detected a second time, which enables a higher resolution of the amino acid sequence [102]. The detection of the fragments is performed on the basis of their mass, which is detected after the first and second mass spectrometry step [102]. Various lengths of the fragmented peptides with their masses allowed to reconstruct the amino acid sequences of each peptide and provide a unique pattern to assign a peptide to a certain protein within the database. The matching between peptides and proteome database facilitates an assignation of unique peptides to proteins. Together with the signal intensity of each peptide, the corresponding protein abundance within and between samples can be assessed, which is known as quantitative proteomics [103]. Metaproteomics include the same procedure as described except that complex microbial communities are investigated [104], which occurs for environmental samples as the one from the Rusitec.

1.4.3 Metabolite analysis

Metabolites of bacteria and in particular from *P. bryantii* B₁₄ were analyzed by targeting specific substrates such as glucose, fermentation products (SCFAs, ammonia, methane) or other molecules (LCFAs, monensin, sodium). Those findings provide an enhanced managing of one of the most dominant rumen microbes to ensure a balanced supplementation of metabolites for the ruminant host. Targeted metabolites were detected by selected methodologies such as: gas chromatography (GC) for SCFAs, gas chromatography coupled mass spectrometry (GC-MS) for LCFAs, inductively coupled plasma mass spectrometry (ICP-

MS) for sodium ions, liquid chromatography coupled with mass spectrometry (LC-MS) for monensin or enzymatic tests kits to determine glucose or glucose-6-phosphate.

For the non-targeted approach, nuclear magnetic resonance (NMR) spectroscopy was used which enabled a search for metabolites via a spectroscopic database. In the present studies ^1H -NMR was used, which enabled to detect all hydrogen atoms of the stable isotope ^1H within a sample. Therefore, samples needed to be dried in order to remove the signal with the most abundant ^1H -hydrogen molecule namely hydrogen dioxide (H_2O). After a solvent substitution with deuterium (D_2O), which has a ^2H isotope (containing an additional neutron), signals of the metabolites can be detected more accurately [105]. For ^1H -NMR a strong magnetic field is applied on molecules in the probe, which affects all ^1H isotopes. By releasing this applied magnetic field, a signal of all those ^1H isotopes within the sample molecules are detected. The signals give evidence about neighbour atoms of those detected hydrogen atoms within a molecule. This means that molecules hydrogen have a certain spectroscopic pattern, which can be matched with a database of diverse metabolites [106]. This non-targeted approach allows to detect also metabolites which were not considered with respect so certain metabolic pathways by using statistical evaluation tools such as linear correlations.

1.5 Motivation, hypotheses & objectives

The family Prevotellaceae is predominantly represented in the rumen microbiome which is why *Prevotella bryantii* B₁₄ became a suitable representative of this family. Nowadays intensified research is found on short-chain fatty acids (SCFAs) and their health beneficial effects on humans and ruminants. However, research about how SCFAs affect microorganisms was rarely conducted down to the biochemical level (Chapter 1.2.3). The main purpose of SCFAs is regarded as being an energy source for the host of the intestinal microbiome. Chapter 2 shall show how versatile the effects of SCFAs are also on microbes such as *P. bryantii* B₁₄.

The strain *P. bryantii* B₁₄ was shown to be remarkably resistant towards monensin (Chapter 1.3.3). This created the starting point and motivation for the second publication (Chapter 3) in order to clarify the existing defence mechanisms. The last manuscript (Chapter 4) should verify the findings from pure culture in mixed culture.

First Hypothesis:

SCFAs are used as growth promoters in defined medium and have different impacts on the metabolism of *Prevotella bryantii* B₁₄.

A complex ecosystem such as the rumen microbiome is inhabited by a vast variety of organisms that produce and consume SCFAs. Since SCFAs are known to have beneficial impact on the host of the microbiome, the impact of SCFA on the ruminal microorganisms itself becomes a topic of great interest too. *P. bryantii* B₁₄ and its relatives are predominant members of the rumen microbiome and are known to produce small organic acids. Previous studies investigated *P. bryantii* under complex growth media based on rumen fluid. Therefore, the influence of SCFAs on bacterial metabolism remained unexplored. This can be overcome by creating a well-defined growth media which allows structured analyses of the cellular metabolism of *P. bryantii* B₁₄ using label-free proteomics and targeted metabolomics analyses.

Second Hypothesis:

***Prevotella bryantii* B₁₄ is counteracting on the ionophoric effect of monensin via the NADH:ubiquinone reductase (NQR).**

Secondly, the causes for monensin resistance in *P. bryantii* have not been fully investigated. The presented research shall confirm earlier findings and extend the list of monensin resistance mechanisms of *P. bryantii* B₁₄. One of the proposed mechanism to cope with the ionophoric effect of monensin is the an enzyme NADH:ubiquinone reductase (NQR) from the aerobic respiration pathway. The NQR is part of the sodium-translocating supercomplex, which is also forming succinate out of fumarate via the included quinone:fumarate reductase (QFR) [107].

Third Hypothesis:

The genus *Prevotella* is an important key player during monensin exposure in the rumen microbiome.

Lastly, the resistance mechanism of *P. bryantii* B₁₄ in mono-cultures are tried to be rediscovered in *Prevotella* spp. within the rumen microbiome. Therefore, the metaproteome and metabolome of the rumen microbiome will be monitored under Rusitec conditions. This will gain in additional information on the impacts of monensin and on other microbes in relation to *Prevotella* and its metabolites.

2. Short-chain fatty acids modulate metabolic pathways and membrane lipids in *Prevotella bryantii* B₁₄

by Andrej Trautmann¹, Lena Schleicher², Simon Deusch¹, Jochem Gätgens³, Julia Steuber² and Jana Seifert^{1,*}

¹ Institute of Animal Science, University of Hohenheim, 70599 Stuttgart, Germany

² Institute of Biology, University of Hohenheim, 70599 Stuttgart, Germany

³ Institute of Bio- and Geosciences, IBG-1: Biotechnology, Forschungszentrum Jülich, 52425 Jülich, Germany

* Correspondence: jseifert@uni-hohenheim.de; Jana Seifert (University of Hohenheim, Institute of Animal Science, Emil-Wolff-Str. 6-10, 70593 Stuttgart, Germany)

Journal: Proteomes 2020, 8(4), 28; <https://doi.org/10.3390/proteomes8040028>

Received: 22 September 2020 / **Revised:** 12 October 2020 / **Accepted:** 13 October 2020 /

Published: 16 October 2020

2.1 Abstract

Short-chain fatty acids (SCFAs) are bacterial products that are known to be used as energy sources in eukaryotic hosts, whereas their role in the metabolism of intestinal microbes is rarely explored. In the present study, acetic, propionic, butyric, isobutyric, valeric, and isovaleric acid, respectively, were added to a newly defined medium containing *Prevotella bryantii* B₁₄ cells. After 8 h and 24 h, optical density, pH and SCFA concentrations were measured. Long-chain fatty acid (LCFA) profiles of the bacterial cells were analyzed via gas chromatography time of flight mass spectrometry (GC-ToF MS) and proteins were quantified using a mass spectrometry-based, label-free approach. Cultures supplemented with single SCFAs revealed different growth behavior. Structural features of the respective SCFAs were identified in the LCFA profiles, which suggests incorporation into the bacterial membranes. The proteomes of cultures supplemented with acetic and valeric acid differed by an increased abundance of outer membrane proteins. The proteome of the isovaleric acid supplementation showed an increase of proteins in the amino acid metabolism. Our findings indicate a possible interaction between SCFAs, the lipid membrane composition, the abundance of outer membrane proteins, and a modulation of branched chain amino acid biosynthesis by isovaleric acid.

Keywords: short-chain fatty acids; long-chain fatty acids; branched-chain amino acids proteome; *Prevotella bryantii* B₁₄; lipid membrane; outer membrane proteins

2.2 Introduction

Short-chain fatty acids (SCFAs) are formed by the microbial turnover of plant-derived materials in the rumen and serve as major energy source for animals [35]. In addition to the utilization of SCFAs by animals, they are also required for the growth of certain microorganisms like *Prevotella bryantii* B₁₄ [41], formerly named *Bacteroides ruminicola* or *Prevotella ruminicola* subsp. *brevis*. Copious SCFA-dependent microorganisms inhabit the gastrointestinal system of animals. The growth of various other bacterial species such as *Ruminococcus albus*, *Porphyromonas gingivalis* and *Fusobacterium prausnitzii* also require SCFAs [39-41]. Some members of the Prevotellaceae family such as *P. gingivalis*, *P. denticola*, or *P. intermedia* are opportunistic pathogens and likewise rely on host derived compounds [20, 22]. *P. bryantii* B₁₄ on the other hand, is commonly found in the rumen and requires strictly anoxic conditions as well as carbon dioxide, heme, and vitamin K for growth promotion [50, 52]. These conditions are usually met by adding rumen fluid to the respective culture media. The SCFAs in rumen fluid are mainly acetic (~50 mM), propionic (~20 mM), and butyric acid (~10 mM) and contain further isoforms of valeric acid (0.5–2 mM), which are well-known to be important for the ruminant metabolism [108]. For the host cells, SCFA are seen as a source of energy, a signal molecule, or a participating molecule in fatty acid and vitamin B biosynthesis [109-111]. Little is known about the role of SCFAs for prokaryotic cells wherefore similar functions are expected to be relevant for *P. bryantii* B₁₄. The use of SCFAs as a C-source can be implemented through coenzyme A attachment and subsequent oxidation. Regarding the anabolic way of the lipid metabolism, SCFAs can be utilized as precursor molecules for long-chain fatty acids (LCFAs). Fatty acid elongation is usually performed by transferring malonyl-CoA to acetyl-CoA by the catalytic activity of the 3-oxoacyl acyl-carrier-protein synthase. Instead of the acetyl-CoA, a SCFA-CoA can be transferred to malonyl-CoA [42]. Thereby, the SCFA-CoA forms the primer molecule and should be detected at the tail of the LCFA. It is also known that branched-chain amino acids (BCAAs) are converted for example into isovaleric acid or 2-methylbutyric acid [112, 113]. It has been described that the amino group of BCAAs was first freed by the aminotransferase and second reduced to 2-oxoacids via the oxidoreductase [112]. A reverse reaction from branched SCFAs to BCAA was not proven yet but the reaction would be theoretically possible via an active incorporation by a ferredoxin oxidoreductase (EC 1.2.7.7).

In order to understand the fate of SCFA in *P. bryantii* B₁₄ cells, the present study established a growth medium enabling the growth of the bacteria on single SCFAs. This elucidates the mode of action of single SCFAs on growth behavior, consumption, and production of SCFAs, as well as on the assembly of membranes (LCFAs). Additionally, the effects of SCFA on overall metabolic routes and cellular mechanisms were analyzed by label-free quantification of the proteome.

2.3 Material & methods

2.3.1 Cultivation in medium M2-A for proteome analysis

P. bryantii B₁₄ (DSM 11371) was cultivated in Hungate tubes under anaerobic conditions. Composition of the medium (M2-A) was derived from the complex M2 medium [114], which is based on rumen fluid and yeast extract. In M2-A media rumen fluid and yeast extract were replaced by a vitamin solution (Table S1) and SCFAs or without SCFA (control) as described in Table S2 [52, 115]. Media M2-B contained only glucose and a mixture of all used SCFAs in various concentrations (Table S2). Resazurin, minerals, sugars, and tryptic digested casein were dissolved, heated, and gassed with CO₂, followed by addition of cysteine. After cooling down while being gassed continuously, the pH was adjusted to 6.8 by using 1 M NaOH. In the case of cultivations with single SCFAs, 15 mM of the respective acid was added to each Hungate tube. The filter sterilized vitamin solution was added by injection to the medium in the autoclaved Hungate tubes containing a final volume of 7.1 mL. The following SCFAs were used for cultivating: acetic acid (Acet; VWR), propionic acid (Prop; Carl Roth), n-butyric acid (But; Merck), isobutyric acid (iBut; Merck), n-valeric acid (Val; Merck) and isovaleric acid (iVal; Merck). *P. bryantii* B₁₄ cells from frozen glycerol stocks were first cultured using M2 medium. Concentrations of SCFA in rumen fluid usually depend on the feed and range from 0.5–50 mM [108]. The average of the sum of SCFAs was around 15 mM, which was therefore used in the present experiments.

Growing cells of the M2 medium (OD = 1.7–2.0) were used to inoculate the M2-A media (4% v/v) to an initial OD of 0.1. To assess successful growth (OD > 1.0) on M2-A media and to eliminate potential remains of the M2 medium, cells were transferred to fresh M2-A media two times. Each single SCFA culture was incubated in triplicates at 39 °C in a static water bath for 8 h to achieve a sufficient cell density. M2-A medium without SCFAs supplementation revealed no growth within 8 h after the second transfer. Cell growth was followed hourly by

non-invasive optical density (OD) measurements in the Hungate tubes ($\lambda = 600$ nm; Bio GenesysTM 10, Thermo Fisher Scientific, Waltham, MA, USA). The pH was determined at the last time point of each growth experiment (pH meter, FE20, Mettler Toledo, Columbus, OH, USA). Cell pellets obtained by centrifugation at 4 °C with 10,000× g for 10 min were stored at –80 °C. Aliquots of the supernatant were stored at –20 °C for subsequent GC coupled to flame ionization detector (FID)-based SCFA quantification.

2.3.2 Cultivation for long-chain fatty acid determination

A cultivation volume of 100 mL in serum bottles containing M2-A medium was used to investigate the incorporation of SCFA into the long-chain fatty acids (LCFAs). Cells of two times transferred Hungate cultures were used for inoculation (7% v/v). Cells were incubated for 8 h or 24 h in order to observe changes in LCFA composition and SCFA depletion. The optical densities and pH were measured as previously described. Aliquots of the culture supernatants were stored at –20 °C for subsequent SCFA quantification. The cell pellets were stored at –80 °C for subsequent LCFA analyses.

2.3.3 Glucose based medium M2-B

The M2-A medium was altered by removing sodium lactate, maltose and cellobiose to establish medium M2-B. Except the adjustment from 2 g/L to 4 g/L of glucose and utilization of a SCFA mixture, the preparation of medium M2-B remained identical, as described above. Cultivation characteristics of *P. bryantii* B14 in M2-B medium were equal to the M2-A media. A two-liter culture was used to allow frequent sampling of the culture. The 2-L culture was inoculated with 10% (v/v) and agitated with 100 rpm by a magnetic stir bar at 39 °C for 7 h. Samples were taken to determine OD, pH and glucose concentration. OD was analyzed photometrically in cuvettes ($\lambda = 600$ nm; Bio GenesysTM 10, Thermo Fisher Scientific). The pH was measured as previously described, and glucose concentration was determined down to the millimolar range using an enzyme kit (BioAnalysis D-Glucose, R-Biopharm, Darmstadt, Germany).

2.3.4 Short-chain fatty acid determination

Determination of SCFAs was conducted using aliquots of the supernatants. The aliquots were thawed, vacuum distilled, and analyzed by a gas chromatograph (GC Hewlett-Packard 6890; Agilent, Santa Clara, CA, USA) equipped with a fused silica capillary column (HP-FFAP, 25 m × 0.32 mm, film thickness 0.5 μ m HP 7683; Agilent) and FID with autosampler as

described previously [93]. As internal standard, 80 mM of 2-methylvaleric acid in 50% formic acid was added to one aliquot for calibration.

2.3.5 Long-chain fatty acid determination

Cell pellets were thawed on ice and washed twice using a 2.7% (w/v) NaCl solution. Cells were lyophilized (Gamma 1–20, Christ, Göttingen Germany) and homogenized, and 10 mg of each sample were mixed with 1.7 mL acidic methanol (10% v/v sulfuric acid) for in-situ transesterification at 60 °C and 750 rpm for 4 h in Pyrex glass tubes. After cooling down, 300 µL of desalted water was added. For methyl ester extraction, 1200 µL of n-heptane (HPLC grade, Chemsolute Th., Geyer, Germany) were added followed by proper vortexing for 20 s. The n-heptane phase was separated and stored at –20 °C until analysis.

Methyl ester derivatized LCFAs were separated by a 30 m Agilent EZ-Guard VF-5ms + 10 m guard column (Agilent, Waldbronn, Germany) connected to an Agilent 6890N gas chromatograph (Agilent, Waldbronn, Germany). Compounds were analyzed by a Waters Micromass GCT Premier high-resolution time of flight mass spectrometer (Waters, Eschborn, Germany). Controlling was performed by the software MassLynx 4.1 (Waters, Eschborn, Germany), and injections were conducted by a Gerstel MPS 2 (Gerstel, Mülheim ad Ruhr, Germany) with Maestro software (Gerstel GmbH & Co. KG, Mülheim an der Ruhr, Germany). Samples of 1 µL were injected into a split/splitless injector at 280°C using altered split modes. A constant helium flow of 1 mL/min was applied. The GC temperature started at 60°C for 2 min and increased by 12°C/min up to a final temperature of 300°C with a hold time of 8 min. Total runtime was 30 min. At 300°C molecules were transferred into the TOF-MS, which operated in positive electron impact (EI)⁺ mode at an electron energy of 70 eV. The temperature at the ionization source was set to 180 °C. Calibration was tuned by Heptacosyl (heptacosylfluoro-tributylamine) fragment patterns. Accurate masses were corrected to a single point lockmass of chloro-pentafluoro-benzene (CPF) as an external reference ($m/z = 201.9609$). Data acquisition was performed in centroid mode with a scan rate of 10 scans per second.

For the identification of known metabolites, a baseline noise subtracted fragment pattern was used and compared to the in-house database JuPoD and the commercial database NIST. Unknown peaks were identified by a structural combination of elemental compositions and verified by virtual derivatization and fragmentation of the predicted structure [116].

The illustration and comparison of LCFAs by the parameters of even or odd chain length and the structuring of linear, iso, or anteiso forms were similarly run as reported in former studies [117, 118]. Quantified peak areas of LCFAs were summarized and represented in percentile contribution, which were used for Pearson correlation with the acidification (pH) and displaying it as the correlation coefficient (R).

2.3.6 Protein extraction

Protein extraction for subsequent LC-ESI-MS/MS analyses was carried out as described by Deusch, S., *et al.* [7]. Thawed cell pellets were kept on ice during the whole procedure. Pellets were washed twice in 300 μ L wash buffer (50 mM Tris/HCl, pH 7.5, 0.1 mg/mL chloramphenicol, 1 mM PMSF) by vortexing and centrifugation at 10,000 \times *g*, 4 °C for 10 min. Pellets were resuspended in 50 μ L wash buffer, and 50 μ L extraction buffer (50 mM Tris/HCl, pH 7.5, 1% SDS) were added, followed by incubation at 1400 rpm and 60 °C for 10 min. Subsequently, 950 μ L of a Benzonase solution (50 mM Tris/HCl, pH 7.5, 1 μ L/mL Benzonase (Merck, Novagen, Germany), 0.1 mg/mL MgCl₂, 1 mM PMSF) were added to the cells, followed by six times of ultra-sonication (UP 50H, Hielscher; 1 min at 60% amplitude and 0.5 per cycle). The samples were incubated at 37 °C and 1400 rpm for 10 min. Finally, the samples were centrifuged at 10,000 \times *g* and 4 °C for 10 min. The supernatants containing the extracted proteins were stored at -20 °C until further processing. Protein concentration was determined using the Bradford assay [119].

2.3.7 In gel protein digestion

A five-fold volume of ice-cold acetone was added to 100 μ g of protein for a 30 min precipitation. The samples were centrifuged for 10 min at 10,000 \times *g* and 4 °C, the supernatant was removed, and the protein pellet was dried at RT by vacuum centrifugation (Eppendorf concentrator, Hamburg, Germany). Protein pellets were resolved in 30 μ L Laemmli buffer and loaded onto a sodium-dedocyl-sulfate (SDS)-polyacrylamide gel electrophoresis (PAGE, 4% stacking gel, 12% separation gel). The gels were run for 100 min at 40 mA. Each sample representing a separation gel lane of 1.0 cm length was cut out and subjected to overnight in-gel trypsin digestion (Promega, Madison, WI, USA) as described by Jehmlich, N., *et al.* [120]. Obtained peptides were cleaned by filtering through Stage-Tips with five layers of Empore™ SPE disks (3M Deutschland GmbH, Neuss, Germany) with a 47 mm diameter, 0.5 mm thickness, and C18 material [121]. The obtained peptides were dried and suspended in 0.1% formic acid before LC-ESI-MS/MS measurement.

2.3.8 LC-ESI-MS/MS

The peptides were separated by an EASY-nLC1000 (Thermo Scientific, Dreieich, Germany) containing an EASY-Spray column PepMap RSLC (particle size 2 μm , 25 cm \times 75 μm , C18). A sample volume of 4 μL was injected and liquid chromatography was run with a flow of 0.25 $\mu\text{L}/\text{min}$. The mobile phase consisted of solvent A (0.1% formic acid) and solvent B (80% acetonitrile, 0.1% formic acid). The gradient of solvent B (2-10-22-45-95%) was run over a time of 260 min (R_t : 1-100-180-235-245 min). The peptides were ionized via electron spray ionization (ESI) before entering the Q-Exactive Plus mass spectrometer (Thermo Scientific) with a survey spectrum range from 300–1600 m/z in the Orbitrap mass analyzer and a resolution of 70,000. The second fragmentation was performed by high-energy collisional dissociation (HCD) with a resolution of 17,500. The 10 most abundant peptide precursors in the linear ion trap were generated by data dependent tandem mass spectra. Internal calibration was performed for all samples using lock-mass ions from ambient air as demonstrated earlier [122].

2.3.9 Data analysis for proteomics

Mass spectrometric (MS) data was analyzed by the software MaxQuant (v 1.6.2.6) [103]. Proteins were determined by searching peptide sequences from tandem MS data against the UniProtKB database of *P. bryantii* B₁₄ (3776 protein entries, 2 July 2019). The identification and label-free quantification (LFQ) considered only proteins with two or more unique peptide identifications. The options re-quantification and “match between runs” were enabled with a match time window of 0.7 min and an alignment time window of 20 min. Oxidation of methionine was set as variable modification and the carbamidomethylation of cysteine as fixed modification. Regarding tryptic digestion, a maximum of two missed cleavages were accepted. The peptides and proteins were filtered using a false discovery rate (FDR) of <1%. The MS data and MaxQuant output have been uploaded to the ProteomeXchange Consortium via PRIDE with the dataset identifier PXD016407 [123].

EggNOG and Ghost Koala were used for functional classification of quantified proteins to retrieve cluster of orthologous groups (COG) and the KEGG Orthology (KO) identifier [124, 125]. KO assignments from both algorithms were combined prioritizing Ghost Koala. The LFQ values (including zeros) were implemented into the statistical software Primer 6 (v 6.1.16) and Permanova (v 1.0.6) (both PRIMER-E, Plymouth Marine Laboratory, Plymouth, UK) to generate PCO plots by standardizing them by the total and applying the Bray Curtis similarity test. LFQ

values (including zeros) were used for SIMPER analysis and were cut-off when contribution was below 1%. The p -values for the LFQ proteins in the PCO plot were calculated by PERMANOVA analysis (9,999 permutations) using the Monte Carlo correction of p -values. A protein was defined as present when least two of three replicates displayed an LFQ-value above zero. Non-quantified proteins can still be present but may be beyond the detection range of the mass spectrometer or MaxQuant. The abundances of core proteins in different metabolic pathways were used to compare incubation conditions. Abundance changes were determined by calculating the fold change of protein in condition with respect to the abundance of the proteins in the Acet supplementation condition:

$$\text{x-fold change} = \frac{(\text{LFQ of Protein Y})_{\text{Condition A}}}{(\text{LFQ}_{\text{Min}} \text{ of Protein Y})_{\text{Acet}}} \quad (1)$$

If the average LFQ value of the Acet cultivation is zero, the smallest LFQ values becomes the reference. Heat maps were created by conditional formatting in Excel 2016 (Microsoft Corporation, Redmond, Washington, USA) and the multi-layer growth curve in was designed using JMP Pro 15 (SAS Institute GmbH, Heidelberg, Germany).

2.4 Results

2.4.1 Cultivation of *P. bryantii* B₁₄ Using Single SCFAs

Growth of *P. bryantii* B₁₄ in M2-A medium was observed if at least one SCFA was added to the medium. Without addition of SCFAs, no growth was detected within the monitored period of 24 h. Applied SCFAs were acetic (Acet), propionic (Prop), butyric (But), iso-butyric (iBut), valeric (Val) and isovaleric acid (iVal) at a concentration of 15 mM. The maximal optical density (OD) in the medium M2-A after 8 and 24 h respectively, was observed for the cultivation with Val (OD_{8h} = 1.73; OD_{24h} = 1.77). In contrast, iVal supplementation exhibited the lowest cell density (OD_{8h} = 1.16; OD_{24h} = 1.54; Table 1). The remaining cultivation conditions (Acet, Prop, But, and iBut) showed different values for the 8 h and the 24 h incubation. Trends of higher cell densities were found in the Val and Acet cultures, while iVal supplementation revealed a lower OD. Replicates of the presented average of the optical density in Table 1 can be seen in Table S3. The relative changes in pH between the beginning and end of the incubation is indicated by the acidification (ΔpH) in Table 1 and can be seen in detail in Table S3. Highest acidifications were found in cultures supplemented with Val ($\Delta\text{pH}_{8\text{h}}$ = 1.47; $\Delta\text{pH}_{24\text{h}}$ = 1.62), followed by But ($\Delta\text{pH}_{8\text{h}}$ = 1.33; $\Delta\text{pH}_{24\text{h}}$ = 1.61). The lowest acidification was also found in cultures with iVal ($\Delta\text{pH}_{8\text{h}}$ = 0.56; $\Delta\text{pH}_{24\text{h}}$ = 1.05). The consumption or production of the single SCFAs was calculated by subtracting the concentration in the non-inoculated media from the final concentration in the cultures. The fermentation products of *P. bryantii* B₁₄ should be formic, succinic, lactic, and acetic acid [126, 127]. Changes in SCFA concentrations are considered as trends, except for acetic acid, which showed a larger variation from 6–12 mM in 8 h and from 11–17 mM in 24 h. Consumption of SCFAs was about 0.5 mM within 8 h and 1.0 mM within 24 h for the other SCFAs. Small amounts of isovaleric acid were found in all cultures, except iVal. In addition, *P. bryantii* B₁₄ exhibited cell sedimentation when isovaleric acid was supplemented.

Table 1. Effect of short-chain fatty acids on growth, acidification, and short-chain fatty acid (SCFA) conversion in *Prevotella bryantii* B₁₄. *P. bryantii* was grown in M2-A medium supplemented with the indicated SCFA. Two sets of experiments were performed, each with three cultures obtained by consecutive transfer of inoculum. In the first set, each of the three cultures was analyzed for optical density (OD), pH, and SCFA composition after 8 h. In the second experiments, these parameters were determined after 24 h. The values for mean and standard deviation (SD) of one set (n = 3) are reported in Table S3. The acidification of the medium (Δ pH) is given as a relative value for each cultivation condition. The consumption (negative value) or production (positive value) of acetic acid (C2), propionic acid (C3), butyric acid (C4), isobutyric acid (iC4), valeric acid (C5), and isovaleric acid (iC5) are displayed in millimolar (n=1). Except for acetic acid (C2), the observed variations in SCFA concentrations were in the range of \pm 1.5 mM and therefore were not considered to be significant.

Cultivation Condition	Mean \pm SD of OD ₆₀₀		Δ pH	Production/Consumption (mM) of						
				C2	C3	iC4	C4	iC5	C5	
8 h incubation	Acet	1.44	\pm 0.19	1.34	9.55	0.00	0.00	0.00	0.06	0.00
	Prop	1.50	\pm 0.17	1.32	10.03	0.70	0.00	-0.04	0.08	0.07
	But	1.43	\pm 0.16	1.33	10.14	-0.05	0.00	-0.10	0.09	0.00
	iBut	1.23	\pm 0.07	0.85	6.06	0.00	-0.49	0.00	0.08	0.00
	Val	1.73	\pm 0.04	1.47	11.77	0.00	0.00	-0.03	0.16	-0.69
	iVal	1.16	\pm 0.09	0.56	6.21	0.00	0.00	0.00	-0.24	0.00
Cultivation Condition	Mean \pm SD of OD ₆₀₀		Δ pH	Production/Consumption (mM) of						
				C2	C3	iC4	C4	iC5	C5	
24 h incubation	Acet	1.67	\pm 0.04	1.38	13.94	0.00	0.00	0.00	0.08	0.00
	Prop	1.64	\pm 0.26	1.57	16.05	0.27	0.00	-0.04	0.07	0.06
	But	1.66	\pm 0.15	1.61	16.79	-0.10	0.00	-0.43	0.10	0.00
	iBut	1.64	\pm 0.06	1.49	14.02	0.00	-0.87	0.00	0.09	0.00
	Val	1.77	\pm 0.13	1.62	15.59	0.00	0.00	-0.01	0.17	-0.89
	iVal	1.54	\pm 0.34	1.05	10.82	0.00	0.00	0.00	-0.46	0.00

Other carboxylic acids, such as lactic, succinic, and formic acid, did not promote growth of *P. bryantii* B₁₄ as the used SCFAs did, which narrows the structural properties of the required acid sources. Growth promoting compounds most likely consist of one carboxyl group and an alkyl attachment of at least one methyl group (CH₃-[CH₂]_n-COOH; n = 0–3).

2.4.2 Proteome inventory of *P. bryantii* B₁₄

Bacterial cells were harvested from M2-A media at the end of the exponential phase. The overall cultivation characteristics for the proteome approach are given in the supplemental data (Figure S1). The number of quantified proteins per sample ranged from 1,518 to 1,599 (Table S4). In total, 1,818 proteins were detected. The proteome shared by all cultures comprised 1,437 proteins with an LFQ-value above zero in at least two out of three replicates. This number covered 38% of all predicted proteins or gene products (3,776 proteins) listed in the UniProt database for *P. bryantii* B₁₄ (2 July 2019). Out of all identified proteins, 1,230 proteins could be assigned to a KEGG orthology (KO) number (68%) and 1,734 proteins to a cluster of orthologous groups (COG) classification (95%).

Comparisons of protein abundances of all samples revealed 84% similarity between all cultures. Cultures clustered in the principle component (PCO) plot mostly regarding their supplementations ($p < 0.03$; Figure 6). A grouping toward the SCFA property (chain length, iso-formation) was not observed. Clustering of cultures according to proteome analysis was accompanied with a change in abundance of several proteins representing specific functional groups (Figure 6). Figures S2 and S3 provide information about most and least abundant COG protein groups within the SCFA supplementations. Note that not all identified proteins could be assigned into COG class or labeled with a KO number. Upon cells cultivated with Val, the proteome contained numerous highly abundant proteins belonging to ribosome and porphyrin metabolism (Figure S4), while iVal cultures revealed most abundant proteins of the amino acid biosynthesis (Figure S5). Val and iVal cultures together showed more abundant proteins for nucleotide metabolism (Figure S2). Similar to the Val supplementation, the Prop cultures led to an increased abundance of ribosomal proteins as well as replication and repair proteins (Figure S6). Heat shock proteins (HSP) and chaperonin increased slightly in the Val, Prop, and iVal cultures (Figure S2). Many outer membrane proteins were elevated in Acet (Figure S7) especially iron import related proteins were elevated together with Val (Figure S8). Cultures with butyric acid and isobutyric acid had a minor number of culture specific proteins including glucosidases and proteins for post translational modification.

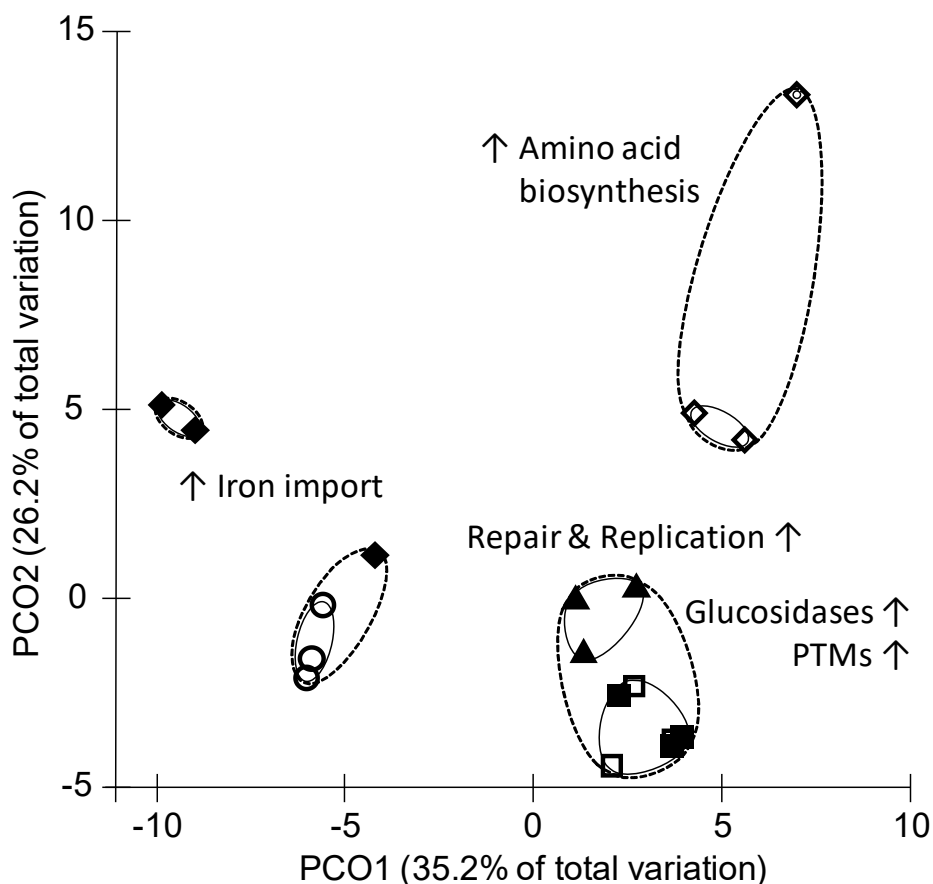


Figure 6: Assignment and comparison of pathways and cellular functions in *P. bryantii* B₁₄ exposed to various short-chain fatty acids based on relative protein abundances. Principle component analysis was done based on S17 Bray Curtis similarity out of the resemblance matrix. Elevated main protein functions causing the separation of the different proteomes are indicated close to the clusters. Clusters illustrate a similarity of either 88% (dotted line) or 92% (solid line). Supplementations with single SCFAs are displayed by following symbols: Acet (○), Prop (▲), But (□), iBut (■), iVal (◇), Val (◆). PTM: post translational modifications. The clustering of supplementation conditions was significant by a p-value < 0.05 (Monte Carlo correction).

Two pathways for acetate utilization were detected in *P. bryantii* (Figure 7). Acetate is most likely formed via the acetate kinase and phosphate acetyltransferase (Figure 7A). Supplementation with acetic acid showed the greatest enzyme elevation in the pathway via acetyl-phosphate. The single enzyme reaction via the acetyl-CoA synthetase with ATP and coenzyme A was elevated (1.3–1.9-fold) in most of cultures except of iBut and Acet (Figure 7B). Enzymes of the two-step reaction (Figure 7A) were in total 22–65-times more abundant for acetate kinase and 3–13-times more abundant in phosphate acetyltransferase as in comparison the acetyl-CoA synthetase, based on the LFQ-values obtained from MaxQuant.

Figure 8 displays the synthesis pathway for the branched-chain amino acids (BCAAs) valine, leucine, and isoleucine including enzymatic cofactors, the EC number, and the enzyme abundance for the respective cultures. An elevation of the BCAA synthesis enzymes was found

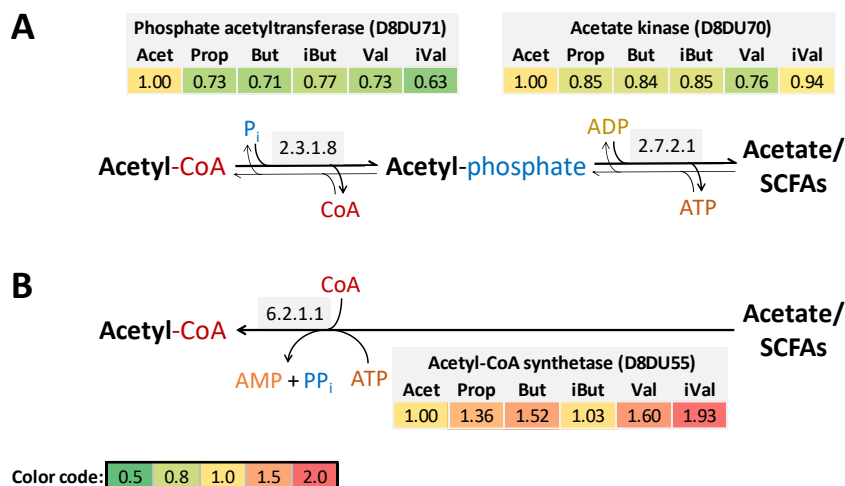


Figure 7: Routes of acetate formation and acetate utilization in response to SCFA exposure of *P. bryantii* B₁4. The abundance of the mentioned enzymes (Uniprot ID) is represented by relative abundance (n = 3) for every treatment. Protein abundance of Acet cultivation is set to one. Above the reaction arrows are the EC numbers of the enzymes displayed. The color code is given in the lower left corner. (A) Acetyl-phosphate path with bidirectional reactions, where production of acetate is more likely due to ATP formation. (B) Reaction via the acetyl-CoA synthetase for SCFA assimilation, explicitly seen for iVal.

especially in the iVal cultures within the reaction path from pyruvate to the final intermediate of the BCAA biosynthesis. Required enzymes for BCAA synthesis were a set of seven enzymes of which six were found in branches for valine, leucine, and isoleucine synthesis. Most of those enzymes were at least two-fold elevated in iVal, except for the acetolactate synthase (EC 2.2.1.6) and the BCAA aminotransferase (EC 2.6.1.42).

The similarity percentage (SIMPER) analysis of the total dataset included mostly proteins with high overall abundance and fold-change (Figure S6). The majority of proteins identified by the SIMPER analysis belonged to the central carbon metabolism (enolase, fructose-1,6-bisphosphate aldolase, glycerin-aldehyde-3-phosphate dehydrogenase, L-fucose isomerase, pyruvate phosphate dikinase, etc.) and were mainly increased in iVal cultures. Proteins related to translation and transcription were elevated in iVal too. Certain iron related proteins, including imelysin, were more abundant in the Acet and Val cultures (Figure S6). The iBut supplementation led also to an elevation of some outer membrane proteins and two tetratricopeptide (TRP) domain proteins, which were also more abundant in iVal.

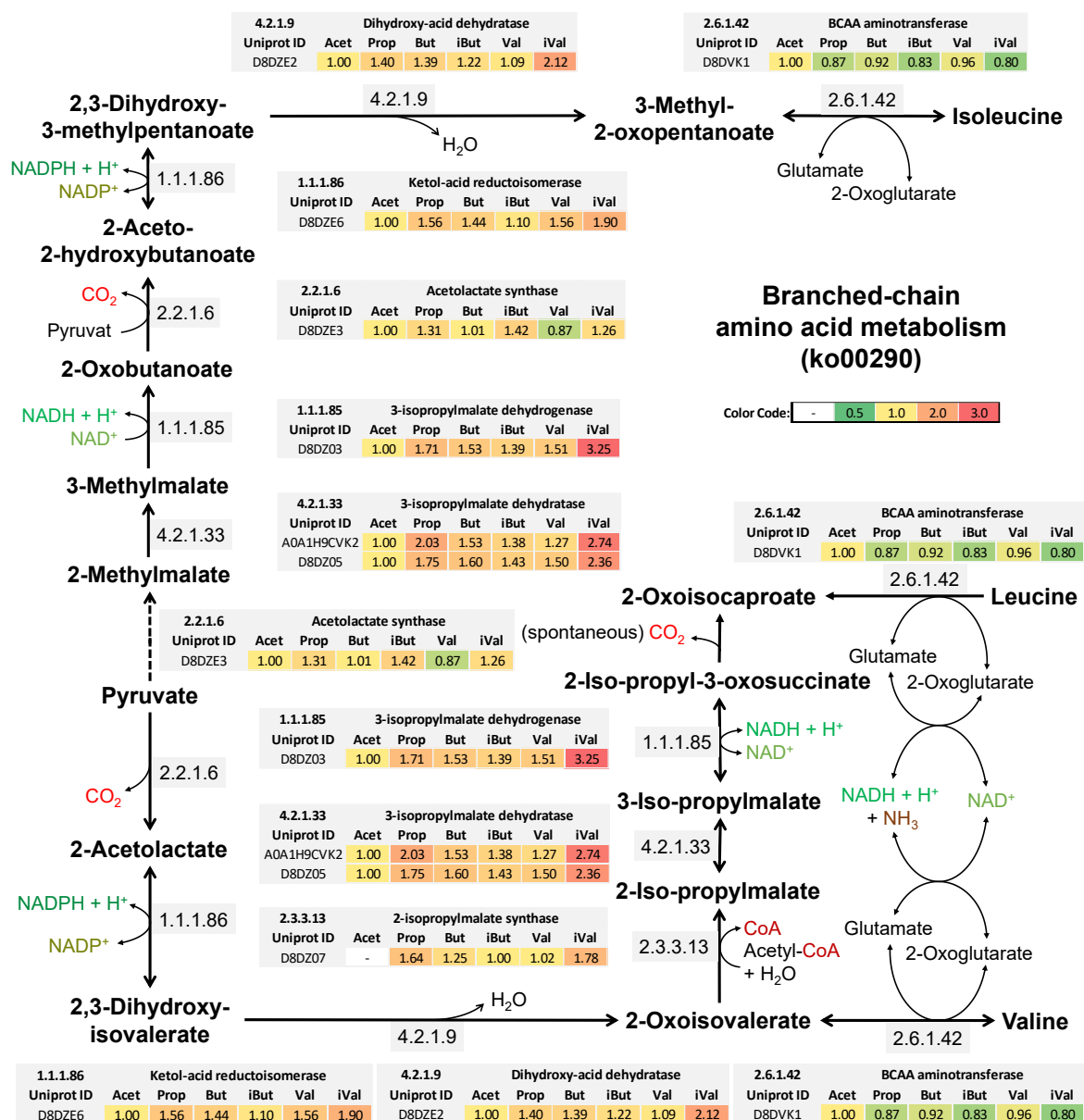


Figure 8: Influence of SCFAs on the relative abundance of enzymes required for the conversion of pyruvate to branched-chain amino acids in *P. bryantii* B₁₄. This pathway is based on the KEGG pathway (ko00290). Grey boxes indicate the mean relative abundance (n=3) of the enzymes (including EC numbers close to the arrows) and their detected subunits or copies, as shown by their Uniprot IDs. The color code on the right side displays fold change with respect to the Acet condition, which is set to one. Dotted arrow illustrates an undetected enzyme.

Proteins related to iron import were found in high abundances in *P. bryantii* B₁₄ cultures Acet and some less in Val (Figure S8). This includes TonB transporters, iron utilization proteins and transcription factors. The heme and ferrienterochelin import is mostly conducted by TonB associated proteins, like HmuY or the ferrienterochelin receptor. The HmuY (D8E002) was found up to 8-times more abundant in Acet and Val when compared to the iVal cultivation condition. In the residual conditions, HmuY was around five-fold less abundant when compared to Acet. The outer membrane receptor for ferrienterochelin (D8E003) showed a 10-

fold increase in Acet cultures and eight-fold in Val cultures while being low abundant (1–2-fold) in the remaining cultures (reference one-fold in iVal). Multiple copies of TonB proteins and uncharacterized proteins with homology to iron transporters were detected (Figure S8). The iron acquisition protein hemolysin (D8DU89) was found in a two-fold amount in the iVal and 1.5-fold in Val while remaining cultures exhibited around one-fold magnitudes.

2.4.3 Effect of SCFA exposure on LCFA in membranes from *P. bryantii*

In order to investigate SCFA incorporation into long-chain fatty acids (LCFAs), the fatty acids of freeze-dried cells from *P. bryantii* B₁₄ were quantified by GC-MS. The analyses showed that an increase of certain iso- and anteiso- LCFA was concomitant to the supplemented iso- and anteiso-SCFA (Figures S9 and S10 and Tables S5 and S6). The iBut supplementation resulted in higher amounts of 12-methyl C13:0 and 14-methyl C15:0 (Figure 9). Both LCFAs were odd-chained and iso-branched like the supplemented isobutyric acid. Compared to the other conditions, iVal showed a small increase of the iso-branched 11-methyl C12:0 after 24 h of incubation. Additionally, a minor amount of the linear C15:0 was measured in iVal, but the major amounts of this odd chained acid were found in Val and Prop. Larger quantities of C16:0 and 15-me C16:0 were found in But, Prop, and Acet. Minor amounts of C17:0 were recovered in Prop and Val. The fatty acid 12-methyl- and 13-methyl C14:0 were the predominant LCFAs in all cultivation conditions, whereby the predominance of 12-methyl C14:0 shifted in some conditions to 13-methyl C14:0 during incubation from 8–24 h. The consumption of the supplemented SCFAs was between 0.2–0.5 mM for 8 h and reached a maximal depletion of 1.0 mM after 24 h of incubation (Table 1). Furthermore, SCFA measurements tend to confirm a minor SCFA consumption in cultivations for LCFA investigations (Table S7) as well as for the proteome investigation (Table S8).

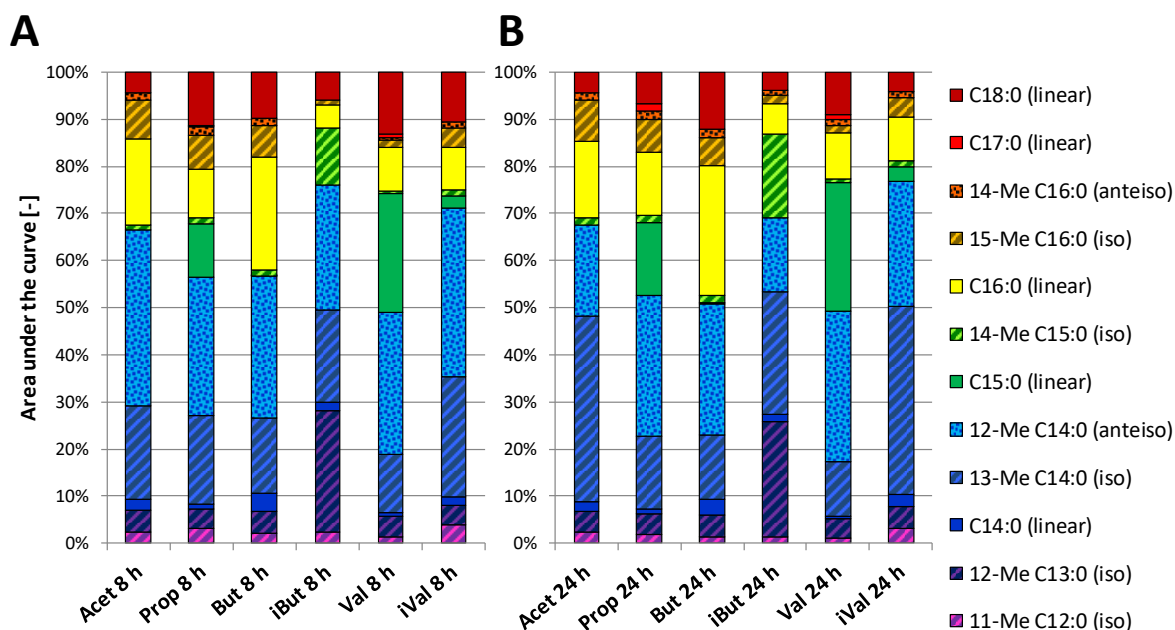


Figure 9. Influence of SCFAs on LCFA profiles in *P. bryantii* B₁₄ cell membranes. (A) LCFA profiles after 8 h and (B) after 24 h incubation are presented as relative abundances of LCFA using AUC values. The nomenclature of the LCFA is defined by the maximal chain length and number of carbon atoms, given by the capital C, followed by the number of carbon double bonds after the colon. The position of methylation (Me) is described by the number in front while the type of branching is given in brackets.

2.4.4 Effect of carbon source on growth of *P. bryantii*

The results described above corroborate the suitability of the M2-A medium to cultivate *P. bryantii* B₁₄ and demonstrate that SCFAs are incorporated in lipid membrane synthesis. Still, the major energy supporting carbon source for *P. bryantii* B₁₄ are sugars derived from polysaccharides like hemicellulose or pectin. It was tested if glucose is usable as a sole energy supporting carbon source by omitting maltose, cellobiose and lactate from the medium (M2-B). Growth kinetics showed a lag-phase of about 120 min and an increase in OD of about 0.9 per hour during the exponential phase.

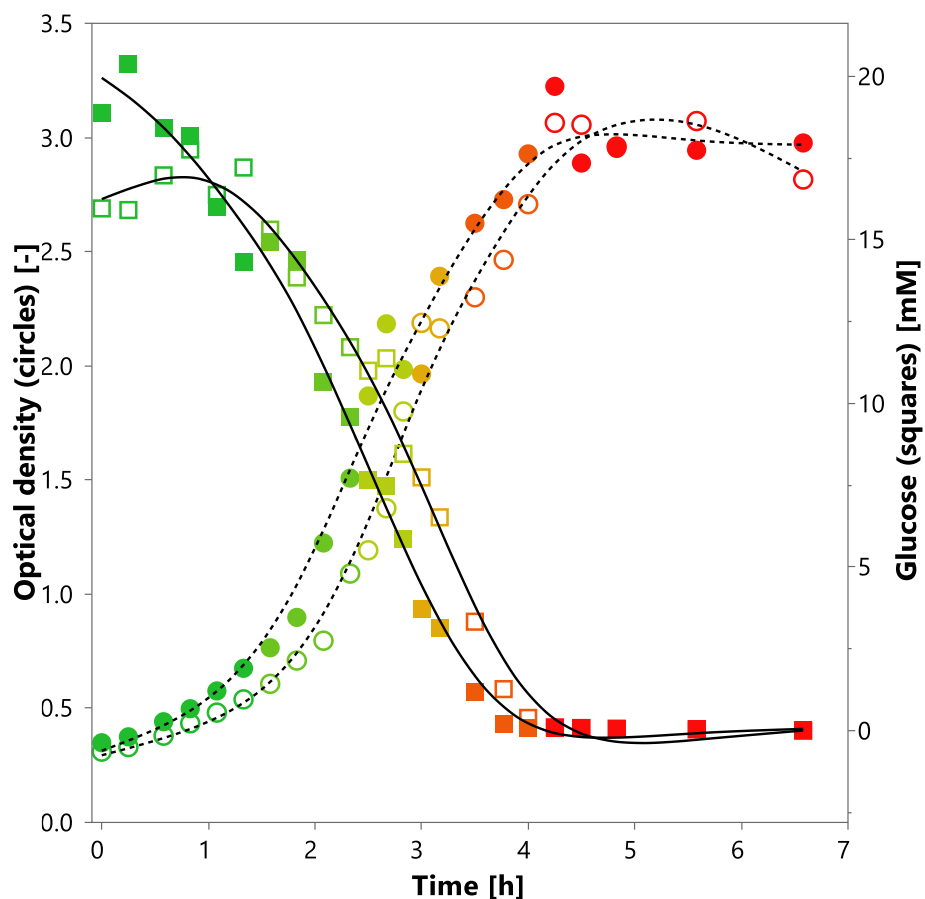


Figure 10. Growth of *P. bryantii* B₁₄ in minimal medium (M2-B) supplemented with glucose as the only carbon source. Following parameters are given for a duplicate (A: empty, B: filled symbols) of a two-liter batch culture: optical density at 600 nm (circles), glucose concentration in millimolar (squares) and pH as a color gradient from pH 7 (green) to pH 5.2 (red). The interpolation curves for optical density (dotted line) and glucose (solid line) represent the trend for each duplicate.

2.5 Discussion

2.5.1 SCFAs replace rumen fluid for cultivation of *P. bryantii* B₁₄

This study verified that rumen fluid can be replaced by various SCFAs to cultivate *P. bryantii* B₁₄. iVal cultures showed the slowest growth indicated by lower optical densities and a tendency of cells to aggregate (Figure S11), which are both indicators of stress [128]. In accordance, cells exposed to iVal showed increased abundance of stress-related chaperones. Absence of any SCFAs resulted in growth of *P. bryantii* B₁₄ only after 36 h of incubation. A further possibility is the selection and reproduction of a sub-population of *P. bryantii* cells, which are less dependent on SCFA. The first culture inoculation allowed a transfer of sufficient amounts of SCFAs from M2-A medium as cells were not washed resulting in a short lag-phase of 3 h (Figure S12). The second transfer in SCFA-free media resulted in a prolonged lag-phase of at least 6 h. Third transfer of *P. bryantii* B₁₄ in SCFA-free media showed the adapted subpopulation as lag-phase was again 3 h (Figure S12). This points towards SCFAs not being essential in the central energy-producing carbon metabolism but enhance growth of *P. bryantii* B₁₄. Figure 2A showed a part of the fermentative branch to generate ATP by producing acetate, a more common reaction. Furthermore, acetate kinase has been described to be responsible for excretion of excessive carbohydrates in form of acetate and is therefore a catabolic repressed enzyme [129, 130]. Despite acetic acid supplementation, further acetate was produced presumably via the acetyl-phosphate pathway, meaning that catabolite repression was not activated under culture conditions of the present study. Assimilation of SCFA via acetyl-CoA synthetase activity was reduced in Acet and iBut compared to Prop, But, Val and iVal supplementations. A catabolite repression especially for Acet is proposed as discussed by Valgepea, K., *et al.* [130]. Although the reported cultivation conditions are artificial and do not represent the natural environment of *P. bryantii*, they may provide a deeper understanding of SCFA requirement, anabolism and related broad range of effects.

2.5.2 SCFA Influence the Abundance of Iron Transport Proteins

P. bryantii is a close relative to pathogenic *Prevotella* species such as *P. denticola* and *P. bivia* that depend on the acquisition of iron, which is important for survival within the host [131]. Enteroferrin, HmuY, TonB, and other outer membrane proteins were elevated in *P. bryantii* cultures containing Acet and iVal. This suggests a regulation of the iron import by supplementation of certain fatty acids or their derivatives. *P. intermedia* 17 showed an increase of a HmuY-like protein and a TonB-linked outer membrane receptor when iron

sources were restricted [57]. Iron deficiency in ruminants is rarely observed in adult ruminants and should not influence growth of *Prevotella* species in the rumen at proper feeding conditions [132]. In the study of Herold, S., *et al.* [47], an increase of TonB was found in a shiga-toxicogenic *E. coli* when multiple SCFAs were supplemented. Another heme importing protein is hemolysin, which was increased in iVal and is usually also expressed under iron deficiency. Iron can be imported in connection to porphyrin or chelating agents such as citrate or enteroferrin. For some *Prevotella* sp., it was demonstrated that heme (an Fe³⁺ bound porphyrin) has to be present in a concentration of at least 10 nM in order to obtain sufficient growth [28]. Investigating the porphyrin biosynthesis pathway revealed enzymes, which convert L-glutamate into protoporphyrinogen IX (PPIX) and coproporphyrinogen. However, the final enzyme for producing porphyrin is not annotated for *P. bryantii* B₁₄ or other *Prevotella* species (Figure S13). The absence of the final enzyme may not be relevant since a PPIX supplementation for *P. intermedia* resulted in sufficient growth [58]. Nevertheless, the presence of functional porphyrin metabolism was not shown in the proteomic dataset. Thus, the role of heme and its supplementation remains uncertain. Possible heme utilization as an oxygen protectant layer on the cell surface was found in *P. nigerescens* and *P. intermedia* [59, 133]. Furthermore, heme can contribute to the performance of cytochrome containing enzymes and the electron transport chains as *P. bryantii* B₁₄ uses anaerobic respiration [134, 135]. In the study from Sperry, J., *et al.* [136], a depletion of heme resulted in an increase of lactate and fumarate, which was not confirmed by the current study. Until now, very little is known about the regulation of the porphyrin biosynthesis in non-photosynthetic bacteria and catabolic repression by heme was already reported for other bacterial species [137]. A higher request for the porphyrin ring instead of iron is indicated by the current findings as well as by the study of Caldwell, D., *et al.* [28]. It can be assumed that acetic and valeric acid increase the abundance of heme import proteins in *P. bryantii*, which in turn enhance heme uptake and regulate the porphyrin biosynthesis as also described by Granick and Beale [137]. An enhanced heme uptake due to the direct aid of SCFAs can be neglected since heme is a large molecule and soluble in alkaline solutions. Absence of mineral iron in the media would have also caused similar patterns among all cultivation conditions and can therefore be also excluded as a trigger. An iron-deficiency was not seen in bacterial density and growth behavior in *P. bryantii* in rumen fluid containing medium (M2) versus newly created growth medium (M2-A) with hemin.

2.5.3 SCFAs incorporated into long-chain fatty acids of lipid membranes

Membranes are composed of LCFAs, which require a malonyl-CoA with an acyl-CoA or acyl-carrier-protein as a primer molecule. This primer molecule is assumed to be a SCFA. The hypothesis is verified by rediscovering features of SCFA in LCFAs. The analyses of LCFA in the current study were similar to LCFA ratios of other *Prevotella* sp. in regard to the predominant fatty acids 13-me C14:0 and 12-me C14:0 [138, 139]. The beneficial effects of incorporating branched SCFAs into the membrane of *P. bryantii* B₁₄ can mirror an adaptation to antibacterial peptides, low temperature and low pH [140-144]. The latter adaptation is expected for the LCFAs 11-me C12:0 (iso) and 13-me C14:0 (iso). Both LCFAs correlated with the pH at 8 h and 24 h with a correlation coefficient between $R = -0.74$ and -0.90 , indicating a possible connection between LCFAs and acidity. Referring to SCFA implementation into LCFAs, acetic acid seems to be the universal building block for the requirements of *P. bryantii* B₁₄ to form all necessary LCFAs with a large fraction of even numbered and branched LCFAs. Other SCFAs shift the LCFA profile regarding their traits (branching, chain length). While traits of SCFAs were recovered for most of the cultures, iVal lacked in larger LCFA with such traits, meaning that isovaleric acid is preferably used for other synthesis pathways like BCAA syntheses. Other rumen bacteria such as *Ruminococci* showed incorporation of larger iso- and odd-chain LCFA [118]. The uptake mechanisms of SCFA to be available in the cell is only known for a few microorganisms and shortly explained in Reiser, K., *et al.* [145] and DiRusso, C.C. and Black, P.N. [146]. In the present dataset, fatty acid transport protein FadL (D8DTK4) showed a decreasing abundance with higher chain length ($R = -0.89$), which may explain the protein elevation for fatty acid related proteins in Acet. Besides FadL, LCFA-transport proteins (AOA1H9JWM8, D8DZW6) are suspected to be also capable of carrying SCFA through the membrane [146]. The two quantified LCFA-transport proteins were twice as much (AOA1H9JWM8) or similarly (D8DZW6) abundant in iVal as in Acet but almost not affected by other SCFAs. Findings on growth, proteome and SCFA assimilation together indicate a bioactive role for isovaleric acid in *P. bryantii* B₁₄ cells.

2.5.4 Isovaleric acid enhance branched-chain amino acid synthesis

Data of SCFA measurements showed low amounts isovaleric acid in all culture conditions, except for iVal, which is most likely connected to the degradation of tryptic digested casein or other high protein substrates [36, 147]. Thus, *P. bryantii* B₁₄ seems to be

capable of producing low amounts of branched SCFA under supplementation of a protein source. Enzymes involved in the BCAA metabolism became elevated in iVal cultures, while other SCFA supplements showed only low abundances of these proteins. Furthermore, a transformation from isovaleric acid to BCAAs is assumed by a lower specificity of the acetyl-CoA synthetase as shown in Glasemacher, J., *et al.* [148]. Especially the 3-isopropylmalate dehydrogenase (3-IPM DH) with an approximate three-fold elevation was highlighting the BCAA metabolism for the iVal condition. All co-elevated enzymes of iVal in the amino acid and carbon metabolism may react to enhanced concentration of isovaleric acid derived compounds, like on BCAAs, to avoid intoxication [149]. The study of Allison, M.J., *et al.* [150] observed a higher activity of the IPM synthase under presence of isovaleric acid plus valine. In contrast, isopropylmalate synthase was inhibited under leucine supplementation in *Bacteroides* species, suggesting a substrate regulation via the CodY operon [151]. The CodY operon seem to react to BCAA and GTP concentration, but was not identified for *P. bryantii* B₁₄ [152]. Atasoglu, C., *et al.* [153] discovered that nitrogen content derived less from ammonia but more from peptides when trypticase supplementation was increased from 1–10 g/L. This means that *P. bryantii* B₁₄ might have shown stronger effects of amino acid synthesis when less trypticase is supplemented. BCAA pathway showed the most prominent elevations of related proteins among all other amino acid synthesis pathways. This reveals a direct impact of isovaleric acid on their abundance. Only the BCAA aminotransferase was low in abundance, which was probably connected to the diminished ammonia assimilation [153].

2.5.5 Conclusions

Driven by exploring the reason for SCFA requirement of *Prevotella bryantii* B₁₄ insights about single SCFA supplementation revealed different outcomes with respect to growth performance and protein inventories. Parts of SCFAs were found in membrane lipids and amino acids. High bacterial cell densities were measured for Val, while OD measurements at 24 h were lowest for the iVal condition. Cell sedimentation in the supplementation with iVal indicated a challenge for *P. bryantii*, which was most likely be caused by the overload of isovaleric acid and peptides from fermentation of tryptic digested casein. The SCFA measurements verified acetic acid production and consumption of supplemented SCFAs. Furthermore, incorporation of SCFA was confirmed by recovering traits in LCFAs of the lipid membrane. Most proteomes of single SCFA cultures shared 80% of their quantified proteome profile. Differences occurred in proteins responsible for carbon metabolism, porphyrin

metabolism (Val), outer membrane proteins, especially porphyrin import related proteins (Acet, Val) and amino acid biosynthesis (iVal). Latter demonstrated the regulation of the BCAA synthesis by isovaleric acid. Nevertheless, proteome analysis of *P. bryantii* B₁₄ cells cultivated with single SCFAs narrowed the range of potential mechanisms and pinpointed contributing of SCFA to growth and other possible functions.

2.6 Miscellaneous information of publication

2.6.1 Funding

The Deutsche Forschungsgemeinschaft (DFG) funded the presented research (SE2059/3-1 and FR1321/7-1).

2.6.2 Acknowledgments

We would like to thank the Deutsche Forschungsgemeinschaft (DFG) for funding. We would like to thank Michael Bott (Forschungszentrum Jülich) for his support and comments to the manuscript. Sincere thanks to the mass spectrometry group of the Core Facility of the University of Hohenheim and Helga Terry for their help with the sample measurements.

2.6.3 Conflicts of interest

The authors declare no conflict of interest.

2.7 Supplementary tables

Table S1: Vitamin Solution for *Prevotella bryantii* B₁₄. Vitamin solution was added after the autoclaving to achieve the final concentration in the media M2-A and –B.

Ingredients	Molecular weight [g/mol]	Weight / Volume	Final concentration in culture
Hemin	651.94	1.00 mg/L	1,534 nM
Menadion	172.18	0.60 mg/L	3,485 nM
Folic acid	441.40	0.05 mg/L	113 nM
Thiamine hydrochloride	337.27	2.00 mg/L	5,930 nM
Riboflavin	376.37	2.00 mg/L	5,314 nM
Nicotinamide	112.12	2.00 mg/L	17,838 nM
Pyridoxamine dihydrochloride	241.11	2.00 mg/L	8,295 nM
Ca-Pantothenate	476.54	2.00 mg/L	4,197 nM
Aminobenzoic acid	137.14	0.10 mg/L	729 nM
Biotin	244.31	0.05 mg/L	205 nM
Cyanocobalamin	1579.60	0.05 mg/L	32 nM

Table S2: Composition of media for growth of *P. bryantii* B₁₄

Ingredients	Weight/Volume	Final concentration in culture
NaHCO ₃	4.00 g/L	47.62 mM
NaCl	0.90 g/L	15.40 mM
(NH ₄) ₂ SO ₄	0.90 g/L	6.81 mM
KH ₂ PO ₄	0.45 g/L	3.31 mM
K ₂ HPO ₄ x 3 H ₂ O	0.45 g/L	1.97 mM
MgSO ₄ x 7 H ₂ O	0.10 g/L	0.61 mM
CaCl ₂ x 2 H ₂ O	0.09 g/L	0.41 mM
Glucose	2.00 g/L	11.1 mM
Maltose ¹	2.00 g/L	5.8 mM
Lactose ¹	2.00 g/L	5.8 mM
Tryptic digested Casein	10.00 g/L	10.0 g/L
Cysteine x HCl x H ₂ O	1.00 g/L	5.7 mM
Acetic acid ²	0.9 / 1.7 g/L	15.0 / 28.3 mM
Propionic acid ²	1.1 / 0.6 g/L	15.0 / 8.1 mM
n-Butyrate ²	1.3 / 0.3 g/L	15.0 / 3.4 mM
Iso-Butyrate ²	1.3 / 0.1 g/L	15.0 / 1.1 mM
n-Valeric acid ²	1.5 / 0.1 g/L	15.0 / 1.0 mM
Iso-Valeric acid ²	1.5 / 0.1 g/L	15.0 / 1.0 mM
Sodium lactate (60% w/v) ¹	10 mL/L	53.5 mM
Resazurin	1.00 mg/L	4.4 nM
CO ₂ (v/v)	100 %	100 % gas phase
Vitamin solution ³	0.1 mL/7 mL	(per Hungate tube)

¹ These ingredients were omitted in the M2-B medium. ² Short-chain fatty acid supplements for M2-A and M2-B. Left-hand values refer to the addition of single SCFAs to M2-A. Concentrations of combined SCFA supplementation to M2-B are given on the right. ³ Composition of vitamin solution see Table S1.

Table S3: Optical density and pH of cultivations for LCFA harvesting.

Cultivation Conditions	OD ₆₀₀			Mean ± SD of OD ₆₀₀	pH		ΔpH	
	Pre (1)	Pre (2)	Main		Sample	Blank		
8 h incubation	Acet	1.26	1.40	1.64	1.44 ± 0.19	5.17	6.51	1.34
	Prop	1.33	1.51	1.68	1.50 ± 0.17	5.18	6.50	1.32
	But	1.46	1.27	1.58	1.43 ± 0.16	5.20	6.53	1.33
	iBut	1.28	1.15	1.25	1.23 ± 0.07	5.73	6.58	0.85
	Val	1.71	1.70	1.77	1.73 ± 0.04	5.08	6.55	1.47
	iVal	1.11	1.11	1.27	1.16 ± 0.09	6.15	6.71	0.56
Cultivation Conditions	OD ₆₀₀			Mean ± SD of OD ₆₀₀	pH		ΔpH	
	Pre (1)	Pre (2)	Main		Sample	Blank		
24 h incubation	Acet	1.68	1.63	1.70	1.67 ± 0.04	5.19	6.57	1.38
	Prop	1.62	1.38	1.91	1.64 ± 0.26	4.93	6.50	1.57
	But	1.63	1.52	1.82	1.66 ± 0.15	4.92	6.53	1.61
	iBut	1.62	1.59	1.71	1.64 ± 0.06	5.17	6.66	1.49
	Val	1.73	1.67	1.92	1.77 ± 0.13	4.93	6.55	1.62
	iVal	1.15	1.64	1.82	1.54 ± 0.34	5.45	6.50	1.05

The cultivations are divided into Pre- and Main cultivations and with incubation time of 8 or 24 h. Pretreatments 1 and 2 represent the chronological order, followed by the main treatment. Mean and standard deviation (SD) of optical density were calculated for each condition (n=3). High SD at 24 h for iVal and Prop indicate deviation in inoculation composition or differences in adaptation time. Acidification is described as ΔpH and calculated as the difference between the pH at the start (blank) and the end of the incubation time (sample)

Table S4: Numbers of peptides and proteins determined by LC-MS/MS measurements.

Replicate	Acet	Prop	But	iBut	Val	iVal	Total peptides detected
A	21,144	21,988	21,599	22,041	20,511	21,025	
B	21,389	21,721	21,575	22,127	21,110	21,620	
C	21,660	22,023	22,160	21,693	20,872	20,667	
Replicate	Acet	Prop	But	iBut	Val	iVal	Proteins detected
A	1,539	1,580	1,588	1,577	1,519	1,534	
B	1,550	1,580	1,566	1,578	1,554	1,543	
C	1,570	1,589	1,599	1,567	1,537	1,518	

Table S5: Cultivation parameters and relative amounts of trait specific long chain fatty acids (LCFAs).

Time	Condition	Acidification	Main OD	Mean OD	Branching			Chain length	
					anteiso	iso	linear	odd	even
8 h	Acet (C2 even)	1.34	1.64	1.44	38.7%	36.3%	25.0%	5.7%	94.3%
	Prop (C3 odd)	1.32	1.68	1.50	31.0%	34.3%	34.7%	17.2%	82.8%
	But (C4 even)	1.33	1.58	1.43	31.4%	30.8%	37.7%	5.9%	94.1%
	iBut (C4 odd)	0.85	1.25	1.23	26.7%	61.0%	12.3%	37.9%	62.1%
	Val (C5 odd)	1.47	1.77	1.73	30.8%	20.2%	49.0%	30.9%	69.1%
	iVal (C5 even)	0.56	1.27	1.16	37.0%	39.0%	24.0%	7.9%	92.1%
	24 h	Acet (C2 even)	1.38	1.70	1.67	21.0%	56.2%	22.8%	5.7%
Prop (C3 odd)		1.57	1.91	1.64	31.5%	30.3%	38.2%	17.2%	82.8%
But (C4 even)		1.61	1.82	1.66	29.6%	27.1%	43.4%	5.9%	94.1%
iBut (C4 odd)		1.49	1.71	1.64	16.8%	71.3%	11.9%	37.9%	62.1%
Val (C5 odd)		1.62	1.92	1.77	33.0%	19.4%	47.6%	30.9%	69.1%
iVal (C5 even)		1.05	1.82	1.54	27.9%	53.0%	19.1%	7.9%	92.1%
Pearson Correlation		Mean OD vs. LCFA type				-0.33	-0.29	0.53	0.16
	Main OD vs. LCFA type				-0.12	-0.38	0.54	-0.05	0.05
	Acidification vs. LCFA type				-0.21	-0.37	0.57	0.11	-0.11

The cultivation parameters like mean optical density of pre- and main culture (OD; n=3), the OD of the respective main culture and the acidification (n=3) were correlated with the LCFA type in the manner of Pearson to obtain the correlation coefficient (R).

Table S6: Percentile amount of long-chain fatty acids found in lipid membrane of *P. bryantii* B₁₄.

LCFA (branching)	Relative amount of LCFA [%] in conditions						
	Acet	Prop	But	iBut	Val	iVal	
8 h	11-Me C12:0 (iso)	2.5	3.0	2.1	2.3	1.4	4.0
	12-Me C13:0 (iso)	4.6	4.1	4.7	25.8	4.4	4.0
	C14:0 (linear)	2.3	1.2	3.8	1.8	0.7	1.8
	13-Me C14:0 (iso)	19.7	18.7	16.1	19.6	12.4	25.5
	12-Me C14:0 (anteiso)	37.3	29.3	30.1	26.7	30.2	35.7
	C15:0 (linear)	-	11.5	0.1	-	25.4	2.7
	14-Me C15:0 (iso)	1.1	1.3	1.2	12.1	0.5	1.2
	C16:0 (linear)	18.3	10.3	24.0	4.7	9.1	9.0
	15-Me C16:0 (iso)	8.4	7.1	6.8	1.2	1.6	4.2
	14-Me C16:0 (anteiso)	1.4	1.7	1.3	-	0.6	1.4
	C17:0 (linear)	-	0.3	-	-	0.6	-
	C18:0 (linear)	4.4	11.4	9.9	5.8	13.2	10.5
	24 h	11-Me C12:0 (iso)	2.5	2.0	1.3	1.3	1.2
12-Me C13:0 (iso)		4.2	4.3	4.8	24.4	4.1	4.7
C14:0 (linear)		2.0	0.9	3.4	1.6	0.4	2.6
13-Me C14:0 (iso)		39.6	15.6	13.6	26.0	11.8	40.0
12-Me C14:0 (anteiso)		19.3	29.7	27.9	15.9	31.8	26.6
C15:0 (linear)		-	15.6	0.2	-	27.3	3.1
14-Me C15:0 (iso)		1.4	1.4	1.5	17.6	0.9	1.3
C16:0 (linear)		16.4	13.5	27.7	6.5	9.8	9.3
15-Me C16:0 (iso)		8.6	7.0	6.0	2.0	1.5	4.0
14-Me C16:0 (anteiso)		1.7	1.8	1.7	1.0	1.2	1.3
C17:0 (linear)		-	1.7	-	-	1.1	-
C18:0 (linear)		4.3	6.6	12.1	3.8	9.1	4.1

Prevotella was incubated with different SCFA, for incubation times at 8 and 24 h. The incubated SCFAs were iso-valeric acid (iVal), valeric acid (Val), iso-butyric acid (iBut), butyric acid (But), propionic acid (Prop) and acetic acid (Acet). The description of the long-chain fatty acids (LCFA) is described by the possible position of methylation, the number of linear carbon atoms behind the letter C and the corresponding type iso or anteiso in brackets.

Table S7: SCFA measurement of cultivation for LCFA analysis

Treatment	C2 [mM]	C3 [mM]	C4I [mM]	C4 [mM]	C5I [mM]	C5 [mM]
Acet 8h_Blank	15.75	0.00	0.00	0.00	0.00	0.00
Acet 24h_Blank	14.76	0.00	0.00	0.00	0.00	0.00
Acet 8h	25.30	0.00	0.00	0.00	0.06	0.00
Acet 24h	28.70	0.00	0.00	0.00	0.08	0.00
Prop 8/24 h_Blank	0.00	14.53	0.00	0.04	0.00	0.00
Prop 8h	10.03	15.22	0.00	0.00	0.08	0.07
Prop 24h	16.05	14.80	0.00	0.00	0.07	0.06
But 8/24 h_Blank	0.00	0.10	0.00	15.50	0.00	0.00
But 8h	10.14	0.06	0.00	15.39	0.09	0.00
But 24h	16.79	0.00	0.00	15.06	0.10	0.00
iBut 8h_Blank	0.65	0.00	15.06	0.00	0.00	0.00
iBut 24h_Blank	0.46	0.00	15.20	0.00	0.00	0.00
iBut 8h	6.71	0.00	14.57	0.00	0.08	0.00
iBut 24h	14.48	0.00	14.33	0.00	0.09	0.00
Val 8/24 h_Blank	0.00	0.00	0.00	0.09	0.00	14.79
Val 8h	11.77	0.00	0.00	0.06	0.16	14.11
Val 24h	15.59	0.00	0.00	0.08	0.17	13.90
iVal 8h_Blank	0.72	0.00	0.00	0.00	14.44	0.00
iVal 24h_Blank	0.41	0.00	0.00	0.00	14.90	0.00
iVal 8h	6.93	0.00	0.00	0.00	14.20	0.00
iVal 24h	11.23	0.00	0.00	0.00	14.44	0.00

Acetic acid (C2), propionic acid (C3), butyric acid (C4), iso-butyric acid (iC4), valeric acid (C5) and iso-valeric acid (iC5) are displayed in mM for each approach in triplicate (n=3) with one blank (n=1). An inaccuracy of ± 1.5 mM can be expected. The number of blanks in the table is depending if the cultivation for 8 or 24 h was performed in one or two runs.

Table S8: SCFA measurement from supernatant of cultivation for proteomic analysis.

Treatment	C2 [mM]	C3 [mM]	C4I [mM]	C4 [mM]	C5I [mM]	C5 [mM]
Acet 8h_Blank	17.30	0.00	0.00	0.00	0.03	0.00
Acet 8h_A	23.48	0.00	0.00	0.00	0.05	0.00
Acet 8h_B	23.19	0.00	0.00	0.00	0.06	0.00
Acet 8h_C	21.97	0.00	0.00	0.00	0.06	0.00
Prop 8h_Blank	0.00	14.99	0.00	0.00	0.02	0.00
Prop 8h_A	7.02	14.92	0.00	0.00	0.06	0.00
Prop 8h_B	6.81	14.92	0.00	0.00	0.05	0.00
Prop 8h_C	8.42	15.30	0.00	0.00	0.06	0.00
But 8h_Blank	0.00	0.00	0.00	15.01	0.00	0.00
But 8h_A	8.48	0.00	0.00	15.73	0.05	0.00
But 8h_B	8.70	0.00	0.00	13.82	0.06	0.00
But 8h_C	9.72	0.00	0.00	13.72	0.06	0.00
iBut 8h_Blank	0.00	0.00	17.03	0.03	0.00	0.00
iBut 8h_A	7.91	0.00	15.26	0.03	0.05	0.00
iBut 8h_B	7.98	0.00	0.55	0.00	0.06	0.00
iBut 8h_C	8.05	0.00	13.36	0.00	0.05	0.00
Val 8h_Blank	0.00	0.00	0.00	0.00	0.00	14.51
Val 8h_A	4.52	0.00	0.00	0.00	0.07	14.60
Val 8h_B	7.06	0.00	0.00	0.00	0.09	14.84
Val 8h_C	5.63	0.00	0.00	0.00	0.07	13.52
iVal 8h_Blank	0.00	0.00	0.00	0.00	14.31	0.06
iVal 8h_A	6.14	0.00	0.00	0.00	15.14	0.06
iVal 8h_B	6.11	0.00	0.00	0.00	13.11	0.00
iVal 8h_C	5.64	0.00	0.00	0.00	22.65	0.04

Acetic acid (C2), propionic acid (C3), butyric acid (C4), iso-butyric acid (iC4), valeric acid (C5) and iso-valeric acid (iC5) are displayed in mM for each approach in triplicate (n=3) with one blank (n=1). All concentrations can deviate ± 1.5 mM. Outliers are written in red.

Table S9: Growth parameters of *P. bryantii* B₁₄ in M2-B.

Time [min]	Glucose (A)	Glucose (B)	pH (A)	pH (B)	OD ₆₀₀ (A)	OD ₆₀₀ (B)	Cell dry mass (A) [mg/mL]	Cell dry mass (B) [mg/mL]
0	15.96	18.88	6.83	6.88	0.31	0.35	0.00	-0.13
15	15.91	20.37	6.79	6.87	0.33	0.38	0.40	-0.20
35	16.97	18.43	6.75	6.87	0.38	0.44	0.00	0.20
50	17.76	18.17	6.83	6.88	0.43	0.50	0.20	0.00
65	16.37	15.99	6.71	6.86	0.48	0.58	0.07	-0.07
80	17.21	14.31	6.65	6.86	0.54	0.68	0.13	-0.07
95	15.31	14.93	6.63	6.71	0.61	0.77	0.07	0.00
110	13.85	14.38	6.57	6.68	0.71	0.90	0.27	0.13
125	12.70	10.66	6.36	6.60	0.80	1.22	0.33	0.10
140	11.72	9.59	6.32	6.59	1.09	1.51	0.20	0.00
150	11.00	7.65	6.16	6.40	1.19	1.87	0.30	0.40
160	11.38	7.48	6.09	6.37	1.38	2.18	0.50	0.56
170	8.46	5.87	5.99	6.26	1.80	1.98	0.72	0.72
180	7.74	3.71	5.90	6.20	2.19	1.96	0.48	0.48
190	6.52	3.14	5.72	6.05	2.16	2.39	0.56	0.88
210	3.33	1.17	5.56	5.79	2.30	2.62	0.96	0.96
226	1.27	0.19	5.44	5.62	2.46	2.73	0.96	1.04
240	0.39	0.08	5.44	5.58	2.71	2.93	1.04	0.88
255	0.10	0.07	5.43	5.51	3.06	3.22	1.09	1.38
270	0.08	0.07	5.42	5.48	3.06	2.89	1.09	1.23
290	0.06	0.06	5.43	5.45	2.96	2.95	0.36	1.09
335	0.04	0.06	5.38	5.42	3.07	2.94	1.23	1.45
395	0.00	0.03	5.39	5.40	2.82	2.98	1.01	1.52

Duplicates are indicated by (A) or (B), each n=1. The glucose is given in milli molar and was determined enzymatically. Optical density (OD) was measured at 600 nm wavelength. Dry mass was calculated by $mass_{(vessel)} - mass_{(vessel + dry\ cells)}$.

2.8 Supplementary figures

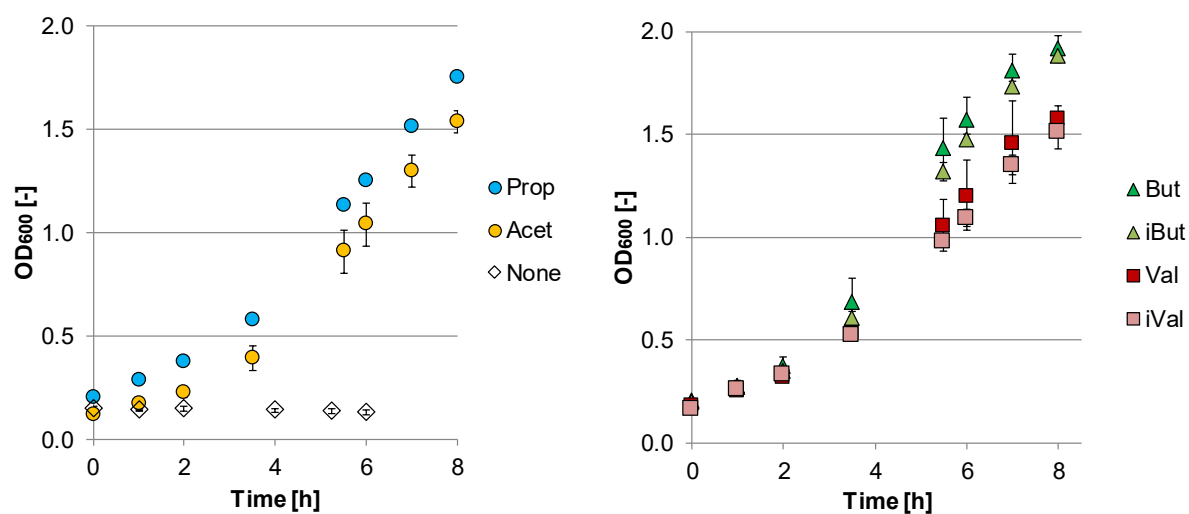


Figure S1: Cultivation of *P. bryantii* B₁₄ in M2-A medium in the presence of various short-chain fatty acids for subsequent proteome analyses. Growth curve of *P. bryantii* culture (A) without SCFAs (None), acetic acid (Acet), propionic acid (Prop) and a second growth curve for better illustration (B) with butyric acid (But), iso-butyric acid (iBut), valeric acid (Val) and iso-valeric acid (iVal). Symbols represent the mean values of biological triplicates with error bars as standard deviation.

Count of maximal abundant COGs per SCFA culture

Treatments	COGs Max count									
	A	ADK	C	CH	CO	CP	D	DK	DM	DZ
Acet	0	0	18	0	3	0	5	0	0	1
Prop	1	0	17	1	0	0	5	0	0	0
But	0	0	6	0	2	1	2	0	1	0
iBut	0	1	9	0	1	0	1	1	0	0
Val	0	0	14	0	2	0	4	0	0	0
iVal	0	0	22	0	3	0	7	0	0	0

Treatments	E	EF	EG	EH	EJ	ET	EU	F	FG	FJ
Acet	11	0	0	1	0	0	0	9	0	0
Prop	10	2	0	0	1	1	0	11	0	0
But	10	0	0	1	0	0	0	2	0	1
iBut	9	0	0	0	1	1	0	6	0	0
Val	21	0	0	0	0	0	1	21	0	0
iVal	54	0	1	3	0	0	1	24	1	3

Treatments	FK	G	GK	GM	H	HP	HQ	I	IM	IQ
Acet	0	24	0	1	13	0	0	10	0	5
Prop	0	13	0	0	11	0	0	1	1	0
But	0	37	0	1	12	0	0	8	0	1
iBut	0	43	0	2	3	0	0	2	0	0
Val	1	15	0	1	24	1	0	6	1	1
iVal	0	32	1	1	31	0	1	17	0	6

Treatments	J	JM	K	KLT	KT	L	LT	M	MNU	MU
Acet	11	0	7	0	1	9	1	27	1	0
Prop	36	0	25	1	2	27	0	25	0	1
But	2	1	9	0	1	13	0	35	0	1
iBut	3	0	7	0	1	2	0	19	0	1
Val	58	2	16	0	0	20	0	30	0	1
iVal	26	0	20	0	1	9	0	46	0	2

Treatments	N	NU	O	OU	P	Q	S	T	U	V
Acet	1	1	13	0	18	3	65	4	0	4
Prop	0	0	13	0	7	2	46	7	5	7
But	0	0	2	0	16	2	44	5	5	6
iBut	1	0	2	0	11	3	32	2	1	2
Val	0	0	19	0	10	1	64	8	2	5
iVal	1	1	13	2	9	4	91	8	2	2

Color code:	0	1	20	50	90
count of the maximal abundant proteins, sorted by COGs and treatments					

A	RNA processing and modification
B	Chromatin Structure and dynamics
C	Energy production and conversion
D	Cell cycle control and mitosis
E	Amino Acid metabolism and transport
F	Nucleotide metabolism and transport
G	Carbohydrate metabolism and transport
H	Coenzyme metabolism
I	Lipid metabolism
J	Translation
K	Transcription
L	Replication and repair
M	Cell wall/membrane/envelop biogenesis
N	Cell motility
O	Post-translational modification, protein turnover, chaperone functions
P	Inorganic ion transport and metabolism
Q	Secondary Structure
R	General Functional Prediction only
S	Function Unknown
T	Signal Transduction
U	Intracellular trafficking and secretion
V	Defense mechanism
Y	Nuclear structure
Z	Cytoskeleton

Figure S2: Count of maximal abundant COGs per treatment. Proteins which were maximal expressed among all treatments were counted and grouped by their functionality using the cluster of orthologous groups (COGs). Colors indicate the number of proteins with maximal abundance within a COG and treatment. The color code is illustrated at the bottom of the graph. COGs are explained on the right side. Proteins with multiple COG assignments can also be found.

Count of least abundant COGs per SCFA culture

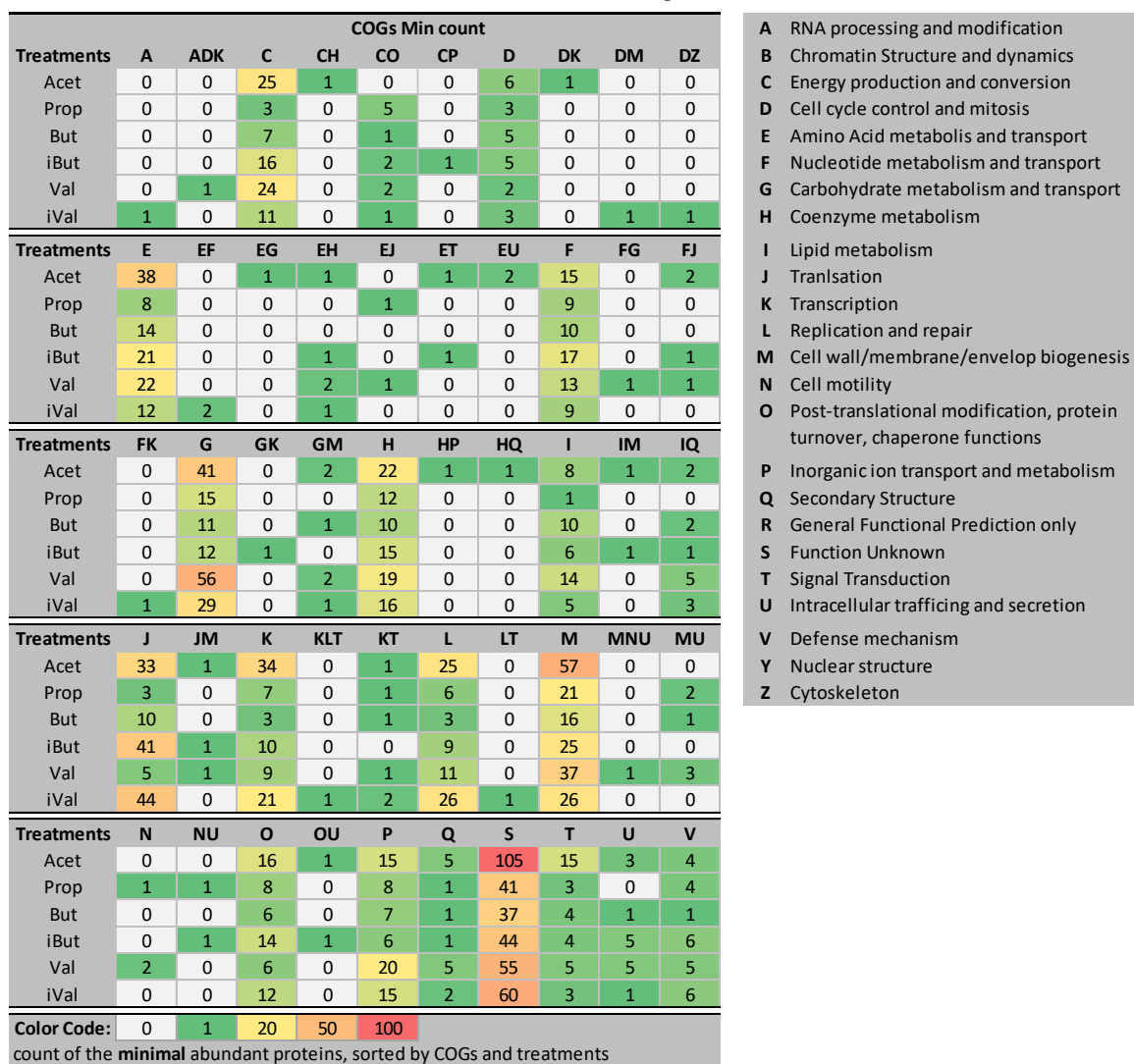


Figure S3: Count of least abundant COGs per treatment. Proteins which were least expressed among all treatments were counted and grouped by their functionality using the cluster of orthologous groups (COGs). Colors indicate the number of proteins with minimal abundance within a COG and treatment. The color code is illustrated at the bottom of the graph. COGs are explained on the right side. Proteins with multiple COG assignments can also be found.

First Publication

Name (Uniprot ID)	Acet	Prop	But	iBut	Val	iVal	Compound	EC
							<i>L-Glutamate</i>	
Glutamate-tRNA ligase (D8DU35)	1.00	1.03	0.92	0.85	1.27	0.97	↓	6.1.1.17
							<i>L-Glutamyl trans (Glu)</i>	
Glutamyl-tRNA reductase (A0A1H9I9M5)	1.00	0.71	1.16	0.83	1.62	1.01	↓	1.2.1.70
							<i>Glutamate-1-semialdehyde</i>	
Glutamate-1-semialdehyde 2,1-aminomutase (D8DTV2)	1.00	0.82	0.97	0.75	1.08	1.15	↓	5.4.3.8
							<i>5-Amino-levulinate</i>	
Porphobilinogen synthase (D8DTV1)	1.00	0.76	0.97	0.74	1.11	1.20	↓	4.2.1.24
							<i>Porphobilinogen</i>	
Hydroxymethylbilane synthase (D8DTU9)	1.00	0.73	0.83	0.76	1.29	0.89	↓	2.5.1.61
							<i>Hydroxymethylbilane</i>	-----
Uroporphyrinogen-III synthase (D8DT34)	1.00	1.24	1.20	1.02	1.18	1.09	↓	4.2.1.75
							<i>Uroporphobilinogen III</i>	
Uroporphyrinogen decarboxylase (D8DTU7)	1.00	0.69	0.77	0.69	0.86	0.96	↓	4.1.1.37
							<i>Coproporphyrinogen III</i>	
Coproporphyrinogen-III oxidase (D8DUC6)	1.00	0.88	1.10	0.75	1.50	1.29	↓	1.3.98.3
							<i>Protoporphyrinogen XI</i>	
Protoporphyrinogen oxidase (D8DUC7)	1.00	0.87	1.19	0.87	1.93	0.75	↓	1.3.3.4
							<i>Protoporphyrin XI</i>	
Spontaneous reaction							<i>Hydroxymethylbilane</i>	←-----
							↓	-
							<i>Uroporphobilinogen I</i>	
Uroporphyrinogen decarboxylase (D8DTU7)	1.00	0.69	0.77	0.69	0.86	0.96	↓	1.3.3.15
							<i>Coproporphyrinogen I / Uroporphobilinogen I</i>	

Color code: 0.6 0.8 1.0 1.2 1.5 2.0

Figure S4: Porphyrin synthesis pathway in *P. bryantii* B₁₄ with enzyme abundances. Protein abundances standardized by protein abundance of the Acet treatment. Enzyme names are given with the Uniprot ID in brackets and the EC number (in the right side). A side reaction of the pathway is illustrated in the lower part. Chemical compounds are written in italic. Color code is given below the figure.

Amino acid biosynthesis

Name (Uniprot ID)	Acet	Prop	But	iBut	Val	iVal
3-isopropylmalate dehydratase large subunit (A0A1H9CVK2)	1.00	2.03	1.53	1.38	1.27	2.74
3-isopropylmalate dehydratase small subunit (D8DZ05)	1.00	1.75	1.60	1.43	1.50	2.36
Argininuccinate synthase (D8DU50)	1.00	1.57	1.41	1.08	1.45	2.33
Gamma-glutamyl Phosphate reductase (D8DU57)	1.00	1.50	1.51	1.34	1.30	2.04
Ribulose-phosphate 3-epimerase (D8DZK5)	1.00	1.24	1.28	0.96	1.52	2.57
Ketol-acid reductoisomerase (D8DZE6)	1.00	1.56	1.44	1.10	1.56	1.90
Aconitase (D8DYN3)	1.00	1.62	1.44	1.32	1.42	1.69
Acetylornithine aminotransferase (D8DU52)	1.00	1.29	1.16	1.01	1.05	2.87
Anthranilate Phosphoribosyltransferase (D8DZK7)	1.00	1.45	1.41	1.45	1.06	1.94
Anthranilate synthase component 1 (A0A1H8ZZV6)	1.00	1.78	1.49	1.39	0.65	1.93
Histidine biosynthesis bifunctional protein (D8DY88)	1.00	1.62	1.24	1.27	1.33	1.47
Glutamate synthase (D8DY67)	1.00	1.53	1.45	1.37	1.11	1.38
S-ribosylhomocysteine lyase (D8DYD4)	1.00	0.96	1.17	1.16	1.57	1.93
Glutamate synthase large subunit (D8DTH3)	1.00	1.71	1.81	1.64	0.00	1.30
Putative oxaloacetate decarboxylase (D8DUR7)	1.00	1.38	1.21	1.05	1.35	1.30
Probable Phosphoglycerate mutase (D8DUV1)	1.00	0.95	1.09	0.94	1.75	1.53
3-phosphohikimate 1-carboxyvinyltransferase (D8DVT2)	1.00	1.14	1.14	1.09	1.12	1.74
Isocitrate dehydrogenase (A0A1H9LFP7)	1.00	1.38	1.16	1.17	0.98	1.47
Aspartokinase (D8DY90)	1.00	1.28	1.15	1.02	1.32	1.26
Tryptophan synthase (D8DUX1)	1.00	1.34	1.36	1.26	0.79	1.24
Methionine synthase (A0A1H9FCA0)	1.00	1.36	1.25	1.12	1.10	1.13
Acetolactate synthase (D8DZE3)	1.00	1.31	1.01	1.42	0.87	1.26
ATP-dependent 6-phosphofructokinase (D8DW45)	1.00	1.12	1.00	1.09	1.13	1.49
Phosphoribosylformimino-5-aminoimidazole carboxamide ribotide isomerase (D8DY86)	1.00	1.07	0.93	1.22	1.14	1.43
Carboxynorspermidine dehydrogenase (D8DYF8)	1.00	1.27	1.00	1.00	1.18	1.30
D-3-phosphoglycerate dehydrogenase (D8DWG1)	1.00	1.23	1.04	1.11	1.22	1.12
Argininsuccinate lyase (D8DXE8)	1.00	1.35	1.09	1.19	0.87	1.16
Phospherine phosphatase (D8DTT3)	1.00	1.27	1.13	0.97	1.15	1.14
Fructose-1,6-bisphosphate aldolase, class II (D8E032)	1.00	1.05	0.93	0.85	1.36	1.44
Triosephosphate isomerase (D8DVS6)	1.00	0.90	0.77	0.87	1.47	1.55
Anthranilate synthase component 2 (D8DZL3)	1.00	1.20	0.82	0.99	0.66	1.76
Histidine biosynthesis bifunctional protein (D8DWS5)	1.00	1.05	1.00	0.78	1.45	0.97
5'-methylthioadenine/S-adenylhomocysteine nucleidase (D8DVQ8)	1.00	0.74	0.75	1.15	1.07	1.53
Homerine O-acetyltransferase (D8DYN0)	1.00	0.99	0.87	0.93	1.31	1.03
ATP Phosphoribosyltransferase (D8DYW0)	1.00	1.10	0.93	1.00	1.12	0.88
S-adenylmethionine synthase (D8DT36)	1.00	0.84	1.01	0.89	1.23	1.05
Bifunctional aspartokinase/homerine dehydrogenase I (D8DYS1)	1.00	0.99	0.92	0.80	1.52	0.73
Ribose-phosphate pyrophosphokinase (A0A1H9J4B5)	1.00	0.98	0.84	0.73	1.49	0.80
3-dehydroquininate dehydratase (D8DT38)	1.00	1.05	0.88	0.83	0.94	1.12
Phospherine aminotransferase (A0A1H9D5W0)	1.00	0.97	1.02	0.89	0.89	0.99
Imidazole glycerol Phosphate synthase subunit (D8DY87)	1.00	0.82	0.73	0.94	0.84	1.29
Threonine ammonia-lyase (D8DZH1)	1.00	0.89	0.88	0.87	0.74	0.89
Glutamate--ammonia ligase (D8DTI2)	1.00	0.72	0.77	0.76	1.33	0.58
Imidazole glycerol Phosphate synthase subunit (D8DY85)	1.00	0.79	0.62	0.82	0.78	1.10
Meso-diaminopimelate D-dehydrogenase (D8DYD8)	1.00	0.85	0.74	0.80	0.84	0.83
L-threonine aldolase (D8DTJ8)	1.00	0.73	0.78	0.68	0.96	0.73
Ribose-5-phosphate isomerase B (D8DYQ0)	1.00	0.75	0.76	0.91	0.58	0.78
N-(5'-phosphoribosyl)anthranilate isomerase (D8DZK9)	1.00	0.63	0.57	0.67	0.83	0.69
Glyceraldehyde-3-phosphate dehydrogenase (D8DZ11)	1.00	0.70	0.48	0.58	0.89	0.75

Color code: 0.00 0.2 1.0 1.5 2.0 2.5

Figure S5: Heat map of enzymes from the amino acid synthesis pathway (ko01230). Label-free quantification (LFQ) values of the amino acid metabolism from KEGG (ko01230) are related and standardized by the Acet treatment and represented the average abundance in form of a heatmap, see color code below. Many enzymes also overlap with The UniprotKB is given in brackets after the protein name.

SIMPER Analysis

Name (Uniprot ID)	Acet	Prop	But	iBut	Val	iVal
Phosphoenolpyruvate carboxykinase (ATP) (D8DZS4)	1.00	1.37	1.23	1.21	1.35	2.80
L-fucose isomerase (D8DSY3)	1.00	1.54	1.38	1.31	0.95	2.24
GGGtGRT protein (D8DZB7)	1.00	1.71	1.48	1.33	1.15	1.66
60 kDa chaperonin (D8DZL6)	1.00	1.30	1.06	0.99	1.52	1.77
Iron complex outer membrane receptor protein (D8DXY3)	1.00	1.13	1.40	1.33	0.75	1.19
Fructose-1,6-bisphosphate aldolase, class II (D8E032)	1.00	1.05	0.93	0.85	1.36	1.44
Formate C-acetyltransferase (D8E078)	1.00	1.16	1.01	0.98	1.17	1.27
Triosephosphate isomerase (D8DVS6)	1.00	0.90	0.77	0.87	1.47	1.55
Phosphoglycerate kinase (D8DY78)	1.00	1.17	0.91	0.98	1.19	1.24
Elongation factor Tu (A0A1H9JXP7)	1.00	1.07	0.78	0.97	0.90	1.65
Outer membrane protein (D8DXY1)	1.00	0.94	1.31	1.19	0.67	1.12
TPR domain protein (D8E017)	1.00	0.70	0.98	1.41	0.27	1.81
3-oxoacyl-[acyl-carrier-protein] synthase 2 (D8DXQ1)	1.00	1.06	0.86	0.93	0.90	1.40
Pyruvate, Phosphate dikinase (D8DWY7)	1.00	1.15	0.84	0.88	1.18	1.03
OmpA family protein (D8DZE1)	1.00	1.00	0.91	0.83	1.09	1.17
2-dehydro-3-deoxygluconokinase (D8DWR0)	1.00	0.92	0.96	1.13	0.83	0.93
Polyribonucleotide nucleotidyltransferase (A0A1H9C5Q4)	1.00	0.98	0.86	0.79	0.94	1.17
50S ribosomal protein L7/L12 (A0A1H9JYE1)	1.00	0.72	0.79	0.71	1.02	1.21
Phosphorylase family protein (D8DYI9)	1.00	0.95	0.72	0.90	0.66	1.17
IPT/TIG domain-containing protein (D8DY17)	1.00	1.12	0.83	1.48	0.40	0.45
Putative lipoprotein (D8DWD4)	1.00	0.74	0.87	0.88	0.73	0.66
Uncharacterized protein (A0A1H9L390)	1.00	0.68	0.71	0.69	0.87	0.83
Phosphoribylaminoimidazolecarboxamide formyltransferase (D8DZZ6)	1.00	0.63	0.69	0.61	1.00	0.69
Glyceraldehyde-3-phosphate dehydrogenase (D8DZJ1)	1.00	0.70	0.48	0.58	0.89	0.75
Putative tetratricopeptide repeat domain protein (D8DZ11)	1.00	0.44	0.58	0.88	0.45	0.92
Pyridoxal 5'-phosphate synthase subunit PdxS (D8DSV8)	1.00	0.39	0.41	0.43	1.49	0.29
Putative lipoprotein (D8DTP2)	1.00	0.36	0.24	0.48	1.67	0.17
Cationic outer membrane protein OmpH (D8DT44)	1.00	0.33	0.41	0.72	0.24	0.64
Enolase (D8E0G3)	1.00	0.36	0.35	0.38	0.83	0.22
Imelysin (D8DZR1)	1.00	0.28	0.29	0.30	1.09	0.16
Flavodoxin (D8DZB4)	1.00	0.34	0.36	0.38	0.80	0.20
Iron complex outer membrane receptor protein (A0A1H9ICS8)	1.00	0.31	0.36	0.29	0.71	0.31

Color code: 0.20 0.50 1.00 1.50 2.00 2.50

Figure S6: Similar percentage (SIMPER) analyzed proteins with >1% contribution. The listed proteins contribute with at least 1% to the differential plotting in the PCO plot of figure 1. Label-free quantification (LFQ) values are related and standardized by the Acet treatment and represented the average abundance in form of a heatmap, see color code below. The UniprotKB is followed in brackets after the protein name.

Outer membrane proteins

Name (Uniprot ID)	Acet	Prop	But	iBut	Val	iVal
Outer membrane protein beta-barrel domain-containing protein (D8DWQ2)	1.00	1.70	3.03	4.23	0.90	2.22
Starch-binding associating with outer membrane (A0A1H9C300)	1.00	1.88	1.42	1.47	2.55	2.43
Outer membrane receptor proteins, mostly Fe transport (D8DZ53)	1.00	1.32	1.18	1.76	0.00	2.57
Outer membrane protein (D8DXI2)	1.00	1.31	1.64	1.43	0.86	1.48
Periplasmic chaperone for outer membrane proteins Skp (D8DSW6)	1.00	1.46	1.32	1.10	1.40	1.30
Outer membrane protein beta-barrel domain-containing protein (D8DZ08)	1.00	1.12	1.32	1.13	1.02	1.45
Outer membrane protein (D8DT53)	1.00	1.34	0.94	1.88	0.92	0.64
Periplasmic chaperone for outer membrane proteins Skp (D8DT43)	1.00	0.99	0.89	0.95	0.88	1.66
Outer membrane protein TolC (D8DVK0)	1.00	0.81	0.92	1.06	1.37	1.19
Outer membrane protein beta-barrel domain-containing protein (D8DWZ7)	1.00	1.02	0.87	1.07	1.00	1.33
Outer membrane lipoprotein-sorting protein (A0A1H9GE28)	1.00	1.00	1.06	0.98	0.97	1.21
Outer membrane protein (D8DXI1)	1.00	0.94	1.31	1.19	0.67	1.12
Starch-binding associating with outer membrane (A0A1H9E645)	1.00	1.10	0.90	1.03	1.09	0.91
Major outer membrane protein OmpA (D8DWD3)	1.00	1.06	1.12	1.00	1.09	0.75
TonB-linked outer membrane protein, SusC/RagA family (A0A1H9B8Y5)	1.00	0.98	1.13	1.48	0.53	0.89
Outer membrane protein (D8DZK0)	1.00	0.94	1.09	1.26	0.61	1.02
Outer membrane protein beta-barrel domain-containing protein (D8DZT1)	1.00	0.57	1.08	1.12	0.67	1.41
Outer membrane receptor proteins, mostly Fe transport (A0A1H9DV15)	1.00	1.16	1.28	0.99	0.67	0.74
Outer membrane receptor proteins, mostly Fe transport (A0A1H9CY22)	1.00	0.88	1.15	0.93	0.87	0.98
Outer membrane protein beta-barrel family protein (A0A1H9HV83)	1.00	1.06	1.15	1.14	0.71	0.75
Outer membrane protein beta-barrel domain-containing protein (D8DUD8)	1.00	0.94	0.94	0.86	0.82	1.23
Outer membrane receptor proteins, mostly Fe transport (D8DTP4)	1.00	0.98	0.99	0.84	0.82	1.08
Outer membrane protein OmpA (A0A1H9DD30)	1.00	0.87	0.87	0.93	1.08	0.92
Outer membrane protein assembly factor BamA (D8DWS2)	1.00	0.80	0.92	0.80	1.14	1.00
Outer membrane efflux protein (D8DYZ4)	1.00	0.90	0.76	0.88	0.67	1.27
Outer membrane protein, cobalt-zinc-cadmium efflux system (A0A1H9FFT0)	1.00	1.07	0.97	1.06	0.52	0.87
TonB-linked outer membrane protein, SusC/RagA family (A0A1H9C2R2)	1.00	0.87	0.86	0.81	0.98	0.91
Outer membrane lipoprotein carrier protein LolA (D8DTI7)	1.00	0.89	0.86	0.85	0.88	0.94
Efflux transporter, outer membrane factor (OMF) lipoprotein, NodT family (D8DVS0)	1.00	0.82	0.67	1.03	0.74	1.13
TonB-linked outer membrane protein, SusC/RagA family (A0A1H9LDK0)	1.00	0.84	0.81	0.85	0.94	0.82
Outer membrane protein beta-barrel family protein (A0A1H8Z174)	1.00	0.80	0.77	0.79	0.75	1.02
Outer membrane protein SusC (D8E073)	1.00	0.87	1.16	1.11	0.00	0.81
Starch-binding associating with outer membrane (D8DV05)	1.00	0.86	1.23	1.07	0.26	0.26
Outer membrane protein beta-barrel domain-containing protein (D8DYY2)	1.00	0.63	0.65	0.76	0.51	0.98
Outer membrane protein beta-barrel domain-containing protein (D8DVA3)	1.00	0.64	0.92	0.82	0.52	0.62
Outer membrane autotransporter barrel domain-containing protein (D8DU39)	1.00	0.76	0.70	0.88	0.46	0.69
Cationic outer membrane protein OmpH (D8DT45)	1.00	0.67	0.66	0.86	0.37	0.88
Outer membrane receptor proteins, mostly Fe transport (D8E0H5)	1.00	0.50	0.64	0.81	0.69	0.70
Outer membrane protein transport protein (OmpP1/fadI/toxI) (D8DTK4)	1.00	0.81	0.62	0.70	0.58	0.61
Starch-binding associating with outer membrane (D8DUK8)	1.00	0.79	0.58	0.95	0.47	0.38
Outer membrane protein beta-barrel domain-containing protein (D8DXU0)	1.00	0.58	0.42	0.54	0.72	0.41
TonB-dependent outer membrane receptor (D8DUK7)	1.00	0.61	0.47	0.75	0.44	0.30
TonB-linked outer membrane receptor P92 (D8DTK2)	1.00	0.54	0.46	0.53	0.51	0.45
Cationic outer membrane protein OmpH (D8DT44)	1.00	0.33	0.41	0.72	0.24	0.64
Outer membrane protein beta-barrel family protein (D8E007)	1.00	0.00	0.00	0.53	1.42	0.00
TonB-dependent outer membrane receptor (D8DXZ1)	0.00	1.69	0.00	0.00	0.00	1.00
Outer membrane receptor for ferrienterochelin and colicins (D8E003)	1.00	0.21	0.16	0.23	0.83	0.10
Outer membrane protein beta-barrel domain-containing protein (D8DWZ3)	1.00	0.00	0.00	0.37	1.07	0.00
Starch-binding associating with outer membrane (D8DVB5)	0.00	1.00	0.00	1.07	0.00	0.00
Outer membrane receptor proteins, mostly Fe transport (D8DSX8)	1.00	0.00	0.00	0.00	0.45	0.00
Starch-binding associating with outer membrane (A0A1H8ZVZ9)	0.00	0.00	0.00	1.00	0.00	0.00

Color code: 0.00 0.2 1.0 1.5 2.0 2.5

Figure S7: Heat map of most found outer membrane proteins. Label-free quantification (LFQ) values are related and standardized by the Acet treatment and represent the average abundance in form of a heatmap, see color code below. In cases where Acet is zero, proteins from treatment with the lowest abundance were set to one. Proteins written in red font indicate proteins involved in iron transport. The UniprotKB is given in brackets after the protein name.

Acet and Val specific proteins

COG	Name (Uniprot ID)	Acet	Prop	But	iBut	Val	iVal
M	Putative integrin, alpha subunit (D8DW34)	1.00	0.20	0.34	0.61	3.07	0.30
M	Acyltransferase (D8DYW5)	1.00	0.63	0.71	0.67	0.94	0.61
M	Biosynthetic peptidoglycan transglycosylase (A0A1H9D129)	1.00	0.86	0.80	0.80	1.00	0.83
M	Outer membrane protein assembly factor BamA (D8DWS2)	1.00	0.80	0.92	0.80	1.14	1.00
M	Outer membrane protein beta-barrel domain-containing protein (D8DW23)	1.00	0.00	0.00	0.37	1.07	0.00
M	Outer membrane protein beta-barrel domain-containing protein (D8DXU0)	1.00	0.58	0.42	0.54	0.72	0.41
M	Outer membrane protein OmpA (A0A1H9DD30)	1.00	0.87	0.87	0.93	1.08	0.92
M	Peptidyl-prolyl cis-trans isomerase (A0A1H8YU86)	1.00	0.75	0.59	0.74	0.78	0.77
M	Putative membrane protein (D8DVX1)	1.00	0.72	0.69	0.85	0.87	0.66
M	Uncharacterized protein (A0A1H9FPB8)	1.00	0.98	0.98	0.93	1.29	0.93
P	Fur family transcriptional regulator, peroxide stress response regulator (D8DTP6)	1.00	0.31	0.08	0.19	1.64	0.07
P	Carboxypeptidase (D8E0I3)	1.00	0.60	0.80	0.86	0.94	0.82
P	Ferrous iron transport protein B (D8DT71)	1.00	0.87	0.84	0.76	1.09	0.67
P	Iron complex outer membrane receptor protein (A0A1H9ICS8)	1.00	0.31	0.36	0.29	0.71	0.31
P	Outer membrane receptor for ferrienterochelin and colicins (D8E003)	1.00	0.21	0.16	0.23	0.83	0.10
P	Outer membrane receptor proteins, mostly Fe transport (D8DSX8)	1.00	0.00	0.00	0.00	0.45	0.00
P	TonB-dependent Receptor Plug Domain (A0A1H8ZS43)	1.00	0.51	0.45	0.63	0.91	0.44
P	TonB-linked outer membrane protein, SusC/RagA family (A0A1H9C2R2)	1.00	0.87	0.86	0.81	0.98	0.91
P	TonB-linked outer membrane protein, SusC/RagA family (A0A1H9LDK0)	1.00	0.84	0.81	0.85	0.94	0.82
P	Uncharacterized protein (D8DZ73)	1.00	0.59	0.78	0.53	1.33	0.64
P	Zinc ABC transporter, ATP-binding protein ZnuC (D8DT91)	1.00	0.75	0.75	0.70	0.90	0.76
S	Imelysin (D8DZR1)	1.00	0.28	0.29	0.30	1.09	0.16
S	AAA domain-containing protein, putative AbiEii toxin (D8DVG6)	1.00	0.90	0.95	0.92	1.03	0.87
S	ATP:cob(I)alamin adenylyltransferase (D8DZF8)	1.00	0.65	0.52	0.63	0.75	0.62
S	DedA family protein (D8DV79)	1.00	0.43	0.55	0.52	0.61	0.43
S	FeS assembly SUF system protein (D8DU67)	1.00	0.60	0.70	0.72	0.98	0.71
S	Glutamate-ammonia ligase (D8DTI2)	1.00	0.72	0.77	0.76	1.33	0.58
S	HmuY protein (D8E002)	1.00	0.25	0.21	0.29	0.98	0.13
S	LruC domain-containing protein (D8DZM3)	1.00	0.39	0.54	0.47	0.92	0.66
S	Membrane protein YfhO (D8DVQ7)	1.00	0.97	0.95	0.82	1.10	0.82
S	PepSY-associated TM helix domain protein (D8DUK5)	1.00	0.51	0.53	0.00	0.58	0.00
S	Peptidase, M16 family (D8DUF2)	1.00	0.35	0.60	0.46	0.71	0.40
S	Predicted ATP-binding protein involved in virulence (A0A1H9KT98)	1.00	0.85	0.90	0.87	0.96	0.84
S	Putative lipoprotein (D8DSX9)	1.00	0.00	0.26	0.25	0.71	0.00
S	Putative lipoprotein (D8DZ94)	1.00	0.53	0.55	0.61	0.70	0.58
S	Putative lipoprotein (D8E004)	1.00	0.31	0.24	0.29	1.04	0.14
S	Putative membrane protein (D8DZ34)	1.00	0.00	0.00	0.00	1.76	0.00
S	RloB-like protein (A0A1H9GW48)	1.00	0.85	0.91	0.00	0.92	0.00
S	RNA polymerase Rpb6 (D8DYA9)	1.00	0.96	0.99	0.75	1.04	0.81

Color code: 0.00 0.2 0.5 1.0 1.5 2.0

Figure S8: Acet and Val treatment specific proteins. Label-free quantification (LFQ) values are related and standardized by the Acet treatment and represent the average abundance in form of a heatmap, see color code below. In cases where Acet is zero, proteins from treatment with the lowest abundance were set to one. Proteins written with a red font indicate proteins involved in iron transport. The UniprotKB is given in brackets after the protein name. Proteins are sorted by the major clusters of orthologous groups (COGs). COG functions: membrane and cell wall assembly (M), inorganic transport (P) and unknown function (S).

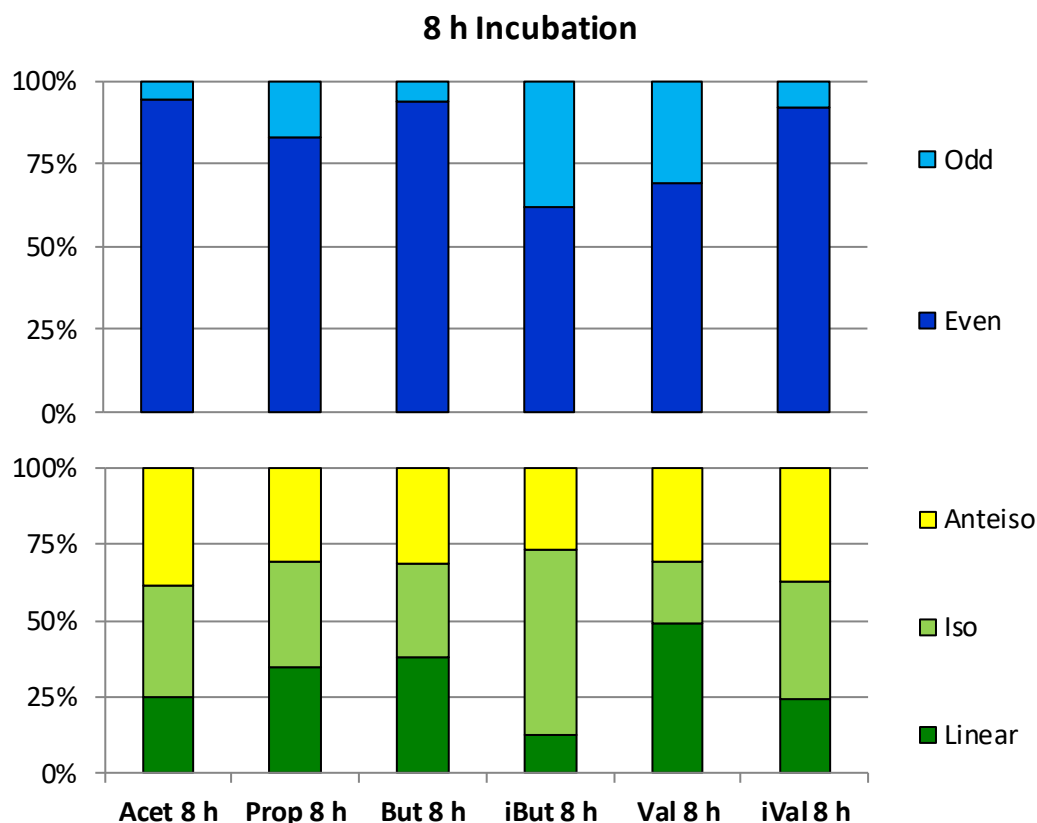


Figure S9: Percentile distribution of long-chain fatty acids (LCFA) by traits of chain length and branching structure after 8 h incubation. The distribution of the trait with odd or even number of the straight chain length of carbon atoms is shown in bluish colors (**upper**). The chain length trait divides the fatty acid length in even for Acet, But and iVal and odd for Prop, iBut and Val. The distribution of non-branched (linear), iso- or anteiso methylated long-chain fatty acids are in yellow-greenish colors (**lower**). SCFAs are grouped by the branching trait in linear for Acet, Prop, But, Val and in iso for iBut and iVal. The two traits are calculated by the sum of the percentile appearance in the LCFA-profile.

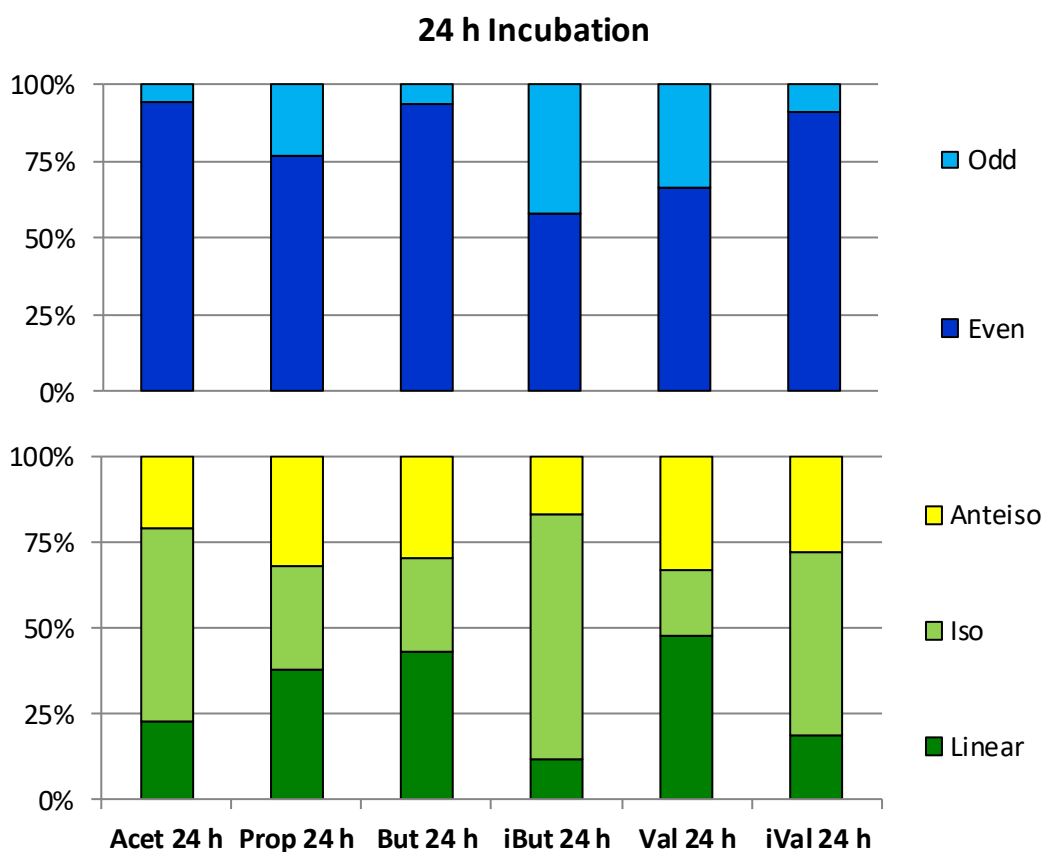


Figure S10: Percentile distribution of long-chain fatty acids (LCFA) by traits of chain length and branching structure after 24 h incubation. The distribution of the trait with odd or even number of the straight chain length of carbon atoms is shown in bluish colors (**upper**). The chain length trait divides the fatty acid length in even for Acet, But and iVal and odd for Prop, iBut and Val. The distribution of non-branched (linear), iso- anteiso methylated long-chain fatty acids are in yellow-greenish colors (**lower**). SCFAs are grouped by the branching trait in linear for Acet, Prop, But, Val and in iso for iBut and iVal. The two traits are calculated by the sum of the percentile appearance in the LCFA-profile.

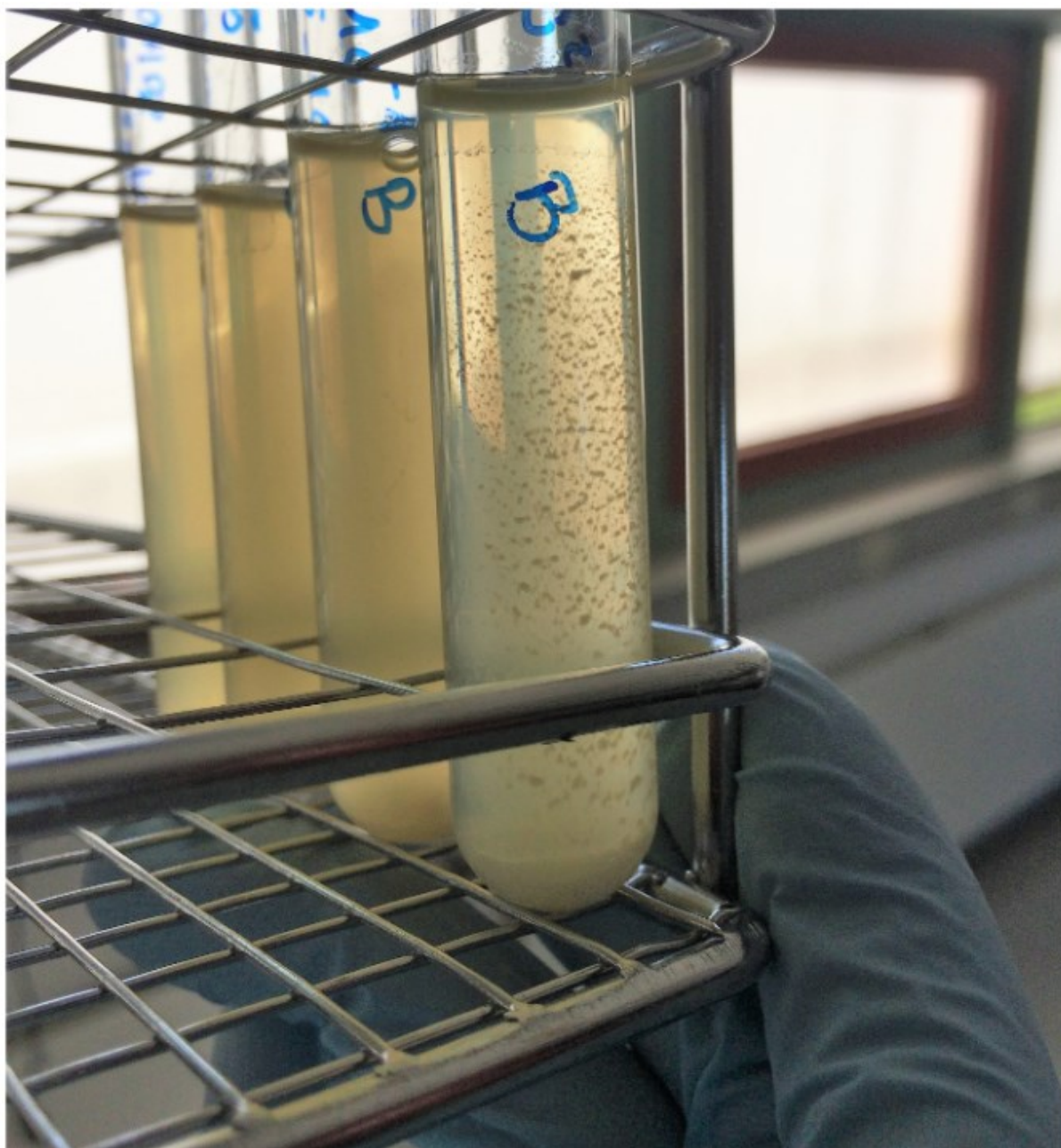


Figure S11: iVal cultivation of *P. bryantii* B₁₄ in Hungate tubes. Cell pellet formation at the bottom of the tube and aggregate formation at the wall of the tube. Cells in other cultivation conditions are homogenously distributed.

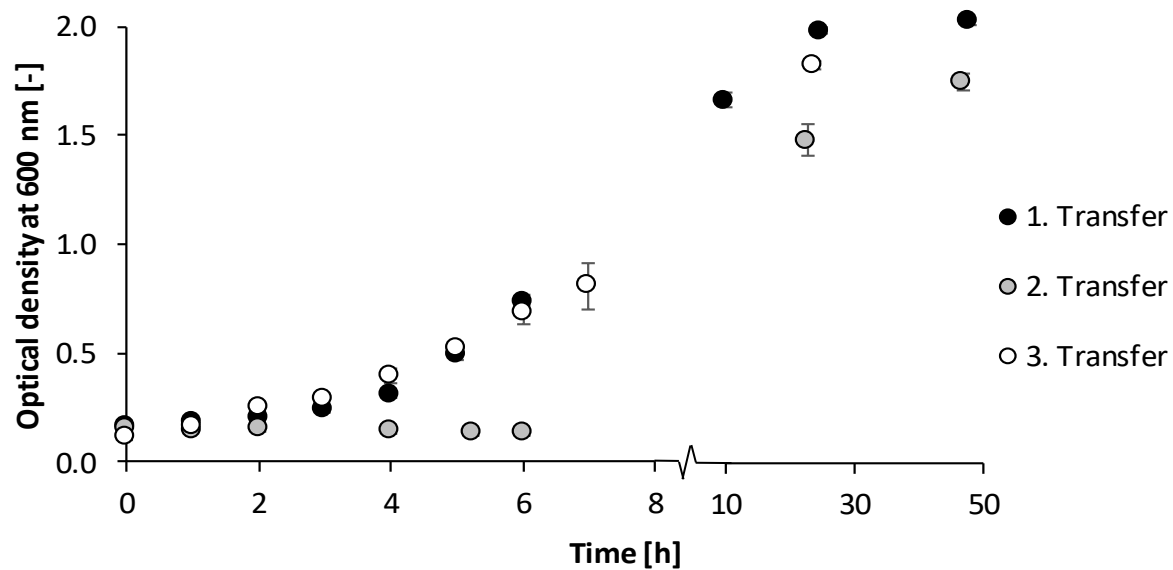
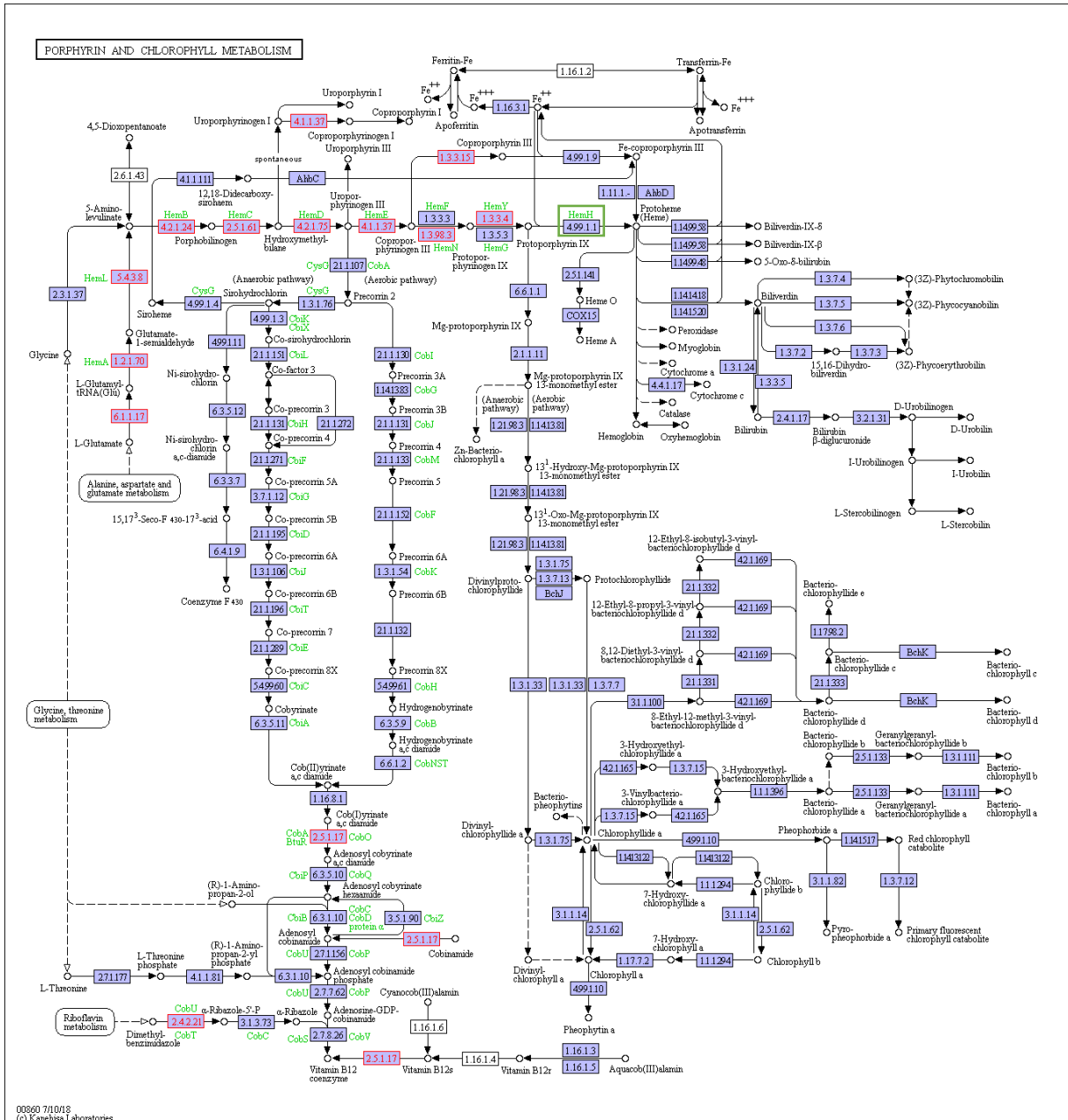


Figure S12: Growth curve of cultures transferred into SCFA-free media. Media composition was similar except the addition of any SCFAs. Inoculation and transfer volume: 4% (v/v). Optical density measurements were conducted in Hungate tubes at a wavelength of 600 nm. Time axis is compressed from 10 to 50 h after inoculation.



00860 7/10/18
(c) Kanehisa Laboratories

Figure S13: KEGG pathway of porphyrin and chlorophyll metabolism found in all treatments. The fields with red letters represent the found enzymes from all treatments combined. The pathway is completed from L-glutamate down to protoporphyrin IX. The orange marked enzyme is the one which annotation is missing.

3. Na⁺-coupled respiration and reshaping of extracellular polysaccharide layer counteract monensin-induced cation permeability in *Prevotella bryantii* B₁₄

by Andrej Trautmann ^{1,2}, Lena Schleicher ^{1,3}, Jana Pfirrmann ², Christin Boldt ⁴, Julia Steuber ^{1,3} and Jana Seifert ^{1,2,*}

¹ HoLMiR - Hohenheim Center for Livestock Microbiome Research, University of Hohenheim, Stuttgart, Germany

² Institute of Animal Science, University of Hohenheim, Stuttgart, Germany

³ Institute of Biology, University of Hohenheim, 70599 Stuttgart, Germany

⁴ Institute of Bioscience, TU Bergakademie Freiberg, 09599 Freiberg, Germany*

Correspondence: jseifert@uni-hohenheim.de; Jana Seifert (University of Hohenheim, Institute of Animal Science, Emil-Wolff-Str. 6-10, 70593 Stuttgart, Germany)

Journal: Int. J. Mol. Sci. 2021, 22(19), 10202; <https://doi.org/10.3390/ijms221910202>

Received: 30 August 2021 / **Revised:** 17 September 2021 / **Accepted:** 20 September 2021 /

Published: 22 September 2021

3.1 Abstract

Monensin is an ionophore for monovalent cations, which is frequently used to prevent ketosis and to enhance performance in dairy cows. Studies showed the rumen bacteria *Prevotella bryantii* B₁₄ being less affected by monensin. As there is still a lack of knowledge about defense mechanisms against monensin, the present study aimed to reveal more information about the respective molecular mechanisms in *P. bryantii*. Cell growth experiments applying increasing concentrations of monensin and incubations up to 72 h were done. Harvested cells were used for label-free quantitative proteomics, enzyme activity measurements, quantification of intracellular sodium and extracellular glucose concentrations and fluorescence microscopy. Our findings confirmed an active cell growth and fermentation activity of *P. bryantii* B₁₄ despite monensin concentrations up to 60 µM. An elevated abundance and activity of the Na⁺-translocating NADH:quinone oxidoreductase counteracted sodium influx caused by monensin. Cell membranes and extracellular polysaccharides were highly influenced by monensin indicated by a reduced number of outer membrane proteins, an increase of certain glucoside hydrolases and an elevated concentration of extracellular glucose. Thus, a reconstruction of extracellular polysaccharides in *P. bryantii* in response to monensin is proposed which is expected to have a negative impact on the substrate binding capacities of this rumen bacterium.

Keywords: Monensin; *Prevotella bryantii* B₁₄; Proteomics; Na⁺-translocating NADH:quinone oxidoreductase; Extracellular Polysaccharides; Biofilms

3.2 Introduction

Use of antibiotics in livestock farming is a crucial aspect for health of a dense stock. A common found antibiotic in poultry farming and cattle fattening is monensin [154]. Since 1996 in Denmark, 1999 in Switzerland and 2006 in the European Union, the application of monensin as a growth promotor in livestock farming became restricted to therapeutic interventions [65-67]. An overuse of antibiotic growth promotors was regarded as concerning due to formation of antibiotic resistance mechanisms. Therefore, utilization of monensin is restricted to the treatment of ruminal ketosis, acidosis and coccidiosis in dairy cows [155-157] and monensin supplementation to poultry feed was permitted again in 2020 by the European Union [68].

Monensin and its derivates were originally isolated from the soil bacteria *Streptomyces cinnamonensis*, which synthesizes the compound via the precursor butyrate and iso-butyrate [80, 81, 158]. A self-intoxication by monensin is prevented due to the anti-isobutyrate factor (AIB), which allows *S. cinnamonensis* to resist not only monensin but also to toxic concentrations of short-chain fatty acids (SCFAs)[159]. Several rumen microorganisms such as *Selenomonas ruminantium* and *Methanobacterium ruminantium* appeared to be insensitive towards monensin, while *Fibrobacter succinogenes*, *Bacteroidetes succinogenes*, *Prevotella ruminicola* and *Bacteroidetes ruminicola* showed a retarded growth in presence of monensin [64, 155]. Monensin is classified as an ionophore, which disrupts gradients of monovalent cations [61]. Multiple studies showed an increased cross-resistance of ruminal microorganisms, after exposure to sub-lethal concentrations of ionophores like lasalocid, nigericin, valinomycin, tetranosin or monensin [61, 64, 85, 160, 161]. Callaway and Russell [61] described several resistance mechanisms like: uncoupler translocase to transfer monensin away from its target location [162], change of membrane fatty acid composition to prevent monensin binding [163], reduction of porin size for passage inhibition [155, 161] and formation of extracellular polysaccharides (EPS) to prevent monensin binding to its target [164]. Monensin cell binding can also be reduced by TRIS-EDTA washing, as it was shown for mixed ruminal bacteria [95].

Only some small subpopulations seem to adapt and are able to establish persistence mechanisms. In comparison to other *Prevotella* species, *P. bryantii* B₁₄ was less affected by high concentrations of monensin (20 µM) and showed a slightly reduced cell density [82]. Especially in the ruminal ecosystem *P. bryantii* B₁₄ seemed to be more resilient towards

monensin exposition [88]. Higher concentrations of monensin (up to 60 μM) were also tolerated by *P. ruminicola* strain 23 and strain GA33 [160].

In the present study, monensin adaptation mechanisms in *P. bryantii* based on proteomic, enzymatic and microscopic results are shown. The study also elucidates upcoming general resistance strategies in bacteria towards ionophore antibiotics involving cell surface modifications promoting for biofilm formation.

3.3 Results

3.3.1 Inhibition of *Prevotella bryantii* B₁₄ growth by increasing monensin concentrations

Dose-dependent effects of monensin on *P. bryantii* growth were tested using 15 concentrations in a range between 0.1 to 60 μM . Optical density (OD) was monitored every 30 min for 7 h. An analysis of variance showed no significant differences between the ODs at 7 and 24 h of incubation ($p=0.486$, Figure 11a). OD decreased gradually from $\text{OD}_{24\text{h}}=1.90$ at 0 μM to the lowest OD at 20 μM monensin ($\text{OD}_{24\text{h}}=1.39$). The minimal inhibitory concentration (MIC) defined by significance in OD was shown at 1 μM ($p<0.01$). The strongest growth inhibition was seen with 20 μM whereas the subsequent monensin treatments (30, 35 and 60 μM) showed a slight increase of the OD indicating a degressive dose-dependent relationship (Figure 11a). A mirrored development was seen for pH values showing the highest pH at 20 μM ($\text{pH}_{24\text{h}}=5.76$; $p<0.01$; Figure 11b). The lowest pH, meaning the highest acid production, was observed under 0.1 μM monensin ($\text{pH}_{24\text{h}}=5.48$). Treatments above 10 μM monensin revealed a lag phase of 3.5–4 h, while without monensin a maximum of 1 h lag-phase was determined. The slowest growth rate was found at 20 μM monensin (Figure S14). Control cultures incubated with EtOH (1.3% (v/v)) showed no effect on final OD, whereas pH was higher with EtOH as without ($p=0.047$)

Four concentrations (0, 10, 20 and 50 μM) were selected for cultivation in up scaled volumes ($v=103$ mL). Six biological replicates per monensin concentration were harvested after 9 h of incubation and OD, pH, intracellular sodium, glucose in culture supernatant and proteome of *P. bryantii* cells were analyzed. A lowered OD was observed at monensin concentrations of 20 μM and 50 μM , as compared to the Hungate tube cultures (OD of 1.4 vs. 1.0 in 20 μM monensin treatments, Figure 12a). The pH changed significantly between the treatments, except for 20 and 50 μM (Figure 12b).

Intracellular sodium concentrations were monitored to determine the effect of the ionophore monensin on *P. bryantii* B₁₄ cells. Mean intracellular Na⁺ concentration of 128 µg sodium per milligram protein was found in the control (without monensin) and set as reference (Figure 12c). In the presence of 10 µM monensin, intracellular Na⁺ was significantly reduced ($p < 0.01$) to 33 µg/mg protein and increased with rising monensin concentration to 105 µg/mg protein (Figure 12c).

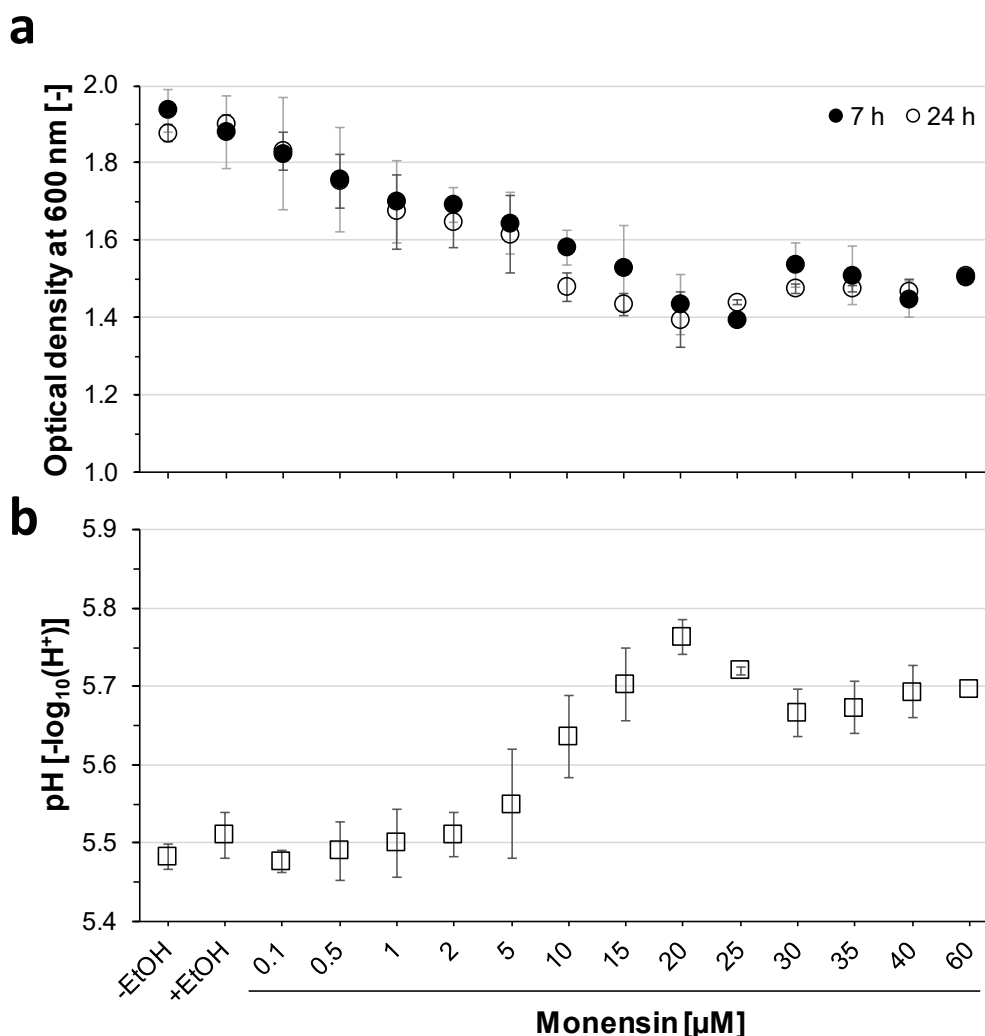


Figure 11: Optical density and pH values of *P. bryantii* B₁₄ using a range of monensin concentrations in Hungate tube cultures. **a:** Mean optical density (OD) after 7 h (black) and 24 h (white) of incubation are given with error bars for standard deviation (n=3). No significant difference was observed between 7 and 24 h (ANOVA: $p = 0.486$). **b:** The pH average after 24 h (white squares) of incubation are given with error bars for standard deviation (n=3). Two controls -without monensin excluded or included (-/+ EtOH). Significances were proven by Fisher LSD-test ($p < 0.01$).

Glucose consumption was measured to determine the effect of monensin towards sugar uptake and fermentation activities. Without monensin almost all glucose was consumed, which resulted in a leftover of 0.06 g/L after 9 h of incubation. A residual amount

of glucose in the medium was found for 10 μM monensin (0.2 g/L), while at higher monensin levels (20 and 50 μM) about 0.8 and 0.9 g/L of glucose remained in supernatant ($p < 0.01$, Figure 12d).

3.3.2 Growth adaptations towards monensin over time

A prolonged incubation (up to 72 h) with 20 μM monensin showed a significantly decreased cell density ($p < 0.001$) at all-time points (Figure 13a), while OD without monensin remained stationary and pH dropped faster and achieved a lower pH as with monensin (Figure 13b). In absence of monensin, glucose was already consumed after 3 h, while with 20 μM

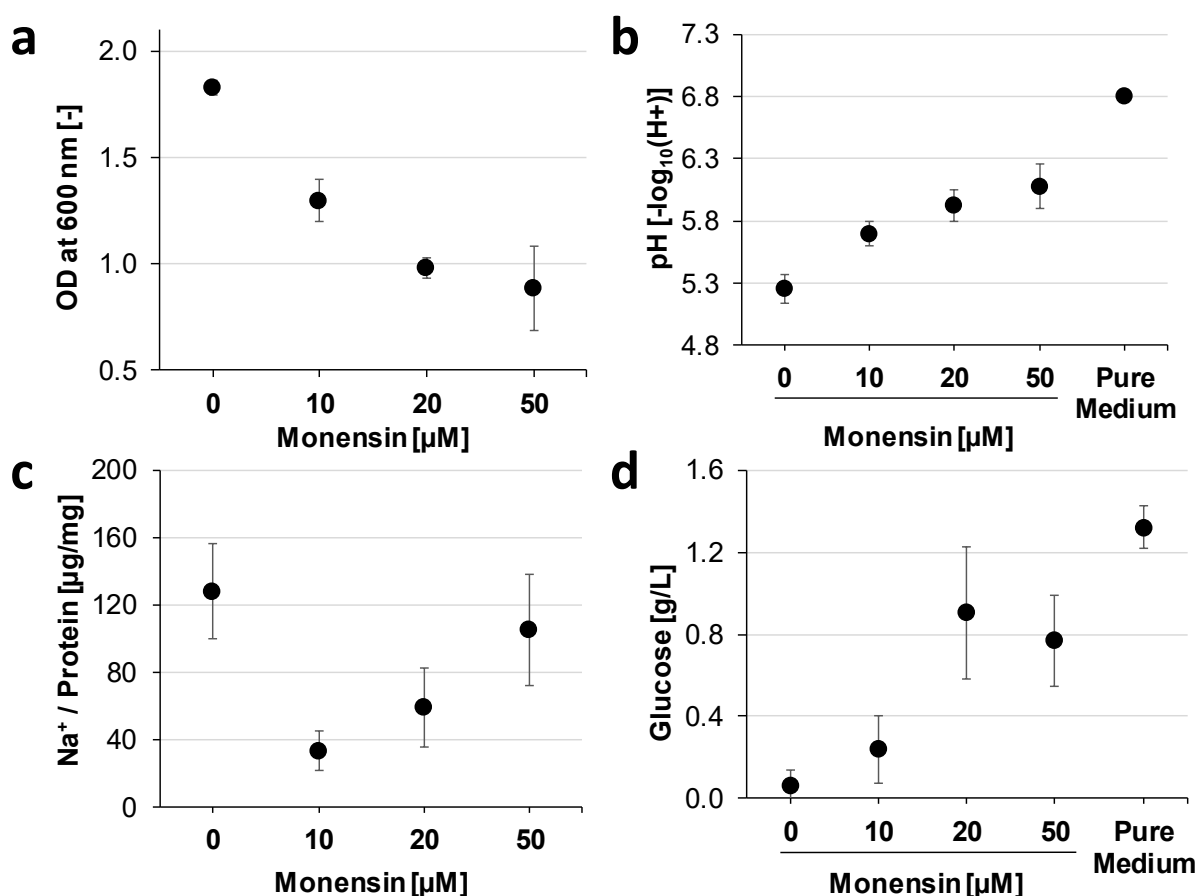


Figure 12: Growth and fermentation reducing monensin triggers intracellular sodium efflux in *P. bryantii* B₁₄. Parameters were obtained from 100 mL cultivations after 9 h growth under monensin concentrations (0, 10, 20 and 50 μM). The average of six biological replicates was displayed for every measurement and condition. Error bars indicate standard deviation if not stated separately. (a) Optical density. (b) pH, adjusted pH of 6.8 is displayed for the non-inoculated pure medium. (c) Intracellular Na⁺ concentration analyzed by ICP-MS and standardized by the protein concentration. The treatment without monensin was set as reference (100%) and error bars indicate standard error mean (SEM). (d) Relative D-glucose concentration in supernatant, which is in pure medium below the supplemented 2 g/L due to the Maillard reaction during autoclaving.

monensin glucose concentration was stable from 6 to 24 h on a low level and increased significantly at 48 and 72 h of incubation ($p < 0.01$, Figure 13c). Glucose-6-phosphate was

quantified concomitantly with glucose showing a significant elevation starting at 48 h ($p < 0.01$, Figure 13d).

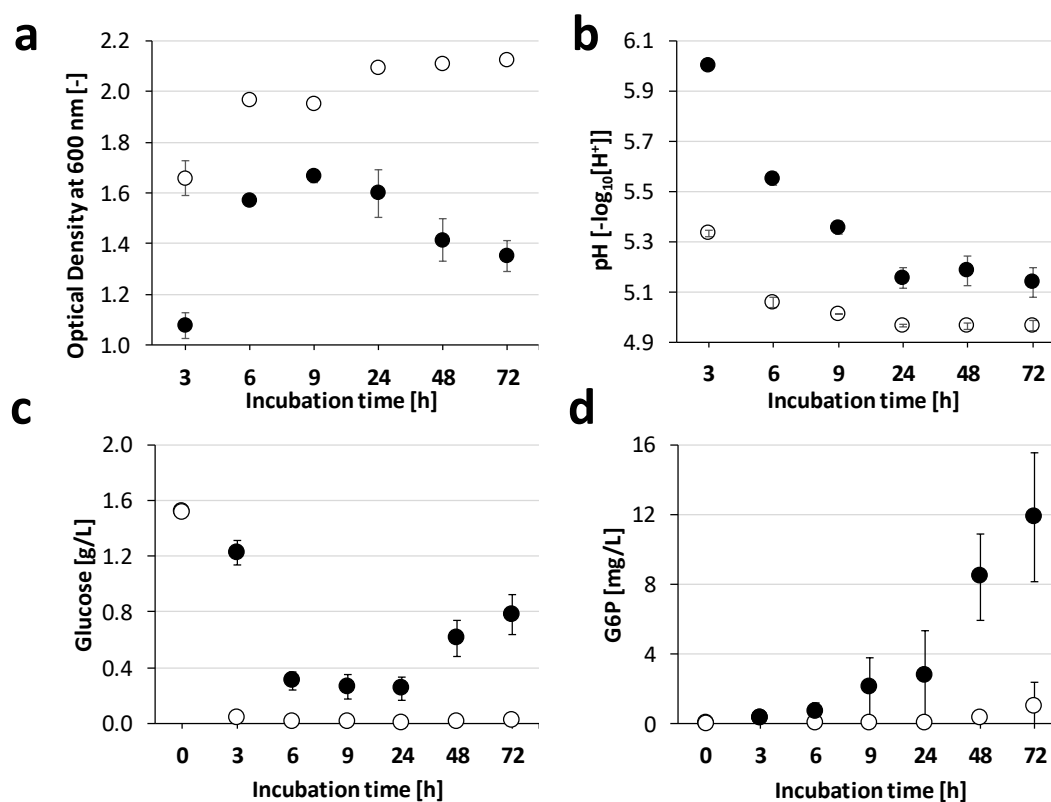


Figure 13: Glucose and glucose-6-phosphate in supernatant are displayed over time in two monensin conditions (○ 0 μM and ● 20 μM). Small letters indicate least significant difference (LSD) between time points for monensin group with p -values indicated in brackets. Measurements for 0 and 20 μM were significantly different ($p < 0.01$). Measuring at 0h was performed with non-inoculated medium. All measurements display the average as a dot and error bars as standard deviation (SD). **(a)** Optical density at 600 nm wavelength ($p < 0.01$). **(b)** pH of cultivation media ($p < 0.01$). **(c)** Extracellular glucose only with LSD-test for 20 μM ($p < 0.01$). **(d)** Extracellular glucose-6-phosphate (G6P) only with LSD-test for 20 μM ($p < 0.05$).

3.3.3 Dose-dependent modulation of the proteome of *Prevotella bryantii* B₁₄ by monensin

P. bryantii B₁₄ cultures were exposed to 0, 10, 20 and 50 μM monensin, from which proteins were extracted after 9 h of cultivation. A total of 1,686 proteins were identified and quantified in at least one sample (Data S1, see Trautmann, A., *et al.* [2]). The number of label-free quantified proteins ranged from 985 to 1,349 proteins per sample (Table S10). All cultivation conditions shared 905 proteins (Figure S15), while all samples shared 742 proteins. The principal component (PCO) analysis (Figure 14) showed a total variation of 95.5% between samples with and without monensin. Both clusters showed a similarity of 80% within each other, while 20% of proteins were shared with a similar expression pattern (Fold-change <

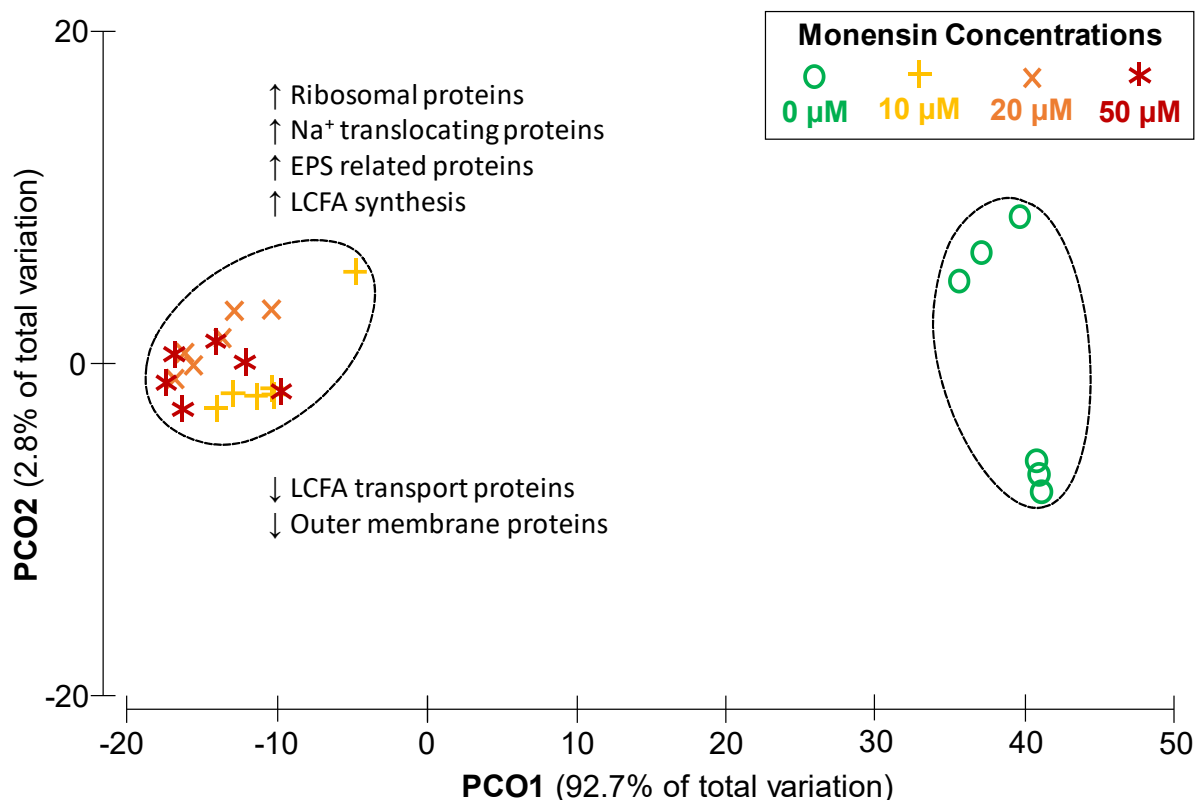


Figure 14: Changes of *P. bryantii* proteomes at different monensin conditions. Each condition consisted of six replicates (n=6). Principal component analysis with 1,686 label-free quantified proteins resulted in two clusters of 80% similarity dividing in with (left) and without monensin (right). Monensin concentrations are depicted in green (0 μM), yellow (10 μM), orange (20 μM), red (50 μM). Arrows with functional assignment indicate a high (↑) or low (↓) abundance of mentioned functional protein groups.

1.5). Minor differences in protein abundances among monensin treated cells were observed in a low fraction of proteins (2%; 35 proteins), whereas most proteins (64.7%; 1,091 proteins) revealed a fold-change difference of more than two.

Changes of functional proteins showed a major shift in clusters of orthologous groups (COGs) during monensin supplementation (Table S11). Proteins belonging to the COGs of translation, ribosomal structures and biogenesis (J), post-translational modification, protein turnover and chaperones (O), transcription (K), energy production (C) and intracellular trafficking, secretion and vesicular transport (U) were significantly elevated in abundance (≥1%) with monensin. COGs responsible for cell wall-, membrane- and envelope biogenesis (M), as well as ion transport and metabolism (P) and a vast number of proteins with unknown functions (S, !S) were significantly depleted in monensin treated cells.

The number of identifications and abundance of outer membrane proteins decreased in monensin treated cells (Table S12). Proteins involved in iron and fatty acid transport as well

as defense mechanisms were less abundant in monensin cultures. Several miscellaneous transporters targeting cations (Na^+ , K^+ , Ca^{2+} and Zn^{2+}), peptides, amino acids, sugars and phosphate were more abundant in monensin treatments (Table S13). Despite enhanced expression of iron related transporters at 0 μM monensin, ferrous iron transport protein B (feoB, D8DT71) was increased around 15–17 fold in presence of monensin (Table S13). Additionally, import related proteins (TonB, RagB/SusD, IPT/TIG domain containing) highly correlated ($R \geq 0.7$) with intracellular Na^+ concentration (Table S14).

A 5-fold higher abundance was seen for the phospholipid/cholesterol transport protein (A0A1H8YR75) in monensin cultures. Abundance of most detected ribosomal proteins increased under monensin supplementation, except 50S subunit ribosomal protein L29 decreased, which was positively correlating with OD and pH ($R^2=0.78$ and $R^2=0.77$).

Special emphasis was given on sodium transport proteins like the Na^+/H^+ antiporter NhaD (D8DYG5) and the phosphate Na^+ -symporter (A0A1H9BJD7), which were increased almost similarly among all monensin doses (Table S13). The sodium/glucose cotransporter (D8DYQ7) was quantified in all treatments and increased gradually with the monensin concentration (Table S13). Subunits of Na^+ -translocating NADH:quinone oxidoreductase (NQR), which are involved in anaerobic respiration and quantified at all culture conditions were analyzed under increasing monensin concentrations (Figure 15a). Similar to Na^+ transporting proteins, NQR subunits were also differently abundant and ranging from 1.5 to 4-fold compared to proteins without monensin, which were set to a fold-change of one. In total, NQR proteins were more abundant during monensin supplementation and increased with prolonged incubation time (Table S15). Observed differences of the NQR abundance in *P. bryantii* cells were confirmed by measurements of NADH oxidation and 2,3-dimethyl-1,4-naphthoquinone reduction activity in isolated membranes of *P. bryantii* grown without or with 10 μM monensin (Figure 15b). The fold-change in activity was set for 0 μM monensin to one and showed a 2–4.3-fold higher activity in 10 μM monensin cultures.

Twenty-four uncharacterized proteins of *P. bryantii* B₁₄ exceeded a fold-change greater than five in monensin cultures. Blast search of five of those resulted in a score of 90 and functional assignments were proposed (Table S16). Protein D8DVZ9 revealed in Blast search the highest similarity to the YghO protein, which is known to act as an N-acetyltransferase.

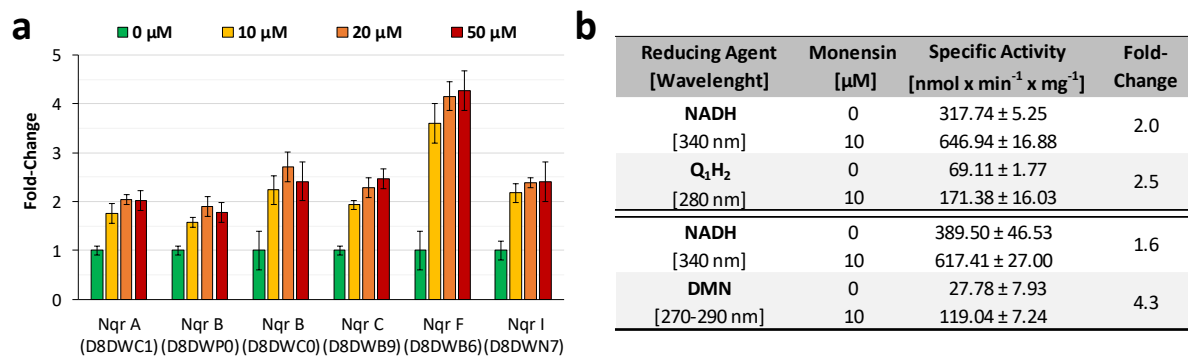


Figure 15: Na⁺-translocating NADH-Quinone reductase (NQR) abundance and activity under presence or absence of monensin. **(a)** Bar plot with mean abundance (n=6) of NQR subunits including their standard deviation represented as error bars. The Uniprot ID is given in brackets. **(b)** Mean specific activity (n=3) and standard deviation of NQR. Oxidation NADH, and formation of ubiquinone (Q₁H₂) and menaquinone (DMNH₂) were followed with membranes of *P. bryantii* B₁₄.

3.3.4 Protein modification in monensin cultures over time

Prevotella bryantii B₁₄ cultivations with 0 and 20 μM monensin were carried out for 72 h taking samples at four different time points. Whole data sets showed a variation of 84.1% in a PCO plot (Figure 16). Samples grouped mainly according to presence and absence of monensin and shifted by time within their grouping along PCO1. Peptide and protein counts are listed in Table S17. Including all time points, 625 proteins for control and 942 proteins for monensin conditions were quantified (Data S2 see Trautmann, A., *et al.* [2], Figure S16). After 9 h, 178 proteins (14%) appeared in the following time points of control group. The monensin exposed proteome showed 222 proteins (18%), shared by all time points except 72 h. Both conditions showed small but dominant fraction (9-11%) of proteins, which appeared only at 9 h. Relative abundance of COG classes, revealed a significant difference between the control and the monensin-supplemented cultivation for the majority of proteins (Table S18). Samples without monensin showed elevated abundances of outer membrane proteins and proteins of post-translational modification (Table S18). Proteins of the monensin cultures shifted in a minor scale as the control and had increased abundances of transferases, ribosomes as well as a higher level of NQR at the beginning of the cultivation. COGs more abundant in monensin-cultivated cells belonged mainly to translation, ribosomal structure and biogenesis (J), energy production and conversion (C) and carbohydrate transport and metabolism (G). Most abundant COGs in the control were belonging to inorganic ion transport and metabolism (P), function unknown (S and S!), cell/membrane/envelope biogenesis (M) and post-translational modification, protein turnover and chaperones (O). Most proteomic differences between time

points appeared between the late exponential phase (9 h) and the residual time points (Figure 16).

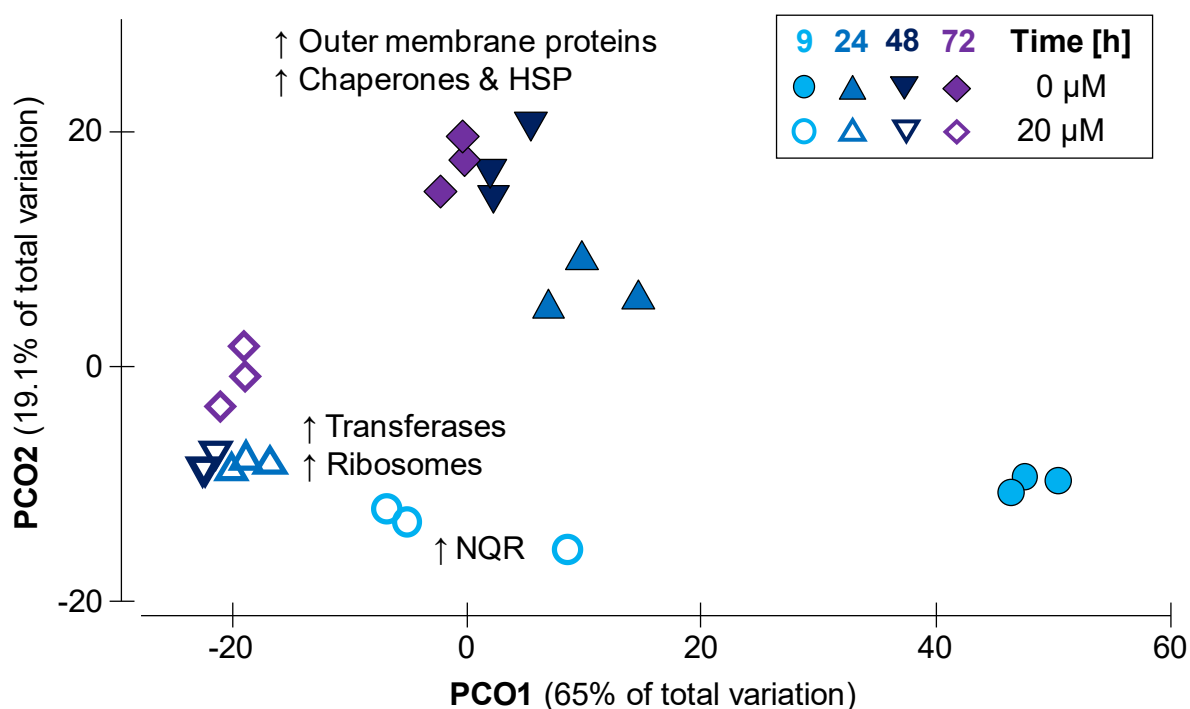


Figure 16: Changes of *P. bryantii* proteomes at 0 and 20 μM monensin after 9, 24, 48 and 72 h of incubation time. Four time points at two monensin conditions contained triplicates (n=3). Data underwent a standardization by total, followed by resemblance matrix formation via Bray Curtis similarity.

Proteins belonging to the COG classes of the energy production and conversion (C) as well as the carbohydrate transport and metabolism (G) were closer investigated due to the observed increase of extracellular glucose in monensin supplemented cells after 24 h (Figure 13c). No clear elevation of proteins connected to gluconeogenesis were observed but an increase of glucosidases responsible for conversion of maltose, cellobiose, dextrin, cellodextrin, starch, and β-glycosides to glucose was identified (Table S19). Seventy-two different carbohydrate-active enzyme families (CAZymes) showed a predominance of GH13 and GH2 in monensin-supplemented cells, while families PL1 and GH43 were predominant in the control (Table S20). Family GH2 was equally distributed while the distribution of proteins belonging to other CAZyme families could not be analyzed since they were underrepresented (Proteins<5).

3.3.5 Altered EPS structure in monensin cultivations

To analyze the effect of monensin on EPS structure, cells were cultured without and with (20 μ M) monensin for 24, 48 and 73 h, harvested, and processed for confocal imaging. Double staining of EPS and nucleic acid (cells) confirmed structural changes in EPS under monensin supplementation (Figure 17). Compact and linear EPS structures were found in monensin cultivations, while EPS from control conditions appeared to be more branched and complex, especially seen in EPS dense regions (Figure 17A). In absence of monensin, cells were mostly embedded into the EPS, while in monensin cultures cells were dissolved out of the EPS (Figure 17B). After 48 h, fringed edges of EPS were observed with monensin-exposed cells, whereas EPS edges from untreated cells were blunt and smooth (Figure 17C). Additionally, a decelerated development of EPS was seen with monensin supplementation over time (Figure 17).

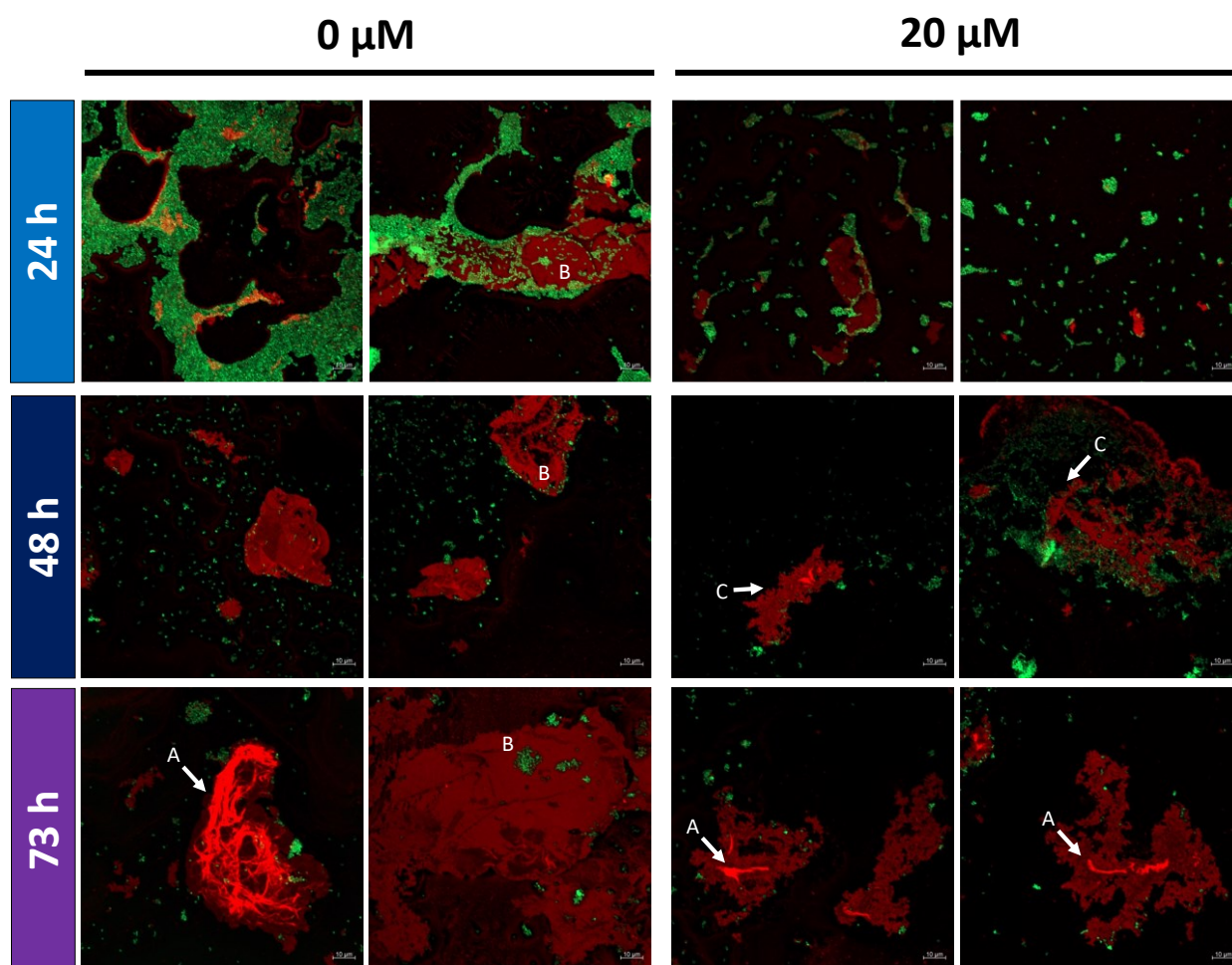


Figure 17: Fluorescence microscopy of *P. bryantii* B₁₄ cells at 24, 48 and 73 h of cultivation with 0 and 20 μ M monensin. Fluorescence stain of EPS (red, Alexa Fluor 594) and DNA (green, SYTO 9). Each condition is presented in duplicates. Lower right corner indicates a size reference of 10 μ M. Capital letters point at dense EPS regions (A), cells embedded in EPS (B) and at fringed edges of EPS layer (C).

3.4 Discussion

3.4.1 Degressive dose-response to monensin

Monitoring OD and pH in the first seven hours of monensin exposure revealed a degressive dose-response relationship and showed that a monensin concentration of 20 μM is the most effective for the inhibition of growth and fermentation activity in *P. bryantii* B₁₄. Callaway and Russell reported only a weak growth inhibition for monensin concentrations up to 20 μM [82]. For *Bacteroides ruminicola* (reassigned as *Prevotella ruminicola* GA33) a linear inhibition and slower growth was shown up to 40 μM monensin, but with less tested concentrations [64]. An explanation for the newly observed stagnation of the antibiotic effect beyond 20 μM monensin might be the maximal capacity of monensin accumulation into the membrane, because of its lipophilic property [82]. Another impact on cell surface composition and cell division is caused by the murein layer deconstruction, which has to be performed in the area of the septal ring [165]. Increased abundance of cell division proteins (Clp, Fts) in monensin cultures (Table S21) with prolonged incubation seemed to compensate slower growth rate and lower OD.

3.4.2 Cation permeability affects proteome and metabolism

Growth inhibition caused by monensin is primarily explained by the disruption of the ion gradient for monovalent cations (K^+ , Na^+ , H^+), which is caused by an increased cation permeability [61]. Considering the increased membrane permeability for protons, the intracellular pH is probably acidified with progressing fermentation [166, 167]. Therefore, inhibition of cytoplasmic metabolism is presumed due to intracellular acidification, which is unfavorable for enzymatic activities. Since fermentation was therefore stopped after 24 h of monensin cultivation, glucose remained in the supernatant. Inhibition of glucose transport can be rejected, as sodium/glucose cotransporter (D8DYQ7) was even almost 3-fold elevated in monensin cultures on proteome level.

In a previous study, a decrease of 85% cytoplasmic K^+ was described when 10 μM monensin was applied [82]. A similar finding was seen in the current study for Na^+ , suggesting an enforced Na^+ efflux by elevated abundance of NQR and other Na^+ -translocating proteins. Since *P. bryantii* possesses only genes encoding for the menaquinone (DMN) synthesis, but not for ubiquinone (Q1) synthesis, the fold-change of NQR activity with DMN appears closer to *in vivo* conditions. The activity fold-change of NQR with DMN was similar to fold-change of the protein abundances. NQR activity and abundance increased not gradually along the

gradient of monensin concentrations, but in a switch-like manner, as seen in the quantitative proteome analysis. This observation points out that the active export of Na⁺ was a countermeasure with respect to the uncontrolled cation permeability caused by monensin. A high correlation ($R \geq 0.7$) of Na⁺ concentrations with the abundances of certain outer membrane proteins might also be used as an indicator for the regulation of protein synthesis by the level of sodium in the cells. The Na⁺/H⁺ antiporter NhaD (D8DYG5) and cation translocating ATPases in *E. coli* and *Enterococcus* showed similar effects [168, 169].

3.4.3 Monensin triggers extracellular polysaccharide degradation by *P. bryantii* with a concomitant release of glucose

Glucose consumption was diminished with increasing monensin concentrations, while further investigation also showed an increase of glucose-6-phosphate, which is most likely derived from cell lysates. However, increasing glucose concentrations at 48 h and 72 h were unlikely to be formed in the gluconeogenesis pathway as proteins responsible for the gluconeogenesis such as fructose biphosphatase (EC 3.1.3.11), were not detectable in the peptide data. Morehead, M. and Dawson, K. [160] described a complete glucose consumption within 36 h for *Prevotella ruminicola* strains under 14 μ M monensin, while remnants of glucose were found in the current approach. Furthermore, increased glucose concentration in the culture supernatant at 48 and 72 h can be explained by the degradation of EPS facilitated through glucosidases and the inhibited glucose uptake mechanism with monensin supplementation. Glucosidase assignments were done based on KEGG orthology (KO), enzyme classification (EC) and CAZyme classification suggesting hydrolytic capacities of *P. bryantii* to convert various poly- and monosaccharides (cellobiose, maltose, dextrin, starch, glycogen) into glucose (Table S22). A β -glucosidase (A0A1H9IED8), with the ability to hydrolyze cellobiose, increased equally in protein abundance to the extracellular glucose in monensin cultures. This possible correlation and influence of the β -glucosidase was supported by supplementary experiments where glucose concentrations were enhanced in the presence of cellobiose and monensin in the cultures (Figure S17). The α -glucosidase (D8DXY7), able to depolymerize non-supplemented starch and dextrin, showed a strong increase in abundance over time in monensin cultures. The corresponding family GH2 uses galactose and mannose as potential substrates, which can be found as main components in EPS of *P. bryantii* [16]. Aside from the mentioned glucosidases, a vast number of transferases, mostly for sugars, as

well as the newly assigned protein N-acetyltransferase (YghO, D8DVZ9), were elevated in monensin cultures and are due to their functionality most likely connected to EPS structure.

Glucose is also used in EPS formation [170], and EPS may serve as a sacrificial layer against ionophore attachment on the cell membrane [164]. In the presented experiments, differences in stickiness of monensin-treated versus untreated cells during centrifugation and cell pellet suspension indicated an altered bacterial surface. This was also seen on proteome level as outer membrane proteins were depleted in abundance. Previous studies described the impact of antibiotics on the phospholipid bilayer, EPS hydrophobicity and lipopolysaccharides in other microorganisms [63, 85, 171-173]. The cell surface and membrane was highly influenced by monensin as outer membrane proteins and a vast number of proteins belonging to COG class M (cell wall/membrane/envelope biogenesis) were quantitatively changed. The Do/DeqQ family serine protease (D8DWJ3), highly abundant in monensin growing cells, decreased during the prolonged incubation time and had therefore a less suppressive effect on EPS formation [174]. Biofilm formation in *A. baumannii* was accompanied by elevated outer membrane proteins and proteins of the histidine metabolism [175]. A similar observation was made for the histidine pathway (Figure S18) in the present experiment but the opposite was found for outer membrane proteins.

Based on the present findings, the detachment and reconstruction of EPS in *P. bryantii* B₁₄ cells during monensin exposure is backed up by the following evidences:

1. An increased amount of EPS degrading enzymes such as glucosidases or COG M class proteins;
2. Elevated amounts of extracellular glucose;
3. Zones with EPS depletions in *P. bryantii* cell clusters

These arguments point towards a partial EPS deconstruction in cells treated with monensin, which is also in line with the two-layer EPS model explained by Nielsen, P.H. and Jahn, A. [176]. The theory states a dense and closely cell-attached inner layer, while the outer EPS layer is loosely bound and soluble. Fluorescence microscopy showed loosely detached EPS layers with signs of decomposition in monensin exposed cells. Stability of EPS in these cells seemed also diminished while handling cell pellets and microscopic slide preparation in comparison to cells grown without monensin. The two-layer EPS theory would explain the findings of Chow, J.M., *et al.* [95], who showed almost no binding of isotope labeled monensin

in *P. bryantii* B₁₄ cells or vesicles. Extensive composition analysis of the outer EPS layer could provide insights about quality and amount of EPS as well as potential monensin and its binding partners such as cations, which are also favorably bound to EPS [177]. This could be done in future experiments using anaerobic flow-cell cultivation techniques.

A degressive dose-response relationship was observed for fermentation and optical density towards incrementing monensin concentration. Protein adaptations to monensin operated in a switch-like manner similarly to the intracellular Na⁺ efflux, which was most likely regulated via elevated NQR activity and other Na⁺ translocating proteins. Monensin showed to have an impact on the outer cell membrane and the degradation of extracellular polysaccharides. An elevated abundance of certain glucoside hydrolases can be correlated to an increase of extracellular glucose. Thus, a detachment and partial degradation of EPS charged with monensin by *P. bryantii* is likely and can be described as a kind of protection or resistance mechanism. This should be evaluated in respect to the strain and its accompanied rumen community members, which need intact cell surfaces to bind and hydrolyze available substrates such as fibers.

3.5 Conclusions

A degressive dose-response relationship was observed for fermentation and optical density towards incrementing monensin concentration. Protein adaptations to monensin operated in a switch-like manner similarly to the intracellular Na⁺ efflux, which was most likely regulated via elevated NQR activity and other Na⁺ translocating proteins. Monensin showed to have an impact on the outer cell membrane and the degradation of extracellular polysaccharides. An elevated abundance of certain glucoside hydrolases can be correlated to an increase of extracellular glucose. Thus, a detachment and partial degradation of EPS charged with monensin by *P. bryantii* is likely and can be described as a kind of protection or resistance mechanism. This should be evaluated in respect to the strain and its accompanied rumen community members, which need intact cell surfaces to bind and hydrolyze available substrates such as fibers.

3.6 Materials and methods

3.6.1 Cultivation

Prevotella bryantii B₁₄ (DSM 11371) was cultivated under anaerobic conditions at 39°C and a starting pH of 6.8 ± 0.05. Medium composition was based on the M2-B medium from Trautmann, A., *et al.* [1] with utilizing glucose, maltose and cellobiose, instead of only glucose. Additionally, 1.4% (v/v) of a vitamin mix and monensin solution were injected into the Hungate tube via sterile filtration (pore size 0.2 µm) resulting in a total volume of 7.5 mL. A 100 µM monensin stock solution was prepared by solving monensin sodium salt (purity ≥ 90% Alfa Aesar) in pure EtOH (purity = 100%; Merck). Cells grown in M2-B without monensin or EtOH supplementation and a final optical density (OD) of at least 1.8 were used for inoculation (4-10% v/v, depending on the used culture volume). Effects of monensin on growth, EPS formation and fermentation parameters were investigated by using Hungate tube cultures (7.5 mL final volume). Cultivation flasks (103 mL final volume) were used additionally for sodium determination and proteomics. Cultivation in serum bottles (1 L final volume) was performed for cell enrichment required for the enzymatic assays.

3.6.2 Growth in presence of monensin

A broad range of monensin concentrations (0, 0.1, 0.5, 1, 2, 5, 10, 15, 20, 25, 30, 35, 40 and 60 µM) was used to determine the effect of monensin on growth parameters (OD, pH) and to define the minimal inhibitory concentration (MIC) by using the first significant difference in optical density compared to the control. EtOH was added to control cultures with equal volumes as used with monensin in EtOH. Hungate tube cultures were incubated for 24 h in triplicates. OD at 600 nm was measured every 30 min within the first 7 h with the help of a densitometer (Bio Genesys™ 10, Thermo Fisher Scientific). After 24h, final OD and pH (pH meter, FE20, Mettler Toledo) were determined.

3.6.3 Determination of intracellular sodium content

P. bryantii B₁₄ was grown in anaerobic cultivation flasks (103 mL) with 0, 10, 20 and 50 µM monensin for 9 h (six replicates each). To the control (0 µM monensin) the respective volume of EtOH was added. OD and pH were measured by transferring four milliliters of the batch culture into a Hungate tube. Both measurements were conducted as described before. After 9 h, supernatant and cells were separated by centrifugation for 10 min at 8,000 x g and 4 °C. Cell pellets were stored at -80 °C.

Cell preparation and sodium measurements were based on previous studies [178, 179] [ENREF 21](#). Cell pellets were suspended in 30 mL of 100 mM Tris/HCl (pH 7.3) and adjusted to OD₆₀₀=30. Cells were centrifuged (10 min; 8,000 x g; 4 °C), disrupted with 3 mL of 5% (w/v) trichloroacetic acid (TCA) by boiling for 20 min at 95 °C. The cell extract was centrifuged (20 min; 10,000 x g; 4 °C) and the supernatant, containing the intracellular sodium, was stored at 4°C. Cell debris were resuspended in 2 mL ddH₂O, and protein content was determined with the Bradford assay [119].

Intracellular sodium concentrations of all six replicates were quantified by inductively coupled plasma mass spectrometry (ICP-MS). An aliquot (1 mL) of the sodium containing supernatant was diluted by adding 3 mL ddH₂O and analyzed in the NexION device (Perkin Elmer). The quantification was conducted as described in the literature for sodium analysis [180]. The amount of sodium was standardized by the amount of protein, determined in the suspended cell debris. K⁺ concentrations were below the limit of quantification by ICP-MS.

3.6.4 Determination of D-glucose and glucose-6-phosphate in cell cultures

D-glucose and glucose-6-phosphate (G6P) concentrations in supernatants from cell cultures. Specific conversion with hexokinase (Roche) and G6P dehydrogenase (Roche) coupled to the conversion of NAD⁺ to NADH in enzymatic assays. NADH concentrations reflecting sugar concentrations were followed at 340 nm [181]. The reaction mixture consisted of 100 µL diluted sample (1:10), 865 µL of Tris HCl (380 mM) with MgSO₄ (6.4 mM) at pH 7.5, 20 µL of 100 mM NAD⁺ (Roth) and 10 µL of 100 mM ATP (Roth). Absorption at 340 nm (E1) was measured before adding 3 µL of G6P dehydrogenase (1000 U/mL) and incubation for 15 min at room temperature. After incubation, second measurement (E2) was performed with subsequent addition of 3 µL hexokinase (1500 U/mL) and further incubation as described before. Final absorption was determined after a stable absorption value was attained (E3). The parameters of sample volume ($v=0.1$ mL), total volume ($V=1$ mL), molecular weight of glucose ($M_w=180.16$ g/mol) and G6P ($M_w=260.14$ g/mol), cuvette thickness ($d=1$ cm), extinction coefficient for NADH at 340 nm ($\epsilon_{340}=6230$ L x cm⁻¹ x mol⁻¹) the absorption difference for glucose-6-phosphate ($\Delta EG6P=E2-E1$) or glucose ($\Delta EGlc=E3-E2$) and the dilution factor (D) were applied in formula 1 to calculate the concentration of D-glucose and G6P. Primary addition of the G6P dehydrogenase and the intermediate measurement (E2)

depicted the formation of NADH by an enzymatic conversion of G6P, while adding the hexokinase glucose was initially converted by a two-step enzymatic reaction.

$$c \left[\frac{g}{L} \right] = \left(\left(\frac{(V \times M_w)}{(\epsilon_{340} \times d \times v)} \right) \times \Delta E \right) \times D \quad (1)$$

3.6.5 Membrane isolation and enzyme kinetics

To isolate membranes containing active NQR, cells were cultivated in serum bottles (1 L). Cells were harvested by centrifugation (9,000 x g, 30 min, 4 °C) and washed twice in 2 mM Tris-H₂SO₄, pH 7.5 with 50 mM K₂SO₄. 10 g of cells were suspended in 30 mL of 20 mM Tris-H₂SO₄ (pH 7.5) containing 50 mM K₂SO₄, 5 mM MgSO₄, 1 mM dithiothreitol, 1 mM phenylmethylsulfonyl fluoride (PMSF), 0.1 mM di-isopropyl fluorophosphate and traces of DNase I (Roche). The suspension was passed three times through an EmulsiFlex®-C3 high-pressure homogenizer (Avestin) at 20,000 psi. Cell debris and unbroken cells were removed by centrifugation at 27,000 g for 30 min and at 4 °C. Membranes were collected by ultracentrifugation at 160,669 x g for 90 min at 4 °C and washed once in 20 mM Tris-H₂SO₄ (pH 7.5) containing 50 mM K₂SO₄ and 5 % (v/v) glycerol and suspended in the same buffer [135].

Enzyme kinetic assays were carried out in a quartz cuvette (1 cm diameter) in a total volume of 1 mL at 25 °C using a Diode-Array spectrophotometer (Analytik Jena Specord S600). NADH oxidation was followed at 340 nm ($\epsilon_{\text{NADH}}=6.22 \text{ mM}^{-1} \times \text{cm}^{-1}$), ubiquinone (Q1) reduction at 280 nm ($\epsilon_{\text{Q1}}=14.5 \text{ mM}^{-1} \times \text{cm}^{-1}$)[182] and DMN reduction at 270-290 nm ($\epsilon_{\text{DMN}}=15.2 \text{ mM}^{-1} \times \text{cm}^{-1}$)[183]. The assays were conducted in buffer containing 20 mM Tris-H₂SO₄ (pH 7.5), 100 mM Na₂SO₄, 100 μM quinone, 100 μM NADH and ~100 μg protein.

3.6.6 Fluorescence microscopy

Cells of *P. bryantii* B₁₄ were cultivated in Hungate tubes and incubated with 0 and 20 μM monensin up to 73 h. Cells were harvested by sampling 0.5 mL after 24, 48 and 73 h of incubation by centrifugation at 4 °C with 1000 x g for 5 min. Cells were washed for 15 min in phosphate buffered saline (PBS) and fixed by shaking for 2 h at 300 rpm in 4% *p*-formaldehyde at 4 °C. Afterwards, cells were washed with ultrapure water and stained with 4 μg/ml SYTO™ 9 and 100 μg/ml Alexa Fluor 594™ Concanavalin A conjugate (ConA-594; both Invitrogen) for 30 min at room temperature in the dark. Stained cells were gently washed with ultrapure

water to remove unbound dye. Finally, cells were suspended in 50 μ L ultrapure water, were mounted on glass slides without cover slip and air-dried.

The biofilms were visualized by a confocal laser scanning microscope (Zeiss LSM 800) and using a non-immersion objective EC Epiplan-Apochromat 50x/0.95 HD DIC M27. The used laser wavelengths were 488 nm for SYTOTM 9 and 561 nm for ConA-594. Images were recorded with a scan speed of two and an averaging number of two. The ZEN Blue 2.6 imaging software (Carl Zeiss GmbH) was used and images were exported as JPEG format.

3.6.7 Proteome analysis preparation

Steps of protein extraction, SDS-PAGE, in-gel digest and STAGE tips were performed as explained in Trautmann, A., *et al.* [1]. Dried peptides were suspended in 0.1 % formic acid before tandem mass spectrometry.

3.6.8 Tandem mass spectrometry

Peptide separation by liquid chromatography and mass spectrometry (MS) analysis were conducted via a Nano-LC-ESI-MS/MS using an Ultimate 3000 RSLC nano system (Dionex, Thermo Fisher Scientific) coupled to a Q-Exactive HF-X mass spectrometer (Thermo Fisher Scientific) using an EASY-Nano Flex ion source (Thermo Fisher Scientific) in the Core Facility module mass spectrometry (University of Hohenheim, Stuttgart). Tryptic digested peptides were injected and passed through a precolumn (μ -precursor C18 PepMap100, 300 μ m, 100 \AA , 5 μ m x 5 mm, Thermo Fisher Scientific) and a NanoEase analytical column (NanoEase M/Z HSS C18 T3, 1.8 μ m 100 \AA 75 μ m x 250 mm column, Waters GmbH). All operations were run at a constant temperature of 35 $^{\circ}$ C and a flow of 300 nL/min. A gradient with solvent A (0,1 % formic acid) and B (0.1 % formic acid and 80 % acetonitrile) was run for 110 min (0-3-34-67-90-110 min) with increasing solvent B (0-2-15-30-45-95 %) and a subsequent isocratic rinsing for 15 min and an equilibration from 95 to 2 % within 10 min. Orbitrap detected at a resolution of 60.000 with 200 m/z, while the survey spectra were performed in a range from 200-2000 m/z. Tandem MS spectra were generated for the 30 most abundant peptide precursors using high energy collision dissociation (HCD) at a resolution of 15,000, normalized by a collision energy of 27. Lock-mass ions from the ambient air were used for internal calibration [122].

3.6.9 Proteome analysis

The obtained tandem mass spectra were used for label-free quantification (LFQ) in MaxQuant (v.1.6.0.16)[103]. Two proteomic datasets were analyzed in separate: first *P. bryantii* B₁₄ exposed to a monensin concentration gradient after 9 h incubation time and second *P. bryantii* B₁₄ grown in absence or presence of monensin in a time series experiment. As a reference database *P. bryantii* B₁₄ proteins from Uniprot (3,757 proteins entries, 12/2019) were used for both searches. Re-quantification was enabled, specific cleavage via trypsin and using only oxidation as a possible modification was set in the adjustments.

Protein quantification within a single cultivation condition was defined by the mean of at least four positive LFQ-values (>0) out of six replicates in the concentration gradient approach or at least two positive LFQ-values out of triplicates in the time series approach. Protein comparison was performed using the fold-change difference by setting the culture without monensin equal to one in the dataset of monensin gradient experiment or setting the incubation time of 9 h to one in time series experiment. If the fold-change of those references was zero, the lowest LFQ average of the different treatments was set equal to one. Two samples with low protein and peptide counts were excluded for fold-change analysis. Functional classification by Kyoto Encyclopedia Genes and Genome (KEGG) Orthologous groups (KO) of the identified proteins was conducted using EggNOG and Kofam, while last one was prioritized in case of discrepancies [125, 184]. Proteins without any COG assignment were set manually as COG class S! (Function unknown). 237 unknown proteins and 130 proteins from the COG class G, originating from protein identifications of proteomic dataset 2, were used in order to obtain specific information about carbohydrate-active enzymes (CAZymes) by using dbCAN2 with the HMMER tool [185]. Twenty-four uncharacterized proteins with a fold-change ≥ 5 were compared via NCBI's protein-protein BLAST to the Uniprot/Swiss-Prot database to find homologous proteins with a described functional annotation. Models (XM/XP) and uncultured/environmental sample sequences were excluded in the blast search. Annotations with a maximal score ≥ 90 were considered as potential candidates for new characterization.

3.6.10 Statistical analysis

Growth parameters (OD and pH), residual glucose concentration in the supernatant and intracellular Na⁺ concentration were examined regarding their significance between the used monensin concentrations and time points of measurement for the OD. Therefore,

analysis of variance (ANOVA) and the least significant difference (LSD) test were performed by using Infostat (version 2018) [186]. Growth rate was determined by identifying the slope of a trend line, which derived from five subsequent time points and their respective OD. Proteomics data were analyzed by a Bray Curtis similarity and principal component (PCO) analysis using the statistical software Primer 6 (v 6.1.16) and Permanova (v 1.0.6). Venn diagram for protein distribution among treatments was conducted using an interactive Venn diagram [187]. Analysis of fold-change and heat map illustrations were conducted using Excel 2016 (Microsoft Corporation, Redmond, Washington, DC, USA). The correlation coefficient (R^2) was used to evaluate a connection among proteins or to other monitored parameters in Excel 2016.

3.7 Miscellaneous information of publication

3.7.1 Data availability statement

Raw mass spectrometric data are stored in the ProteomeXchange Consortium including the data set identifier PXD026085 for the monensin concentration variants and PXD026057 for the time series [123]. Analyzed data are provided as supplementary information.

3.7.2 Acknowledgement

The authors would like to thank the Deutsche Forschungsgemeinschaft (DFG) for funding (project number 327953272). We thank the mass spectrometry group of the Core Facility of the University of Hohenheim for excellent support.

3.7.3 Competing interest

The authors declare no conflict of interest.

3.8 Supplementary tables

Table S10: Protein and peptide count from replicates among monensin treatments. A to F indicate the replicates while the treatments with monensin are given from 0 to 50 μM . Count of proteins represents the number of proteins that were quantified. Count of peptides indicate number of quantified peptides.

Monensin [μM]	A	B	C	D	E	F	
0	1,130	1,141	985	1,041	1,070	1,096	Proteins
10	1,321	1,323	1,349	1,303	1,294	1,286	
20	1,248	1,292	1,299	1,289	1,287	1,283	
50	1,289	1,274	1,307	1,290	1,294	1,290	
0	13,352	13,936	10,861	12,154	12,464	12,463	Peptides
10	14,969	14,620	14,792	14,818	14,764	14,560	
20	13,212	14,954	14,992	14,611	14,608	14,473	
50	14,573	14,044	14,862	14,608	14,586	14,328	

Second Publication

Table S11: Differences in clusters of orthologous group (COG) classes depending on 0, 10, 20 or 50 μM monensin. Mean of proteins (n=6) belonging to the displayed COG classes was standardized by total and compared for each concentration. COGs with a difference $\geq 1\%$ were displayed in red lettering. Cultivation parameters were attached below and display the mean of six replicates. Intermediate columns display with a reddish color an elevation and with bluish color a decrease of functional class proteins under monensin supplementation. A least significant difference (LSD, $p < 0.01$) test was performed for all displayed COG classes and cultivation parameters (small letters in right columns).

(COG) Description	___ Mean Contribution ___				_Differences to 0 μM _			___ Fisher LSD ($p < 0.01$) ___			
	0 μM	10 μM	20 μM	50 μM	10 μM	20 μM	50 μM	0 μM	10 μM	20 μM	50 μM
(C) Energy production and conversion	7.6%	8.7%	9.2%	8.8%	1.14%	1.65%	1.28%	a	b	b	b
(D) Cell cycle control, cell division, chromosome partitioning	0.1%	0.4%	0.4%	0.4%	0.30%	0.36%	0.34%	a	b	c	c
(E) Amino acid transport and metabolism	4.7%	4.3%	4.6%	4.6%	-0.36%	-0.06%	-0.11%	a	b	ab	ab
(F) Nucleotide transport and metabolism	3.6%	3.9%	3.8%	3.9%	0.26%	0.21%	0.31%	a	b	ab	b
(G) Carbohydrate transport and metabolism	15.3%	14.4%	15.3%	15.5%	-0.86%	-0.02%	0.18%	-	-	-	-
(H) Coenzyme transport and metabolism	1.6%	1.1%	1.1%	1.2%	-0.46%	-0.44%	-0.42%	a	b	b	b
(I) Lipid transport and metabolism	1.8%	1.7%	1.7%	1.6%	-0.12%	-0.13%	-0.17%	-	-	-	-
(J) Translation, ribosomal structure and biogenesis	6.2%	24.4%	25.5%	26.3%	18.20%	19.27%	20.10%	a	b	b	b
(K) Transcription	0.6%	2.8%	3.2%	3.0%	2.16%	2.55%	2.39%	a	b	c	bc
(L) Replication, recombination and repair	0.3%	1.1%	1.2%	1.2%	0.83%	0.89%	0.90%	a	b	b	b
(M) Cell wall/membrane/envelope biogenesis	16.9%	8.7%	7.7%	7.5%	-8.19%	-9.17%	-9.36%	a	b	b	b
(N) Cell motility	0.8%	0.9%	1.0%	0.9%	0.08%	0.16%	0.11%	-	-	-	-
(O) Post-translational modification, protein turnover, and chaperones	7.1%	9.9%	8.5%	8.7%	2.82%	1.44%	1.59%	a	c	b	b
(P) Inorganic ion transport and metabolism	7.2%	1.9%	1.9%	1.9%	-5.31%	-5.35%	-5.36%	a	b	b	b
(Q) Secondary metabolites biosynthesis, transport, and catabolism	0.0%	0.0%	0.1%	0.1%	0.02%	0.03%	0.03%	a	b	b	b
(S) Function unknown	16.9%	9.0%	8.4%	8.0%	-7.88%	-8.50%	-8.82%	a	b	b	b
(IS) Function unknown (manually assigned)	8.7%	4.0%	3.6%	3.6%	-4.74%	-5.14%	-5.13%	a	b	b	b
(T) Signal transduction mechanisms	0.2%	0.6%	0.7%	0.7%	0.36%	0.44%	0.47%	a	b	c	c
(U) Intracellular trafficking, secretion, and vesicular transport	0.3%	1.8%	1.8%	1.7%	1.50%	1.53%	1.41%	a	b	b	b
(V) Defense mechanisms	0.1%	0.2%	0.3%	0.3%	0.17%	0.20%	0.19%	a	b	c	bc
Cultivation Parameters	_____ Mean _____				_Differences to 0 μM _			___ Fisher LSD ($p < 0.01$) ___			
	0 μM	10 μM	20 μM	50 μM	10 μM	20 μM	50 μM	0 μM	10 μM	20 μM	50 μM
Optical density [-] at 600 nm	1.83	1.30	0.98	0.89	-0.53	-0.85	-0.94	a	b	c	c
pH [-log ₁₀ [H ⁺]] in supernatant	5.25	5.70	5.92	6.08	0.44	0.67	0.82	a	b	c	c
Glucose [g/L] in supernatant	0.06	0.24	0.90	0.77	0.18	0.84	0.71	a	a	b	b
intracellular Na ⁺ per Protein [$\mu\text{g}/\text{mg}$]	128	33	59	105	-95	-69	-23	a	c	bc	ab

Table S12: Outer membrane (OM) related proteins under different monensin concentrations. Protein abundances are illustrated as a heat map with a fold-change indicated by the color code (below heat map) and standardized by 0 μ M monensin (set equal to one). Protein names are listed with the Uniprot ID in brackets.

Name (Uniprot ID)	10 μ M	20 μ M	50 μ M
Starch-binding associating with OM (A0A1H9C300)	0.03	0.02	0.03
OM receptor for ferrienterochelin and colicins (D8E003)	0.06	0.08	0.06
Starch-binding associating with OM (D8DV05)	0.09	0.06	0.09
OM protein assembly factor BamA (D8DWS2)	0.14	0.07	0.10
OM receptor proteins, mostly Fe transport (A0A1H9CY22)	0.15	0.11	0.09
OM protein, cobalt-zinc-cadmium efflux system (A0A1H9FFT0)	0.14	0.11	0.11
OM protein (D8DX2)	0.11	0.12	0.14
OM protein (D8DX1)	0.11	0.12	0.14
OM protein beta-barrel domain-containing protein (D8DZT1)	0.21	0.13	0.12
TonB-linked OM protein, SusC/RagA family (A0A1H9B8Y5)	0.14	0.13	0.14
OM protein transport protein (Omp1/fadl/todx) (D8DTK4)	0.18	0.15	0.13
TonB-dependent OM receptor (D8DUK7)	0.15	0.20	0.23
Cationic OM protein OmpH (D8DT44)	0.32	0.15	0.15
OM protein beta-barrel family protein (A0A1H8Z174)	0.17	0.16	0.16
OM autotransporter barrel domain-containing protein (D8DU39)	0.26	0.19	0.17
Starch-binding associating with OM (A0A1H9E645)	0.23	0.18	0.19
TonB-linked OM protein, SusC/RagA family (A0A1H9C2R2)	0.24	0.21	0.18
TonB-linked OM protein, SusC/RagA family (A0A1H9LDK0)	0.27	0.23	0.19
OM protein TolC (D8DWK0)	0.31	0.21	0.22
OM protein beta-barrel domain-containing protein (D8DYY2)	0.41	0.25	0.21
TonB-linked OM receptor P92 (D8DTK2)	0.37	0.26	0.22
Efflux transporter, OM factor (OMF) lipoprotein, NodT family (D8DVS0)	0.28	0.24	0.23
Starch-binding associating with OM (D8DUK8)	0.23	0.32	0.41
Major OM protein OmpA (D8DWD3)	0.27	0.24	0.25
OM protein (D8DZK0)	0.34	0.27	0.24
OM receptor proteins, mostly Fe transport (D8E0H5)	0.31	0.27	0.25
OM protein beta-barrel domain-containing protein (D8DWZ7)	0.26	0.25	0.27
OM receptor proteins, mostly Fe transport (A0A1H9DV15)	0.26	0.30	0.31
OM protein OmpA (A0A1H9DD30)	0.40	0.29	0.28
OM protein beta-barrel domain-containing protein (D8DVA3)	0.36	0.30	0.00
Cationic OM protein OmpH (D8DT45)	0.52	0.33	0.36
OM protein beta-barrel domain-containing protein (D8DWQ2)	0.43	0.33	0.46
OM efflux protein (D8DYZ4)	0.47	0.38	0.34
OM protein (D8DT53)	0.35	0.47	0.53
Periplasmic chaperone for OM proteins Skp (D8DT43)	0.55	0.39	0.39
OM protein beta-barrel domain-containing protein (D8DUD8)	0.60	0.48	0.50
OM lipoprotein-sorting protein (A0A1H9GE28)	0.75	0.64	0.59
OM lipoprotein carrier protein LolA (D8DTI7)	0.78	0.64	0.60
Periplasmic chaperone for OM proteins Skp (D8DSW6)	1.32	1.17	1.20

Color Code:	0.10	0.50	1.00
-------------	------	------	------

Second Publication

Table S13: Transport related proteins under different monensin concentrations.

Protein abundances are illustrated as a heat map with a fold-change indicated by the color code (below heat map). Protein names are listed with the Uniprot ID in brackets. Bluish marked proteins (upper part) indicate protein elevated in absence of monensin while reddish marked proteins (lower part) show increased abundance under monensin presence.

Name (Uniprot ID)	0 μ M	10 μ M	20 μ M	50 μ M
Putative auto-transporter adhesin, head GIN domain (D8DVY5)	1.00	0.15	0.08	0.06
Outer membrane receptor proteins, mostly Fe transport (A0A1H9CY22)	1.00	0.15	0.11	0.09
Outer membrane protein transport protein (D8DTK4)	1.00	0.18	0.15	0.13
Long-chain fatty acid transport protein (A0A1H9JWM8)	1.00	0.19	0.19	0.15
Outer membrane autotransporter protein (D8DU39)	1.00	0.26	0.19	0.17
Efflux transporter, outer membrane factor lipoprotein (D8DVS0)	1.00	0.28	0.24	0.23
Outer membrane receptor proteins, mostly Fe transport (D8E0H5)	1.00	0.31	0.27	0.25
Outer membrane receptor proteins, mostly Fe transport (A0A1H9DV15)	1.00	0.26	0.30	0.31
Long-chain fatty acid transport protein (D8DZW6)	1.00	0.44	0.34	0.31
Outer membrane receptor proteins, mostly Fe transport (D8DSX8)	1.00	0.00	0.00	0.00
Outer membrane receptor proteins, mostly Fe transport (D8DTP4)	1.00	0.00	0.00	0.00
Outer membrane receptor proteins, mostly Fe transport (D8DZ53)	1.00	0.00	0.00	0.00
Ferrous iron transport protein B (D8DT71)	1.00	15.92	17.06	15.32
Phospholipid/cholesterol/gamma-HCH transport system (A0A1H8YR75)	1.00	4.87	4.69	4.62
ABC transporter, ATP-binding protein (D8DYR5)	1.00	3.04	3.25	3.14
ABC transporter, ATP-binding protein (D8DZW0)	1.00	2.81	3.30	3.22
Sodium/glucose cotransporter (D8DYQ7)	1.00	2.22	3.00	3.12
ABC-type amino acid transport/signal transduction system (D8DYU7)	1.00	2.08	2.89	2.71
Biopolymer transport protein ExbB (D8DVL9)	1.00	2.09	2.60	2.63
Hexuronate transporter (D8DVQ2)	1.00	2.11	2.61	2.62
Electron transport complex protein RnfG (D8DXV4)	1.00	2.08	2.41	2.73
Electron transport complex protein RnfG (D8DYE1)	1.00	2.82	1.93	2.37
Di-tripeptide ABC transporter (D8DWZ5)	1.00	2.00	2.13	2.07
Biopolymer transport protein ExbD/ToIR (D8E014)	1.00	1.94	1.84	1.67
Glutamine ABC transporter, ATP-binding protein GlnQ (D8DYU8)	1.00	1.92	1.92	1.84
Cell division transport system ATP-binding protein (D8DY89)	1.00	1.65	2.21	1.90
NitT/TauT family transport system substrate-binding protein (D8DY75)	1.00	1.46	1.77	1.65
Phosphate transport system substrate-binding protein (D8E016)	1.00	1.36	1.39	1.40
Biopolymer transport protein, ExbD/ToIR family (D8E013)	1.00	1.12	1.05	1.08
Maltose/moltooligosaccharide transporter (D8DXY5)	0.00	1.00	1.65	1.82
Transporter (D8DT67)	0.00	1.00	1.53	1.89
MFS transporter, FHS family, L-fucose permease (D8DYR0)	0.00	1.21	1.26	1.00
ABC-type sugar transport system (D8DUK6)	0.00	1.00	1.19	1.25
Ca ²⁺ -transporting ATPase (D8DXJ6)	0.00	1.00	1.30	1.10
ABC transporter, ATP-binding protein (D8E0H6)	0.00	1.00	1.35	1.05
Putative ABC transport system permease protein (A0A1H9F867)	0.00	1.00	1.32	1.03
Putative transport protein (A0A1H9JA50)	0.00	1.00	1.23	1.08
ABC transporter, ATP-binding protein, MsbA family (D8DZU9)	0.00	1.00	1.23	1.04
Na ⁺ /H ⁺ antiporter NhaD (D8DYG5)	0.00	1.00	1.16	1.11
Phosphate:Na ⁺ symporter (A0A1H9BJD7)	0.00	1.05	1.20	1.00
ABC transporter, ATP-binding protein (D8DSX4)	0.00	1.00	1.16	1.07
ABC transporter domain protein (D8DWC8)	0.00	1.00	1.11	1.08
ABC transporter, ATP-binding protein (D8DWW0)	0.00	1.04	1.00	1.14
ABC transporter domain protein (D8DY72)	0.00	1.00	1.12	1.03
ABC transporter, ATP-binding protein (D8DZ98)	0.00	1.00	1.08	1.03
Kef-type K ⁺ transport system, membrane component KefB (D8DZH8)	0.00	0.00	1.09	1.00
Zinc ABC transporter, ATP-binding protein ZnuC (D8DT91)	0.00	0.00	1.05	1.00
Cation ABC transporter, periplasmic-binding protein (D8DT92)	0.00	0.00	0.00	1.00

Color Code: 0.00 0.10 2.00 5.00

Second Publication

Table S14: Proteins with highly correlating intracellular sodium. Proteins abundances (natural logarithm of LFQ values) are displayed in color code to show also the magnitude of differences between the proteins. Only proteins with correlations ≥ 0.7 are shown. Intracellular Na⁺ concentration is presented in last row.

Name (Uniprot ID)	Monensin				Correlation with Na ⁺
	0 μ M	10 μ M	20 μ M	50 μ M	
N-carbamoylputrescine amidase (A0A1H9EHL1)	20.32	20.83	20.74	20.68	-0.74
ATP-dependent Clp protease ATP-binding subunit ClpX (A0A1H8YR68)	18.46	21.18	21.19	21.03	-0.70
Beta-glucosidase (D8DY03)	20.70	19.08	19.37	19.61	0.70
TonB-dependent receptor, plug (D8DVB1)	20.73	19.13	19.52	19.77	0.71
Putative lipoprotein (D8DU09)	21.17	19.70	20.19	20.35	0.72
IPT/TIG domain-containing protein (A0A1H9LFB0)	22.19	20.99	21.36	21.42	0.73
RagB/SusD domain protein (D8DT52)	22.05	20.86	21.31	21.44	0.74
IPT/TIG domain-containing protein (D8DY17)	23.19	22.10	22.29	22.36	0.76
TonB-dependent receptor, plug (D8DY14)	20.92	19.88	20.17	20.28	0.78
Putative lipoprotein (D8DY15)	22.42	21.49	21.85	21.91	0.78
Outer membrane protein (D8DT53)	19.95	19.51	19.50	19.70	0.79
Intracellular Na ⁺ standardized by protein [μ g/mg]	128	33	59	105	1.00

Color Code: 18 19 21 23

Second Publication

Table S15: NADH:Quinone Reductase (NQR) in a time series with and without monensin.

Name (Uniprot ID)	0 μ M Monensin (Con)				20 μ M Monensin (Mon)				Ratio Mon : Con			
	9h	24h	48h	72h	9h	24h	48h	72h	9h	24h	48h	72h
NQR subunit A (D8DWC1)	1.00	7.76	11.49	11.83	1.00	1.54	1.83	2.54	3.68	0.73	0.59	0.79
NQR subunit B (D8DWC0)	-	1.00	1.65	1.89	1.00	1.13	1.63	2.79	Mon	0.99	0.86	1.29
NQR subunit B (D8DWP0)	1.00	2.36	4.69	4.41	1.00	1.11	1.49	1.92	4.27	2.01	1.35	1.86
NQR subunit C (D8DWB9)	1.00	6.14	8.87	10.10	1.00	1.28	1.56	2.07	3.57	0.74	0.63	0.73
NQR subunit F (D8DWB6)	1.00	6.86	9.88	8.73	1.00	1.37	1.57	1.50	13.45	2.69	2.13	2.30
NQR subunit H (D8DWN8)	-	1.00	-	-	1.00	1.56	2.30	-	Mon	0.98	Mon	-
NQR subunit I (D8DWN7)	1.00	5.53	9.30	10.04	1.00	1.17	1.29	2.09	6.34	1.34	0.88	1.32
NQR subunit J (D8DWN6)	-	1.00	-	-	1.00	1.42	2.05	-	Mon	0.73	Mon	-
NQR subunit L (AOA1H9A8K0)	-	1.00	-	-	1.00	1.81	3.38	4.04	Mon	1.24	Mon	Mon
NQR subunit M (AOA1H9A8A6)	-	-	-	-	-	1.00	2.02	-	-	Mon	Mon	-

Color code: 0 1 2 5 10 Color code: Con 0.5 1 5 Mon

Table S16: pBLAST results of uncharacterized proteins ranked by best score combined with fold change.

Left part illustrates the fold change of identified uncharacterized proteins. Color code is below the table. Right part shows the candidate matches with the best score and other parameters.

Name (Uniprot ID)	Monensin				Lenght	Max Score	E-value	Query Cover	% Ident	Protein Name	pBLAST	
	0 μ M	10 μ M	20 μ M	50 μ M							Acession No.	Organism
UP, UPF0371 family (D8DTQ4)	1.00	16.25	19.68	17.55	595	576	0.0E+00	0.98	56.9	UPF0371 protein cu0538 [Corynebacterium...	B1VFF9.1	<i>Corynebacterium</i>
UP (D8DVZ9)	1.00	10.53	13.16	13.49	210	140	3.0E-41	0.96	31.6	Protein YghO [Escherichia coli K-12]	Q46840.3	<i>Escherichia coli</i> K-12
UP (D8DYX8)	1.00	0.33	0.17	0.15	197	130	1.0E-35	0.75	33.3	Radial spoke head 10 homolog B [Danio rerio]	Q08CH7.1	<i>Danio rerio</i> (Zebra fish)
UP (D8DZRO)	1.00	0.23	0.18	0.19	318	121	4.0E-33	0.88	19.6	Uncharacterized protein aq_1259; Flags: Precurso...	O67300.1	<i>Aquifex aeolicus</i> VF5
UP (AOA1H8YRX1)	1.00	4.47	5.17	5.26	490	96	7.0E-26	0.84	23.0	Uncharacterized protein YitL [Bacillus subtilis...	O06747.2	<i>Bacillus subtilis</i> subsp. <i>subtilis</i> str. 168

UP: Uncharacterized protein 0.00 0.10 0.25 5.00 15.00 Color Code

Table S17: Protein and peptide count from replicates among 0 and 20 μ M monensin cultivations over time. A, B, C indicate the replicates while time points reach from 9, 24, 48 to 72 h. Count of proteins represents the number of proteins that were quantified. Count of peptides indicate number of quantified peptides. Red numbers indicate low counts and were excluded for fold-change calculations.

Time [h]	Con (0 μ M)			Mon (20 μ M)			
	A	B	C	A	B	C	
9	903	941	896	1,339	1,383	1,380	Proteins
24	1,089	1,117	1,016	1,258	1,290	1,293	
48	646	1,006	905	1,300	1,280	1,285	
72	891	1,008	846	1,146	1,027	532	
9	8,721	10,350	9,508	14,575	14,609	14,331	Peptides
24	10,869	12,210	10,191	13,831	14,011	14,070	
48	4,184	9,581	7,121	13,021	12,725	12,963	
72	6,917	10,139	6,537	9,389	7,484	3,811	

Second Publication

Table S18: Differences in COG classes and cultivation parameters at 9, 24, 48 and 72 h of cultivation with 20 µM monensin or without.

Mean occurrence of proteins (n=3 and for control 48 h and monensin 72 h) belonging to the displayed COG classes were standardized by total and compared for each time point. COG classes with red font were mostly affected (>1 %) at a time point in their abundance between Con and Mon, displayed in the right column with blue (more abundant in Mon) and red (more abundant in Con). Cultivation parameters were attached below and display the mean of triplicates. For all displayed parameters significance with respect to cultivation condition over all time points (* in front of parameter description) and time (displayed by different small letters in right columns) was determined with p<0.05.

(COG) Description	Control [0 µM]				Monensin [20 µM]				Differences (Con-Mon)				Time (p<0.05)			
	9h	24h	48h	72h	9h	24h	48h	72h	9h	24h	48h	72h	9h	24h	48h	72h
* (C) Energy production and conversion	3.5%	7.9%	7.8%	8.4%	8.2%	9.6%	9.8%	9.1%	-4.7%	-1.7%	-2.0%	-0.7%	a	b	b	b
* (D) Cell cycle control, cell division, chromosome partitioning	0.0%	0.1%	0.1%	0.1%	0.3%	0.4%	0.4%	0.3%	-0.3%	-0.3%	-0.3%	-0.2%	a	b	b	a
* (E) Amino acid transport and metabolism	2.6%	3.5%	3.6%	3.9%	4.2%	4.2%	4.3%	3.1%	-1.6%	-0.7%	-0.7%	0.8%	a	b	b	b
* (F) Nucleotide transport and metabolism	1.2%	2.6%	2.6%	2.8%	3.1%	3.7%	3.8%	3.1%	-1.9%	-1.1%	-1.2%	-0.3%	a	b	b	b
* (G) Carbohydrate transport and metabolism	12.0%	15.6%	12.5%	12.1%	16.0%	17.0%	16.5%	14.8%	-4.0%	-1.4%	-4.0%	-2.6%	a	b	ab	a
* (H) Coenzyme transport and metabolism	0.5%	1.0%	0.9%	0.9%	1.0%	1.1%	1.1%	0.7%	-0.5%	-0.1%	-0.3%	0.2%	a	b	b	b
(I) Lipid transport and metabolism	1.8%	2.0%	1.7%	1.7%	1.9%	1.8%	1.8%	1.3%	-0.1%	0.2%	-0.1%	0.4%	a	a	ab	b
* (J) Translation, ribosomal structure and biogenesis	3.6%	15.0%	18.7%	19.1%	18.0%	22.2%	22.8%	24.4%	-14.4%	-7.2%	-4.1%	-5.3%	a	b	b	b
* (K) Transcription	0.2%	1.1%	1.2%	1.4%	1.9%	2.4%	2.7%	2.3%	-1.7%	-1.3%	-1.5%	-0.9%	a	b	b	b
* (L) Replication, recombination and repair	0.3%	0.5%	1.1%	1.3%	0.9%	1.2%	1.4%	1.4%	-0.5%	-0.7%	-0.3%	-0.1%	a	b	c	d
* (M) Cell wall/membrane/envelope biogenesis	16.6%	9.7%	9.4%	8.3%	9.6%	7.5%	6.5%	6.8%	6.9%	2.2%	2.9%	1.5%	a	b	b	b
* (N) Cell motility	1.3%	0.6%	1.7%	1.6%	0.9%	0.6%	0.9%	1.6%	0.3%	0.0%	0.8%	0.0%	a	b	a	a
* (O) Post-translational modification, protein turnover, and chaperones	8.3%	11.9%	14.3%	16.2%	10.1%	10.6%	10.5%	13.0%	-1.8%	1.3%	3.8%	3.2%	a	b	b	c
* (P) Inorganic ion transport and metabolism	13.0%	6.9%	5.5%	4.8%	3.9%	1.9%	1.7%	1.7%	9.2%	5.0%	3.7%	3.1%	a	b	b	b
(Q) Secondary metabolites biosynthesis, transport, and catabolism	0.2%	0.0%	0.0%	0.0%	0.1%	0.1%	0.1%	0.0%	0.1%	0.0%	-0.1%	0.0%	a	b	b	b
* (S) Function unknown	19.8%	11.7%	9.7%	9.2%	11.1%	8.1%	7.8%	5.8%	8.6%	3.5%	2.0%	3.4%	a	b	b	b
* (S!) Function unknown [manually annotated]	14.8%	8.3%	7.2%	6.4%	6.4%	3.9%	3.7%	3.6%	8.4%	4.4%	3.4%	2.8%	a	b	b	b
* (T) Signal transduction mechanisms	0.1%	0.2%	0.2%	0.2%	0.4%	0.6%	0.7%	0.4%	-0.3%	-0.4%	-0.4%	-0.2%	a	b	c	b
* (U) Intracellular trafficking, secretion, and vesicular transport	0.1%	1.1%	1.3%	1.4%	1.6%	2.5%	3.0%	2.7%	-1.5%	-1.4%	-1.7%	-1.3%	a	b	c	ab
* (V) Defense mechanisms	0.0%	0.1%	0.2%	0.2%	0.2%	0.3%	0.3%	0.2%	-0.2%	-0.1%	-0.1%	0.0%	a	b	b	c

Cultivation Parameters [Unit]	Control [0 µM]				Monensin [20 µM]				Differences (Con-Mon)				Time (p<0.01)			
	9h	24h	48h	72h	9h	24h	48h	72h	9h	24h	48h	72h	9h	24h	48h	72h
* Optical Density [-] at 600 nm	1.95	2.09	2.11	2.12	1.67	1.60	1.41	1.35	0.28	0.50	0.70	0.77	-	-	-	-
* pH [-log ₁₀ [H ⁺]] of supernatant	5.01	4.96	4.96	4.97	5.35	5.15	5.18	5.14	-0.34	-0.19	-0.22	-0.17	a	b	b	b
* Glucose [g/L] in supernatant	0.00	0.00	0.01	0.01	0.26	0.25	0.61	0.78	-0.26	-0.25	-0.60	-0.77	a	a	ab	b
* Glucose-6-phosphate [mg/L] in supernatant	0.00	0.00	0.28	0.96	2.06	2.75	8.40	11.84	-2.06	-2.75	-8.12	-10.87	a	ab	ab	b

Second Publication

Table S19: Enzymes of the starch metabolism (ko00500) with gradually ascending or descending abundance.

The green-yellow-red color code illustrates the fold-change within conditions control (Con) and monensin (Mon), while blue-yellow-brown shows the ratio of protein abundance of Mon:Con. Fields without quantification are displayed by a grey-filled field with a dash. Fields with Mon or Con indicate that in this sample the protein was only quantified in the monensin (Mon) or the control (Con) condition. Protein names written in red point out enzymes with glucose as a product.

Protein Name (Uniprot ID)	0 μ M Monensin (Con)				20 μ M Monensin (Mon)				Ratio Mon : Con			
	9h	24h	48h	72h	9h	24h	48h	72h	9h	24h	48h	72h
Alpha-L-arabinofuranosidase (D8E0G9)	1.00	0.03	-	-	1.00	0.28	0.10	-	0.29	2.45	Mon	-
Alpha-glucosidase (D8DXY7)	1.00	0.08	0.00	-	1.00	0.42	0.27	0.12	0.35	1.87	176.36	Mon
Beta-galactosidase (D8DV08)	1.00	0.19	0.08	-	1.00	0.29	0.31	0.40	0.34	0.52	1.28	Mon
Putative glycosyl hydrolase, family 13 (D8DXY9)	1.00	0.11	-	0.00	1.00	0.36	0.13	0.14	0.24	0.75	Mon	12.96
Beta-glucosidase (A0A1H9IED8)	1.00	0.10	-	0.07	1.00	0.96	1.70	4.95	0.13	1.25	Mon	9.27
Fructan beta-(2,6)-fructosidase (D8DUL1)	1.00	0.25	0.03	0.01	1.00	0.49	0.37	0.31	0.26	0.50	3.12	6.10
4-deoxy-L-threo-5-hexosulose-uronate ketol-isomerase (D8DVQ3)	1.00	0.14	0.05	0.05	1.00	0.29	0.31	0.36	0.48	0.99	2.89	3.22
Aldose 1-epimerase (A0A1H9EVQ9)	1.00	1.15	0.50	0.34	1.00	1.66	1.53	1.72	0.36	0.52	1.11	1.79
Beta-galactosidase (D8E0G2)	1.00	0.24	0.07	0.07	1.00	0.48	0.48	0.74	0.18	0.35	1.23	1.83
Transketolase (D8DYQ1)	1.00	6.12	6.50	6.76	1.00	1.62	1.78	1.49	3.19	0.85	0.87	0.71
Starch phosphorylase (A0A1H9J3G8)	1.00	8.48	12.87	13.26	1.00	1.60	1.71	1.84	5.25	0.99	0.70	0.73
4-alpha-glucanotransferase (D8DXY6)	1.00	16.19	24.25	25.60	1.00	2.37	3.01	2.33	6.62	0.97	0.82	0.60
Galactitol PTS, EIIc (D8DVQ4)	-	1.00	1.85	2.17	1.00	1.21	1.60	1.64	Mon	0.86	0.62	0.54
Hexuronate transporter (D8DVQ2)	-	1.00	1.29	1.47	1.00	1.72	1.59	1.09	Mon	0.97	0.69	0.42

Color code:	-	0.1	1	5	10	Color code:	Con	0.5	1	5	Mon
-------------	---	-----	---	---	----	-------------	-----	-----	---	---	-----

Second Publication

Table S20: Ratio of CAZyme families distribution between control and monensin out of 72 identified CAZymes. Depending if proteins of corresponding class were more abundant in control, monensin or in between, a related distribution was assigned depending on the intensity with an increasing number of plus signs (+). In families without a sufficient amount of total hits (<5), distribution assignation was omitted.

Enzyme Classes	Total Hits	Most found in condition			Most found in condition			Distribution
		Control	In between	Monensin	Control	In between	Monensin	
GH2	10	2	4	4	20%	40%	40%	+ Mon
GH43	6	4	1	1	67%	17%	17%	++ Con
GH13	5	0	1	4	0%	20%	80%	+++ Mon
PL1	5	4	0	1	80%	0%	20%	+++ Con
GH3	4	1	2	1	25%	50%	25%	-
GH51	4	0	2	2	0%	50%	50%	-
GH5	3	1	1	1	33%	33%	33%	-
GH97	3	1	0	2	33%	0%	67%	-
CE8	2	1	1	0	50%	50%	0%	-
GH106	2	0	0	2	0%	0%	100%	-
GH26	2	1	1	0	50%	50%	0%	-
GH28	2	2	0	0	100%	0%	0%	-
GH31	2	1	0	1	50%	0%	50%	-
GH32	2	1	1	0	50%	50%	0%	-
GH35	2	0	1	1	0%	50%	50%	-
GH53	2	1	1	0	50%	50%	0%	-
CBM20	1	0	1	0	0%	100%	0%	-
GH105	1	0	1	0	0%	100%	0%	-
GH127	1	0	0	1	0%	0%	100%	-
GH133	1	0	0	1	0%	0%	100%	-
GH141	1	0	1	0	0%	100%	0%	-
GH154	1	0	0	1	0%	0%	100%	-
GH163	1	0	1	0	0%	100%	0%	-
GH36	1	0	0	1	0%	0%	100%	-
GH57	1	0	0	1	0%	0%	100%	-
GH67	1	1	0	0	100%	0%	0%	-
GH78	1	0	0	1	0%	0%	100%	-
GH9	1	0	1	0	0%	100%	0%	-
GH94	1	0	0	1	0%	0%	100%	-
GT35	1	0	1	0	0%	100%	0%	-
GT5	1	0	0	1	0%	0%	100%	-
PL29	1	0	1	0	0%	100%	0%	-

Second Publication

Table S21: Cell division proteins (Fts) with and without monensin over time. The green-yellow-red color code illustrates the fold-change within conditions control (Con) and monensin (Mon), while blue-yellow-brown shows the ratio of protein abundance of Mon:Con. Fields without quantification are displayed by a grey-filled field with a dash. Fields with Mon or Con indicate that in this sample the protein was only quantified in the monensin (Mon) or the control (Con) condition.

Name (Uniprot ID)	0 μ M Monensin (Con)				20 μ M Monensin (Mon)				Ratio Mon : Con			
	9h	24h	48h	72h	9h	24h	48h	72h	9h	24h	48h	72h
ATP-dependent zinc metalloprotease FtsH (D8DT63)	1.00	7.73	11.68	15.74	1.00	0.98	0.78	1.11	16.76	2.13	1.13	1.18
Cell division protein FtsA (D8DUA2)	-	1.47	1.42	1.00	1.00	1.56	1.74	1.04	Mon	4.12	4.75	4.04
Signal recognition particle receptor FtsY (D8DXW7)	-	1.22	1.00	1.04	1.00	1.27	1.63	0.95	Mon	2.91	4.58	2.55
Cell division protein FtsZ (D8DUA3)	-	1.00	1.65	1.50	1.00	1.11	1.32	1.44	Mon	3.06	2.20	2.64
Ftsk/spoiiie family protein (D8DYX1)	-	-	-	-	1.00	0.97	0.81	0.98	Mon	Mon	Mon	Mon
Cell division protein FtsI (Penicillin-binding protein 3) (D8DU94)	1.00	-	-	-	1.00	0.47	0.34	-	1.39	Mon	Mon	-
Cell division protein FtsX (D8DVR7)	-	-	-	-	-	1.00	1.42	3.81	-	Mon	Mon	Mon
Cell division protein FtsZ (D8DTR9)	-	-	-	-	-	-	1.00	-	-	-	Mon	-

Color code:	-	0.1	1	5	10	Color code:	Con	0.5	1	5	Mon
-------------	---	-----	---	---	----	-------------	-----	-----	---	---	-----

Second Publication

Table S22: Glucose forming glucosidases with gradually descending abundance cells with and without monensin over time. The green-yellow-red color code illustrates the fold-change within conditions control (Con) and monensin (Mon), while blue-yellow-brown shows the ratio of protein abundance of Mon:Con. Fields without quantification are displayed by a grey-filled field with a dash. Fields with Mon or Con indicate that in this sample the protein was only quantified in the monensin (Mon) or the control (Con) condition.

Name (Uniprot ID)	KO Number	0 μ M Monensin (Con)				20 μ M Monensin (Mon)				Ratio Mon : Con			
		9h	24h	48h	72h	9h	24h	48h	72h	9h	24h	48h	72h
Alpha-glucosidase (D8DXY7)	K21574	1.00	0.08	0.00	-	1.00	0.42	0.27	0.12	0.35	1.87	176.36	Mon
Putative glycosyl hydrolase, family 13 (D8DXY9)	K21575	1.00	0.11	-	0.00	1.00	0.36	0.13	0.14	0.24	0.75	Mon	12.96
Beta-glucosidase (AOA1H9IED8)	K05349	1.00	0.10	-	0.07	1.00	0.96	1.70	4.95	0.13	1.25	Mon	9.27
Alpha-L-arabinofuranosidase A (D8DZD6)	K01209	1.00	0.11	0.08	0.05	1.00	0.33	0.30	0.19	0.59	1.87	2.12	2.36
Fructan beta-(2,6)-fructosidase (D8DUL1)	K03332	1.00	0.25	0.03	0.01	1.00	0.49	0.37	0.31	0.26	0.50	3.12	6.10
Beta-galactosidase (D8DV08)	K12308	1.00	0.19	0.08	-	1.00	0.29	0.31	0.40	0.34	0.52	1.28	Mon
Beta-galactosidase (D8E0G2)	K01190	1.00	0.24	0.07	0.07	1.00	0.48	0.48	0.74	0.18	0.35	1.23	1.83
Glycosyl hydrolases family 2 (D8DWD5)	K01190	1.00	0.44	0.40	0.45	1.00	0.56	0.54	0.74	0.43	0.55	0.57	0.71
Beta-galactosidase (D8DW02)	K01190	1.00	0.33	0.22	0.28	1.00	0.60	0.55	0.78	0.23	0.42	0.59	0.66

Color code:	-	0.1	1	5	10		Color code:	Con	0.5	1	5	Mon
-------------	---	-----	---	---	----	--	-------------	-----	-----	---	---	-----

3.9 Supplementary figures

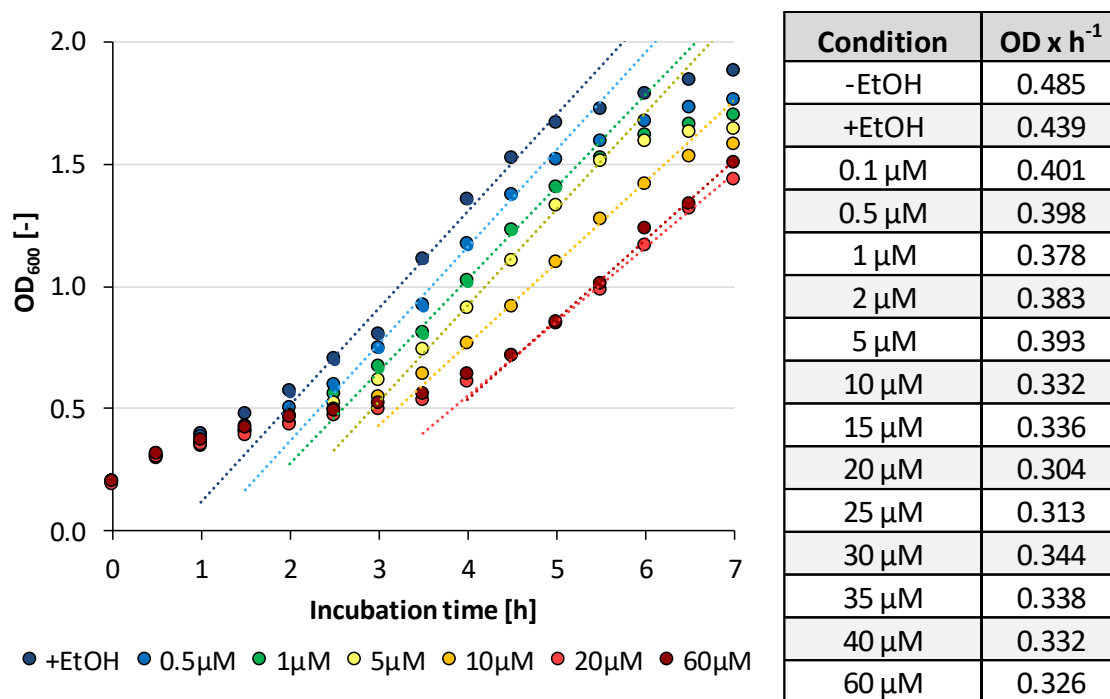


Figure S14: Growth curves with table of growth rates per hour at various monensin concentrations. Average optical density (OD; n=3) was determined at a wavelength of 600 nm and a linear trend line was fitted through the measure points during the exponential growth phase. Table on the right side displays the growth rates during exponential phase of *P. bryantii* B₁₄ under various monensin concentrations.

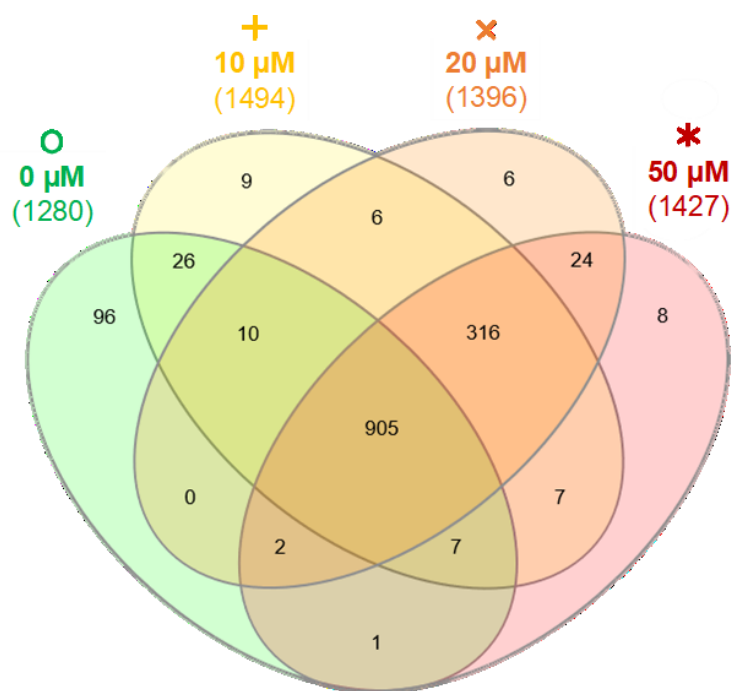


Figure S15: Venn diagram of proteomes under monensin. Each treatment contained six replicates (n=6). A protein was only counted if at least 4 of 6 replicates were quantified.

Time points				Control		Monensin	
9 h	24 h	48 h	72 h	n	%	n	%
○				136	11%	116	9%
	○			78	6%	18	1%
		○		5	0%	35	3%
			○	14	1%	2	0%
○	○			96	8%	44	4%
○		○		0	0%	17	1%
○			○	2	0%	5	0%
	○		○	30	2%	0	0%
		○	○	9	1%	3	0%
	○	○		14	1%	39	3%
○	○	○		21	2%	222	18%
○	○		○	28	2%	3	0%
○		○	○	1	0%	5	0%
	○	○	○	178	14%	15	1%
○	○	○	○	625	51%	942	76%
Total:				1237		1466	

Figure S16: Dot plot of proteomes at 9, 24, 48 and 72 h of incubation time under control, monensin or combined conditions. Each time point at each condition consists of triplicates (n=3). Percental contribution to total number of quantified proteins for each condition and combination were given below the diagram.

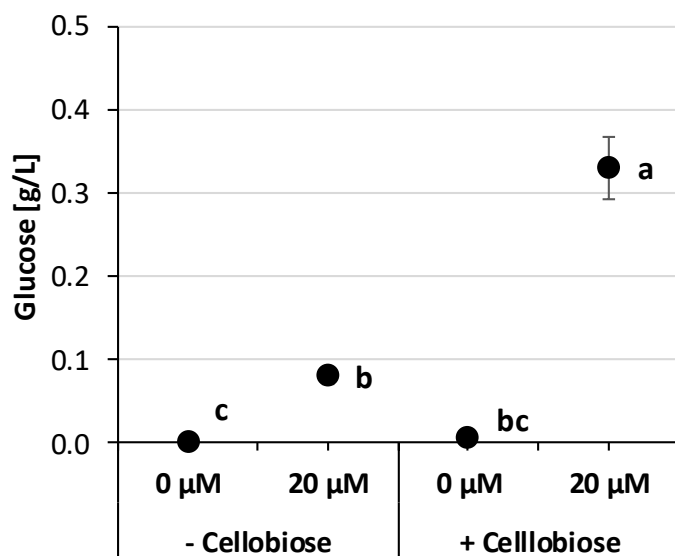


Figure S17: Glucose concentrations in supernatant of cultures with and without cellobiose and with and without monensin after 73 h. Black dots represent glucose with the left y-axis. Error bars indicate standard deviation. Not commonly shared letters indicate significant difference by the Fisher-LSD test ($p < 0.01$) for glucose.

a

Name (Uniprot ID)	EC Number	0 μ M Monensin (Con)				20 μ M Monensin (Mon)				Ratio Mon : Con			
		9h	24h	48h	72h	9h	24h	48h	72h	9h	24h	48h	72h
ATP phosphoribosyltransferase (D8DYW0)	2.4.2.17	1.00	16.42	26.57	24.58	1.00	1.98	2.38	1.57	11.91	1.43	1.07	0.76
Histidine biosynthesis bifunctional protein HisE (D8DY88)	3.5.4.19 / 3.6.1.31	-	2.18	1.44	1.00	1.00	1.28	1.47	0.82	Mon	0.65	1.13	0.91
1-phosphoribosylformimino-5-aminoimidazole-4-carboxamide isomerase (D8DY86)	5.3.1.16	1.00	0.10	-	0.14	1.00	0.45	0.47	-	0.18	0.78	Mon	Con
Imidazole glycerol phosphate synthase subunit HisH (D8DY85)	4.3.2.10 / 3.5.1.2	1.00	-	-	-	1.00	0.52	0.53	-	1.02	Mon	Mon	-
Imidazole glycerol phosphate synthase subunit HisF (D8DY87)	4.3.2.10	1.00	-	-	-	1.00	0.57	0.49	-	1.26	Mon	Mon	-
Histidine biosynthesis bifunctional protein HisB (D8DWS5)	3.1.3.15 / 4.2.1.19	-	-	-	-	1.00	1.74	2.59	1.91	Mon	Mon	Mon	Mon
Histidinol-phosphate aminotransferase (D8DYV8)	2.6.1.9	-	1.00	-	2.24	1.00	1.49	1.80	0.60	Mon	16.60	Mon	2.98
Histidinol dehydrogenase (D8DYV9)	1.1.1.23	-	1.00	-	-	1.00	0.99	1.24	0.87	Mon	8.04	Mon	Mon

Color code: - 0.1 1 5 10 Color code: Con 0.5 1 5 Mon

b

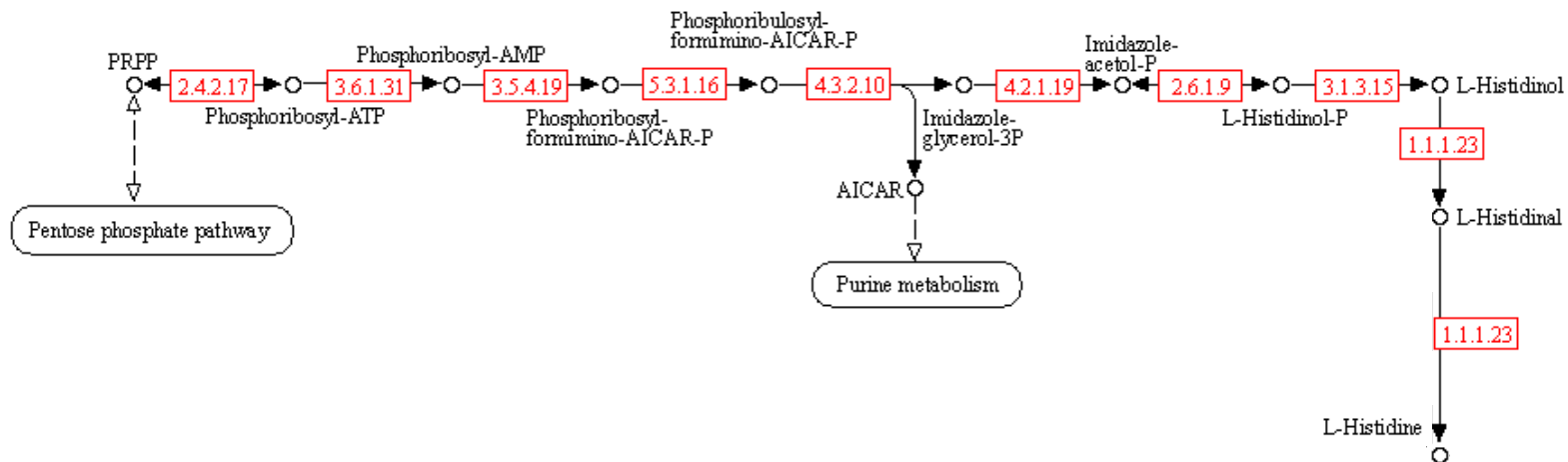


Figure S18: Histidine biosynthesis pathway with enzymes and their abundance within a time series between monensin absence or presence. (a) Displays the abundance on respective enzymes in their order for histidine synthesis. The green-yellow-red color code illustrates the fold-change within conditions control (Con) and monensin (Mon), while blue-yellow-brown shows the ratio of protein abundance of Mon:Con. Fields without quantification are displayed by a grey-filled field with a dash. Fields with Mon or Con indicate that in this sample the protein was only quantified in the monensin (Mon) or the control (Con) condition. (b) The KEGG pathway (ko00350) for histidine biosynthesis. Red written EC numbers can be found also in a of this graph.

4. A shift towards succinate-producing *Prevotella* in the ruminal microbiome challenged with monensin

By Andrej Trautmann ^{1,2}, Lena Schleicher ^{1,3}, Ariane Koch ³, Johannes Günther ³, Julia Steuber ^{1,3}, Jana Seifert ^{1,2*}

¹ HoLMiR - Hohenheim Center for Livestock Microbiome Research, University of Hohenheim, Stuttgart, Germany

² Institute of Animal Science, University of Hohenheim, Stuttgart, Germany

³ Institute of Biology, University of Hohenheim, Stuttgart, Germany

Correspondence: jseifert@uni-hohenheim.de; Jana Seifert (University of Hohenheim, Institute of Animal Science, Emil-Wolff-Str. 6-10, 70593 Stuttgart, Germany)

Journal: Proteomics; **Manuscript No.:** pmic.202200121.R1

Received: 03.June 2022 / **Revised:** 30.September 2022

4.1 Abstract

The time-resolved impact of monensin on the active rumen microbiome in a rumen-simulating technique (Rusitec) was studied with metaproteomic and metabolomic approaches. Monensin treatment, decreased catabolism linked to fiber degradation was observed by the reduced abundance of proteins assigned to fibrolytic bacteria and glycoside hydrolases, sugar transporters and carbohydrate metabolism. Reduced amounts of ammonium as well as branched-chain fatty acids refer to a decreased proteolytic activity. The family Prevotellaceae exhibited increased resilience in the presence of monensin, with a switch of metabolism from acetate to succinate production. *Prevotella* species harbor a membrane bound electron transfer complex, which drives the reduction of fumarate to succinate, the substrate for propionate production in the rumen habitat. Besides the increased succinate production, a concomitant depletion of methane concentration was observed upon monensin exposure. Our study demonstrates that *Prevotella* sp. shifts its metabolism successfully in response to monensin exposure and Prevotellaceae represents the key bacterial family stabilizing the rumen microbiota during exposure to monensin.

Keywords: Metaproteome, Metabolome, Monensin, *Prevotella*, Rumen

4.2 Introduction

The ionophore monensin is primarily used for treating metabolic disorders in ruminants [188] and coccidiosis in poultry farming [79]. Due to the reduced methane production and enhanced feed utilization [189, 190], monensin became a promising feed supplement in animal farming. The overuse of monensin as a growth promotor provided the development of resistances towards monensin and other ionophores [191, 192], even if such

a scenario seems to be unlikely for livestock consumers [193]. In the European Union and within other European countries the use of monensin was declared solely for therapeutic and preventive interventions [65, 194]. Monensin is used to treat coccidiosis in broilers and ketosis, acidosis and acute bovine pulmonary edema and emphysema in cattle [79, 188, 195, 196]. In the rumen, monensin inhibits acetate formation which results in a lower amount of hydrogen [197]. Since hydrogen is need for methanogenesis, the formation of methane is limited [198, 199]. The rumen microbiome is a highly diverse ecosystem and consists of several microbial groups covering a broad metabolic capacity [200]. Monensin is an ionophore which preferentially complexes and transports Na^+ across lipid membranes, hereby dissipating electrochemical sodium gradients of bacterial membranes. It is most effective against Gram-positive bacteria [193]. *Prevotella* is a major key genus in the rumen. It was found to be resilient towards monensin, with *P. bryantii* B₁₄ exhibiting the highest resilience [201]. Former *in vivo* and *in vitro* studies of the rumen microbiome treated with monensin showed reduced methane and increased propionate and succinate formation [89, 90]. Also, a reduced proteolytic activity was observed by Wallace et al. (1981) [90]. As a consequence, monensin induced cattle fattening was explained by an increased hepatic gluconeogenesis originating from the elevated propionate levels [190, 202]. However, the detailed metabolic routes affected by monensin treatment and the molecular mechanisms leading to resilience of *Prevotella* sp. against monensin remained unclear.

In the past, effects of monensin were studied using the Rusitec or similar *in vitro* systems focusing on a narrow range of specific microbial groups and metabolites [203-207]. Former Rusitec experiments revealed adaptation phases between of 2 to 13 days, with a tendency closer to 2 days, after which the treatment with an established microbial consortium can be done [208]. In the present study, the adaptation period was adjusted to one week and the use of a multiomics approach revealed a novel mechanism applicable in *Prevotella*: the dissipation of the Na^+ -gradient by monensin is counteracted by the increased activity of a Na^+ -translocating membrane protein complex which reduces fumarate to succinate. The implications of this catabolic route on the cellular and metabolic functions of the ruminal bacteria challenged with monensin are discussed.

4.3 Material and methods

4.3.1 Diet and treatment preparation

A total mixed ratio (TMR) including 40% dried maize silage, 20% dried grass silage, 20% soybean meal extract and 20% dried corn grains (dried for 48 h at 60°C and percentage refers to weight). All ingredients were milled through a sieve of 0.5 mm (SM1, Retsch) and mixed for 15 min with the M200 (GLP, Gebrüder Lödige Paderborn). Nylon bags (100 x 50 mm, pore size=0.1 mm) were filled with 15 ± 0.01 g of TMR and were sealed with a cable tie. Filled bags were stored under dry conditions and in absence of light at 8°C until further usage. During treatment phase, 1 mL of a monensin stem solution (280 mg monensin / 45 mL ethanol) was added to TMR in nylon bags to gain in a final concentration of 415 mg monensin / kg TMR. The control treatment was supplemented the TMR only with ethanol. In all bags, ethanol was evaporated before TMR bag was placed in the reactor vessel. The buffer was prepared one day before usage as described in the study of McDougall (1948) [209].

4.3.2 Inoculation and Rusitec design

Four lactating Jersey cows were fed *ad libitum* with straw and TMR, with same composition as described before, for at least one week before rumen fluid sampling. Sampling was done through the rumen fistula using a tube connected to a vacuum pump to sample rumen fluid, rumen solid material was sampled manually. Rumen fluid from all cows was combined and filtered through two layers of cheesecloth at a temperature of 39°C. Six thermostatic reaction vessel (Gassner Glastechnik GmbH) were run in parallel, each was filled with 500 mL rumen fluid and 500 mL of buffer with same composition as in Wischer et al. (2013) [203]. Two nylon bags were placed into the agitating cage inside the filled vessel. One bag contained TMR and was replaced by a fresh bag every 48 h. The second nylon bag contained an equal amount of ruminal solid phase from each cow (totally - change 60 g) and was replaced after 24 h by a fresh TMR bag. The change of the TMR bag of every 24 h simulates the feed intake of the ruminant and additionally the fiber attached microbes are allowed to colonize the newly introduced solid matter. The vessel content was kept at $39 \pm 0.5^\circ\text{C}$ and mixed by agitating the feed container up- and downwards (12 rpm) to simulate the peristaltic movement of the rumen. Artificial saliva, represented by the buffer [203], was introduced into the vessel by a peristaltic pump (IPC, ISMATEC) with a flow of approximately 31.2 mL/h, resulting in a 75% volume exchange within one day. Produced gas and superfluous liquid eluted via the overflow into a cooled gas trap (ca. 0°C) separating liquid and gas phase. The

liquid phase was directed into waste containers and discarded, while the produced gas amount was channelled to the gas meter (BlueVCount, BlueSens), which exhausted the measured gas into a gas proof bag (Plastigas, Linde). Total gas emission was measured online from day 1 until day 17. The technical setup is illustrated in Figure 18a.

4.3.3 Parameter measurement and sampling

Daily temperature measurements via a rod thermometer (TFA Dostmann) were required to maintain and mimic the optimal rumen temperature. The volume of the overflow in the waste vessels was measured daily to evaluate the continuous buffer supply. Total gas production was determined by the gas meters (BlueVCount, BlueSens). Methane concentration of accumulated gas was daily determined by channeling the accumulated gas through the Advanced Gasmitter (Pronova). Liquid phase of the reaction vessel (18 mL) was retrieved via a syringe for metabolic analysis. A FiveEasy pH meter (Mettler Toledo) was used to determine pH within a sample tube directly after the collection. TMR was sampled after 48 h of incubation from the nylon bag to investigate solid phase adherent microbes with

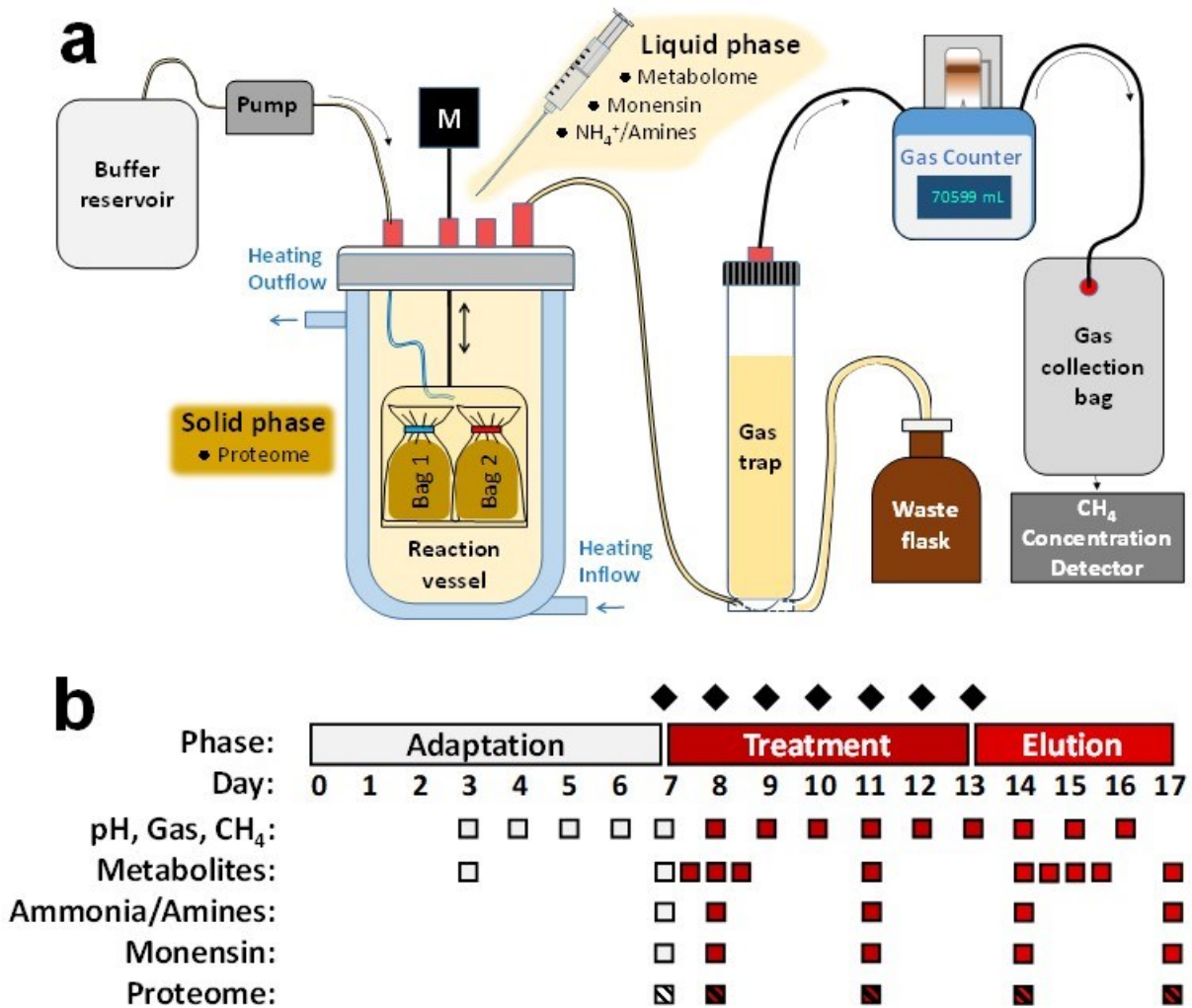


Figure 18: Experimental setup. **a:** Technical setup of the rumen simulation technique (Rusitec) with indication of sampling material and gas measurement, including methane. **b:** Timepoints of sampling for respective analysis are marked by a square (□). Striped squares indicate that total mixed ratio was sampled as solid material for the respective analysis. Daily addition of monensin in the treatment phase is indicated by black diamonds above the phase description (◆).

proteomic analyses. Sampling and daily TMR exchange was always conducted under CO₂ gassing on the exposed reactor content, to maintain anaerobic conditions. Samples were transferred directly on ice before storage at -80°C. Time points for sampling are illustrated in Figure 18b. During the first two days of treatment and elution phase, samples for metabolome analyses were taken in an interval of 12 instead of 24 h.

4.3.4 Experimental setup

The experiment was divided in three phases starting with: adaptation, treatment and elution. Three reaction vessels were set up for either monensin presence (MON) or absence (CON). In the adaptation phase (first 7 days), ruminal microorganisms adapted primarily to the *in vitro* conditions without monensin. Monensin was supplemented to the MON group only during the treatment phase (day 7 to 14). Elution phase was defined as day 15 to 18 (Figure 18b).

4.3.5 Gas slope calculations

Gas production behavior was monitored by calculating the linear slope by hour, using measurements of every minute starting from day 3 to 17. Slope calculation was performed by using Excel (Microsoft Office, v.2016).

4.3.6 Monensin quantification via LC-MS

Fluid samples of three reactor vessels (MON) were combined and centrifuged from selected time points (7, 8, 11, 14, 17 d). Supernatants were purified by means of an SPE column (Phenomenex Strata, C18), which was loaded and washed with 2 mL ddH₂O. Elution of the trapped substances was conducted with 1 mL methanol and eluent was dried under N₂ gassing before resuspension in methanol. For compound separation 5 µL purified sample were loaded on an ACQUITY UPLC CSH Fluoro-Phenyl column (50 x 2.1 mm, 1.7 µm, 130 Å; Waters). With a flow of about 0.3 mL/min a gradient, consisting of solvent A (0.2% formic acid in ddH₂O) and solvent B (0.2% formic acid in methanol), was used. Solvent B increased from 40-60-80-100-100% within 0-3.50-10.00-10.30-12.00 min. Components were fragmented using the Q-Exactive plus (Thermo Fisher Scientific) with positive ionization and a resolution of 70,000. Fragment detection was in the m/z range from 150 to 1,100 with a TopN of five.

4.3.7 Quantification of [NH₃ + NH₄⁺]

Collected liquid phase of the Rusitec was centrifuged (21,130 x g, 15 min, 4°C) and 100 µL of 1:10 diluted supernatant was added to 800 µL of water and 100 µL of Nessler reagent (Roth). Mixture was incubated for 5 min at room temperature without agitation before absorbance was measured at λ = 425 nm photometrically (Bio Genesys 10, Thermo Fisher). Calibration curve with Nessler reagent was established with NH₄SO₄ in a range from 0.25 to 5 mM (R²=0.995).

4.3.8 Metabolome analysis by ¹H-NMR spectroscopy

Metabolite concentrations were obtained by quantitative ¹H-NMR [210]. Liquid samples from selected time points (3, 7, 7.5, 8, 8.5, 11, 14, 14.5, 15, 15.5 and 17 d) were centrifuged (10,000 x g, 30 min, 4°C) and supernatant was filtered through a 0.2 µm cellulose acetate filter (C. Roth, Germany). Three milliliters were dried in a vacuum centrifuge (program: V-AQ at 22°C, Concentrator Plus, Eppendorf). Metabolites were two-fold concentrated by suspending in 1.5 mL deuterated potassium-phosphate buffer (50 mM, pH 7), including 5 mM 3-trimethylsilyl-propionic acid 2,2,3,3-d₄ (TSP) as an internal standard. Freshly solved samples were centrifuged (13,000 x g, 30 min, 4°C) and the soluble part was transferred into an NMR-tube (d=5 mm). ¹H-NMR was performed subsequently with a 600 MHz spectrometer (Avance IIIHD, Bruker Corporation) equipped with a Cryoprobe Prodigy BBO. 1D ¹H-NMR experiments based on the first increment of a 2D NOESY pulse sequence (1D NOESY) with 16 scans, 100 ms mixing time, 12 ppm sweep width and 4 s acquisition time (about 57k data points) were run at room temperature with Topspin software (Version 3.6.1, Bruker Corporation). Processing (phase correction and baseline correction, manually performed) and metabolite quantification was conducted by using the Chenomx NMR suit (Chenomx Inc., v.8.6).

4.3.9 Protein extraction and purification

Solid sample material from nylon bags were retrieved from three reactors per treatment group (CON, MON) at selected time points (7, 8, 11, 14, and 17 d), while time point 0 d was a unique sample (fresh rumen material). These single solid samples of each treatment group and time point were pooled to a total mass of 4 g solid sample material, and incubated with 35 mL methylcellulose buffer (200 mM NaCl, 50 mM Tris-HCl, 0.1% (w/v) methylcellulose, pH 8) under 30 min rotation at 4°C and subsequent vigorous mixing. After sonicating the samples in the water bath (RT = 20±1°C) for 1 min, they were vacuum filtrated through a 2-layered sterile cheesecloth via a strainer and washed twice with 25 mL of rinsing buffer (200 mM NaCl, 50 mM Tris-HCl, pH 8). Samples were centrifuged (200 x g, 10 min, 4°C), and the resulting supernatants were centrifuged once again (10,000 x g, 15 min, 4°C). Obtained pellets were washed twice with 5 mL wash buffer (50 mM Tris-HCl, 0.1 g/L chloramphenicol, 1 mM PMSF, pH 7.5). Pellets were stored at -20°C until protein extraction. Protein extraction and purification was performed as described by Trautmann, A., *et al.* [1] and modified by adapting the amount of precipitated protein to 80 µg.

4.3.10 Tandem mass spectrometry

Nano-LC-ESI-MS/MS experiments were performed on an EASY-nLC 1200 (Thermo Fisher Scientific, Germany) coupled to a Q-Exactive HF mass spectrometer (Thermo Fisher Scientific, Germany) equipped using a NanosprayFlex source (Thermo Fisher Scientific, Germany) in the University of Hohenheim, Stuttgart, Germany. Tryptic digested peptides were directly injected to a NanoEase analytical column (NanoEase M/Z HSS C18 T3, 1.8 μm 100 \AA 75 μm x 250 mm column, Waters GmbH, Germany) at a constant temperature of 35°C by a PRSO-V2 column oven (Sonation GmbH, German) and a flow of 250 nL/min. A gradient with solvent A (0.1% formic acid) and B (0.1% formic acid and 80% acetonitrile) was run for 140 min (0-115-130-140 min) with increasing solvent B (1-50-56-95%). The Orbitrap of the Q-Exactive HF enabled a resolution of 60,000 with a range from 200 to 2000 m/z and a TopN of 20. Tandem MS spectra were generated for the 20 most abundant peptide precursors using high-energy collision dissociation (HCD) at a resolution of 15,000, normalized by a collision energy of 27. Lock-mass ions from the ambient air were used for internal calibration [211].

4.3.11 Metaproteomic data analysis

Tandem mass spectra from selected time points (7, 8, 11, 14, and 17 d) of CON and MON were analyzed by Metalab (v.2.1.1.7) [212]. Default settings were used to obtain label-free quantification (LFQ) values of proteins. Protein identification was based on a freely available rumen metagenomic database [213]. Functional annotation was conducted using EggNOG [214] and the predetermined labels from Stewart, R.D., *et al.* [213]. LFQ values of proteins with the same KEGG orthology ID were summed up for KEGG pathway analysis of the total quantified microbiome for each time point. Comparative analysis of protein numbers was always performed by subtracting the number of quantified proteins of the monensin group from the control group (CON - MON). For comparative analysis with quantitative protein measurements, LFQ ratios between monensin versus control group, were used to display a fold-change within the ratio (MON/CON). Pearson correlation was performed with relative abundance values in Excel (Microsoft Office, v.2016). Proteins aligning in number and abundance with treatment duration and monensin concentration underwent a closer investigation. For KEGG mapper analysis, at least three of five time points required to be elevated in CON or MON in terms of summed LFQ values and number of proteins for a certain KEGG orthology ID. Additionally, a similar pattern as the monensin concentration and the experimental phases were elucidated for further investigation and demonstration.

4.3.12 Data analysis

Principal coordinate analysis (PCoA) was performed using a Bray-Curtis similarity matrix with standardized LFQ values in PRIMER 6 & PERMANOVA+ (v.1.0.6). Differential analysis in number were always calculated by subtracting the number of quantified peptides or proteins of the monensin group from the control group. LFQ-values from the monensin group were divided by the control group for each time point and formed a ratio for quantitative analysis. COG classes were additionally analyzed using the number of proteins from CON minus the number of MON, which shows information about differences of the absolute quantity. Statistical analysis were conducted using the least significant difference (LSD) test in Infostat (v.2008) [186].

4.4 Results

4.4.1 Gas and methane emission

The gas production rate and the methane concentration of the monensin reactors decreased directly after the first monensin supply (Figure S19a, b). Methane concentration decreased significantly in the monensin group (MON, $p < 0.05$), while the control group increased (CON, Figure S19b, c). The difference in methane concentration remained until the end of the elution phase (17 d), where methane concentrations increased slightly in monensin group. Total amount of daily gas production was fluctuating between mean volumes of 600 and 1000 mL/d during the experiment in all vessels (Figure S19c).

4.4.2 Fermentation and metabolites

The pH of medium was mostly not affected among the two treatment groups along the whole experiment (Figure S21). An overall increase of fermentation products was found at time point 7.5 d in MON, when monensin was already introduced for 12 h (Figure 19). Concentrations of acetate, propionate and valerate decreased initially after 24 h of monensin introduction and not directly after 12 h (day 7.5). Summed averages of organic acid concentrations, including formate, acetate, propionate, butyrate, valerate, isobutyrate, isovalerate and succinate, remained stable during all phases in CON. A decrease of summed averages of organic acids was observed during treatment phase and an increase during the elution phase in MON (Figure S20). Fermentation products showed a decrease of multiple compounds after 24 h of the first monensin supply (Figure 19, Figure S22) with high variations in low concentrated metabolites (Figure S22). In the elution phase, propionate and valerate

increased significantly ($p < 0.05$) in MON (Figure 19). Low concentrated fermentation products such as formate and succinate showed fluctuations in MON along the complete experimental period (Figure 20). A decreasing trend in concentrations of isobutyrate (Figure 20a) and isovalerate (Figure 20b) was shown during the treatment phase in MON, which aligned with the ammonium and amine concentration (Figure 20c). These proteolytic side products, especially ammonia, decreased significantly at day 11, 14 and 17 from about 3.5 mM to 1.5–2.0 mM (Figure 20c).

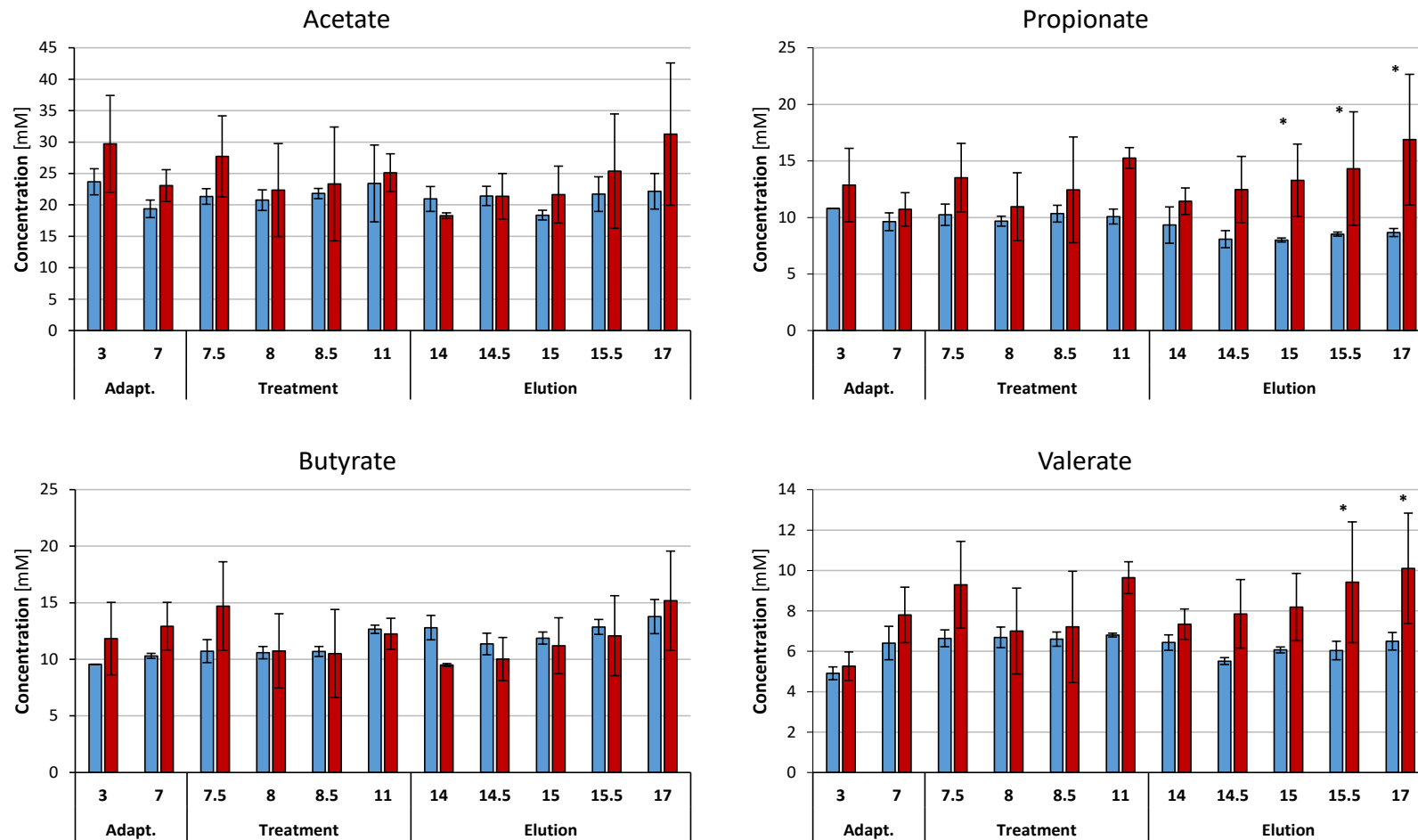


Figure 19: Average metabolite difference between CON and MON from Rusitec supernatant determined by $^1\text{H-NMR}$. Metabolite excess in control are positive concentration while excess in monensin group are negative concentrations. Error bars indicate standard deviation ($n=3$) while asterisk (*) indicates a significant difference between both groups (LSD-Fisher, $p<0.05$). Time point zero is represented the inoculation sample ($n=1$). **a)** Higher abundant fermentation products. **b)** Low concentrated metabolites.

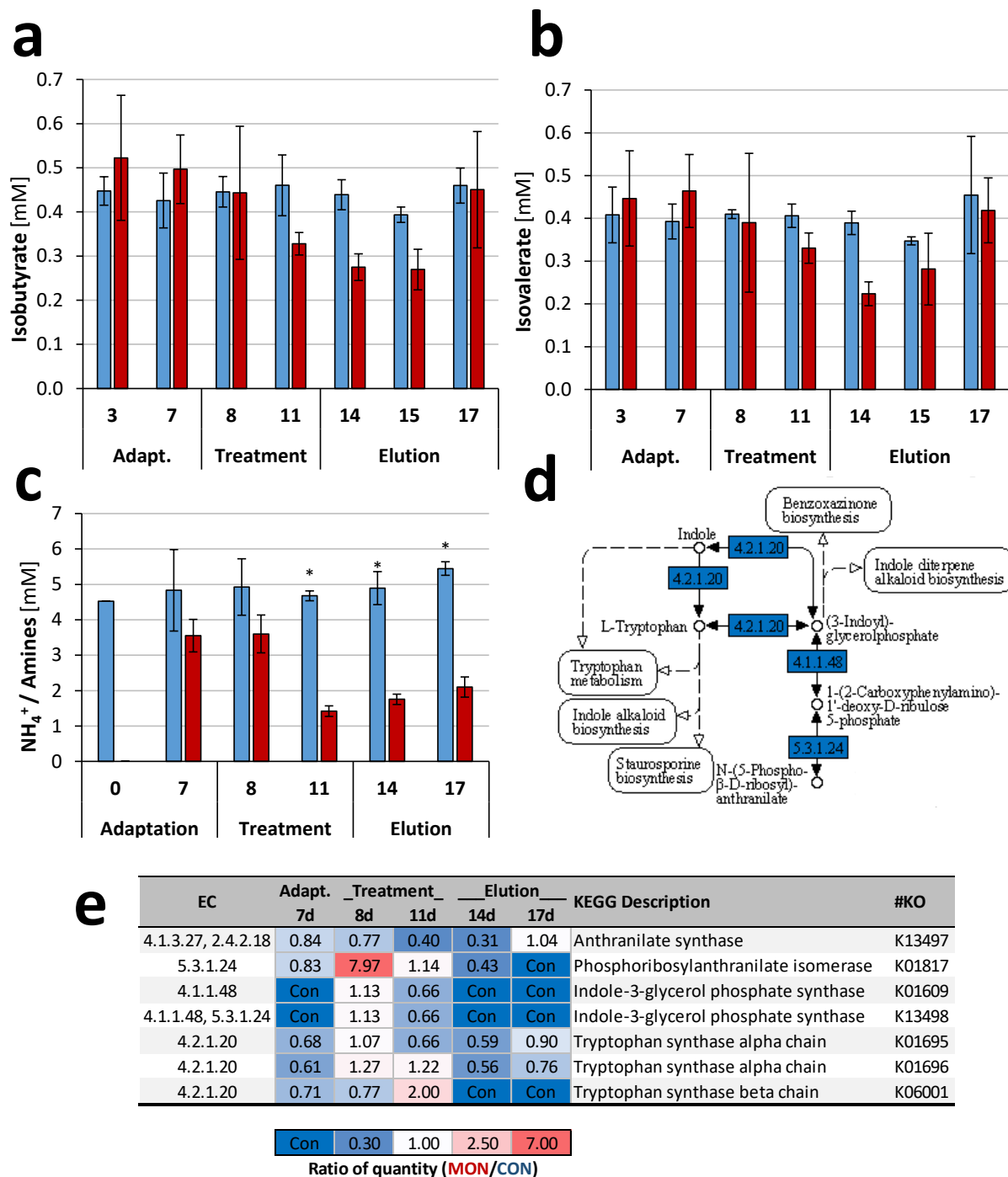


Figure 20: Monensin treatment results in a decrease in proteins involved in proteolysis and tryptophan biosynthesis. Mean proteolysis indicators (n=3) with standard deviations and asterisks (*) as significant differences (LSD-Fisher; p<0.05) between CON (blue) and MON (red) were shown like **a**) Isobutyrate **b**) Isovalerate and **c**) Ammonia and amines. **d**) Phenylalanine, tyrosine and tryptophan biosynthesis KEGG map (ko00350) with blue marked enzymes elevated in quantity (LFQ-values) and number in CON (blue) during treatment and elution phase. **e**) Ratio of summed LFQ-values based on EC corresponding to KEGG map ko00350.

4.4.3 Monensin in reactor effluent

Relative monensin quantifications showed a linear increase of monensin in the reactor fluid starting from day 8 (Figure S23). The maximum monensin concentration was most likely achieved after the last monensin supplementation between day 13 and 14. An approximate monensin elution of 200% per day can be calculated when monensin supplementation was ceased after day 13 to 17.

4.4.4 Metaproteome is altered by monensin exposure

In total 9,159 protein groups were identified, and out of this 7,149 protein groups were quantified with LFQ values at the time points 0, 7, 8, 11, 14 and 17 d. A core proteome of 2,532 protein groups were found among all time points and both treatment groups (Table S23). A peptide identification rate of 18.7% (Total peptides found: 28,419) was achieved with the

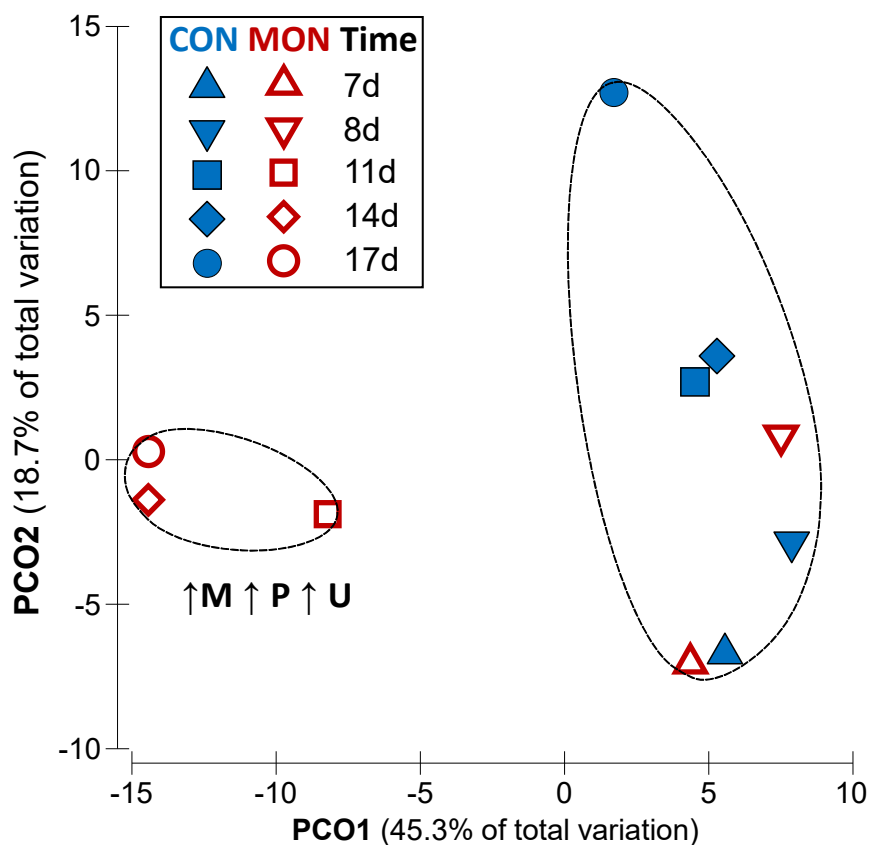


Figure 21: Principal Coordinate plot of proteins obtained from solid samples retrieved from Rusitec consortia with or without monensin treatment. 7149 quantified proteins were standardized by total and underwent a resemblance by Bray Curtis similarity. Dashed line indicate sample clustering with 80% similarity. The legend displays the CON (blue) and MON (red) conditions with different symbols for each time point. Adaptation phase (7d), treatment phase (8, 11, 14d) and post-treatment phase (17d). Selected cluster of orthologous groups (COG) are indicated as an elevated (↑) unique feature for certain samples and clusters. COG: membrane biogenesis (M); inorganic transport and metabolism (P); intracellular trafficking and secretion (U).

database from Stewart et al. [213]. Measurements at time point 0 d were excluded for direct comparison between both groups. Distribution of metaproteomic datasets of the reactor samples based on time points and groups is depicted in Figure 21. Two sample clusters with 80% Bray-Curtis similarity can be identified. The first cluster, including three samples from MON group, was characterized by an increase of proteins from membrane biogenesis, inorganic transport and metabolism and intracellular trafficking.

Among all detected proteins, about 32% were assigned to *Prevotella*, showing the dominance of this genus in the active community. Proteins affiliated to *Selenomonas* (6.2%), Lachnospiraceae (4.4%) and *Treponema* (3.9%) followed with a descending average contribution (Table S24). LFQ values were used to calculate the ratio of the metaproteomes between MON and CON at respective time points. Bacterial taxons identified on single protein groups were divided into monensin fast and slow responding groups. Slow responders were defined by a correlation coefficient (R^2) >0.6 with the relative monensin concentration and MON/CON ratio for taxons that had a contribution of at least eleven peptides which was set as a threshold for this dataset (Table S25). Meaning that slow responders seem to react corresponding to the amount of monensin in the Rusitec. A gradual decrease over time was seen for *Actinobacteria* in MON, which was verified on deeper taxonomical ranks in the genus *Bifidobacterium* (Figure 22). Linear trends in MON | CON (\searrow | \nearrow) showed the effect of monensin on the amount of Bifidobacteriaceae, which was contributing about 0.3% to the total LFQ-value at family level. Other slow responding families were Acidaminococcaceae, increased slightly within MON, and Ruminococcaceae which increased in CON.

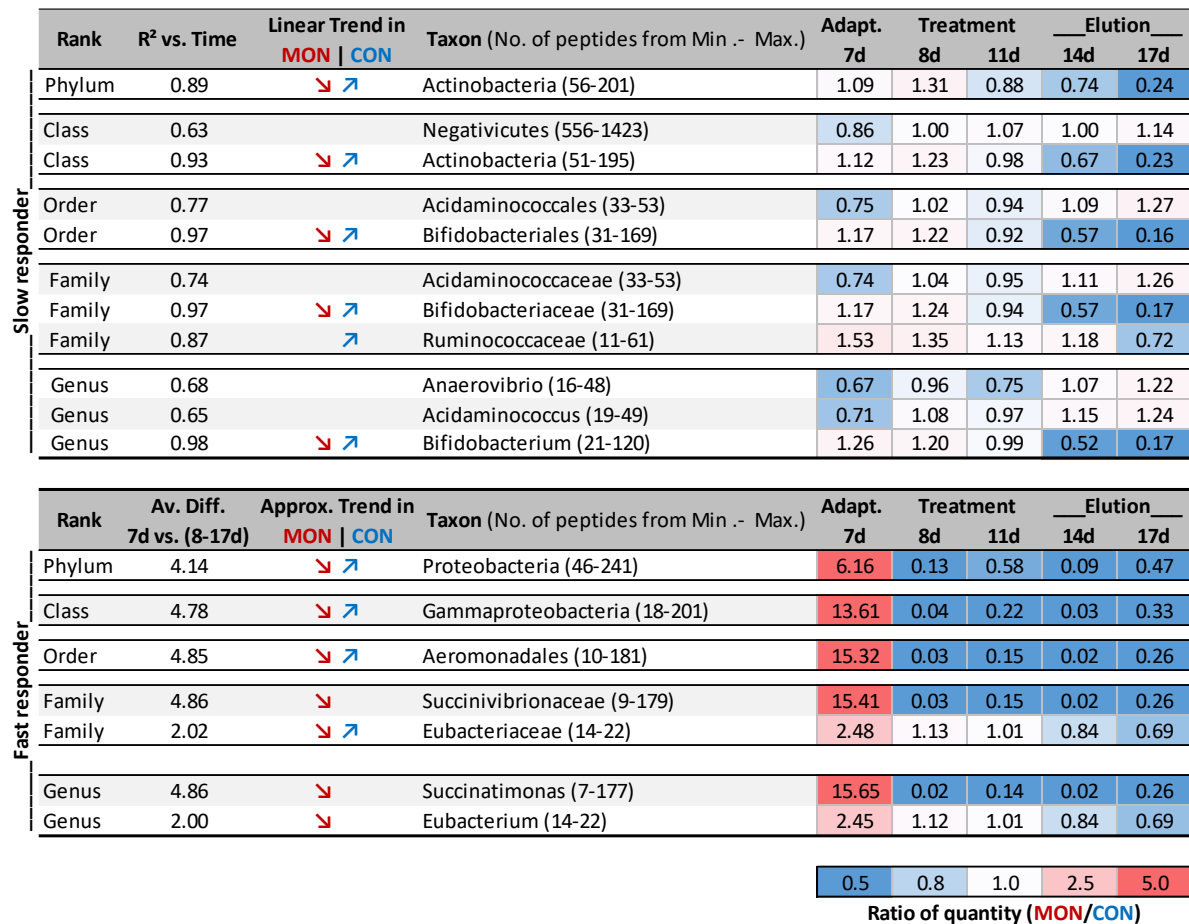


Figure 22: Time course of relative peptide abundances from Rusitec consortia with or without monensin treatment reveal slow and fast responding microorganisms. Slow responding microbes appeared with a linear relation to monensin concentration, wherefore $R^2 \geq 0.6$ was used. Fast responding microbes had an exponential relation to monensin concentration, which is why fold-change ≥ 2 between ratio of time point 7d and the average of ratios from 8–17 d was used. More abundance in MON is displayed in red while for CON in blue. Taxon assignment was indicated with the minimal and maximal number of contributed peptides over time in brackets. Ratio was calculated by dividing the relative abundance of the MON by CON. Trends for MON (red) and the CON (blue) either increased (\nearrow), decreased (\searrow) or remained unchanged over time (absent arrow).

4.4.5 *Prevotella* species are less affected by monensin

The highest number of quantified proteins with the used database from Stewart et al. (2019) belonged to the dominant genus *Prevotella* (Table S24) and proteins of seven *Prevotella* species were identified with at least ten species-specific peptides (Figure S24). *Prevotella* species with most unique peptides were *P. multisaccharivorax*, *P. ruminicola* and *P. bryantii*. Latter two species were two- to three fold more abundant in MON from day 11 on. *P. multisaccharivorax* was more abundant in CON, while at day 11 and 17 they were elevated in MON. Most *Prevotella* species showed a gradual elevation to its maximum at day 17, when monensin was absent for three days. Most *Prevotella* species appeared to have a decreasing trend over time in CON, except *P. ruminicola* and *P. copri* (Figure S24). Linear trends in MON

were only found in *P. dentalis* and *P. copri*. *P. brevis* (formerly *P. ruminicola* 23 [34]) increased about 3-fold in the MON at day 11 and decreased at day 14 and 17. *P. bryantii* also increased in MON at day 11 about 2-fold and decreased proportional in both groups over time. *Prevotella* sp. S7-1-8 remained mostly unchanged until day 17, where an approximate 2.8-fold decrease was seen in CON. These predominant *Prevotella* species were represented by proteins from COG classes for carbohydrate metabolism (G), translation (J), membrane and cell wall biogenesis (M) and inorganic transport (P). Although *Prevotella* proteins are so dominant here, it must be clarified that these results were generated with the currently most suitable database for ruminants, which may not include rare microbes or have too less proteins of single taxa.

4.4.6 Functional metaproteome influenced by monensin

The variation of the metaproteomic data and the evolution of the bacterial functions among the control and monensin incubations over time were also detectable by the analyses of the COG classes (Figure 23). Proteins belonging to COGs of intracellular trafficking and secretion (U), cell wall/membrane/envelope biogenesis (M) and inorganic transport (P) were quantitatively predominant in MON (Figure 23). The LFQ ratio between MON and CON was slightly lower in proteins assigned to COG class G of the carbohydrate metabolism and transport (Figure 23). The alternate unweighted perspective showed a tremendous depletion of the total number of these proteins in MON from day 11 to 17 (Figure S7). Deeper insight was provided via KEGG pathway analysis of the quantified proteins resulting in 1,215 unique KEGG orthologues (KO). Major changes were detected in the starch and sucrose metabolism (ko00500), the amino acid metabolism (ko01230) and the carbon metabolism (ko01200). KO that appeared in number and quantity in either the CON or MON were shown in the KEGG mapper for the carbon metabolism (Figure S25). Several enzymatic reactions belonging to glycolysis, amino acid biosynthesis and fatty acid metabolisms were mainly elevated in CON during the experiment (Figure S25). An elevated number and quantity of proteins belonging to the TCA cycle (Figure 24a) was found in MON at day 11, 14 and 17. The prior fermentation product of the TCA cycle is succinate, which on average was always slightly higher in MON (Figure 24b). Elevated enzymes of the TCA cycle and especially the quinol:fumarate reductase (QFR) originated mainly from *Prevotella* species (Table S26). Elevated enzyme activity of the fumarate reductase was also found in a monensin supplemented Rusitec study pointing to an prevalence of less monensin-sensitive succinate producers [90].

A decrease of multiple proteins that were involved in tryptophan biosynthesis was identified in MON with a minimum at day 14 (Figure 20e). Proteins assigned to amino acid metabolism showed a similar trend to the depleted products of proteolysis (Figure 20b, d). Microorganisms such as *Prevotella ruminicola*, *Lactobacillus mucosae*, *Mitsuokella jalaludinii*, *Treponema sp. JC4*, *Prevotella dentalis* correlated with proteolytic side products in MON with an absolute average ≥ 0.6 and a minimum of 10 peptides per taxon (Table S25).

COG	COG Description	Adapt.	Treatment			Elution		Total Number [n]
		7d	8d	11d	14d	17d		
A	RNA processing and modification	0.970	Con	0.985	Con	1.003	6	
B	Chromatin Structure and dynamics	MON	-	-	-	-	3	
C	Energy production and conversion	0.999	1.000	0.998	1.001	0.997	2187	
D	Cell cycle control and mitosis	0.999	1.004	0.999	1.003	1.003	282	
E	Amino acid metabolism and transport	0.998	1.000	0.997	0.998	0.995	1428	
F	Nucleotide metabolism and transport	0.998	0.997	0.996	0.994	1.001	615	
G	Carbohydrate metabolism and transport	1.001	0.998	0.996	1.001	0.997	2493	
H	Coenzyme metabolism	1.000	0.997	0.997	1.001	0.995	546	
I	Lipid metabolism	1.000	1.007	0.997	0.996	0.988	351	
J	Translation	0.998	1.001	0.998	1.001	0.999	4059	
K	Transcription	0.992	1.001	0.996	0.997	1.004	645	
L	Replication and repair	0.984	0.999	0.999	1.001	0.999	249	
M	Cell wall/membrane/envelop biogenesis	1.000	0.999	1.010	1.011	1.008	1185	
N	Cell motility	1.000	0.997	0.998	0.998	0.995	774	
O	PTM, protein turnover, chaperone functions	0.999	1.000	1.002	1.005	0.997	1263	
P	Inorganic ion transport and metabolism	1.001	0.994	1.006	1.005	1.008	1188	
Q	Secondary Structure	1.000	0.999	1.001	1.004	1.004	60	
T	Signal Transduction	0.991	1.001	0.991	0.999	0.999	141	
U	Intracellular trafficking and secretion	1.003	1.001	1.010	1.014	1.011	417	
Z	Cytoskeleton	1.000	0.999	1.000	0.998	1.007	3	
S	Function Unknown	0.998	0.998	1.003	1.006	1.007	1149	
IS	Function Unknown (manually assigned)	0.998	1.002	1.009	1.012	1.002	828	

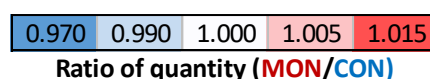


Figure 23: Shift in relative abundance of annotated proteins in solid phase of Rusitec consortia with or without monensin treatment over time. More abundance in MON is displayed in red while for CON in blue. Summed label-free quantification values of clusters of orthologous groups (COGs) from control and monensin group were divided (MON/CON). Right column indicates total amount of proteins detected. Color code of heat map is illustrated at the bottom of the differential and the relational approach. PTM in the COG description stands for post-translational modifications. One protein can belong to multiple COGs, which leads to a higher number sum of total counts than proteins are quantified.

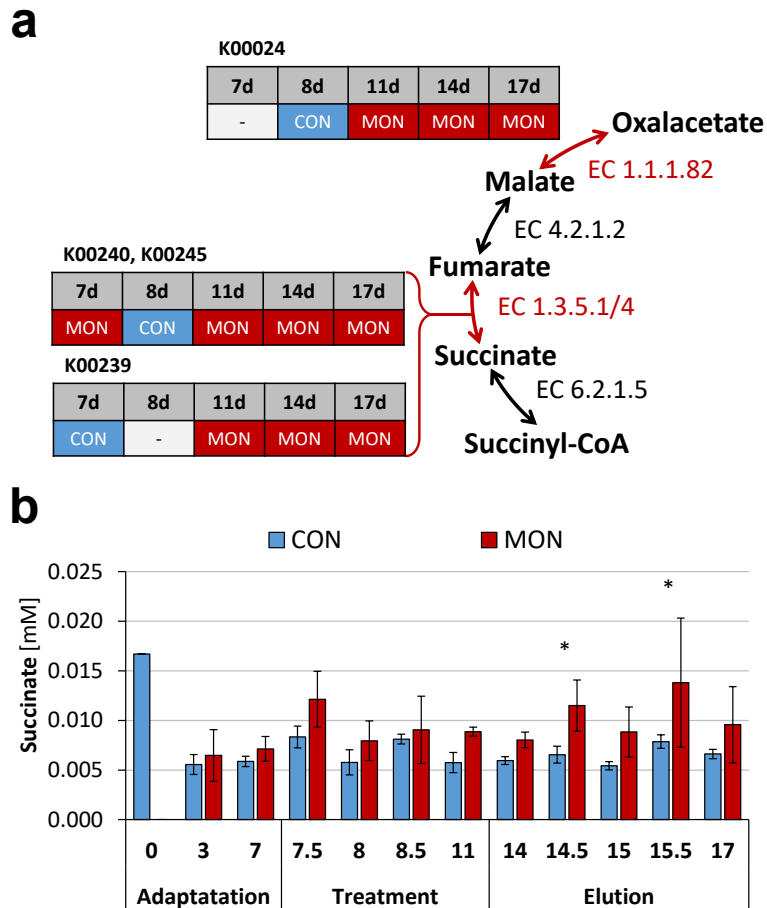


Figure 24: Enhanced succinate production in Rusitec consortium exposed to monensin. **a)** Highest protein number and abundance in group. Proteins of groups (CON, MON) exceeding number and summed quantity were displayed per time points. In case of a dash number or summed quantity was lacking. Red reaction arrows point out reactions elevated mainly in the monensin group. KEGG orthology numbers are indicated above the boxes. Enzyme commission number is located close to the reaction arrows. **b)** Mean Succinate concentrations with error bars standard deviations and asterisk as indicator for significance ($p < 0.05$, LSD-Fisher).

4.4.7 Monensin leads to reduced fiber digesting and assimilating capabilities of the microbiome

The downstream functional analyses revealed 1,401 proteins with one or more carbohydrate active enzyme (CAZyme) IDs out of 135 unique CAZyme families. Glycoside hydrolase (GH) 16 was the largest CAZyme family including 19 identified proteins, aligned with a decrease of the quantitative ratio over time ($R=0.73$) and were mostly represented by *Prevotella* species. Changes of protein abundance of CAZymes contributing to plant fiber degradation were listed in Figure 8. Day 14 marked the lowest ration for CAZyme families in MON among all time points, indicating a minimum of GH abundance. Carbohydrate esterases (CE) 1, CE12 and GH16 increased in MON over time, whereas most of the GHs decreased along

the treatment (Figure 25). Most of the selectively presented CAZymes were targeting cellulose β -1,4/1,3 glucan linkages (n=36), followed by pectin linkages (n=42), β -1,4 arabinoxylan (n=27) and β -1,4 xyloglucan (n=8). *Prevotella ruminicola* were majorly assigned to 21 proteins from GH35, followed by *Prevotella* sp. ne3005 with 11 proteins. The species with the most diverse set of CAZymes was *Prevotella multisaccharivorax* DSM 17128 with 28 different CAZymes families found in the present metaproteomics dataset followed by *Selenomonas bovis* with 19 diverse CAZymes (Table S23).

CAZy Family	Target	Detected Proteins [n]	Adapt. 7d	Treatment			Elution	
				8d	11d	14d	17d	
CE1	Pectin	13	0.87	0.86	1.42	1.71	1.35	
CE12	Pectin	8	1.01	0.88	1.32	2.46	2.77	
GH1	Cellulose β -1,4/1,3 Glucan	8	1.84	0.46	1.05	0.12	0.85	
GH10	β -1,4 Arabinoxylan	15	0.97	0.74	1.12	0.80	1.24	
GH12	β -1,4 Arabinoxylan	6	0.38	3.31	1.13	1.83	1.63	
GH16	Cellulose β -1,4/1,3 Glucan	19	1.11	0.85	0.89	1.43	2.30	
GH28	Pectin	17	0.95	1.01	1.14	0.92	1.05	
GH3	Cellulose β -1,4/1,3 Glucan	9	1.08	1.02	1.09	0.55	1.08	
GH51	β -1,4 Xyloglucan	7	0.76	1.04	1.18	0.52	1.25	
GH53	β -1,4 Xyloglucan	1	1.68	1.01	0.98	0.72	1.07	
GH78	Pectin	4	1.20	0.72	0.56	0.45	0.91	
GH95	β -1,4 Arabinoxylan	6	1.13	0.60	1.16	0.17	0.85	

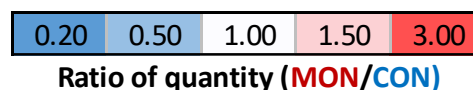


Figure 25: Monensin exposure of the microbial consortium affects fibrolytic CAZyme families. More abundance in MON is displayed in red while for CON group in blue. Ratio was calculated by dividing the LFQ-value of MON from the CON. CAZyme families were assigned to their targets of plant fiber degradation.

A gradual increase of proteins belonging to inorganic transport and metabolism (COG: P) was identified in MON over time (Figure 23, Figure S25). This general change was observed also on the individual level of iron transporting proteins. COG P included also ATP-binding proteins from multiple sugar transport system (K10112), such as maltose/maltodextrin transport system permease proteins (K10109) during monensin exposition (Table S23).

4.5 Discussion

4.5.1 Proteolytic activities influenced by monensin

Diminished ammonium and branched-chain fatty acid (BCFA) levels indicated a reduced proteolytic activity in the monensin supplemented reactors (MON). Species such as *Prevotella bryantii* and *Prevotella ruminicola* were found to be hyper ammonia producing and have been associated with protein degradation in rumen [215, 216]. Despite of *Prevotella* for their prominent proteolytic activity [14], correlations with proteolytic side products were found with a sufficient amount of peptide evidence (at least 11 unique peptides/time point) in *P. ruminicola* and *P. dentalis* under MON (Table S3). Correlations with proteolytic products showed that individual species either prefer BCFA or ammonia formation. A decreased diversity and quantity of proteins assigned to amino acid metabolism was found in MON, pointing towards a hampered tryptophan metabolism in *Prevotella* species and demonstrating the intermediate step to prevent acute bovine pulmonary edema by monensin [188]. The lack of BCFAs inhibited most likely the formation of branched-chain amino acid (BCAA) due to the structure similarity of BCAA to isovalerate and isobutyrate [1]. We therefore agree with the statement of Wallace, R. [23] that a smaller part of high-active rumen microorganisms are most likely responsible for the proteolysis [23]. Proteolytic activity may also be uncoupled from abundance of bacterial species and therefore regulated by availability of cofactors, such as NADH. However further research is required to verify the major key players for proteolysis in rumen microbiome.

4.5.2 Reduced fibre degradation in the presence of monensin

Functional changes in the metaproteome were induced by the first monensin supplementation at time point 8 d and continued for at least 24 h. The elevation of translation and transcription proteins was often seen in proteomic studies with antibiotic supplementation or in microorganisms under stressful conditions [217]. The large drop in proteins for carbohydrate metabolism (COG G) gave rise to suspicion, that carbohydrate degradation is reduced in the variety of degradation as shown by Poos, M., *et al.* [218] who observed a diminished dry matter digestibility via fecal analysis after monensin supplementation in lambs [218]. Haimoud, D.A., *et al.* [92] documented similar findings for ruminal fiber digestion under monensin in cows but total fiber digestion remained unchanged when compared to control [92]. The current study underlined findings of reduced fiber digestion by a drop of bacterial glycoside hydrolases GH1, GH3, GH51, GH53, GH78 and GH95

which contribute to plant fiber deconstruction [219]. However, the CAZymes of protozoa or fungi were not included in the used database and may also have a relevant contribution. The decline of polysaccharide degradation appears to be connected to changes of the monomer uptake. Results indicated a reduced presence of ATP-binding protein of the multiple sugar transport systems that enforces the perspective of a diminished sugar uptake too, which was also seen under monoculture conditions [220].

4.5.3 Monensin affects fermentation activities

Proteins contributing to glycolysis were also lowered, meaning that either a switch to hibernation or an alternative energy generation via anaerobic respiration is made as described in *P. bryantii* B₁₄ [221]. Reduced glycolysis induced by monensin was also described in studies with *P. bryantii* [220] and *Streptococcus faecalis* [222], which reveal a reduction of the whole ruminal carbohydrate degenerative system. Analyses of the fermentation products showed significantly enhanced concentrations of succinate and propionate at late MON incubations. This can be directly linked to the protein abundances of the respective metabolic pathways. An incorporation of propionate into valerate can explain the similar trend at the elution phase since both are linear organic acids with an odd number of carbon atoms [1]. Protein abundance of the succinate-producing genus *Succinatimonas* [223] showed that this bacteria belonged to the fast-responders, which decreased almost 5-fold, as soon as monensin was introduced (8 d). Thus, the formation of succinate has to be linked to other succinate-producers as the level of succinate was constant and even increased during the treatment phase in MON. Similar SCFA ratios were observed by Kaplan-Shabtai, V., *et al.* [224] showing that the succinate-dependent propionate production is associated with Succinivibrionaceae, *Bulleidia* and *Prevotella* [224]. *Prevotella* appears to be the main candidate since Succinivibrionaceae were depleted in the present study and proteins for *Bulleidia* were not identified which is due to a very low number in the database (six proteins).

In vitro and *in vivo* studies also demonstrated monensin tolerance and resistance of several *Prevotella* species [192, 225, 226], which largely contributed to the ruminal microbiome under monensin supplementation [227]. This was verified by the predominance of protein counts from genus *Prevotella* in the present study. *Prevotella* was able to consolidate its ecological niche within the monensin environment and was able to utilize the provided nutrients for acetate and succinate biosynthesis. In *P. bryantii* B₁₄, succinate is the product of a respiratory supercomplex which oxidizes NADH and reduces fumarate under

formation of an electrochemical Na⁺-gradient [221]. Furthermore, less sugar is assimilated in *Prevotella* under monensin [220], which point to an increased metabolic shift to succinate production in order to maintain its concentration. By shifting its metabolism from acetate to succinate production [201], a conversion from succinate into propionate becomes very likely and beneficial for maintaining the monensin-disrupted sodium gradient [220]. Previous studies and current findings also indicated an increase of propionate during monensin supplementation [228], whereas a significant elevated propionate concentration was only determined after monensin supplementation was stopped. Defense mechanisms seem to require an adjustment time longer than 24 h and non-increasing monensin concentrations. *Prevotella ruminicola* was shown to produce elevated propionate levels under monensin [201] and propionate production was only occurring in presence of the cofactor vitamin B₁₂ [51]. An inhibition of vitamin B₁₂ synthesis by monensin appears to be less likely since the microbial-borne vitamin B₁₂ concentration in the blood serum of monensin treated lambs remained unchanged [229]. Some species of the genus *Prevotella* seem to use the niche created by monensin and act as the main trader for metabolites like acetate and succinate [11]. This perspective is supported by the high abundance of *Prevotella*, the elevated amount of succinate [11, 201] and the detected increase of succinate forming pathways under monensin in the present study.

Further ruminal propionate producers are Rikenellaceae and Ruminococcaceae [227], which showed a decreasing quantity with progressing time after initial day of treatment. Some Succinivibrionaceae species were shown to be resistant towards monensin [230], but the current findings demonstrated a fast responding sensitivity towards monensin. The presented data showed a decrease of *Butyrivibrio* sp. specific proteins in MON, which may have caused an inhibition of the propionate consumer *Butyrivibrio fibrosolvens* leading to a propionate enrichment by monensin. Schären, M., *et al.* [227] assumed that monensin is leading rather to an increase of the substrate succinate than affecting the propionate producers [227]. According to this, *Prevotella* species are assumed to be the main mediator for the increase of propionate during the elution phase, where the dwindling antibiotic pressure enabled countermeasures of *Prevotella* against monensin. Furthermore, a negative correlation trend in MON for succinate and Prevotellaceae was found (R=-0.94), while succinate correlated positively with Lachnospiraceae and *Megasphaera* (R=0.94). Those two conspicuous trends align with the production of propionate by *Megasphaera*, which belongs to the family

Veillonellaceae [231], and butyrate by a certain Lachnospiraceae [232]. The positive relationship between propionate with *Lachnospira* and *Shuttleworthia* described by Xue, M., *et al.* [233] was rediscovered in the correlation analysis of the current study and verified “that some species belonging to this genus may positively interact with propionate-producing taxa” [233]. Another propionate producer is Acidaminococcaceae [234], which together with Veillonellaceae is correlating ($R \geq 0.8$) with propionate and succinate resulting in the responsive families for propionate production under monensin exposition. Species from the family Veillonellaceae were shown to synthesize propionate out of succinate and lactate [235]. Assuming that the lactate pathway may be inhibited due to monensin, the production of propionate may take place mainly via succinate. However, the exact process of succinate production by *Prevotella* and assimilation via *Megasphaera* and Veillonellaceae species over time has to be shown in a co-cultivation under monensin. Veillonellaceae appeared to be insensitive towards monensin up to concentrations, which were exceeded in this experiment [230]. The intermediate sampling points 14.5 d and 15.5 d showed an elevation of succinate in MON that is probably due to the monensin binding or elution after the supplementation.

Methane production was reduced in presence of monensin, which was already demonstrated in previous studies [90, 228]. The study of Wallace, R., *et al.* [90] indicated a drop in methane production during continuous monensin administration independently of the applied dosage [90]. Their highest added dosage of monensin per day was similar to the applied dosage of the current study (6.2 mg/d). The decline of methane was associated with reduced formation of acetate, increased formation of propionate and an elevated presence of the genus *Prevotella* [236]. Those findings align with the observation of *Prevotella* being a key player in the rumen which is responsible for the metabolic shift by redirecting reducing equivalents from CO₂ reduction (and methane formation) to fumarate reduction (and succinate production). This paves the way for increased propionate formation from succinate [221]. In summary, our study demonstrates that the ionophoric effect of monensin induces the modulation of metabolic routes in rumen bacteria without causing a major phylogenetic reconstruction.

4.5.4 Accumulation and elution of monensin

In a previous study, we assumed that monensin is bound and accumulated in extracellular polysaccharides (EPS) but at a certain point monensin is released due to a deconstruction of EPS via CAZymes [220]. Together with a periodical supplementation of

monensin, this situation results in a prolonged effect of monensin, meaning that the rumen microorganisms require more time to recover despite monensin supplementation was stopped. The current data does not provide a full explanation and illustration of the monensin accumulation and elution in a ruminal *in vitro* system, but it shows that there is an undiscovered field of how long drugs remain in the gastro-intestinal tract before being washed out. The consequences for a prolonged retention of monensin are difficult to assess, however, current data showed that a reduction or even eradication of certain low abundant microbes is a probable outcome.

4.6 Miscellaneous information of manuscript

4.6.1 Associated Data

The mass spectrometry proteomics data have been deposited to the ProteomeXchange Consortium via the PRIDE [237] partner repository with the dataset identifier PXD034099.

4.6.1 Acknowledgments

The authors would like to thank the Deutsche Forschungsgemeinschaft (DFG) for funding (project number 327953272). We greatly acknowledge the support given by Jessica Walter, Paula Truelsen, Ronja Hepp, Anna-Lena Schweiger and Anna Hanauska for Rusitec preparation, maintenance and sample analysis. Thanks to the spectroscopy and mass spectrometry unit of the Core Facility of Hohenheim for ¹H-NMR and MS/MS measurement and to Johan S. Saenz for help with data analyses.

4.7 Supplementary tables

Table S23: List of identified proteins per time point and treatment including LFQ (column G-Q), and protein affiliations and grouping. Please see separate Excel sheet attached as supplementary material of the publication.

Table S24: Protein counts and their percentile contribution (>0.1%) based on generic name of quantified protein from solid phase samples over all time points. Generic name may include various taxa levels depending on protein designation. Names without clear designation were highlighted in grey.

Generic Name	Count [n]	Contribution [%]
Prevotella	2902	31.68%
Selenomonas	569	6.21%
Lachnospiraceae	398	4.35%
Treponema	354	3.87%
Bacteroides	214	2.34%
unclassified	195	2.13%
Megasphaera	194	2.12%
Fibrobacter	180	1.97%
Mitsuokella	177	1.93%
Prevotellaceae	153	1.67%
Bacteroidales	150	1.64%
Ruminococcus	145	1.58%
Clostridiales	142	1.55%
Succinatimonas	140	1.53%
Lactobacillus	139	1.52%
bacterium	129	1.41%
Firmicutes	121	1.32%
Clostridium	119	1.30%
Eubacterium	114	1.24%
uncultured	99	1.08%
Dialister	86	0.94%
Ruminobacter	73	0.80%
Butyrivibrio	65	0.71%
Succinivibrio	59	0.64%
Alistipes	58	0.63%
Pseudoscardovia	55	0.60%
Bifidobacterium	52	0.57%
Ruminococcaceae	46	0.50%
Succiniclasticum	46	0.50%
Bacteroidetes	45	0.49%
Roseburia	36	0.39%
Bacteria	34	0.37%
Sarcina	32	0.35%
Muribaculaceae	31	0.34%
Aeromonas	30	0.33%
Acidaminococcus	30	0.33%
Succinivibrionaceae	30	0.33%
Clostridia	28	0.31%
Succinimonas	26	0.28%
Kandleria	25	0.27%
Parabacteroides	24	0.26%
Anaerovibrio	24	0.26%
Schwartzia	22	0.24%
Streptococcus	21	0.23%
Olsenella	21	0.23%
Alloprevotella	21	0.23%
Paraprevotella	21	0.23%
Shuttleworthia	20	0.22%
Erysipelotrichaceae	17	0.19%
Lachnobacterium	17	0.19%
Sharpea	16	0.17%
Blautia	15	0.16%
Faecalibacterium	15	0.16%
Lachnoclostridium	15	0.16%
Tolomonas	15	0.16%
Oscillibacter	14	0.15%
Coprococcus	13	0.14%
Anaeromassilibacill	12	0.13%
Methanobrevibacter	12	0.13%
Porphyromonadace	11	0.12%
Lentisphaerae	11	0.12%
Barnesiella	11	0.12%
Oribacterium	10	0.11%
Pseudobutyrvibrio	10	0.11%
Anaerotruncus	10	0.11%
Dysgonomonas	9	0.10%

Table S25: Correlation table for metabolites, monensin with phylogenetic levels. Positive correlations indicated with red and negative correlations with blue by using conditional formatting. Pre-last column shows the average by using absolute values of correlations from proteolysis indicators: isobutyrate, isovalerat and ammonia. Last column shows the slow responders by a correlation of the MON/CON ration of phylogenetic levels with relative monensin concentrations. Please see separate Excel sheet attached as supplementary material of the publication.

Table S26: Genus counts for “succinate dehydrogenase” and “fumarate reductase” as protein description

Genus name	Count
Prevotella	10
Fibrobacter	5
Aeromonas	3
Mitsuokella	3
Bacteroides	3
Selenomonas	2
Bacteroidales	2
Stylophora	1
Succinatimonas	1
Alloprevotella	1
Schwartzia	1
Succinivibrio	1

4.8 Supplementary figures

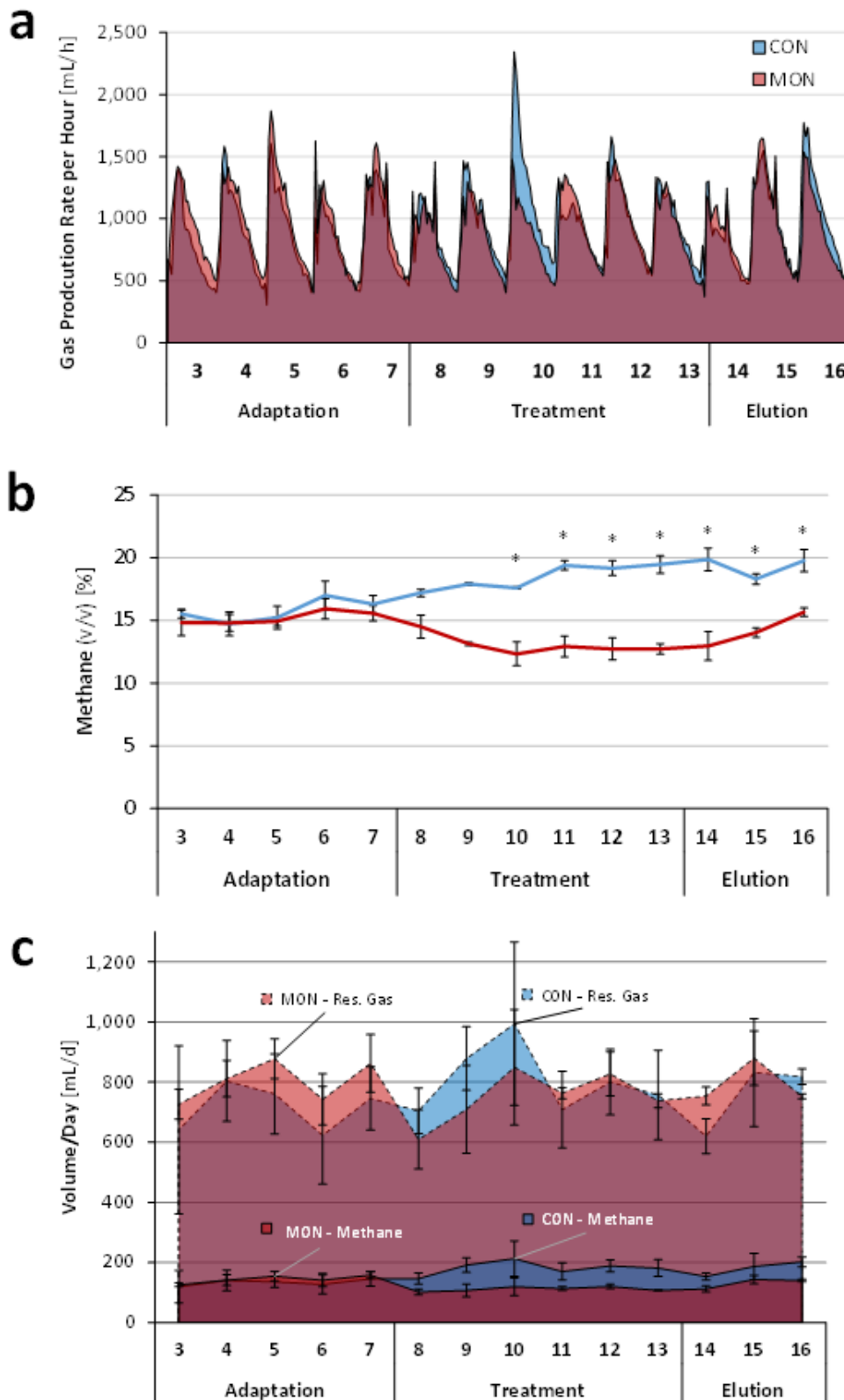


Figure S19: Gas production under monensin (MON, red) and control (CON, blue) group over time. Error bars indicate standard deviation from average ($n=3$). a: production velocity of total gas volume in milliliter per hour for each hour; b: daily methane concentration with asterisks (*) indicating significant differences (LSD-Fisher; $p<0.05$) between groups; c: The solid line in the lower part of the graph displays the daily produced methane volume while the dashed line displays the total gas volume of methane and the residual gas that has been produced per day.

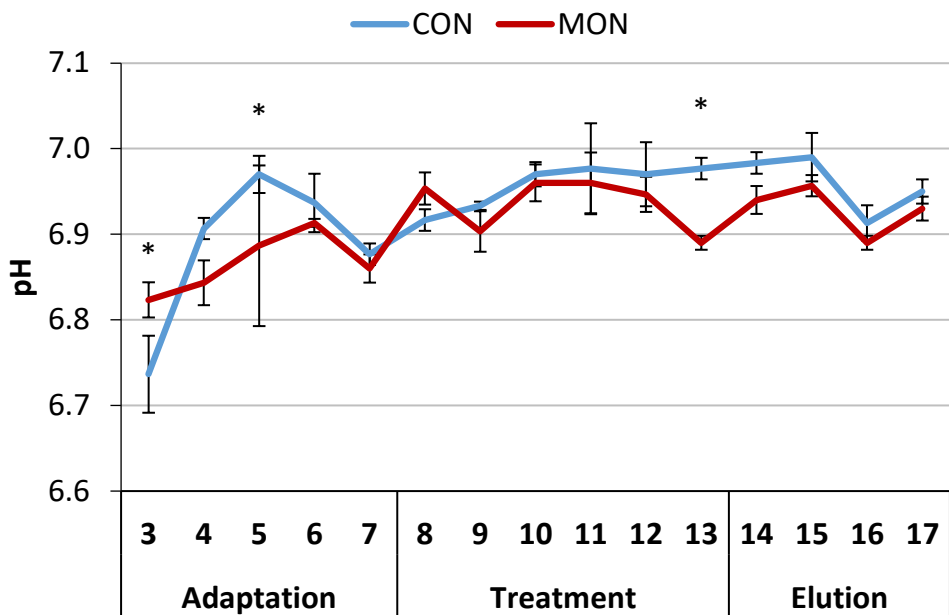


Figure S21: Development of the pH in the liquid phase. Error bars indicate standard deviation (n=3). Asterisk (*) mark significances between groups (LSD Fisher, p<0.05).

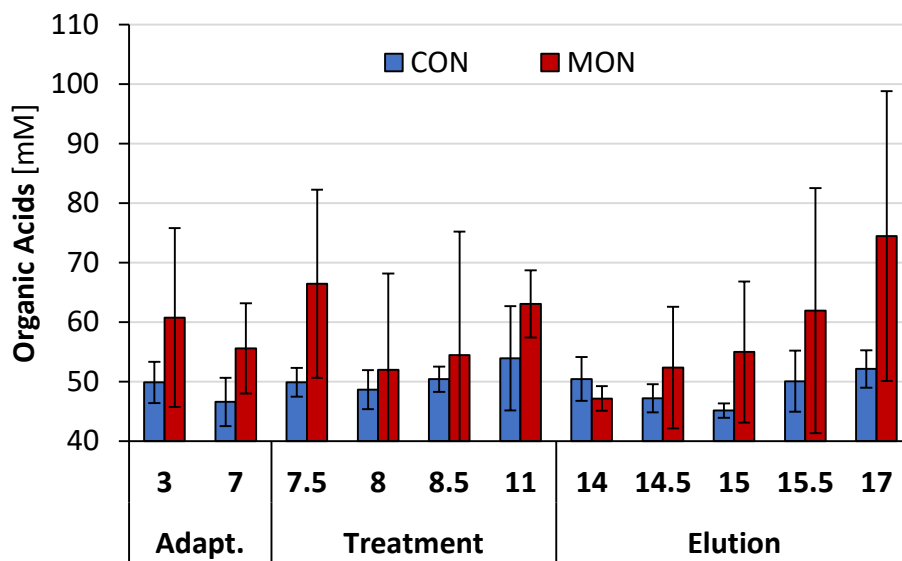


Figure S20: Summed concentration of averages of quantified organic acids. Included are formate, acetate, propionate, butyrate, valerate, isobutyrate, isovalerate and succinate.

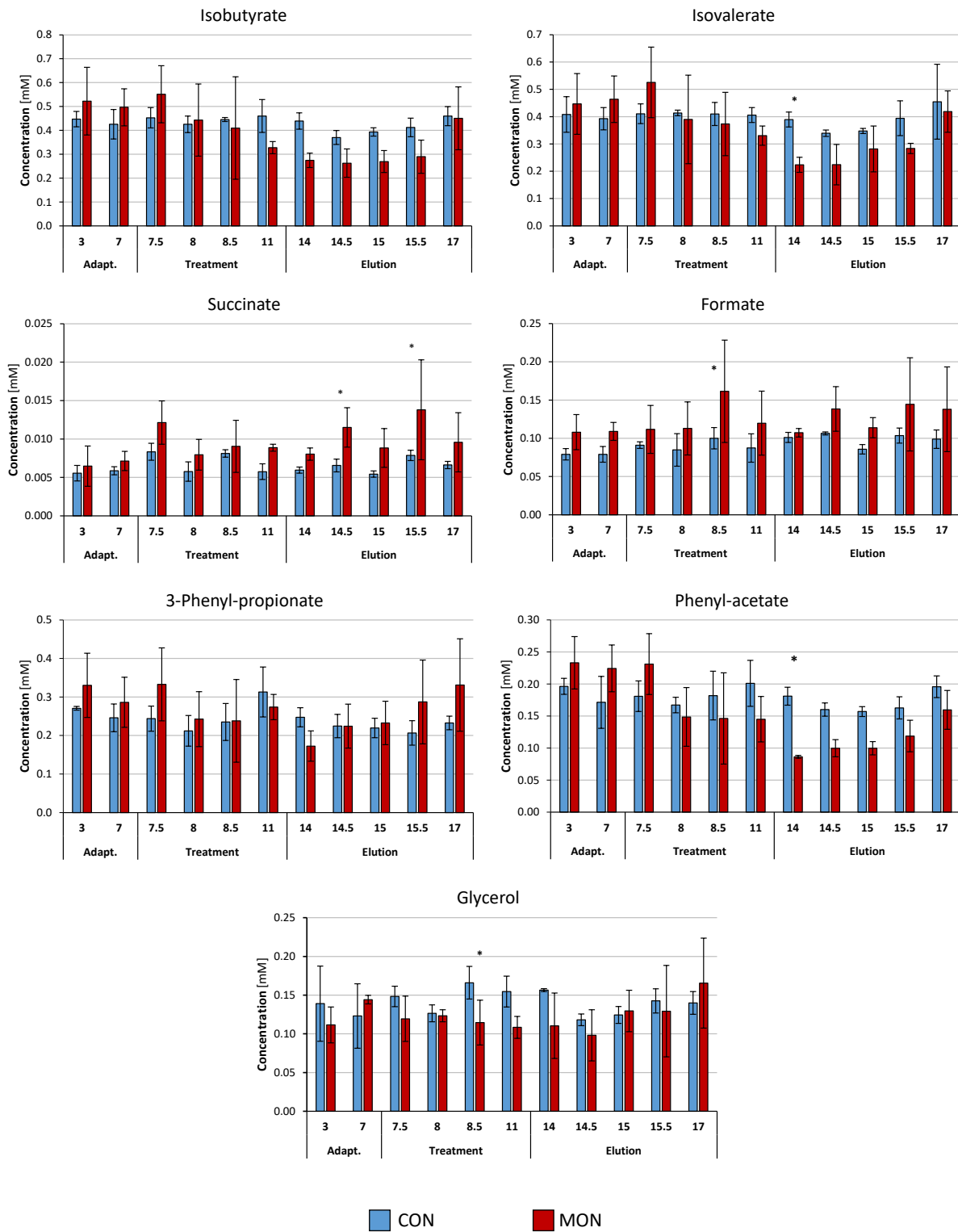


Figure S22: Fermentation products in culture supernatant detected via $^1\text{H-NMR}$. Error bars indicated standard deviation while asterisk indicated significance between groups at certain time point (* $p < 0.05$, Fisher LSD-Test).

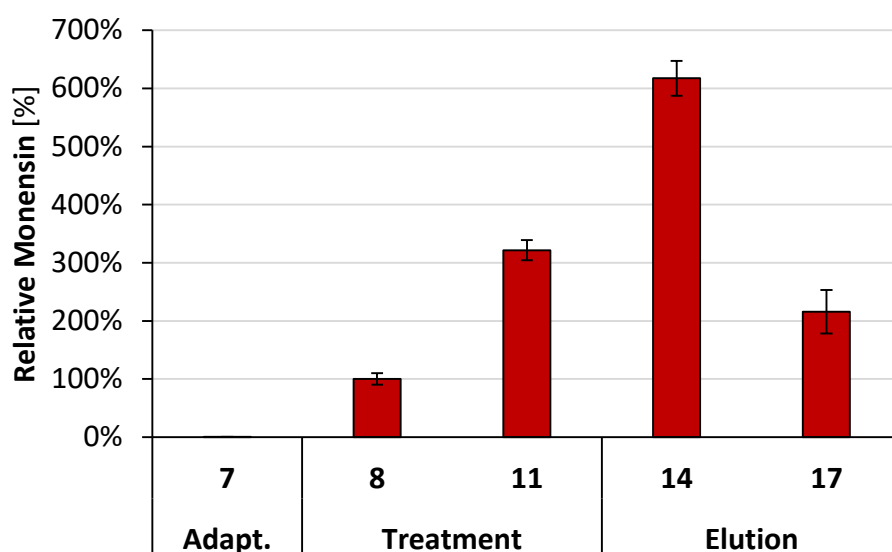


Figure S23: Relative monensin amount after dissolving and eluting monensin directly before supplementation. Monensin concentration at day 8 was set to 100%. Samples were taken before monensin supplementation during treatment phase. Mean and standard deviation (n=3) of monensin was calculated. Outlier at day 8 was excluded.

Prevotella species	Total unique peptides	Linear Trend in MON CON	Adapt.	Treatment		Elution	
			7d	8d	11d	14d	17d
Prevotella multisaccharivorax	348	↘	0.84	0.85	0.98	0.68	1.17
Prevotella ruminicola	181		1.09	1.55	3.01	2.37	1.69
Prevotella bryantii	105	↘	1.01	0.97	1.84	1.75	2.08
Prevotella dentalis	28	↘ ↘	0.97	0.78	1.19	0.60	0.94
Prevotella buccae	20	↘	0.93	0.75	1.05	1.16	1.75
Prevotella copri	15	↗	1.09	0.52	1.06	1.11	2.88
Prevotella sp. S7-1-8	10	↘	0.99	1.34	1.21	1.06	2.79

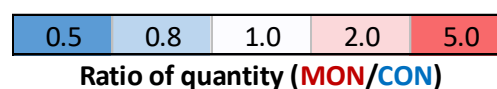


Figure S24: Summed peptide ratios of *Prevotella* species with their contribution to cluster of orthologous groups (COG) over time. More abundance in monensin group is displayed in red while for control group in blue. Ratio is calculated by summed LFQ-values of species-specific peptides, where the monensin group is divided by the control group. The total peptide count gives evidence about number of species-specific peptides found among all time points. A linear trend over time for the monensin and the control group over time was either increasing (↗, Pearson>0.7), decreasing (↘, Pearson<0.7) or remained unchanged over time (missing arrow).

COG	COG Description	Adapt. 7d	Treatment		Elution		Total Number [n]
			8d	11d	14d	17d	
A	RNA processing and modification	0	2	0	2	-1	6
B	Chromatin Structure and dynamics	-1	0	0	0	0	3
C	Energy production and conversion	13	-15	-1	19	13	2187
D	Cell cycle control and mitosis	2	0	-3	0	3	282
E	Amino acid metabolism and transport	38	-23	22	23	30	1428
F	Nucleotide metabolism and transport	1	-8	14	15	-15	615
G	Carbohydrate metabolism and transport	14	-5	55	45	45	2493
H	Coenzyme metabolism	-12	-9	7	5	16	546
I	Lipid metabolism	7	-7	10	17	15	351
J	Translation	44	-65	3	38	-2	4059
K	Transcription	5	-9	14	13	2	645
L	Replication and repair	1	1	8	10	0	249
M	Cell wall/membrane/envelop biogenesis	9	8	-19	-3	-22	1185
N	Cell motility	4	1	3	6	0	774
O	PTM, protein turnover, chaperone functions	12	-10	25	30	10	1263
P	Inorganic ion transport and metabolism	16	16	0	-8	-23	1188
Q	Secondary Structure	2	4	-1	1	-2	60
T	Signal Transduction	6	9	8	13	-7	141
U	Intracellular trafficking and secretion	1	-16	-8	-9	3	417
Z	Cytoskeleton	0	0	-2	-1	-4	3
S	Function Unknown	10	-22	6	9	-6	1149
!S	Function Unknown (manually assigned)	15	-18	21	14	28	828

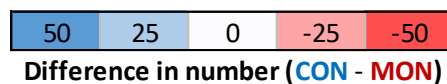


Figure S25: Heat map of functionally annotated proteins with difference between MON and CON group of solid phase over time. More abundance in monensin group is displayed in red while for control group in blue. Number of quantified proteins belonging to specific clusters of orthologous groups (COGs) of the monensin group were subtracted from the control group (CON – MON). Right column indicates total amount of proteins detected. Color code of heat map is illustrated at the bottom of the differential approach. PTM in the COG description stands for post-translational modifications. LFQ is described as label-free quantification value. One protein can belong to multiple COGs, which leads to a higher number sum of total counts than proteins are quantified.

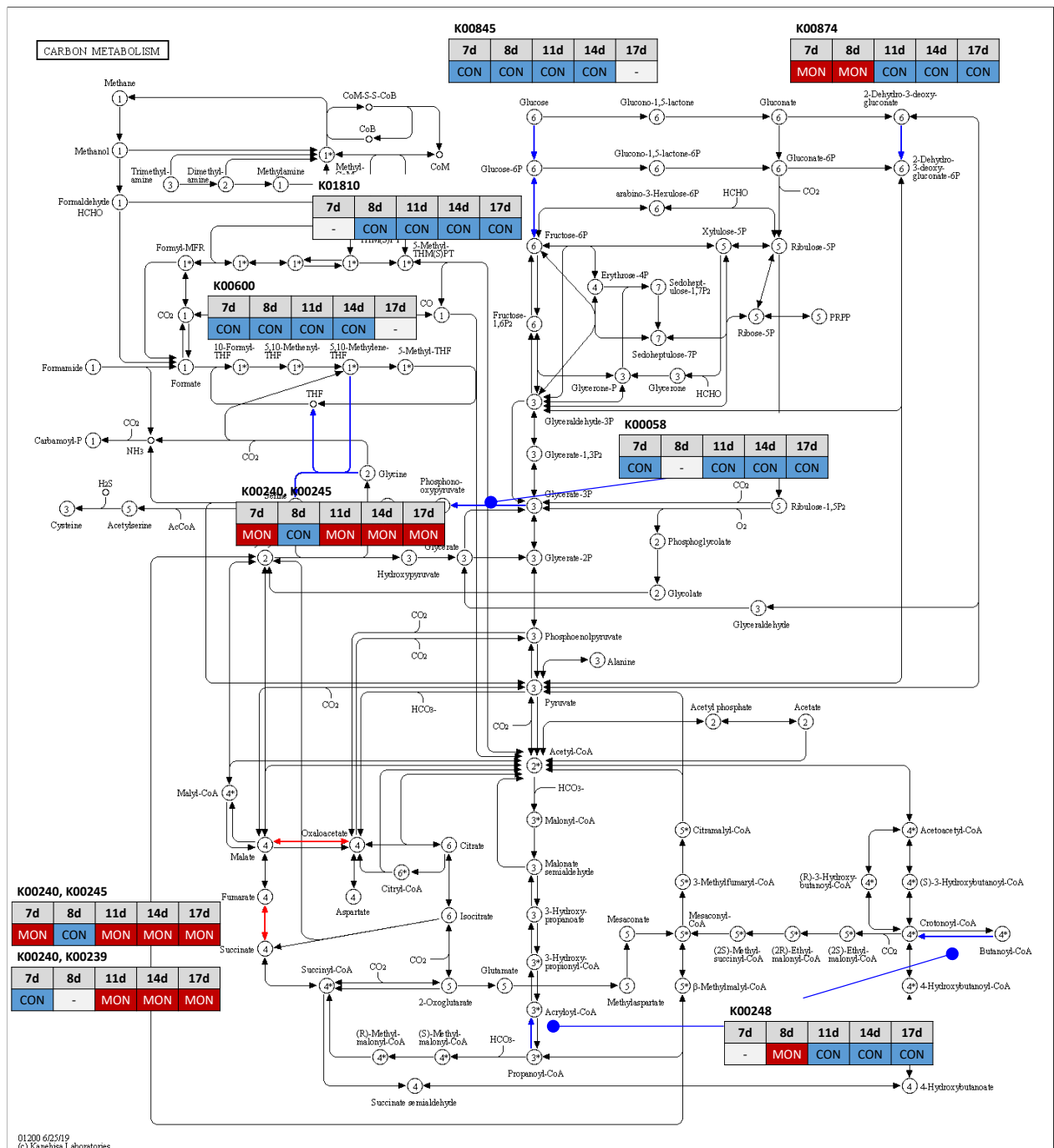


Figure S26: Increased group specific reactions in carbon metabolism of KEGG map (ko1200). Proteins from various ruminal microbes with similar KEGG orthology (KO) ID were displayed as higher in control (CON, blue) or monensin (MON, red) group, when summarized quantity (LFQ-values) and number of quantified proteins was showing a common trend for one of the groups. Boxes with KO ID illustrated close to condition specific colored arrow points out the time points of common indication. A dash in the boxes was meant when trend in number and quantity was contradicting. None indicated reactions were either not found or had less than four trends in five time points.

5. Requirements of semi-defined media for *Prevotella bryantii* B₁₄

In the process of the current thesis further findings were made regarding requirements for *P. bryantii*, which were partially or not included in the stories of chapter 2, 3 and 4. In order to document the obtained helpful knowledge for working with *P. bryantii*. The subsequent chapters shall give clarification about the optimal growth conditions and the requirements of *P. bryantii*.

5.1 Gas phase requirements

Cultivation of *P. bryantii* B₁₄ in M2-A medium with gaseous nitrogen (N₂) instead of carbon dioxide (CO₂) failed and showed that bicarbonate supplementation is insufficient for growth. The coloring of the M2-A media with N₂ was also more into orange as the usual yellow. Cultivation experiments with drastically reduced gas volume from 50 to 1.5% showed no difference in optical density measurements (Figure 26). With respect to the methodology it seems that the liquid media requires to be saturated with CO₂ gas but the volume of the gas-phase in the Hungate tube appears to be irrelevant. Carbon dioxide appears to be required for the implementation via the phosphoenol-pyruvate (PEP) pathway into succinate [238], but further dependencies remain to be investigated.

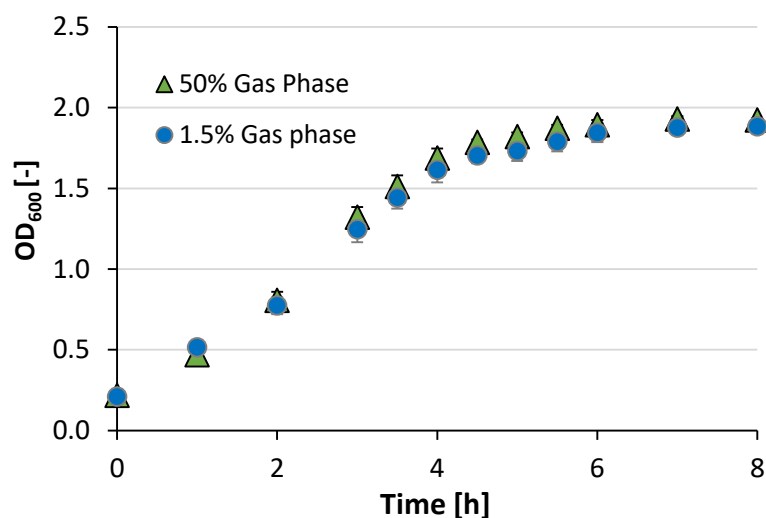


Figure 26: Cultivation of *P. bryantii* B₁₄ under two gas phase volumes. The gas volumes of the total Hungate tube volume were 1.5% (blue filled circle) and 50% (green filled triangle). Optical density at 600 nm was measured over the time until stationary phase was reached. Cultivations were performed for each approach in triplicates (n=3). Error bars indicate standard deviation in grey for 1.5% and black for 50% gas volume.

5.2 Optimal starting pH

The impact of the optimal starting pH was conducted by using a sodium-phosphate buffer for the pH range from 5.8 to 7.2. Measurements indicated that a starting pH optimum around pH 6.7 resulted in the fastest growth (Figure 27). Regarding chapter 2 a starting pH of 6.8 was used.

For the mixed culture in chapter 4, a pH of 6.95 ± 0.05 was maintained (Figure S21). OD was measured 5 h after inoculation in the pH range from 5.8 to 7.2. Findings indicate the best starting pH for fastest growth, but not for the maximal OD.

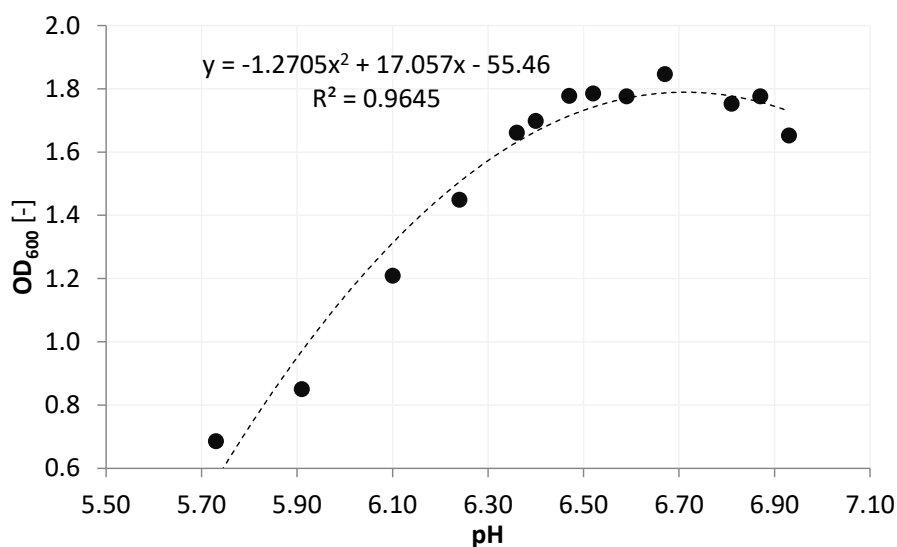


Figure 27: Starting pH vs. optical density of *Prevotella bryantii* B₁₄ after 5 h growth. Cell growth in Hungate tubes is detected by OD₆₀₀ with biological triplicates (n=3) for each pH. Starting pH values were obtained by measuring non-inoculated medium (n=1). Dotted polynomial trend line (x²) represents an approximation to the general trend with the coefficient of determination (R²).

5.3 Dispensable supplements

Additional research in the field of supplement requirements revealed and verified that the growth of *P. bryantii* B₁₄ is independent of the supplemented vitamin mix as described in the thesis of Pflüger, S. [239]. The results revealed significant but small difference in OD when omitting menadion, biotin, cobalamin and/or hemin from the vitamin mix [239]. The study of Pflüger, S. [239] verified the finding of Mannarelli, B.M., *et al.* [16] that the role of hemin has almost no effect as a growth promotor. The indicated growth of *P. bryantii* B₁₄ in the work of Pflüger, S. [239] were around an OD=2.0, while the growth under single-supplement deletion had only a small reduction to an OD=1.9. Those findings illustrate that the investigated supplements are non-essential for the growth of *P. bryantii* B₁₄. Furthermore, no protective effects against oxygen was shown when ascorbic acid (Vitamin C) was supplemented as an

Additional Findings

anti-oxidative [239], although such effects were found for certain anaerobic species [240]. Similar protective effects were suggested for hemin in *P. intermedia* [57]. Hemin was also not growth-promoting, which may be due to autonomous production of protoporphyrin IX (PPIX) in *P. bryantii* (Figure S4). By observing the supplementary requirements of *P. bryantii*, the role as a generalist in the realm of rumen microbiota becomes more evident. Despite the findings of the independency of micro-supplements for *P. bryantii*, the beneficial role of the growth promoting trypticase is not solved, which may contain supplements which were omitted in the work of Pflüger, S. [239] and as similarly seen when SCFAs were replaced by trypticase [15].

6. Discussion

6.1 Major findings

Three hypotheses were stated at the beginning and were examined during the present thesis. This resulted in five major findings which are summarized below:

Chapter Findings

- 2 Supplemented short-chain fatty acids (SCFAs) are incorporated into long-chain fatty acids (LCFAs) of membrane lipids of *Prevotella bryantii* B₁₄, leading to a change of membrane characteristics and outer membrane proteins.
- 2 Branched-chain fatty acids (BCFAs) are utilized for branched-chain amino acid (BCAA) synthesis in *Prevotella bryantii* B₁₄ via the acetyl-CoA synthetase and the 3-isopropylmalate (3-IPM) pathway.
- 3 During monensin exposure *Prevotella bryantii* B₁₄ reduces its intracellular sodium levels by elevating sodium transporters, in particular the NADH:ubiquinone reductase (NQR).
- 3 The sacrificial layer of extracellular polysaccharides (EPS) is actively detached from *Prevotella bryantii* B₁₄ cells, which prevents the binding of monensin to the cell membrane.
- 4 The genus *Prevotella* acts in a rumen microbiome under monensin exposure as a key player by shifting its metabolism from acetate to succinate production, which provides a precursor for propionate synthesis and diminishes NADH for methane synthesis.

6.2 Versatile functions of SCFA in *Prevotella bryantii* B₁₄

6.2.1 SCFA a non-essential growth promotor

Current works verified findings of Pittman, K. and Bryant, M. [29] and showed growth of *P. bryantii* with trypticase but without SCFAs is feasible. However, after the second transfer into SCFA-free media a lag-phase of about 24 h was observed and vanished in the third transfer (Chapter 2.5.1, Figure S12). Findings of chapter 2 pointed towards the SCFA utilization in form of precursors for membrane lipids and the conversion of BCFA into BCAA (Chapter 2.5.4). This showed, that minor amounts of SCFAs are able to enhance growth and also an independency of *P. bryantii* towards SCFAs as similarly seen in additional experiments. Even though the question about the necessity of SCFA for *P. bryantii* is solved, the question about a dosage-dependent growth promotion by SCFAs remains open.

6.2.2 Influence of SCFA on LCFA and membrane proteins

The first study of this thesis focused on the effects of supplementing *P. bryantii* with various SCFAs (Chapter 2) and it was possible to prove that the use of any SCFA promote the growth of *P. bryantii*. Furthermore, an incorporation of SCFAs into LCFAs was shown, which can be found in membrane lipids of *P. bryantii*. This finding indicates that SCFA have an effect on membrane fluidity via LCFAs in *P. bryantii* [241]. It is also assumed that membrane fluidity impacts the appearance of outer membrane proteins [43]. This assumption is supported by the differences in abundance detected for outer membrane proteins in acetate (Acet) and valerate (Val) supplemented treatments. Lee, A.G. [45] pointed that the length of LCFA in membrane lipids also affect the implementation of membrane-associated proteins. This was clearly seen for valerate (C5-chain) in contrast to acetate (C2-chain) with respect to the appearance of TonB proteins (Figure S8). The beneficial effects and pathways of SCFA on bacterial cells are rarely described, but these current findings provided a foundation for further investigations on this perspective. Unfortunately, SCFA are mainly regarded from the perspective of having a negative impact by acidifying the environment and regulate virulence genes in enteric pathogens [242], while having a beneficial effect on the intestine and body of the host [243]. The SCFA impact on the membrane and its proteins was proven throughout all chapters to be important and connected to the abundance of *P. bryantii*. Based on the knowledge that this bacterium is dominating the rumen microbiome, future research activities should consider these findings.

6.2.3 Iron uptake via SCFAs

Monensin resistance in *P. bryantii* B₁₄ were shown to be decisive by strong cation regulation mechanisms. This reinforces the idea that growth promoting SCFA supplementation for *Prevotella* species is maybe due to acting as a cation co-transporter through the cell membrane. SCFA are generally constituted out of carboxyl group for cation binding and an alkyl residue, which allows to pass the membrane when the SCFA is uncharged [244]. Elevated levels of TonB-associated proteins in acetate (Acet) and valerate supplemented cultivations (Val) indicate an acetate- and valerate-mediated transport of iron (Fe²⁺/Fe³⁺). Iron is found in iron-sulfur clusters of proteins but also as the central atom of the porphyrin ring, which can be produced by *P. bryantii* but needs to be filled by an iron ion. Iron import proteins, like TonB, HmuY, outer membrane receptor for ferrienterochelin, LemA, are highly influenced and were found mostly in fast growing cultures [1] (Chapter 2, Figure S8), including pathogenic species, such as *Listeria monocytogenes* and *Pseudomonas gingivalis* [245-248]. The findings presented in chapter 2.4.2 showed similar results for cells without monensin and displayed a correlation coefficient (R^2) ≥ 0.8 between imelysin and outer membrane proteins like OmpA and the IPT/TIG domain containing protein [2]. A newly assigned protein (UniprotKB: D8DTQ4), which is conserved through several bacterial species, was found to be elevated in cells growing with monensin exposure (Supplementary data of Trautmann, A., *et al.* [2]) and found to be decreased under iron chelation [249]. This protein is involved in iron acquisition and may be induced by limitations of iron even though hemin was supplemented as a kind of iron source. The question of an iron deficiency of *P. bryantii* can only be answered by additional experiments with inorganic iron supplementation and subsequent proteomic analysis. It is clear that iron-import related proteins of *P. bryantii* B₁₄ are only present under favorable conditions with increased cellular growth [1], whereas exposure to antibiotics or a lack of certain SCFAs resulted in an absence of iron import proteins [2]. An alternate iron transport system may be via chelating iron ions with SCFAs, which may be a capable mediator through the membrane. This hypothesis aligns also with the lack of SCFA consumption in *P. bryantii* because SCFA were not fully utilized and can pass through membranes via non-ionic diffusion as shown in colon cells of rats [244]. Literature research displayed a lack of investigation about how SCFA may affect the ion transport in microorganism. Familiar research in this topic focused mainly on eukaryotic cells of the host [250-252] and the sole complex formation of SCFA with ions [253, 254]. In order gain more

insight into the topic of SCFA-metal complexes and their possible uptake in bacterial cells, intracellular cation concentration had to be measured under various SCFA quantities and qualities. Similar SCFA complexation may be seen for cations such as iron, calcium, sodium or potassium.

6.2.4 Production and deconstruction of BCAAs and BCFA

BCFAs such as isovalerate and 2-methylbutyrate were most likely converted into BCAA, since the reverse reaction was already described in other *Prevotella* spp. [112]. *P. bryantii* produced small amounts of BCFA by its proteolytic activity. The 3-IPM pathway plays a crucial role in the BCAA metabolism, where 2-oxoisovalerate is converted into 2-oxoisocaproate by using NAD⁺ and acetyl-CoA as cofactors. All three enzymes involved in the 3-IPM pathway (EC 2.3.3.12, EC 4.2.1.33, and EC 1.1.1.85) were elevated under isovalerate supplementing conditions (iVal) and demonstrated a potentially assimilating effect for isovalerate or its derivatives. Those findings demonstrated the capability of *P. bryantii* B₁₄ to form BCFA via proteolysis, to construct BCAA and that isovalerate stimulate a regulative effect. Those findings provide deeper insight into the utilization of BCFA for BCAA production and the degradation from proteins via BCAA into BCFA. To prove a production of valine and leucine, additional cultivation experiments with stable isotope-labeled isovalerate would be required. Subsequent proteomics could provide evidence about integration of stable isotope-labeled amino acids into proteins. Those findings could be adopted to complement studies using feed with supplemented small amounts of isovalerate to enhance bacterial protein synthesis. Together with isobutyrate it was shown to lower the ruminal ammonia level of isobutyrate supplemented cattle [255]. The less available ruminal ammonia indicated most likely an incorporation of NH₃ into amino acid formation, especially of BCAA as seen in chapter 4.4.2.

6.3 Reactions & countermeasures of *P. bryantii* towards monensin

Several changes in *P. bryantii* towards monensin were already observed in former studies [82, 88]. Figure 28 summarizes the discoveries that were made in chapter 3. Protein

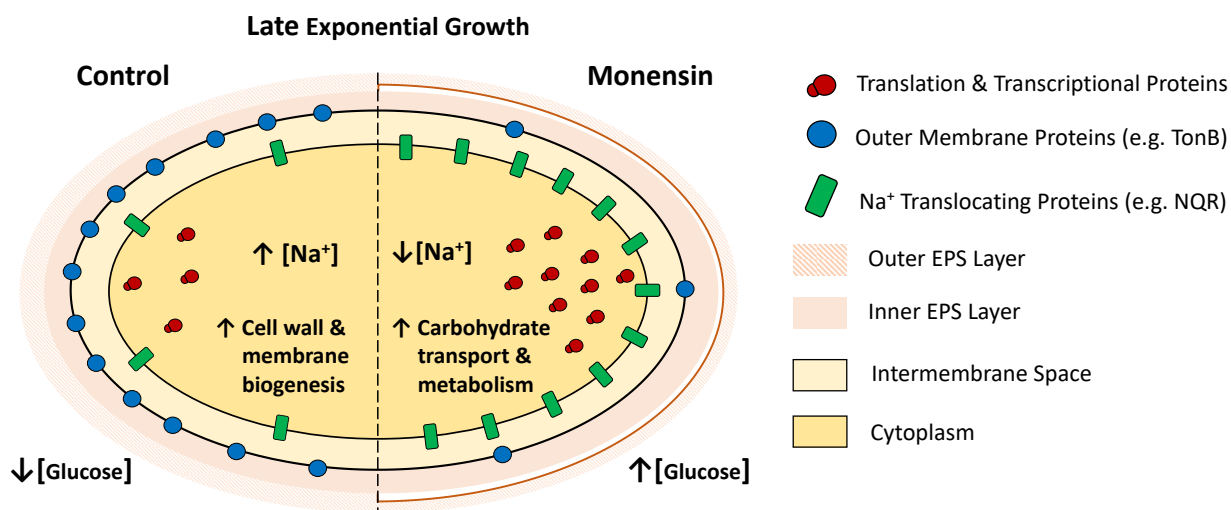


Figure 28: Comparison of diverging parameters and features from a *P. bryantii* cell between control and monensin condition. EPS: Extracellular polysaccharide. Proportions of parameters between control and monensin are just for illustration and do not reflect the observed quantity.

abundance of translational and transcriptional proteins were increased under monensin exposure (Chapter 3.3.3, Table S11). Monensin affected an increase of proteins involved in the carbohydrate transport and metabolism (Chapter 3.3.4, Table S18), while intracellular sodium was decreased depending on the applied monensin concentrations (Chapter 3.3.2, Figure 12c). Sodium translocating proteins (Chapter 3.3.3, Table S13) and the activity of NQR were increased under monensin supplementation (Chapter 3.3.4, Figure 15). Meanwhile outer membrane protein abundance was decreased in the monensin group (Chapter 3.3.3, Table S12, Table S13). The unaffected growth of cells in the control group without monensin (Chapter 3.3.1, Figure 11a) was reflected by the abundance of cell wall and membrane biogenesis proteins in the late exponential phase (Chapter 3.3.3, Table S11). The outer EPS layer was found detached from the inner EPS layer under monensin, which was shown by following findings: fluorescence microscopy (Chapter 3.3.5, Figure 17), increased levels of extracellular glucose (Chapter 3.3.2, Figure 12d, Figure 13c) and higher abundance of CAZymes (Chapter 3.3.4, Table S19, Table S20).

6.3.1 Increased Na⁺-translocating proteins, NQR and QFR promote succinate formation

The disruption of the Na⁺ gradient and the resulting increase of sodium concentrations in the cytoplasm, is one of the described effects of monensin [61]. However, *P. bryantii* B₁₄ showed a reversed effect during monensin exposure by having less intracellular Na⁺ concentration. The intrusion of Na⁺ via monensin seemed to work on *P. bryantii* with an increasing monensin-dosage. However, the high abundance of Na⁺-translocating proteins kept the intracellular sodium still lower than under normal conditions (chapter 3.3.2). The increased amount of sodium transporters included the NADH:ubiquinone reductase (NQR), which is besides translocating Na⁺ also involved in the production of succinate via coupling to the quinol:fumarate reductase (QFR). Findings showed that besides the increased amount of the NQR, the activity also increased which means that the enzyme has a strong impact on the maintenance of the Na⁺-gradient (chapter 3.3.3). Having a reduced intracellular Na⁺ concentration would also mean to have an increased membrane potential, but Schleicher, L., *et al.* [238] showed the opposite by having a decreased membrane potential. This finding leads to the assumption that other cations (H⁺, K⁺ or others) are most likely involved and their intrusion by monensin cannot be compensated. But, this has to be interpreted with care as the monensin exposure times were shorter in Schleicher, L., *et al.* [238]. This type of anaerobic respiration shall also produce more succinate under the influence of monensin. To verify this hypothesis, an accurate carbon balance measurement has to be performed, to show the favored succinate production under monensin conditions. For an adequate comparison the amount of substrate and products needs to be standardized by the amount of cells. The reduced glucose consumption under monensin need to be taken into account. Acetate and succinate have to be considered as products but also lactate might be important, as shown for the close relative *P. bryantii* 25A [256].

6.3.2 Prevent monensin binding

Another reason why glucose can be found in supernatant even after 72 h of incubation is the degradation of the extracellular polysaccharides (EPS) layer. To avoid monensin binding to the membrane of *P. bryantii*, EPS act as a sacrificial layer to capture monensin with its included cations [177]. Over time, *P. bryantii* strips itself out of the monensin contaminated EPS, which was shown by increased CAZymes and the degradation zones around active cells [2]. The sacrificial layer of EPS was actively detached from *P. bryantii* B₁₄ cells (Chapter 3.4.3), which

prevent monensin from binding the cell membrane. The activity of a partial deconstruction of the EPS layer by in-house produced CAZymes may point out a general strategy of Gram-negative bacteria. A rougher surface of Gram-negative bacteria as compared to Gram-positive ones as seen in atomic force microscope images of Umeda, A., *et al.* [257]. This dynamic fortress of EPS may explain the successful strategy of *P. bryantii* B₁₄ against monensin. The mechanism of preventing antibiotics to reach their target, by covering with an EPS layer, was found in other microorganisms too [258]. The mechanism of separating the microorganism from an existing EPS-layer (turning into a planktonic form) was observed in Gram negative bacteria, such as *Pseudomonas aeruginosa* and *Streptococcus mutans* when a nutrient depletion appeared [259]. Also the decomposition of the EPS layer during prolonged incubation was found for *Pseudomonas fluorescens* [260], which was similar to the observed situation in chapter 3.3.5. The mechanism for detaching bacterial cells from EPS antibiotic exposure was not described yet in particular. The assumption that the EPS detachment may be caused by the prolonged incubation time, could be denied by the observation of the control group in chapter 3.3.5.

6.3.3 Increased transcription & translation

Monensin triggered low intracellular Na⁺, K⁺ or H⁺ concentration can be the mediators for adaptation processes [261] in form of elevated translation and transcription proteins in pure cultures (Chapter 3.3.3 and 3.3.4). Transcriptional and translational proteins also increased in the control group but only when stationary phase of growth was reached. However, the abundance in the control group still remained lower than under monensin conditions. Clearly are the reasons for adapting the quantity of transcription and translation proteins are different, but they provide a set of proteins that can be assigned to a certain function. Monensin supplemented cells revealed for example a presence of ribosomal RNA methyltransferases, which are also seen to be important for antibiotic resistances [262, 263]. The newly assigned protein (UniprotKB: A0A1H8YRX1) is similar to the YitL protein from *Bacillus subtilis*, which is most likely involved in translation, due to its RNA binding domain (Chapter 3.3.3, Table S16). However, antibiotic supplemented cells had specifically more methyltransferases for activation of genes [264]. In order to obtain a clear image about protein expression mechanisms of this vast amount of RNA-methyl transferases, various conditions with their metadata have to be tested for *P. bryantii* in order to understand the complex pattern and the role of functionally unknown proteins.

6.3.4 Outer membrane proteins as biomarkers

Monensin treatment and single-SCFA incubations were challenging conditions for *P. bryantii*, which was often reflected by the differential abundance of outer membrane proteins in chapter 2, 3 and 4. Cell aggregation was observed under isovaleric acid (Chapter 2.5.1, Figure S11) and monensin exposure (Chapter 3.3.3 with Figure 14, Chapter 3.3.4 with Figure 16 and [85]) which can be most likely connected to a decline of outer membrane proteins. Out of all outer membrane proteins, TonB related proteins seemed to play an important role as an indicator for physiologic challenging conditions. Those proteins are usually responsible for transport of porphyrin- and pyrrole-ring structures, as hemin (including iron) or cyanocobalamin (Vitamin B₁₂), siderophores and also carbohydrates [245, 246, 265]. Biochemical functions and requirement of hemin, iron and cyanocobalamin for *P. bryantii* are discussed in chapter 5.3. The lowered abundance of outer membrane proteins under monensin and most likely under other stressful conditions (Chapter 3.3.3, Table S12) underlines that this mechanism supports the hibernation type metabolism. Under those condition the enzymatic activity is concentrated in the central carbon metabolism in order to react fast to upcoming changes and maintain a steady state with low metabolic flux. However, the direct path from stress perception to TonB, as a highly abundant biomarker, still needs to be investigated. A suitable approach would be to perform correlation studies with label-free quantitative proteomics to identify possible interaction partners and elucidate causalities.

6.3.5 Key role of *Prevotella* under monensin exposure

Rusitec experiments with rumen microbiota under monensin supplementation verified the major role of *Prevotella* due to the adaptive response of the QFR (Chapter 4.4.6). Abundance of QFR assigned to *Prevotella* was increased under monensin and a concomitant activity of QFR (Figure 15) was shown with an elevated fumarate reduction to succinate (Figure 23). Therefore, less acetate is formed by responsible microbes, due to the preference for the QFR in *Prevotella*. Succinate also appears to be a propionate precursor [127, 266], which is why succinate is assumed to be rapidly converted and kept at an equilibrium and not accumulating in the cells (Figure 24). Metaproteomic (Chapter 4.4.5, Figure S24) and qPCR resulting from DNA extracts of the Rusitec study (Chapter 4) also showed a significant increase of *Prevotella* and its representative 16S rRNA copies in the MON group when compared to CON (Figure 29). Figure 29 underlines the persistence of *Prevotella* and in particular *P. bryantii* under monensin exposure not only in pure but in mixed culture. This success of *Prevotella* surviving under monensin exposure can be explained by the expressed pathway for anaerobic respiration via the QFR. The QFR utilizes the available H₂ (in form of NADH) and reduces fumarate into succinate and diminishes the methanogenesis by removing the important substrate H₂ as also described by Henderson, C., *et al.* [266].

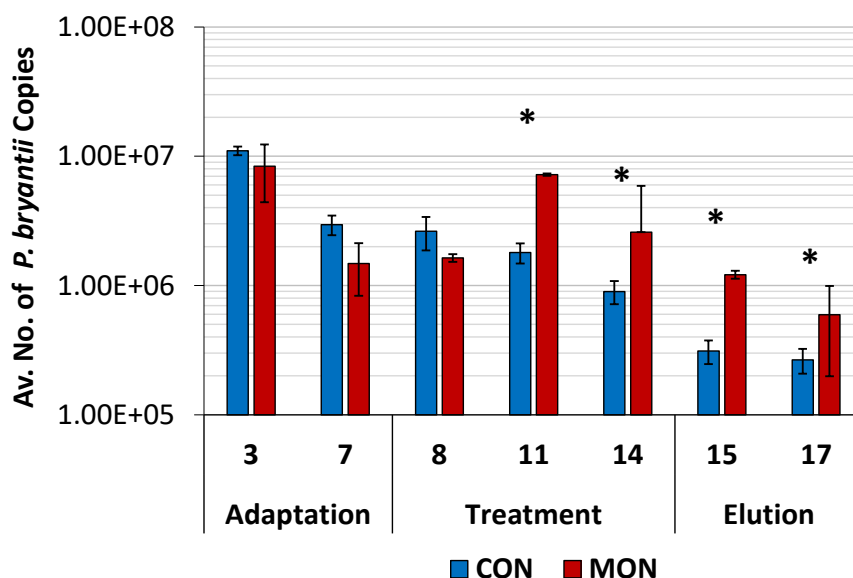


Figure 29: Average number of variable 16S rRNA region of *Prevotella bryantii* in monensin treatments (MON) and control group (CON) in the solid phase of the Rusitec experiment. Significant differences indicated by asterisk (*, LSD-Fisher, $p < 0.05$). Error bars indicate standard deviation. qPCR methodology including primers of *P. bryantii* originated from Stevenson and Weimer (2007) and Witzig *et al.* (2018).

Prevotella sp. and especially *P. bryantii* is discussed in chapter 6.3.1 – 6.3.3, one of the most important metabolic key player in the rumen microbiome. Metabolic pathways regarding polysaccharide fermentation and protein degradation are displayed in Figure 30. Proteolytic *Prevotella* sp. such as *P. bryantii*, *P. ruminicola* and *P. brevis* are known to be responsible for ruminal proteolysis [14] which is reduced via the quantity of tryptophan metabolizing enzymes (Chapter 4.4.2, Figure 20). Concerning the reduced ruminal plant fibre degradation under monensin, several CAZymes were identified (Figure 25) for being responsible for the reduced degradation (Chapter 4.4.7). The responsible fibre degraders in the genus *Prevotella* were identified by Terry, S.A., *et al.* [219] to be *P. bryantii*, *P. ruminicola* and *P. multisaccharivorax*. The special feature of being able to perform anaerobic respiration via the NQR, connected to the QFR was shown by the investigation of Hackmann, T.J., *et al.* [127] combined with findings Schleicher, L., *et al.* [107]. Browsing the obtained data from chapter 4 gave the list of *Prevotella* sp. with a NQR (*P. ruminicola*, *P. albensis*, *P. multisaccharivorax*) and QFR (*P. bryantii*, *P. ruminicola*, *P. albensis*, *P. buccae*). Figure 30 summarizes the impact of monensin on ruminal metabolism and indicate the findings (Chapter 3.3.3, 4.4.6 and 4.5.2) and improves our understanding of ruminal metabolism regulation under monensin when comparing Figure 4 with Figure 30.

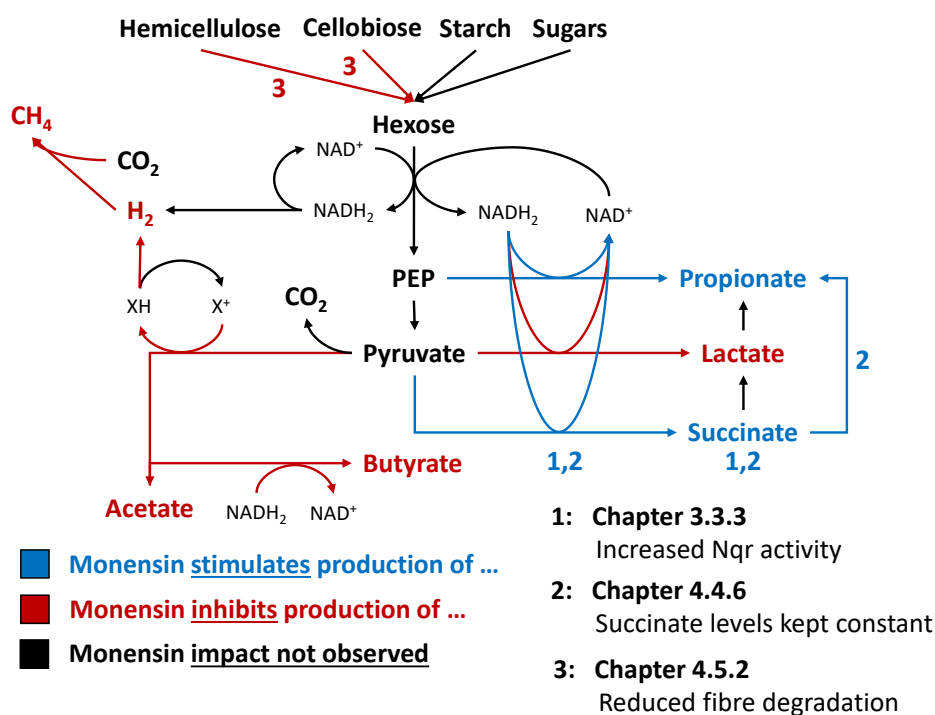


Figure 30: Ruminal fermentation pathways under monensin. X⁺ and XH represent a proton carrying redox cofactor.

6.4 Reclassification of *P. bryantii* to *Segatella bryantii*

Before completion of this thesis, *Prevotella bryantii* has been reclassified as *Segatella bryantii*, which classification is based on “comparative genome approaches (marker gene-based genome phylogeny, core genome phylogeny, average amino acid identity, percentage of conserved proteins and clade-specific marker genes) to identify large differences between the 53 species”[267].

7. Outlook

The presented thesis provided several new insights but in the same way also the next questions for future research. A clearer understanding of how SCFA can be used on a biochemical level in *P. bryantii* was provided in the present work and can be adapted for other bacterial species. The reason for the growth promoting ability of SCFA could not be clearly illuminated but showed a clear involvement into the LCFA metabolism. The interesting aspect about LCFAs is their implementation into the membrane of microorganisms. Depending on the membrane lipid composition, incorporation of certain membrane proteins may be favoured. Membrane proteins manage the crucial part of interacting with the environment, which is why their favourable conditions are crucial to be known. Together with the methodologies of LCFA analysis, proteomics, protein-structure analysis and bioinformatics, a favourable membrane lipid environment, modulated by SCFA supplementation, can be identified. The gained information can be applied in the fields of nutrition, by supplementing the correct amount of SCFAs for adjusting cellular processes. This knowledge can also be applied in upscale processing, when certain membrane proteins are desired to be enriched in a cell culture.

The elucidated mechanisms of how *P. bryantii* B₁₄ can cope with monensin are the degradation of the outer EPS layer under monensin supplementation. Connected to this finding further new tasks emerged, that require a verification of the assumed defence mechanism of *P. bryantii* B₁₄ by letting monensin bind to its outer EPS layer. This hypothesis of monensin binding the EPS layer was supported by the low recovery rate of radioactive labelled monensin in cells of *P. bryantii* [95]. This defence mechanism of binding antibiotics via a biofilm is not a new discovery [268]. Therefore, the mechanism of how to reduce or enhance the binding of monensin will become an important field of research in our time of rising antibiotic resistances. New drugs with different mode of actions may be required, for which this research on antibiotic will create the basis. In order to further understand the monensin binding to the EPS, the EPS composition with its adherent components will be required. New methodologies for sample preparation will be most likely needed to analyse the complex mixture of saccharides and other components. The preferred analytical methodology will be LC-MS, due to its sharp compound wide spectra for compound identification. Especially the binding capacity of the EPS on ions will be interesting, since monensin favours sodium ions which may be the link for its binding. Methodologies such as

microfluidic bioreactors [245] may provide technical solutions for required experimental setups and improve sample preparation for extracellular polymeric substrates. Knowledge about monensin binding to EPS can be applied in the field of medicine, where antibiotic resistance can be reduced by supplementing CAZymes in order to degrade EPS. Involved CAZymes for the EPS degradation were specified in Table S20 but needs to be verified for *P. bryantii* B₁₄.

The metabolic reactions of the rumen microbiome under monensin exposure *ex vivo* were investigated with a metaproteomic approach, which showed that *Prevotella* acts as a key player in the rumen microbiome under monensin exposure. The observed shift of a preferred production of acetate to succinate by *Prevotella* indicated the flexibility of this genus and family, which explains their strong abundance. Other propionate producing microbes such as Veillonellaceae [231] correlated positively with propionate and were documented to be able to use succinate and lactate as a substrate [235]. In order to verify the Prevotellaceae provided succinate dependency of Veillonellaceae, a co-cultivation with and without monensin could verify the described metabolic shift. An increase of propionate would also enhance the support of butyrate and valerate production, since the alkyl chain can be extended more easily. Those insights can allow us to understand interactions and dependencies, respectively, and use metabolites and antibiotics like monensin to shift the microbiome metabolism. The future idea would be to customize gut microbiotas of ruminants or other animals in order to provide a desired amount of nutrients for the host. Research showed that those health promoting metabolites appear to be SCFA [269, 270]. Since a direct supplementation of SCFA may be unpractical for ruminants, a supplementation of the respective precursors and probiotics may be useful to modulate ruminal SCFAs homeostasis [271]. But in order to maintain this balance permanently, a suitable diet and environment for the health promoting ruminal key player are required. Holistic approaches, as for example the study from Belanche, A., *et al.* [272], described that concentrate feed provides a higher yield of SCFAs with a smaller diversity of microbes. In comparison to feed concentrate showed ryegrass pasture a wider distribution of metabolites with a larger diversity of rumen microbes [272]. The current world-wide dominating strategy in animal farming display the use of feed concentrate as well as the use of growth promoters, such as monensin. This strategy results in a higher yield of animal product but bear an increased risk for pathogenic invasion, correlated with a less diverse eco system [273]. Both types of feed provide their specific

features which need to be taken into account, when it is upon to decide which strategy aligns with our desired way of life.

8. Literature References

1. Trautmann, A.; Schleicher, L.; Deusch, S.; Gätgens, J.; Steuber, J.; Seifert, J. Short-chain fatty acids modulate metabolic pathways and membrane lipids in *Prevotella bryantii* B14. *Proteomes* **2020**, *8*, 28.
2. Trautmann, A.; Schleicher, L.; Pfirrmann, J.; Boldt, C.; Steuber, J.; Seifert, J. Na⁺-coupled respiration and reshaping of extracellular polysaccharide layer counteract monensin-induced cation permeability in *Prevotella bryantii* B14. *International Journal of Molecular Science* **2021**, *2*, 10202.
3. Millen, D.D.A., Mario De Beni; Pacheco, Rodrigo Dias Lauritano. *Rumenology*. Switzerland: Springer, **2016**, *9*, 63-102.
4. Zehavi, T.; Probst, M.; Mizrahi, I. Insights into culturomics of the rumen microbiome. *Frontiers In Microbiology* **2018**, *9*, 1999.
5. Watson, M. The genomic and proteomic landscape of the rumen microbiome revealed by comprehensive genome-resolved metagenomics. **2018**. Content was later published under literature reference number [213]
6. Bailoni, L.; Carraro, L.; Cardin, M.; Cardazzo, B. Active rumen bacterial and protozoal communities revealed by RNA-based amplicon sequencing on dairy cows fed different diets at three physiological stages. *Microorganisms* **2021**, *9*, 754.
7. Deusch, S.; Camarinha-Silva, A.; Conrad, J.; Beifuss, U.; Rodehutschord, M.; Seifert, J. A structural and functional elucidation of the rumen microbiome influenced by various diets and microenvironments. *Frontiers of Microbiology* **2017**, *8*, 1605.
8. Deusch, S.; Tilocca, B.; Camarinha-Silva, A.; Seifert, J. News in livestock research — use of omics-technologies to study the microbiota in the gastrointestinal tract of farm animals. *Computational Structural Biotechnology Journal* **2015**, *13*, 55–63.
9. Stevenson, D.M.; Weimer, P.J. Dominance of *Prevotella* and low abundance of classical ruminal bacterial species in the bovine rumen revealed by relative quantification real-time PCR. *Applied Microbiology and Biotechnology* **2007**, *75*, 165–174.
10. Shah, H.N.; Collins, D.M. *Prevotella*, a new genus to include *Bacteroides melanogenicus* and related species formerly classified in the genus *Bacteroides*. *International Journal of Systematic and Evolutionary Microbiology* **1990**, *40*, 205-208.
11. Purushe, J.; Fouts, D.E.; Morrison, M.; White, B.A.; Mackie, R.I.; Coutinho, P.M.; Henrissat, B.; Nelson, K.E.; Bacteria, N.A.C.f.R. Comparative genome analysis of *Prevotella ruminicola* and *Prevotella bryantii*: Insights into their environmental niche. *Microbial Ecology* **2010**, *60*, 721-729.
12. Avguštin, G.; Wallace, R.J.; Flint, H.J. Phenotypic diversity among ruminal isolates of *Prevotella ruminicola*: Proposal of *Prevotella brevis* sp. Nov., *Prevotella bryantii* sp. Nov., and *Prevotella albensis* sp. Nov. and redefinition of *Prevotella ruminicola*. *International Journal of Systematic and Evolutionary Microbiology* **1997**, *47*, 284-288.
13. Dodd, D.; Moon, Y.-H.; Swaminathan, K.; Mackie, R.I.; Cann, I.K. Transcriptomic analyses of xylan degradation by *Prevotella bryantii* and insights into energy

- acquisition by xylanolytic *Bacteroidetes*. *Journal of Biological Chemistry* **2010**, 285, 30261-30273.
14. Griswold, K.E.; White, B.A.; Mackie, R.I. Diversity of extracellular proteolytic activities among *Prevotella* species from the rumen. *Current Microbiology* **1999**, 39, 187-194.
 15. Bryant, M.; Small, N.; Bouma, C.; Chu, H. *Bacteroides ruminicola* n. sp. and *Succinimonas amylolytica* the new genus and species: Species of succinic acid-producing anaerobic bacteria of the bovine rumen. *Journal of Bacteriol* **1958**, 76, 15.
 16. Mannarelli, B.M.; Ericsson, L.D.; Lee, D.; Stack, R.J. Taxonomic relationships among strains of the anaerobic bacterium *Bacteroides ruminicola* determined by DNA and extracellular polysaccharide analysis. *Applied Environmental Microbiology* **1991**, 57, 2975-2980.
 17. Avguštin, G.; Wright, F.; Flint, H.J. Genetic diversity and phylogenetic relationships among strains of *Prevotella (Bacteroides) ruminicola* from the rumen. *International Journal of Systematic and Evolutionary Microbiology* **1994**, 44, 246-255.
 18. Pybus, V.; Onderdonk, A.B. Evidence for a commensal, symbiotic relationship between *Gardnerella vaginalis* and *Prevotella bivia* involving ammonia: Potential significance for bacterial vaginosis. *Journal of Infectious Diseases* **1997**, 175, 406-413.
 19. Wu, C.-C.; Johnson, J.; Moore, W.; Moore, L. Emended descriptions of *Prevotella denticola*, *Prevotella loescheii*, *Prevotella veroralis*, and *Prevotella melaninogenica*. *International Journal of Systematic and Evolutionary Microbiology* **1992**, 42, 536-541.
 20. Torrungruang, K.; Jitpakdeebordin, S.; Charatkulangkun, O.; Gleebua, Y. *Porphyromonas gingivalis*, *Aggregatibacter actinomycetemcomitans*, and *Treponema denticola/Prevotella intermedia* co-infection are associated with severe periodontitis in a Thai population. *PLoS One* **2015**, 10, e0136646.
 21. Nadkarni, M.A.; Caldon, C.E.; Chhour, K.-L.; Fisher, I.P.; Martin, F.E.; Jacques, N.A.; Hunter, N. Carious dentine provides a habitat for a complex array of novel *Prevotella*-like bacteria. *Journal of Clinical Microbiology* **2004**, 42, 5238-5244.
 22. Tompkins, G.R.; Wood, D.P.; Birchmeier, K.R. Detection and comparison of specific heme binding by *Porphyromonas gingivalis* and *Pprevotella intermedia*. *Journal of Bacteriology* **1997**, 179, 620-626.
 23. Wallace, R. "The proteolytic systems of ruminal microorganisms." Paper presented at the *Annales de Zootechnie* **1996**, 45, 301-308.
 24. Spencer, H. *A system of synthetic philosophy: The Principles of Biology*. D. Appleton, **1873**, 2.
 25. Baldwin, R.; Allison, M. Rumen metabolism. *Journal of Animal Science* **1983**, 57, 461-477.
 26. Huang, Y.; Marden, J.; Julien, C.; Bayourthe, C. Redox potential: An intrinsic parameter of the rumen environment. *Journal of Animal Physiology and Animal Nutrition* **2018**, 102, 393-402.
 27. Demain, L.; Wolfe, R.F. Marvin P. Bryant. *Biographical Memoirs of* **2002**, 81, 66-377.
 28. Caldwell, D.; White, D.; Bryant, M.; Doetsch, R. Specificity of the heme requirement for growth of *Bacteroides ruminicola*. *Journal of Bacteriology* **1965**, 90, 1645-1654.

Literature References

29. Pittman, K.; Bryant, M. Peptides and other nitrogen sources for growth of *Bacteroides ruminicola*. *Journal of Bacteriology* **1964**, 88, 401-410.
30. Boguhn, J.; Kluth, H.; Rodehutsord, M. Effect of total mixed ration composition on fermentation and efficiency of ruminal microbial crude protein synthesis *in vitro*. *Journal of Dairy Science* **2006**, 89, 1580-1591.
31. Lou, J.; Dawson, K.; Strobel, H. Glycogen biosynthesis via udp-glucose in the ruminal bacterium *Prevotella bryantii* B1(4). *Applied and Environmental Microbiology* **1997**, 63, 4355-4359.
32. Colleoni, C. Storage polysaccharide metabolism in micro-organisms. *Enzymology of Complex Alpha-Glucans* **2021**, 61.
33. Aoki, K.F.; Kanehisa, M. Using the KEGG database resource. *Current protocols in bioinformatics* **2005**, 11, 1.12. 11-11.12. 54.
34. Bergman, E. Energy contributions of volatile fatty acids from the gastrointestinal tract in various species. *Physiological Reviews* **1990**, 70, 567-590.
35. Flint, H.J.; Bayer, E.A. Plant cell wall breakdown by anaerobic microorganisms from the mammalian digestive tract. *Annals of the New York Academy of Sciences* **2008**, 1125, 280-288.
36. El-Shazly, K. Degradation of protein in the rumen of the sheep. 2. The action of rumen micro-organisms on amino-acids. *Biochemical Journal* **1952**, 51, 647-653.
37. Neis, E.P.; Dejong, C.H.; Rensen, S.S. The role of microbial amino acid metabolism in host metabolism. *Nutrients* **2015**, 7, 2930-2946.
38. Liu, Q.; Wang, C.; Pei, C.; Li, H.; Wang, Y.; Zhang, S.; Zhang, Y.; He, J.; Wang, H.; Yang, W. Effects of isovalerate supplementation on microbial status and rumen enzyme profile in steers fed on corn stover based diet. *Livestock Science* **2014**, 161, 60-68.
39. Dehority, B.; Scott, H.; Kowaluk, P. Volatile fatty acid requirements of cellulolytic rumen bacteria. *Journal of Bacteriology* **1967**, 94, 537-543.
40. Duncan, S.H.; Hold, G.L.; Harmsen, H.J.; Stewart, C.S.; Flint, H.J. Growth requirements and fermentation products of *Fusobacterium prausnitzii*, and a proposal to reclassify it as *Faecalibacterium prausnitzii* gen. Nov., comb. Nov. *International Journal of Systematic and Evolutionary Microbiology* **2002**, 52, 2141-2146.
41. Dehority, B. Characterization of several bovine rumen bacteria isolated with a xylan medium. *Journal of Bacteriology* **1966**, 91, 1724-1729.
42. Fujita, Y.; Matsuoka, H.; Hirooka, K. Regulation of fatty acid metabolism in bacteria. *Molecular Microbiology* **2007**, 66, 829-839.
43. DiRienzo, J.M.; Inouye, M. Lipid fluidity-dependent biosynthesis and assembly of the outer membrane proteins of *E. coli*. *Cell* **1979**, 17, 155-161.
44. Lee, A. Lipids and their effects on membrane proteins: Evidence against a role for fluidity. *Progress in Lipid Research* **1991**, 30, 323-348.
45. Lee, A.G. How lipids affect the activities of integral membrane proteins. *Biochimica et Biophysica Acta (BBA)-Biomembranes* **2004**, 1666, 62-87.

46. Hoseinifar, S.H.; Sun, Y.Z.; Caipang, C.M. Short-chain fatty acids as feed supplements for sustainable aquaculture: An updated view. *Aquaculture Research* **2017**, *48*, 1380-1391.
47. Herold, S.; Paton, J.C.; Srimanote, P.; Paton, A.W. Differential effects of short-chain fatty acids and iron on expression of iha in shiga-toxigenic *Escherichia coli*. *Microbiology* **2009**, *155*, 3554-3563.
48. Schwarzenbach, v.G. Der Chelateffekt. *Helvetica Chimica Acta* **1952**, *35*, 7, 2344-2359.
49. Lu, Q.; Yang, Y.-T.; Chen, C.-S.; Davis, M.; Byrd, J.C.; Etherton, M.R.; Umar, A.; Chen, C.-S. Zn²⁺-chelating motif-tethered short-chain fatty acids as a novel class of histone deacetylase inhibitors. *Journal of Medicinal Chemistry* **2004**, *47*, 467-474.
50. Scott, H.; Dehority, B. Vitamin requirements of several cellulolytic rumen bacteria. *Journal of Bacteriology* **1965**, *89*, 1169-1175.
51. Strobel, H.J. Vitamin B12-dependent propionate production by the ruminal bacterium *Prevotella ruminicola* 23. *Applied and Environmental Microbiology* **1992**, *58*, 2331-2333.
52. Gibbons, R.J.; Macdonald, J.B. Hemin and vitamin K compounds as required factors for the cultivation of certain strains of *Bacteroides melaninogenicus*. *Journal of Bacteriology* **1960**, *80*, 164-170.
53. Sybesma, W.; Starrenburg, M.; Tijsseling, L.; Hoefnagel, M.H.; Hugenholtz, J. Effects of cultivation conditions on folate production by lactic acid bacteria. *Applied and Environmental Microbiology* **2003**, *69*, 4542-4548.
54. Downey, R. Vitamin K-mediated electron transfer in *Bacillus subtilis*. *Journal of Bacteriology* **1964**, *88*, 904-911.
55. Guchhait, R.B.; Polakis, S.E.; Dimroth, P.; Stoll, E.; Moss, J.; Lane, M.D. Acetyl coenzyme a carboxylase system of *Escherichia coli*: Purification and properties of the biotin carboxylase, carboxyltransferase, and carboxyl carrier protein components. *Journal of Biological Chemistry* **1974**, *249*, 6633-6645.
56. Carlsson, J.; Höfling, J.; Sundqvist, G. Degradation of albumin, haemopexin, haptoglobin and transferrin, by black-pigmented *Bacteroides* species. *Journal of Medical Microbiology* **1984**, *18*, 39-46.
57. Yu, F.; Anaya, C.; Lewis, J.P. Outer membrane proteome of *Prevotella intermedia* 17: Identification of thioredoxin and iron-repressible hemin uptake loci. *Journal of Proteomics* **2007**, *7*, 403-412.
58. Leung, K.-P.; Folk, S.P. Effects of porphyrins and inorganic iron on the growth of *Prevotella intermedia*. *FEMS Microbiology Letters* **2002**, *209*, 15-21.
59. Smalley, J.W.; Silver, J.; Birss, A.J.; Withnall, R.; Titler, P.J. The haem pigment of the oral anaerobes *Prevotella nigrescens* and *Prevotella intermedia* is composed of iron (iii) protoporphyrin ix in the monomeric form. *Microbiology* **2003**, *149*, 1711-1718.
60. Bergen, W.G.; Bates, D.B. Ionophores: Their effect on production efficiency and mode of action. *Journal of Animal Science* **1984**, *58*, 1465-1483.

Literature References

61. Callaway, T.; Edrington, T.; Rychlik, J.; Genovese, K.; Poole, T.; Jung, Y.S.; Bischoff, K.; Anderson, R.; Nisbet, D.J. Ionophores: Their use as ruminant growth promotants and impact on food safety. *Current Issues in Intestinal Microbiology* **2003**, *4*, 43-51.
62. Bogaert, C.; Jouany, J.; Jeminet, G. Effects of the ionophore antibiotics monensin, monensin-propionate, abierixin and calcimycin on ruminal fermentations *in vitro* (Rusitec). *Animal Feed Science and Technology* **1990**, *28*, 183-197.
63. Russell, J.B.; Houlihan, A.J. Ionophore resistance of ruminal bacteria and its potential impact on human health. *FEMS Microbiology Reviews* **2003**, *27*, 65-74.
64. Chen, M.; Wolin, M. Effect of monensin and lasalocid-sodium on the growth of methanogenic and rumen saccharolytic bacteria. *Applied and Environmental Microbiology* **1979**, *38*, 72-77.
65. Perreten, V. Use of antimicrobials in food-producing animals in Switzerland and in the European Union (EU). *Mitteilungen aus Lebensmitteluntersuchung und Hygiene* **2003**, *94*, 155-163.
66. Castanon, J. History of the use of antibiotic as growth promoters in european poultry feeds. *Poultry Science Journal* **2007**, *86*, 2466-2471.
67. Kirchhelle, C. Pharming animals: A global history of antibiotics in food production (1935–2017). *Palgrave Communications* **2018**, *4*, 1-13.
68. European Commission. Commission implementing regulation (EU) 2020/994 of 9th July 2020 concerning the authorisation of monensin and nicarbazin (monimax) as a feed additive for turkeys for fattening, chickens for fattening and chickens reared for laying (holder of authorisation huvepharma nv). **2020**.
69. U.S. Food & Drug Administration (FDA) 2020 summary report on antimicrobials sold or distributed for use in food-producing animals. *49*, **2021**.
70. Miller, S.; Wu, R.; Oremus, M. The association between antibiotic use in infancy and childhood overweight or obesity: A systematic review and meta-analysis. *Obesity Reviews* **2018**, *19*, 1463-1475.
71. Lin, J. Effect of antibiotic growth promoters on intestinal microbiota in food animals: A novel model for studying the relationship between gut microbiota and human obesity? *Frontiers in Microbiology* **2011**, *2*, 53.
72. Wang, H.; Ren, L.; Yu, X.; Hu, J.; Chen, Y.; He, G.; Jiang, Q. Antibiotic residues in meat, milk and aquatic products in Shanghai and human exposure assessment. *Food Control* **2017**, *80*, 217-225.
73. Kivits, T.; Broers, H.P.; Beeltje, H.; Van Vliet, M.; Griffioen, J. Presence and fate of veterinary antibiotics in age-dated groundwater in areas with intensive livestock farming. *Environmental Pollution* **2018**, *241*, 988-998.
74. Martini, M.; Verità, P.; Cecchi, F.; Cianci, D. Monensin sodium use in lambs from the second week of life to slaughter at 105 days. *Small Ruminant Research* **1996**, *20*, 1-8.
75. Todd, G.; Novilla, M.; Howard, L. Comparative toxicology of monensin sodium in laboratory animals. *Journal of Animal Science* **1984**, *58*, 1512-1517.
76. Hall, J.O. Toxic feed constituents in the horse. *Veterinary Clinics of North America: Equine Practice* **2001**, *17*, 479-489.

77. Basu, S.K.; Goldstein, J.L.; Anderson, R.G.; Brown, M.S. Monensin interrupts the recycling of low density lipoprotein receptors in human fibroblasts. *Cell* **1981**, 24, 493-502.
78. Wileman, T.; Boshans, R.L.; Schlesinger, P.; Stahl, P. Monensin inhibits recycling of macrophage mannose-glycoprotein receptors and ligand delivery to lysosomes. *Biochemical Journal* **1984**, 220, 665-675.
79. Chapman, H.; Jeffers, T.; Williams, R. Forty years of monensin for the control of coccidiosis in poultry. *Poultry Science* **2010**, 89, 1788-1801.
80. Łowicki, D.; Huczyński, A. Structure and antimicrobial properties of monensin a and its derivatives: Summary of the achievements. *BioMed Research International* **2013**, Article ID: 742149, 14 pages.
81. Saleh, O.; Bonitz, T.; Flinspach, K.; Kulik, A.; Burkard, N.; Mühlenweg, A.; Vente, A.; Polnick, S.; Lämmerhofer, M.; Gust, B. Activation of a silent phenazine biosynthetic gene cluster reveals a novel natural product and a new resistance mechanism against phenazines. *MedChemComm* **2012**, 3, 1009-1019.
82. Callaway, T.R.; Russell, J.B. Variations in the ability of ruminal gram-negative *Prevotella* species to resist monensin. *Current Microbiology* **2000**, 40, 185-189.
83. Wischer, G. Effects of monensin and tannin extract supplementation on methane production and other criteria of rumen ermentation *in vitro* and in long-term studies with sheep. Dr. agr., University of Hohenheim, **2012**, 7.
84. Strobel, H.; Russell, J. Non-proton-motive-force-dependent sodium efflux from the ruminal bacterium *Streptococcus bovis*: Bound versus free pools. *Applied and Environmental Microbiology* **1989**, 55, 2664-2668.
85. Callaway, T.R.; Russell, J.B. Selection of a highly monensin-resistant *Prevotella bryantii* subpopulation with altered outer membrane characteristics. *Applied and Environmental Microbiology* **1999**, 65, 4753-4759.
86. Callaway, T.R.; Adams, K.A.; Russell, J.B. The ability of "low g+ c gram-positive" ruminal bacteria to resist monensin and counteract potassium depletion. *Current Microbiology* **1999**, 39, 226-230.
87. Hook, S.E.; Northwood, K.S.; Wright, A.-D.; McBride, B.W. Long-term monensin supplementation does not significantly affect the quantity or diversity of methanogens in the rumen of the lactating dairy cow. *Applied and Environmental Microbiology* **2009**, 75, 374-380.
88. Weimer, P.J.; Stevenson, D.M.; Mertens, D.R.; Thomas, E.E. Effect of monensin feeding and withdrawal on populations of individual bacterial species in the rumen of lactating dairy cows fed high-starch rations. *Applied Microbiology and Biotechnology* **2008**, 80, 135-145.
89. Van Maanen, R.W.; Herbein, J.H.; McGilliard, A.D.; Young, J.W. Effects of monensin on *in vivo* rumen propionate production and blood glucose kinetics in cattle. *The Journal of Nutrition* **1978**, 108, 1002-1007.
90. Wallace, R.; Czerkawski, J.; Breckenridge, G. Effect of monensin on the fermentation of basal rations in the rumen simulation technique (Rusitec). *British Journal of Nutrition* **1981**, 46, 131-148.

Literature References

91. Callaway, T.R.; De Melo, A.M.C.; Russell, J.B. The effect of nisin and monensin on ruminal fermentations *in vitro*. *Current Microbiology* **1997**, *35*, 90-96.
92. Haimoud, D.A.; Vernay, M.; Bayourthe, C.; Moncoulon, R. Avoparcin and monensin effects on the digestion of nutrients in dairy cows fed a mixed diet. *Canadian Journal of Animal Science* **1995**, *75*, 379-385.
93. Wischer, G.; Boguhn, J.; Steingäß, H.; Schollenberger, M.; Hartung, K.; Rodehutschord, M. Effect of monensin on *in vitro* fermentation of silages and microbial protein synthesis. *Archives of Animal Nutrition* **2013**, *67*, 219–234.
94. Newbold, C.; Wallace, R.; Watt, N.D. Properties of ionophore-resistant *Bacteroides rurninicola* enriched by cultivation in the presence of tetronasin. *Journal of Applied Bacteriology* **1992**, *72*, 65-70.
95. Chow, J.M.; Van Kessel, J.A.S.; Russell, J.B. Binding of radiolabeled monensin and lasalocid to ruminal microorganisms and feed. *Journal of Animal Science* **1994**, *72*, 1630-1635.
96. Hungate, R.; Macy, J. The roll-tube method for cultivation of strict anaerobes. *Bulletins from the Ecological Research Committee* **1973**, 123-126.
97. Griswold, K.; Mackie, R. Degradation of protein and utilization of the hydrolytic products by a predominant ruminal bacterium, *Prevotella ruminicola* B14. *Journal of Dairy Science* **1997**, *80*, 167-175.
98. Czerkawski, J.; Breckenridge, G. Design and development of a long-term rumen simulation technique (Rusitec). *British Journal of Nutrition* **1977**, *38*, 371-384.
99. Berg, J.M.; Stryer, L.; Tymoczko, J.L.; Gatto, G.J. *Biochemistry*: Macmillan Learning, **2013**, *2*, 257-249.
100. Bjerrum, J.T. *Metabonomics: Methods and protocols*. Vol. 1. New York, NY ; Heidelberg: Humana Press: Springer, **2015**, 1277, 1-14.
101. Wilkins, M.R.; Pasquali, C.; Appel, R.D.; Ou, K.; Golasz, O.; Sanchez, J.-C.; Yan, J.X.; Gooley, A.A.; Hughes, G.; Humphery-Smith, I. From proteins to proteomes: Large scale protein identification by two-dimensional electrophoresis and amino acid analysis. *Bio/technology* **1996**, *14*, 61-65.
102. Matthiesen, R.; Bunkenborg, J. "Introduction to mass spectrometry-based proteomics." In *Mass Spectrometry Data Analysis in Proteomics*, 1-58: Springer, **2020**.
103. Cox, J.; Hein, M.Y.; Lubner, C.A.; Paron, I.; Nagaraj, N.; Mann, M. Accurate proteome-wide label-free quantification by delayed normalization and maximal peptide ratio extraction, termed maxlfr. *Molecular & Cellular Proteomics* **2014**, *13*, 2513–2526.
104. Wilmes, P.; Bond, P.L. Metaproteomics: Studying functional gene expression in microbial ecosystems. *Trends in Microbiology* **2006**, *14*, 92-97.
105. Giraudeau, P.; Silvestre, V.; Akoka, S. Optimizing water suppression for quantitative NMR-based metabolomics: A tutorial review. *Metabolomics* **2015**, *11*, 1041-1055.
106. Ellinger, J.J.; Chylla, R.A.; Ulrich, E.L.; Markley, J.L. Databases and software for NMR-based metabolomics. *Current Metabolomics* **2013**, *1*, 28-40.
107. Schleicher, L.; Trautmann, A.; Stegmann, D.P.; Fritz, G.; Gätgens, J.; Bott, M.; Hein, S.; Simon, J.; Seifert, J.; Steuber, J. A sodium-translocating module linking succinate

- production to formation of membrane potential in *Prevotella bryantii*. *Applied and Environmental Microbiology* **2021**, 87, e01211-01221.
108. Alvarez, H.; Santini, F.J.; Rearte, D.H.; Elizalde, J.C. Milk production and ruminal digestion in lactating dairy cows grazing temperate pastures and supplemented with dry cracked corn or high moisture corn. *Animal Feed Science and Technology* **2001**, 91, 183-195.
 109. Byrne, C.; Chambers, E.; Morrison, D.; Frost, G. The role of short chain fatty acids in appetite regulation and energy homeostasis. *International journal of obesity* **2015**, 39, 1331-1338.
 110. Von Engelhardt, W.; Rönnau, K.; Rechkemmer, G.; Sakata, T. Absorption of short-chain fatty acids and their role in the hindgut of monogastric animals. *Animal Feed Science and Technology* **1989**, 23, 43-53.
 111. LeBlanc, J.G.; Chain, F.; Martín, R.; Bermúdez-Humarán, L.G.; Courau, S.; Langella, P. Beneficial effects on host energy metabolism of short-chain fatty acids and vitamins produced by commensal and probiotic bacteria. *Microbial Cell Factories* **2017**, 16, 79.
 112. Takahashi, N.; Yamada, T. Pathways for amino acid metabolism by *Prevotella intermedia* and *Prevotella nigrescens*. *Oral Microbiology and Immunology* **2000**, 15, 96-102.
 113. Bhatia, S.K.; Yang, Y.-H. Microbial production of volatile fatty acids: Current status and future perspectives. *Reviews in Environmental Science and Bio/Technology* **2017**, 16, 327-345.
 114. Hobson, P.N. "Rumen bacteria." In *Methods in microbiology*, edited by J. R. Norris and D. W. Ribbons, London, UK: Elsevier Ltd., **1969**, 3, 133–149..
 115. Cotta, M.A.; Russell, J.B. Effect of peptides and amino acids on efficiency of rumen bacterial protein synthesis in continuous culture. *Journal of Dairy Science* **1982**, 65, 226–234.
 116. Paczia, N.; Nilgen, A.; Lehmann, T.; Gätgens, J.; Wiechert, W.; Noack, S. Extensive exometabolome analysis reveals extended overflow metabolism in various microorganisms. *Microbial Cell Factories* **2012**, 11, 122.
 117. Vlaeminck, B.; Fievez, V.; Cabrita, A.; Fonseca, A.; Dewhurst, R. Factors affecting odd- and branched-chain fatty acids in milk: A review. *Animal Feed Science and Technology* **2006**, 131, 389-417.
 118. Allison, M.J.; Bryant, M.; Katz, I.; Keeney, M. Metabolic function of branched-chain volatile fatty acids, growth factors for *Ruminococci* II.: Biosynthesis of higher branched-chain fatty acids and aldehydes. *Journal of Bacteriology* **1962**, 83, 1084-1093.
 119. Bradford, M.M. A rapid and sensitive method for the quantitation of microgram quantities of protein utilizing the principle of protein-dye binding. *Analytical Biochemistry* **1976**, 72, 248–254.
 120. Jehmlich, N.; Schmidt, F.; Hartwich, M.; Bergen, M.v.; Richnow, H.-H.; Vogt, C. Incorporation of carbon and nitrogen atoms into proteins measured by protein-based stable isotope probing (protein-sip). *Rapid Communications in Mass Spectrometry* **2008**, 22, 2889–2897.

121. Rappsilber, J.; Mann, M.; Ishihama, Y. Protocol for micro-purification, enrichment, pre-fractionation and storage of peptides for proteomics using stagetips. *Nature Protocols* **2007**, 2, 1896–1906.
122. Olsen, J.V.; Godoy, L.M.F.d.; Li, G.; Macek, B.; Mortensen, P.; Pesch, R.; Makarov, A.; Lange, O.; Horning, S.; Mann, M. Parts per million mass accuracy on an orbitrap mass spectrometer via lock mass injection into a c-trap. *Molecular & Cellular Proteomics* **2005**, 4, 2010–2021.
123. Vizcaíno, J.A.; Csordas, A.; Del-Toro, N.; Dienes, J.A.; Griss, J.; Lavidas, I.; Mayer, G.; Perez-Riverol, Y.; Reisinger, F.; Ternent, T. 2016 update of the pride database and its related tools. *Nucleic Acids Research* **2016**, 44, D447-D456.
124. Kanehisa, M.; Sato, Y.; Morishima, K. Blastkoala and ghostkoala: Kegg tools for functional characterization of genome and metagenome sequences. *Journal of Molecular Biology* **2016**, 428, 726–731.
125. Huerta-Cepas, J.; Forslund, K.; Coelho, L.P.; Szklarczyk, D.; Jensen, L.J.; von Mering, C.; Bork, P. Fast genome-wide functional annotation through orthology assignment by EggNOG-mapper. *Molecular Biology and Evolution*. **2017**, 34, 2115-2122.
126. Hungate, R.E. *The rumen and its microbes*. London, UK: Academic Press Inc., 1966.
127. Hackmann, T.J.; Ngugi, D.K.; Firkins, J.L.; Tao, J. Genomes of rumen bacteria encode atypical pathways for fermenting hexoses to short-chain fatty acids. *Environmental Microbiology* **2017**, 19, 4670-4683.
128. Conner, R.L.; Reilly, A.E. The effects of isovalerate supplementation on growth and fatty acid composition of *Tetrahymena pyriformis* w. *Biochimica et Biophysica Acta (BBA)-Lipids and Lipid Metabolism* **1975**, 398, 209-216.
129. Grundy, F.J.; Waters, D.A.; Allen, S.; Henkin, T. Regulation of the *Bacillus subtilis* acetate kinase gene by CcpA. *Journal of Bacteriology* **1993**, 175, 7348-7355.
130. Valgepea, K.; Adamberg, K.; Nahku, R.; Lahtvee, P.-J.; Arike, L.; Vilu, R. Systems biology approach reveals that overflow metabolism of acetate in *Escherichia coli* is triggered by carbon catabolite repression of acetyl-CoA synthetase. *BMC Systems Biology* **2010**, 4, 1-13.
131. Holt, S.C.; Ebersole, J.L. *Porphyromonas gingivalis*, *Treponema denticola*, and *Tannerella forsythia*: The 'red complex', a prototype polybacterial pathogenic consortium in periodontitis. *Periodontology 2000* **2005**, 38, 72-122.
132. Lindt, F.; Blum, J.W. Occurrence of iron deficiency in growing cattle. *Zentralbl Veterinarmed A*. **1994**, 41, 237-246.
133. Henry, C.A.; Judy, M.; Dyer, B.; Wagner, M.; Matthews, J.L. Sensitivity of *Porphyromonas* and *Prevotella* species in liquid media to argon laser. *Photochemistry and Photobiology* **1995**, 61, 410-413.
134. Macy, J.; Probst, I.; Gottschalk, G. Evidence for cytochrome involvement in fumarate reduction and adenosine 5'-triphosphate synthesis by *Bacteroides fragilis* grown in the presence of hemin. *Journal of Bacteriology* **1975**, 123, 436-442.
135. Deusch, S.; Bok, E.; Schleicher, L.; Seifert, J.; Steuber, J. Occurrence and function of the Na⁺-translocating NADH: Quinone oxidoreductase in *Prevotella* spp. *Microorganisms* **2019**, 7, 117.

136. Sperry, J.; Appleman, M.; Wilkins, T.D. Requirement of heme for growth of *Bacteroides fragilis*. *Applied Environmental Microbiology* **1977**, *34*, 386-390.
137. Granick, S.; Beale, S.I. Hemes, chlorophylls, and related compounds: Biosynthesis and metabolic regulation. *Advances in Enzymology and Related Areas of Molecular Biology* **1978**, *46*, 33-203.
138. Minato, H.; Ishibashi, S.; Hamaoka, T. Cellular fatty acid and sugar composition of representative strains of rumen bacteria. *Journal of General and Applied Microbiology* **1988**, *34*, 303-319.
139. Logar, R.M.; Zorec, M.; Kopečný, J. Reliable identification of *Prevotella* and *Butyrivibrio* spp. From rumen by fatty acid methyl ester profiles. *Folia Microbiologica* **2001**, *46*, 57-59.
140. Sun, Y.; Wilkinson, B.J.; Standiford, T.J.; Akinbi, H.T.; O'Riordan, M.X. Fatty acids regulate stress resistance and virulence factor production for *Listeria monocytogenes*. *Journal of Bacteriology* **2012**, *194*, 5274-5284.
141. Mitchell, N.J.; Seaton, P.; Pokorny, A. Branched phospholipids render lipid vesicles more susceptible to membrane-active peptides. *Biochimica et Biophysica Acta (BBA)-Biomembranes* **2016**, *1858*, 988-994.
142. Singh, V.K.; Hattangady, D.S.; Giotis, E.S.; Singh, A.K.; Chamberlain, N.R.; Stuart, M.K.; Wilkinson, B.J. Insertional inactivation of branched-chain α -keto acid dehydrogenase in *Staphylococcus aureus* leads to decreased branched-chain membrane fatty acid content and increased susceptibility to certain stresses. *Applied and Environmental Microbiology* **2008**, *74*, 5882-5890.
143. Kaneda, T. Iso-and anteiso-fatty acids in bacteria: Biosynthesis, function, and taxonomic significance. *Microbiological Reviews* **1991**, *55*, 288-302.
144. Sirobhushanam, S. Alternative pathway for provision of acyl CoA precursors for fatty acid biosynthesis: Purification and kinetic characterization of phosphotransbutyrylase and butyrate kinase from *Listeria monocytogenes*. *Illinois* **2016**, 3-4.
145. Reiser, K.; Davis, M.A.; Hynes, M.J. *Aspergillus nidulans* contains six possible fatty acyl-CoA synthetases with FaaB being the major synthetase for fatty acid degradation. *Archives of Microbiology* **2010**, *192*, 373-382.
146. DiRusso, C.C.; Black, P.N. Bacterial long chain fatty acid transport: Gateway to a fatty acid-responsive signaling system. *Journal of Biological Chemistry* **2004**, *279*, 49563-49566.
147. De Filippis, F.; Pasolli, E.; Tett, A.; Tarallo, S.; Naccarati, A.; De Angelis, M.; Neviani, E.; Cocolin, L.; Gobetti, M.; Segata, N. Distinct genetic and functional traits of human intestinal *Prevotella copri* strains are associated with different habitual diets. *Cell Host Microbe* **2019**, *25*, 444-453. e443.
148. Glasemacher, J.; Bock, A.K.; Schmid, R.; Schönheit, P. Purification and properties of acetyl-CoA synthetase (ADP-forming), an archaeal enzyme of acetate formation and ATP synthesis, from the hyperthermophile *Pyrococcus furiosus*. *European Journal of Biochemistry* **1997**, *244*, 561-567.

149. Harris, R.A.; Joshi, M.; Jeoung, N.H. Mechanisms responsible for regulation of branched-chain amino acid catabolism. *Biochemical and Biophysical Research Communications* **2004**, 313, 391-396.
150. Allison, M.J.; Baetz, A.L.; Wiegel, J. Alternative pathways for biosynthesis of leucine and other amino acids in *Bacteroides rumenicola* and *Bacteroides fragilis*. *Applied and Environmental Microbiology* **1984**, 48, 1111-1117.
151. Commichau, F.M.; Forchhammer, K.; Stülke, J. Regulatory links between carbon and nitrogen metabolism. *Current Opinion in Microbiology* **2006**, 9, 167-172.
152. den Hengst, C.D.; Groeneveld, M.; Kuipers, O.P.; Kok, J. Identification and functional characterization of the *Lactococcus lactis* CodY-regulated branched-chain amino acid permease BcaP (CtrA). *Journal of Bacteriology* **2006**, 188, 3280-3289.
153. Atasoglu, C.; Valdés, C.; Walker, N.D.; Newbold, C.J.; Wallace, R.J. *De novo* synthesis of amino acids by the ruminal bacteria *Prevotella bryantii* B14, *Selenomonas ruminantium* HD4, and *Streptococcus bovis* ES1. *Applied and Environmental Microbiology* **1998**, 64, 2836-2843.
154. Butaye, P.; Devriese, L.A.; Haesebrouck, F. Antimicrobial growth promoters used in animal feed: Effects of less well known antibiotics on gram-positive bacteria. *Clinical Microbiology Reviews* **2003**, 16, 175-188.
155. Newbold, C.; Wallace, R.; Walker, N.D. The effect of tetronasin and monensin on fermentation, microbial numbers and the development of ionophore-resistant bacteria in the rumen. *Journal of Applied Microbiology* **1993**, 75, 129-134.
156. Witzig, M.; Zeder, M.; Rodehutschord, M. Effect of the ionophore monensin and tannin extracts supplemented to grass silage on populations of ruminal cellulolytics and methanogens *in vitro*. *Anaerobe* **2018**, 50, 44-54.
157. Thornton, J.; Owens, F. Monensin supplementation and *in vivo* methane production by steers. *Animal Science Journal* **1981**, 52, 628-634.
158. Pospíšil, S. Resistance of *Streptomyces cinnamonensis* to butyrate and isobutyrate: Production and properties of a new anti-isobutyrate (AIB) factor. *Microbiology* **1991**, 137, 2141-2146.
159. Pospíšil, S.; Váňová, M.; Machurová, V. Activity of the aib factor observed in prokaryotic and eukaryotic microorganisms. *Folia Microbiol.* **1993**, 38, 147.
160. Morehead, M.; Dawson, K. Some growth and metabolic characteristics of monensin-sensitive and monensin-resistant strains of *Prevotella (Bacteroides) rumenicola*. *Applied and Environmental Microbiology* **1992**, 58, 1617-1623.
161. Newbold, C.; Wallace, R. Changes in the rumen bacterium, *Bacteroides rumenicola*, grown in the presence of the ionophore, tetronasin. *Asian-Australasian Journal of Animal Sciences* **1989**, 2, 452-453.
162. Lewis, K.; Naroditskaya, V.; Ferrante, A.; Fokina, I. Bacterial resistance to uncouplers. *Journal of Bioenergetics and Biomembranes* **1994**, 26, 639-646.
163. Dunkley, E.; Clejan, S.; Krulwich, T. Mutants of *Bacillus* species isolated on the basis of protonophore resistance are deficient in fatty acid desaturase activity. *Journal of Bacteriology* **1991**, 173, 7750-7755.

164. Rychlik, J.L.; Russell, J.B. The adaptation and resistance of *Clostridium aminophilum* f to the butyriovibriocin-like substance of *Butyriovibrio fibrisolvens* JL5 and monensin. *FEMS Microbiology Letters* **2002**, 209, 93-98.
165. Bisson-Filho, A.W.; Hsu, Y.-P.; Squyres, G.R.; Kuru, E.; Wu, F.; Jukes, C.; Sun, Y.; Dekker, C.; Holden, S.; VanNieuwenhze, M.S. Treadmilling by FtsZ filaments drives peptidoglycan synthesis and bacterial cell division. *Science* **2017**, 355, 739-743.
166. Chow, J.; Russell, J. Effect of ionophores and pH on growth of *Streptococcus bovis* in batch and continuous culture. *Applied and Environmental Microbiology* **1990**, 56, 1588-1593.
167. Russell, J.B. A proposed mechanism of monensin action in inhibiting ruminant bacterial growth: Effects on ion flux and protonmotive force. *Animal Science Journal* **1987**, 64, 1519-1525.
168. Karpel, R.; Alon, T.; Glaser, G.; Schuldiner, S.; Padan, E. Expression of a sodium proton antiporter (NhaA) in *Escherichia coli* is induced by Na⁺ and Li⁺ ions. *Journal of Biological Chemistry* **1991**, 266, 21753-21759.
169. Murata, T.; Yamato, I.; Igarashi, K.; Kakinuma, Y. Intracellular Na⁺ regulates transcription of the ntp operon encoding a vacuolar-type Na⁺-translocating ATPase in *Enterococcus hirae*. *Journal of Biological Chemistry* **1996**, 271, 23661-23666.
170. Yamanaka, T.; Yamane, K.; Furukawa, T.; Matsumoto-Mashimo, C.; Sugimori, C.; Nambu, T.; Obata, N.; Walker, C.B.; Leung, K.-P.; Fukushima, H. Comparison of the virulence of exopolysaccharide-producing *Prevotella intermedia* to exopolysaccharide non-producing periodontopathic organisms. *BMC Infectious Diseases*. **2011**, 11, 228.
171. Sanin, S.L.; Sanin, F.D.; Bryers, J.D. Effect of starvation on the adhesive properties of xenobiotic degrading bacteria. *Process Biochemistry* **2003**, 38, 909-914.
172. Yun, S.-H.; Choi, C.-W.; Park, S.-H.; Lee, J.C.; Leem, S.-H.; Choi, J.-S.; Kim, S.; Kim, S.I. Proteomic analysis of outer membrane proteins from *Acinetobacter baumannii* DU202 in tetracycline stress condition. *Research Journal of Microbiology* **2008**, 46, 720-727.
173. Urfer, M.; Bogdanovic, J.; Monte, F.L.; Moehle, K.; Zerbe, K.; Omasits, U.; Ahrens, C.H.; Pessi, G.; Eberl, L.; Robinson, J.A. A peptidomimetic antibiotic targets outer membrane proteins and disrupts selectively the outer membrane in *Escherichia coli*. *Journal of Biological Chemistry* **2016**, 291, 1921-1932.
174. King, L.B.; Pangburn, M.K.; McDaniel, L.S. Serine protease pkf of *Acinetobacter baumannii* results in serum resistance and suppression of biofilm formation. *Journal of Infectious Diseases* **2013**, 207, 1128-1134.
175. Cabral, M.P.; Soares, N.C.; Aranda, J.; Parreira, J.R.; Rumbo, C.; Poza, M.; Valle, J.; Calamia, V.; Lasa, Í.; Bou, G. Proteomic and functional analyses reveal a unique lifestyle for *Acinetobacter baumannii* biofilms and a key role for histidine metabolism. *Journal of Proteome Research*. **2011**, 10, 3399-3417.
176. Nielsen, P.H.; Jahn, A. "Extraction of EPS." In *Microbial extracellular polymeric substances*, edited by J. Wingender, Thomas R Neu and H.C. Felming, Heidelberg Berlin: Springer-Verlag, **1999**, 49-72.
177. Ding, Z.; Bourven, I.; Guibaud, G.; van Hullebusch, E.D.; Panico, A.; Pirozzi, F.; Esposito, G. Role of extracellular polymeric substances (EPS) production in bioaggregation:

- Application to wastewater treatment. *Applied Microbiology and Biotechnology* **2015**, 99, 9883-9905.
178. Vorburger, T.; Nedielkov, R.; Brosig, A.; Bok, E.; Schunke, E.; Steffen, W.; Mayer, S.; Götz, F.; Möller, H.M.; Steuber, J. Role of the Na⁺-translocating NADH: Quinone oxidoreductase in voltage generation and Na⁺ extrusion in *Vibrio cholerae*. *Biochimica et Biophysica Acta (BBA), Bioenergetics* **2016**, 1857, 473-482.
179. Terahara, N.; Sano, M.; Ito, M. A bacillus flagellar motor that can use both Na⁺ and K⁺ as a coupling ion is converted by a single mutation to use only Na⁺. *PloS one* **2012**, 7, e46248.
180. VDLUFA. "VDLUFA-methodenbuch." In *Band VII Umweltanalytik* Darmstadt: VDLUFA, **2011**, 65, 262-263.
181. Burtis, C.A.; Ashwood, E.R. Tietz textbook of clinical chemistry. **1999**, 2238.
182. Juárez, O.; Ahearn, K.; Gillespie, P.; Barquera, B. Acid residues in the transmembrane helices of the Na⁺-pumping NADH: Quinone oxidoreductase from *Vibrio cholerae* involved in sodium translocation. *Biochemistry* **2009**, 48, 9516-9524.
183. Geisler, V.; Ullmann, R.; Kröger, A. The direction of the proton exchange associated with the redox reactions of menaquinone during electron transport in *Wolinella succinogenes*. *Biochimica et Biophysica Acta (BBA), Biomembranes* **1994**, 1184, 219-226.
184. Aramaki, T.; Blanc-Mathieu, R.; Endo, H.; Ohkubo, K.; Kanehisa, M.; Goto, S.; Ogata, H. KofamKOALA: KEGG ortholog assignment based on profile HMM and adaptive score threshold. *Bioinformatics* **2020**, 36, 2251-2252.
185. Zhang, H.; Yohe, T.; Huang, L.; Entwistle, S.; Wu, P.; Yang, Z.; Busk, P.K.; Xu, Y.; Yin, Y. DbCAN2: A meta server for automated carbohydrate-active enzyme annotation. *Nucleic Acids Research* **2018**, 46, W95-W101.
186. Di Rienzo, J.; Casanoves, F.; Balzarini, M.G.; Gonzalez, L.; Tablada, M.; Robledo, C. Infostat, versión 2008. *Grupo infostat, fca, Universidad Nacional de Córdoba, Argentina* **2008**, 268.
187. Heberle, H.; Meirelles, G.V.; da Silva, F.R.; Telles, G.P.; Minghim, R. Interactivenn: A web-based tool for the analysis of sets through VENN diagrams. *BMC Bioinformatics* **2015**, 16, 169.
188. Hammond, A.; Breeze, R. Monensin and the prevention of tryptophan-induced acute bovine pulmonary edema and emphysema. *Science* **1978**, 201, 153-155.
189. Thornton, J.; Owens, F. Monensin supplementation and *in vivo* methane production by steers. *Journal of Animal Science* **1981**, 52, 628-634.
190. Russell, J.B.; Strobel, H. Effect of ionophores on ruminal fermentation. *Applied and Environmental Microbiology* **1989**, 55, 1-6.
191. Russell, J.B.; Houlihan, A.J. Ionophore resistance of ruminal bacteria and its potential impact on human health. *FEMS Microbiology Reviews* **2003**, 27, 65-74.
192. Newbold, C.; Wallace, R.; Walker, N.D. The effect of tetronasin and monensin on fermentation, microbial numbers and the development of ionophore-resistant bacteria in the rumen. *Journal of Applied Bacteriology* **1993**, 75, 129-134.

Literature References

193. Callaway, T.; Edrington, T.; Rychlik, J.; Genovese, K.; Poole, T.; Jung, Y.S.; Bischoff, K.; Anderson, R.; Nisbet, D.J. Ionophores: Their use as ruminant growth promotants and impact on food safety. *Current Issues in Intestinal Microbiology* **2003**, 4, 43-51.
194. Castanon, J. History of the use of antibiotic as growth promoters in european poultry feeds. *Poultry Science Journal* **2007**, 86, 2466-2471.
195. Duffield, T.; Sandals, D.; Leslie, K.; Lissemore, K.; McBride, B.; Lumsden, J.; Dick, P.; Bagg, R. Efficacy of monensin for the prevention of subclinical ketosis in lactating dairy cows. *Journal of Dairy Science* **1998**, 81, 2866-2873.
196. Nagaraja, T.; Avery, T.; Bartley, E.; Galitzer, S.; Dayton, A. Prevention of lactic acidosis in cattle by lasalocid or monensin. *Journal of Animal Science* **1981**, 53, 206-216.
197. Bergen, W.G.; Bates, D.B. Ionophores: Their effect on production efficiency and mode of action. *Journal of Animal Science* **1984**, 58, 1465-1483.
198. Wallace, R.J.; Snelling, T.J.; McCartney, C.A.; Tapio, I.; Strozzi, F. Application of meta-omics techniques to understand greenhouse gas emissions originating from ruminal metabolism. *Genetic Selection Evolution* **2017**, 49, 9.
199. Pitta, D.; Indugu, N.; Narayan, K.; Hennessy, M. Symposium review: Understanding the role of the rumen microbiome in enteric methane mitigation and productivity in dairy cows. *Journal of Dairy Science* **2022**, 105, 8569-8585.
200. Gharechahi, J.; Vahidi, M.F.; Bahram, M.; Han, J.L.; Ding, X.Z.; Salekdeh, G.H. Metagenomic analysis reveals a dynamic microbiome with diversified adaptive functions to utilize high lignocellulosic forages in the cattle rumen. *ISME Journal* **2021**, 15, 1108-1120.
201. Morehead, M.; Dawson, K. Some growth and metabolic characteristics of monensin-sensitive and monensin-resistant strains of *Prevotella (Bacteroides) ruminicola*. *Applied Environmental Microbiology* **1992**, 58, 1617-1623.
202. Perry, T.; Beeson, W.; Mohler, M. Effect of monensin on beef cattle performance. *Journal of Animal Science* **1976**, 42, 761-765.
203. Wischer, G.; Boguhn, J.; Steingäß, H.; Schollenberger, M.; Hartung, K.; Rodehutschord, M. Effect of monensin on *in vitro* fermentation of silages and microbial protein synthesis. *Archives of Animal Nutrition* **2013**, 67, 219-234.
204. Weimer, P.J.; Stevenson, D.M.; Mertens, D.R.; Hall, M.B. Fiber digestion, VFA production, and microbial population changes during *in vitro* ruminal fermentations of mixed rations by monensin-adapted and unadapted microbes. *Animal Feed Science Technology* **2011**, 169, 68-78.
205. Johnson, M.C.; Devine, A.A.; Ellis, J.C.; Grunden, A.M.; Fellner, V. Effects of antibiotics and oil on microbial profiles and fermentation in mixed cultures of ruminal microorganisms. *Journal of Dairy Science* **2009**, 92, 4467-4480.
206. Karnati, S.K.; Sylvester, J.T.; Ribeiro, C.V.; Gilligan, L.E.; Firkins, J.L. Investigating unsaturated fat, monensin, or bromoethanesulfonate in continuous cultures retaining ruminal protozoa. I. Fermentation, biohydrogenation, and microbial protein synthesis. *Journal of Dairy Science* **2009**, 92, 3849-3860.
207. Karnati, S.K.; Yu, Z.; Firkins, J.L. Investigating unsaturated fat, monensin, or bromoethanesulfonate in continuous cultures retaining ruminal protozoa. II.

- Interaction of treatment and presence of protozoa on prokaryotic communities. *Journal of Dairy Science* **2009**, 92, 3861-3873.
208. Lengowski, M.B.; Zuber, K.H.; Witzig, M.; Möhring, J.; Boguhn, J.; Rodehutschord, M. Changes in rumen microbial community composition during adaptation to an *in vitro* system and the impact of different forages. *PLoS One* **2016**, 11, e0150115.
209. McDougall, E. Studies on ruminant saliva. 1. The composition and output of sheep's saliva. *Biochemical Journal* **1948**, 43, 99.
210. Deusch, S.; Camarinha-Silva, A.; Conrad, J.; Beifuss, U.; Rodehutschord, M.; Seifert, J. A structural and functional elucidation of the rumen microbiome influenced by various diets and microenvironments. *Frontiers in Microbiology* **2017**, 8, 1605.
211. Olsen, J.V.; Godoy, L.M.F.d.; Li, G.; Macek, B.; Mortensen, P.; Pesch, R.; Makarov, A.; Lange, O.; Horning, S.; Mann, M. Parts per million mass accuracy on an orbitrap mass spectrometer via lock mass injection into a c-trap. *Molecular and Cellular Proteomics* **2005**, 4, 2010–2021.
212. Cheng, K.; Ning, Z.; Zhang, X.; Li, L.; Liao, B.; Mayne, J.; Figeys, D. Metalab 2.0 enables accurate post-translational modifications profiling in metaproteomics. *Journal of the American Society for Mass Spectrometry* **2020**, 31, 1473-1482.
213. Stewart, R.D.; Auffret, M.D.; Warr, A.; Walker, A.W.; Roehe, R.; Watson, M. Compendium of 4,941 rumen metagenome-assembled genomes for rumen microbiome biology and enzyme discovery. *Nature Biotechnology* **2019**, 37, 953-961.
214. Huerta-Cepas, J.; Forslund, K.; Coelho, L.P.; Szklarczyk, D.; Jensen, L.J.; von Mering, C.; Bork, P. Fast genome-wide functional annotation through orthology assignment by EggNOG-mapper. *Molecular Biology and Evolution* **2017**, 34, 2115-2122.
215. Ferme, D.; Banjac, M.; Calsamiglia, S.; Busquet, M.; Kamel, C.; Avguštin, G. The effects of plant extracts on microbial community structure in a rumen-simulating continuous-culture system as revealed by molecular profiling. *Folia Microbiologica* **2004**, 49, 151-155.
216. Bach, A.; Calsamiglia, S.; Stern, M. Nitrogen metabolism in the rumen. *Journal of Dairy Science* **2005**, 88, E9-E21.
217. El-Rami, F.; Kong, X.; Parikh, H.; Zhu, B.; Stone, V.; Kitten, T.; Xu, P. Analysis of essential gene dynamics under antibiotic stress in *Streptococcus sanguinis*. *Microbiology* **2018**, 164, 173-185.
218. Poos, M.; Hanson, T.; Klopfenstein, T. Monensin effects on diet digestibility, ruminal protein bypass and microbial protein synthesis. *Journal of Animal Science* **1979**, 48, 1516-1524.
219. Terry, S.A.; Badhan, A.; Wang, Y.; Chaves, A.V.; McAllister, T.A. Fibre digestion by rumen microbiota—a review of recent metagenomic and metatranscriptomic studies. *Canadian Journal of Animal Science* **2019**, 99, 678-692.
220. Trautmann, A.; Schleicher, L.; Pfirrmann, J.; Boldt, C.; Steuber, J.; Seifert, J. Na⁺-coupled respiration and reshaping of extracellular polysaccharide layer counteract monensin-induced cation permeability in *Prevotella bryantii* B14. *International Journal of Molecular Science* **2021**, 22.

221. Schleicher, L.; Trautmann, A.; Stegmann, D.; Fritz, G.; Gätgens, J.; Bott, M.; Hein, S.; Simon, J.; Seifert, J.; Steuber, J. A sodium-translocating module linking succinate production to formation of membrane potential in *Prevotella bryantii*. *Applied and Environmental Microbiology* **2021**, *87*, e0121121.
222. Delort, A.-M.; Dauphin, G.; Guyot, J.; Jeminet, G. Study by NMR of the mode of action of monensin on *Streptococcus faecalis* de-energized and energized cells. *Biochimica et Biophysica Acta (BBA)* **1989**, *1013*, 11-20.
223. Morotomi, M.; Nagai, F.; Watanabe, Y.; Tanaka, R. *Succinatimonas hippei* gen. nov., sp. nov., isolated from human faeces. *International Journal of Systematic and Evolutionary Microbiology* **2010**, *60*, 1788-1793.
224. Kaplan-Shabtai, V.; Indugu, N.; Hennessy, M.L.; Vecchiarelli, B.; Bender, J.S.; Stefanovski, D.; De Assis Lage, C.F.; Räsänen, S.E.; Melgar, A.; Nedelkov, K. Using structural equation modeling to understand interactions between bacterial and archaeal populations and volatile fatty acid proportions in the rumen. *Frontiers in Microbiology* **2021**, *12*, 611951.
225. Callaway, T.; Russell, J. Variations in the ability of ruminal gram-negative *Prevotella* species to resist monensin. *Current Microbiology* **2000**, *40*, 185-189.
226. Ogunade, I.; Schweickart, H.; Andries, K.; Lay, J.; Adeyemi, J. Monensin alters the functional and metabolomic profile of rumen microbiota in beef cattle. *Animals* **2018**, *8*, 211.
227. Schären, M.; Drong, C.; Kiri, K.; Riede, S.; Gardener, M.; Meyer, U.; Hummel, J.; Urich, T.; Breves, G.; Dänicke, S. Differential effects of monensin and a blend of essential oils on rumen microbiota composition of transition dairy cows. *Journal of Dairy Science* **2017**, *100*, 2765-2783.
228. Jalč, D.; Baran, M.; Vondrák, T.; Siroka, P. Effect of monensin on fermentation of hay and wheat bran investigated by the rumen simulation technique (Rusitec) 1. Basal parameters of fermentation. *Archives of Animal Nutrition* **1992**, *42*, 147-152.
229. Daugherty, M.; Galyean, M.; Hallford, D.; Hageman, J. Vitamin B12 and monensin effects on performance, liver and serum vitamin B12 concentrations and activity of propionate metabolizing hepatic enzymes in feedlot lambs. *Journal of Animal Science* **1986**, *62*, 452-463.
230. Dennis, S.; Nagaraja, T.; Bartley, E. Effect of lasalocid or monensin on lactate-producing or using rumen bacteria. *Journal of Animal Science* **1981**, *52*, 418-426.
231. Weimer, P.; Moen, G. Quantitative analysis of growth and volatile fatty acid production by the anaerobic ruminal bacterium *Megasphaera elsdenii* T81. *Applied Microbiology and Biotechnology* **2013**, *97*, 4075-4081.
232. Haas, K.N.; Blanchard, J.L. *Kineothrix alysoides*, gen. nov., sp. nov., a saccharolytic butyrate-producer within the family Lachnospiraceae. *International Journal of Systematic and Evolutionary Microbiology* **2017**, *67*, 402-410.
233. Xue, M.; Sun, H.; Wu, X.; Guan, L.L.; Liu, J. Assessment of rumen microbiota from a large dairy cattle cohort reveals the pan and core bacteriomes contributing to varied phenotypes. *Applied and Environmental Microbiology* **2018**, *84*, e00970-00918.

Literature References

234. Marchandin, H.; Teyssier, C.; Campos, J.; Jean-Pierre, H.; Roger, F.; Gay, B.; Carlier, J.-P.; Jumas-Bilak, E. *Negativicoccus succinicivorans* gen. nov., sp. nov., isolated from human clinical samples, emended description of the family Veillonellaceae and description of negativicutes classis nov., Selenomonadales ord. nov. and Acidaminococcaceae fam. nov. In the bacterial phylum Firmicutes. *International Journal of Systematic and Evolutionary Microbiology* **2010**, 60, 1271-1279.
235. Distler, W.; Kröncke, A. The lactate metabolism of the oral bacterium *Veillonella* from human saliva. *Archives of Oral Biology* **1981**, 26, 657-661.
236. Aguilar-Marin, S.B.; Betancur-Murillo, C.L.; Isaza, G.A.; Mesa, H.; Jovel, J. Lower methane emissions were associated with higher abundance of ruminal *Prevotella* in a cohort of colombian buffalos. *BMC Microbiology* **2020**, 20, 364.
237. Perez-Riverol, Y.; Bai, J.; Bandla, C.; Garcia-Seisdedos, D.; Hewapathirana, S.; Kamatchinathan, S.; Kundu, D.J.; Prakash, A.; Frericks-Zipper, A.; Eisenacher, M.; Walzer, M.; Wang, S.; Brazma, A.; Vizcaino, J.A. The pride database resources in 2022: A hub for mass spectrometry-based proteomics evidences. *Nucleic Acids Research* **2022**, 50, D543-D552.
238. Schleicher, L.; Herdan, S.; Fritz, G.; Trautmann, A.; Seifert, J.; Steuber, J. Central carbon metabolism, sodium-motive electron transfer, and ammonium formation by the vaginal pathogen *Prevotella bivia*. *International Journal of Molecular Sciences* **2021**, 22, 11925.
239. Pflüger, S. Einfluss von ausgewählten zusatzstoffen auf das wachstum von *Prevotella bryantii* B14. Bachelor, Bachelor of Science, University of Hohenheim, Stuttgart, **2019**.
240. La Scola, B.; Khelaifia, S.; Lagier, J.-C.; Raoult, D. Aerobic culture of anaerobic bacteria using antioxidants: A preliminary report. *European Journal of Clinical Microbiology & Infectious Diseases* **2014**, 33, 1781-1783.
241. Cybulski, L.E.; Albanesi, D.; Mansilla, M.C.; Altabe, S.; Aguilar, P.S.; De Mendoza, D. Mechanism of membrane fluidity optimization: Isothermal control of the *Bacillus subtilis* acyl-lipid desaturase. *Molecular Microbiology* **2002**, 45, 1379-1388.
242. Sun, Y.; O'Riordan, M.X. Regulation of bacterial pathogenesis by intestinal short-chain fatty acids. *Advances in Applied Microbiology* **2013**, 85, 93-118.
243. Haenen, D.; Zhang, J.; Souza da Silva, C.; Bosch, G.; van der Meer, I.M.; van Arkel, J.; van den Borne, J.J.; Pérez Gutiérrez, O.; Smidt, H.; Kemp, B. A diet high in resistant starch modulates microbiota composition, SCFA concentrations, and gene expression in pig intestine. *The Journal of Nutrition* **2013**, 143, 274-283.
244. Charney, A.N.; Micic, L.; Egnor, R.W. Nonionic diffusion of short-chain fatty acids across rat colon. *American Journal of Physiology-Gastrointestinal and Liver Physiology* **1998**, 274, G518-G524.
245. Noinaj, N.; Guillier, M.; Barnard, T.J.; Buchanan, S.K. TonB-dependent transporters: Regulation, structure, and function. *Annual Review of Microbiology* **2010**, 64, 43-60.
246. Simpson, W.; Olczak, T.; Genco, C.A. Characterization and expression of HmuRmur, a TonB-dependent hemoglobin receptor of *Porphyromonas gingivalis*. *Journal of Bacteriology* **2000**, 182, 5737-5748.

247. Wójtowicz, H.; Guevara, T.; Tallant, C.; Olczak, M.; Sroka, A.; Potempa, J.; Solà, M.; Olczak, T.; Gomis-Rüth, F.X. Unique structure and stability of HmuY, a novel heme-binding protein of *Porphyromonas gingivalis*. *PLoS Pathogens* **2009**, *5*, e1000419.
248. Grünberg, K.; Wawer, C.; Tebo, B.M.; Schüler, D. A large gene cluster encoding several magnetosome proteins is conserved in different species of magnetotactic bacteria. *Applied and Environmental Microbiology* **2001**, *67*, 4573-4582.
249. Jiménez-Munguía, I.; Calderón-Santiago, M.; Rodríguez-Franco, A.; Priego-Capote, F.; Rodríguez-Ortega, M.J. Multi-omic profiling to assess the effect of iron starvation in *Streptococcus pneumoniae* TIGR4. *PeerJ* **2018**, *6*, e4966.
250. Dostal, A.; Baumgartner, J.; Riesen, N.; Chassard, C.; Smuts, C.M.; Zimmermann, M.B.; Lacroix, C. Effects of iron supplementation on dominant bacterial groups in the gut, faecal scfa and gut inflammation: A randomised, placebo-controlled intervention trial in south african children. *British Journal of Nutrition* **2014**, *112*, 547-556.
251. Mayneris-Perxachs, J.; Moreno-Navarrete, J.M.; Fernández-Real, J.M. The role of iron in host–microbiota crosstalk and its effects on systemic glucose metabolism. *Nature Reviews Endocrinology* **2022**, 1-16.
252. Kortman, G.A.; Raffatellu, M.; Swinkels, D.W.; Tjalsma, H. Nutritional iron turned inside out: Intestinal stress from a gut microbial perspective. *FEMS Microbiology Reviews* **2014**, *38*, 1202-1234.
253. Trinidad, T.P.; Wolever, T.M.; Thompson, L.U. Interactive effects of calcium and short chain fatty acids on absorption in the distal colon of man. *Nutrition Research* **1993**, *13*, 417-425.
254. Bougle, D.; Vaghefi-Vaezadeh, N.; Roland, N.; Bouvard, G.; Arhan, P.; Bureau, F.; Neuville, D.; Maubois, J.-L. Influence of short-chain fatty acids on iron absorption by proximal colon. *Scandinavian Journal of Gastroenterology* **2002**, *37*, 1008-1011.
255. Misra, A.; Thakur, S. Effect of dietary supplementation of sodium salt of isobutyric acid on ruminal fermentation and nutrient utilization in a wheat straw based low protein diet fed to crossbred cattle. *Asian-Australasian Journal of Animal Sciences* **2001**, *14*, 479-484.
256. Rodríguez, F. Control of lactate accumulation in ruminants using *Prevotella bryantii*. Doctoral degree, PhD, Iowa State University, **2003**, 61.
257. Umeda, A.; Saito, M.; Amako, K. Surface characteristics of gram-negative and gram-positive bacteria in an atomic force microscope image. *Microbiology and Immunology* **1998**, *42*, 159-164.
258. Dufour, D.; Leung, V.; Lévesque, C.M. Bacterial biofilm: Structure, function, and antimicrobial resistance. *Endodontic Topics* **2010**, *22*, 2-16.
259. O'Toole, G.; Kaplan, H.B.; Kolter, R. Biofilm formation as microbial development. *Annual Reviews in Microbiology* **2000**, *54*, 49-79.
260. Allison, D.G.; Ruiz, B.; SanJose, C.; Jaspe, A.; Gilbert, P. Extracellular products as mediators of the formation and detachment of *Pseudomonas fluorescens* biofilms. *FEMS Microbiology Letters* **1998**, *167*, 179-184.
261. Silver, S.; Walderhaug, M. Gene regulation of plasmid-and chromosome-determined inorganic ion transport in bacteria. *Microbiological Reviews* **1992**, *56*, 195-228.

262. Sebald, M. Genetic basis for antibiotic resistance in anaerobes. *Clinical Infectious Diseases* **1994**, 18, S297-S304.
263. Stojković, V.; Fujimori, D.G. Mutations in rna methylating enzymes in disease. *Current Opinion in Chemical Biology* **2017**, 41, 20-27.
264. Osterman, I.; Dontsova, O.; Sergiev, P. rRNA methylation and antibiotic resistance. *Biochemistry (Moscow)* **2020**, 85, 1335-1349.
265. Schauer, K.; Rodionov, D.A.; de Reuse, H. New substrates for TonB-dependent transport: Do we only see the 'tip of the iceberg'? *Trends in Biochemical Sciences* **2008**, 33, 330-338.
266. Henderson, C.; Stewart, C.; Nekrep, F.V. The effect of monensin on pure and mixed cultures of rumen bacteria. *Journal of Applied Bacteriology* **1981**, 51, 159-169.
267. Hitch, T.C.; Bisdorf, K.; Afrizal, A.; Riedel, T.; Overmann, J.; Strowig, T.; Clavel, T. A taxonomic note on the genus *Prevotella*: Description of four novel genera and emended description of the genera *Hallella* and *Xylanibacter*. *Systematic and Applied Microbiology* **2022**, 126354.
268. Moreau-Marquis, S.; Bomberger, J.M.; Anderson, G.G.; Swiatecka-Urban, A.; Ye, S.; O'Toole, G.A.; Stanton, B.A. The $\delta f508$ -CftR mutation results in increased biofilm formation by *Pseudomonas aeruginosa* by increasing iron availability. *American Journal of Physiology-Lung Cellular and Molecular Physiology* **2008**, 295, L25-L37.
269. Hijova, E.; Chmelarova, A. Short chain fatty acids and colonic health. *Bratislavské Lekárske Listy* **2007**, 108, 354.
270. Gill, P.; Van Zelm, M.; Muir, J.; Gibson, P. Short chain fatty acids as potential therapeutic agents in human gastrointestinal and inflammatory disorders. *Alimentary Pharmacology & Therapeutics* **2018**, 48, 15-34.
271. Castillo, C.; Benedito, J.; Méndez, J.; Pereira, V.; Lopez-Alonso, M.; Miranda, M.; Hernández, J. Organic acids as a substitute for monensin in diets for beef cattle. *Animal Feed Science and Technology* **2004**, 115, 101-116.
272. Belanche, A.; Kingston-Smith, A.H.; Griffith, G.W.; Newbold, C.J. A multi-kingdom study reveals the plasticity of the rumen microbiota in response to a shift from non-grazing to grazing diets in sheep. *Frontiers in Microbiology* **2019**, 10, 122.
273. Karimi, B.; Maron, P.A.; Chemidlin-Prevost Boure, N.; Bernard, N.; Gilbert, D.; Ranjard, L. Microbial diversity and ecological networks as indicators of environmental quality. *Environmental Chemistry Letters* **2017**, 15, 265-281.

9. Author contributions

The supervisors (J.Seifert and J.Steuber) confirm here that the author (A.T.) was the contributor to the respective sections mentioned for the manuscripts and publications below (Chapter 9.1 to 9.3).

_____, _____ the _____
J.Seifert (Signature) Place Date

_____, _____ the _____
J.Steuber (Signature) Place Date

_____, _____ the _____
A.Trautmann (Signature) Place Date

9.1 First publication in chapter 2

Conceptualization, A.T., J.Seifert; methodology, A.T., L.S., S.D., and J.G.; formal analysis, A.T. L.S. and J.G.; investigation, A.T. and L.S.; data curation, A.T.; writing—original draft preparation, A.T.; writing—review and editing, J.Steuber, J. Seifert, L.S., S.D., and J.G.; supervision, J. Seifert; project administration, J. Seifert and J.Steuber; funding acquisition, J.Steuber and J. Seifert

9.2 Second publication in chapter 3

Conceptualization, A.T., J.Steuber, J.Seifert; methodology, A.T., L.S., C.B. and J.P.; formal analysis, A.T., L.S., C.B. and J.P.; investigation, A.T., L.S., C.B. and J.P.; data curation, A.T.; writing—original draft preparation, A.T.; writing—review and editing, J.Steuber, J.Seifert and L.S.; supervision, J. Seifert; project administration, J.Seifert and J.Steuber; funding acquisition, J.Steuber and J.Seifert. All authors have read and agreed to the published version of the manuscript.

9.3 Third publication/manuscript in chapter 4

Conceptualization, Andrej Trautmann, Jana Seifert; methodology, Andrej Trautmann, Lena Schleicher, Ariane Koch; formal analysis, Andrej Trautmann, Lena Schleicher, Ariane Koch; investigation, Andrej Trautmann, Ariane Koch; data curation, Andrej Trautmann; writing—original draft preparation, Andrej Trautmann; writing—review and editing, Julia Steuber, Jana Seifert and Lena Schleicher; supervision, Jana Seifert; project administration, Jana Seifert and Julia Steuber; funding acquisition, Julia Steuber and Jana Seifert. All authors have read and agreed to include this version of the manuscript in this thesis.

Curriculum Vitae (CV)

Andrej Trautmann born in Moscow (Russia), 06. February 1993

Higher Education

Ph.D. Thesis

University of Hohenheim

2017 Oct. - 2023 March

Thesis: Adaptations of *Prevotella bryantii* B₁₄ to Short-Chain Fatty Acids and Monensin Exposure

Facility: Institute of Animal Science, Functional Microbiology, Prof. Dr. Jana Seifert

Master of Science

Food Microbiology and Biotechnology,

University of Hohenheim

2015 Oct. – 2017 Oct.

Thesis: Light dependent gene regulation and biosynthesis of sesquiterpene lactones in sunflower trichomes

Facility: Institute of Botany, Group of Biodiversity and Plant Interaction, Prof. Dr. Otmar Spring

Bachelor of Science

Biology, University of Hohenheim

2012 Oct. – 2015 Oct.

Thesis: HPLC-Unterstützte Analyse von Sesquiterpenen in Drüsenhaaren der Sonnenblume unter Einfluss verschiedener Entwicklungsstadien und Lichtqualitäten

Facility: Institute of Botany, Group of Biodiversity and Plant Interaction, Prof. Dr. Otmar Spring

A.Trautmann (Signature) _____, _____ the _____
Place Date

Publications

“Short-chain fatty acids modulate metabolic pathways and membrane lipids in *Prevotella bryantii* B14”. 2020. [Trautmann A.](#), Schleicher L., Deusch S., Gätgens J., Steuber J., Seifert J. Proteomes. doi: 10.3390/proteomes8040028.

“Na⁺-coupled respiration and reshaping of extracellular polysaccharide layer counteract monensin-induced cation permeability in *Prevotella bryantii* B14”. [Trautmann A.](#), Schleicher L., Pfirrmann, J. Boldt C., Steuber J., Seifert J. 2021. International Journal of Molecular Science. doi: 10.3390/ijms221910202.

“A sodium-translocating module linking succinate production to formation of a membrane potential in *Prevotella bryantii*”. 2021. Schleicher L., [Trautmann A.](#), Stegmann DP., Fritz G., Gätgens J., Bott M., Hein S., Simon J., Seifert J., Steuber J. Applied and Environmental Microbiology. doi: 10.1128/AEM.01211-21.

“Central carbon metabolism, sodium-motive electron transfer, and ammonium formation by the vaginal pathogen *Prevotella bivia*”. 2021. Schleicher L., Herdan S., Fritz G., [Trautmann A.](#), Seifert J., Steuber S. International Journal of Molecular Science. doi: 10.3390/ijms222111925.

„A shift towards succinate-producing *Prevotella* in the ruminal microbiome challenged with monensin”. 2022. [Trautmann A.](#), Schleicher L., Koch A., Günther J., Steuber J., Seifert J. Proteomics; Manuscript No.: pmic.202200121.R1

Acknowledgements

Jana Seifert – My sincere gratefulness for your trust, patience, your advice and clear communication. You are the Alpha and the Omega for this work and I am glad to have you as my supervisor. We shared a lot of intense events and experiences, which I will remember as my good old times, “When I was young”.

Julia Fritz-Steuber – I was always amazed and inspired by your spirit for discovery and scientific adventures. Your alternate perspectives broadened my view and enforced me to reconsider findings carefully. Thank you for sharing this motivation and engagement for science during my time as a student up to my PhD.

Lena Schleicher – I really appreciate your chilled vibes and our subject related interchange that gave me the feeling having companion with similar issues and a common history.

Johanna Tröscher-Mußotter – The valuable and cheering office mate and friend. I am honoured to meet and work beside such a socially empathic, smart and authentic person.

Christine Rau – Who inspired and led me to become a better version of myself. Without your carrying support, this thesis would not be completed.

Simon Deusch – The man of the hour who saved my day when things went wrong. Your humour was my painkiller. Thanks a lot!

Specialists:

Thanks to *Jens Pfannstiel*, *Berit Würtz*, *Iris Klaiber* and *Philipp Hubel* who provided flawless MS raw data and good vibes during my visits. *Johannes Günther* was a great help with optimizing the NMR measurements to identify metabolites. *Margit Schollenberger* & *Helga Terry* provided fast and efficient results with SCFA measurements. *Michael Bott* and *Jochen Gätgens* enabled us to see the wonderful world of membrane lipids and *Christin Boldt* showed us the world of biofilms. Thanks to all of you and your crucial contribution to this thesis!

The Team:

Being around and interacting with you gave me the inspiration, motivation and input to overcome challenges and hard ships. However, especially the fun times we shared were the fuel for the fulfilment of this work. Therefor many thanks to *Amélia Silva, Daniel Borda, Angelica Hernandez, Daniel Rissi, Katrin Röhm, Alina Renz, Bibiana Rios Galicia, Nida Amin, Johan Sebastian Saenz, Petra Miller-Rostek, Beate Metzger, Tanja Sims, Susanne Künzel, Katharina Wild, Heike Trapp, Lisa Uhland* and all the others from the whole institute!

Bachelors, Masters & Hiwis:

Big thanks for the adventurers at the frontline of science: *Jana Pfirrmann, Svenja Pflüger, Paula Truelsen, Jessica Walter, Anna Hanauska, Ariane Koch, Anna-Lena Schweiger, and Ronja Hepp*. Your ideas and efforts supported this contribution to natural sciences and it meant a lot to me!

Deutsche Forschungsgesellschaft (DFG):

I would like to express my gratitude the DFG, which made this research even possible.

Eidesstattliche Versicherung

Annex 2 to the University of Hohenheim doctoral degree regulations for Dr. rer. nat.

Affidavit according to Sec. 7(7) of the University of Hohenheim doctoral degree regulations for Dr. rer. nat.

For the dissertation submitted on the topic

“Adaptations of *Prevotella bryantii* B₁₄ to Short-Chain Fatty Acids and Monensin Exposure”

1. I hereby declare that I independently completed the work.
2. I only used the sources and aids documented and only made use of permissible assistance by third parties. I properly documented any contents which I used – either by directly quoting or paraphrasing – from other works.
3. I did not accept any assistance from commercial doctoral agency or consulting firm.
4. I am aware of the meaning of this affidavit and the criminal penalties of an incorrect or incomplete affidavit.

I hereby confirm the correctness of the above declaration: I hereby affirm in lieu of oath that I have, to the best of my knowledge, declared nothing but the truth and have not omitted any information.

Place and Date

Signature

Eidesstattliche Versicherung

This work was funded by a doctoral fellowship of the Deutsche Forschungsgemeinschaft (DFG, SE2059/3-1 and FR1321/7-1), which is gratefully acknowledged.

The presented studies were realized at the Institutes of Animal Science of the University of Hohenheim in Stuttgart, Germany. The experimental work was performed in the time between October 2017 and May 2021 under the supervision of Prof. Dr. Jana Seifert (University of Hohenheim, Head of the “Feed-Gut Microbiota Interaction” Group).

The Faculty of Natural Sciences at the University of Hohenheim accepted this thesis as a doctoral thesis (dissertation) in fulfillment of the regulations to acquire the doctoral degree “Doktor der Naturwissenschaften” on 17.Mar.2023 (date when review by the professors is completed).

Dean of the Faculty of Natural Sciences: Prof. Dr. Uwe Beifuss

Date of the oral examination: 17.Mär.2023

Chairperson of the oral examination: Prof. Dr. Jana Seifert

Dissertation supervisor: Prof. Dr. Jana Seifert

Second examiner: Prof. Dr. Julia Fritz-Steuber

Third examiner: Prof. Dr. Armin Huber